Dissertation zur Erlangung des Doktorgrades
der Fakultät für Chemie und Pharmazie
der Ludwig-Maximilians-Universität München

MICROSCALE THERMOPHORESIS (MST) FOR PROTEIN FORMULATION DEVELOPMENT

Randy Lee Wanner
aus
San Antonio, USA

2019

Erklärung

Diese Dissertation wurde im Sinne von § 7 der Promotionsordnung vom 28. November 2011 von Herrn Prof. Dr. Gerhard Winter betreut.

Eidesstattliche Versicherung

Diese Dissertation wurde eigenständig und ohne unerlaubte Hilfe erarbeitet.

München, den 18.02.2019

_____

Randy Wanner

Dissertation eingereicht am: 19.02.2019

1. Gutachter: Prof. Dr. Gerhard Winter
2. Gutachter: Prof. Dr. Wolfgang Frieß

Mündliche Prüfung am: 18.03.2019

Acknowledgements

The present thesis was prepared at the Department of Pharmacy, Pharmaceutical Technology and Biopharmaceutics at the Ludwig-Maximilians-Universität München under the supervision of Prof. Dr. Gerhard Winter. The method developments in the field of high-throughput protein stability screenings based on MicroScale Thermophoresis (MST) were performed in close collaboration with NanoTemper Technologies GmbH, Munich.

First and foremost, I want to express my deepest gratefulness to my doctoral advisor and mentor Prof. Dr. Gerhard Winter for the excellent guidance and continuous support throughout my time at the university and during the preparation of this thesis. I profited a lot from his outstanding expertise in the field of protein formulation development and the great confidence that was shown in me. Right from day one, I very much enjoyed our good cooperation and open communication that always gave me the feeling to meet at eye level. Moreover, he encouraged me to work independently and realize own ideas anytime, but was there to support whenever needed.

Moreover, I am indebted to my co-supervisor Dr. Ahmed Besheer for the possibility to work on this fascinating research topic. Although, in the end, our time together at the chair was limited, he is greatly acknowledged for initiating and shaping this project with many innovative ideas that sustainably stimulated our scientific investigations.

Prof. Wolfgang Frieß is kindly acknowledged for serving as the co-referee of this thesis. Furthermore, I want to thank him for always spreading a very warm atmosphere and the great fun we had during seminars, conferences and social activities.

The chair of pharmaceutical technology offered an outstanding framework for this project, combining a very homogeneous group of scientists with the possibility to access a broad range of state-of-the-art analytical equipment. I want to thank the whole groups of Prof. Winter and Prof. Frieß for the good time during everyday life at university, but also on hikes, ski trips, and scientific conferences. Especially Alice Hirschmann is mentioned for being the best office mate I could wish for, often being open for a little fun and distraction, while steadily challenging me with questions about chansonniers, conquerors or composers.

I very much appreciate the help of my internship students Daniel Kullmann (bachelor's thesis), Tanja Ebbing (bachelor's thesis), Antonia Lang (bachelor's thesis), and Andreas Stelzl (master practical course A). You did a great job and it was always a lot of fun working with you.

I owe my deepest gratitude to Dr. Stefan Duhr, Dr. Philipp Baaske and Dr. Dennis Breitsprecher, our cooperation partners at NanoTemper Technologies, for the constructive scientific and technical input and the numerous fruitful discussions throughout the project. The unique possibility to become part of your interdisciplinary and highly skilled team, working together at the cutting edge of analytical development inspired me professionally and personally – an experience I do not want to miss.

Dr. Neil Ferguson and Dr. Crispin Alexander from the University College Dublin are acknowledged for the great collaboration and for sharing their scientific expertise in the field of isothermal chemical denaturation.

I would like to thank the Bavarian Research Foundation for the generous funding of our project (AZ-992-11). Roche Diagnostics GmbH, Sanofi S.A., and Wacker Biotech GmbH are acknowledged for providing the protein materials used in this thesis.

Finally, I want to address heartfelt thanks to my family for always encouraging me in my aims and being there whenever I needed them. Christina, I am eternally grateful for your continuous support and unconditional love. To have you by my side and to start our own little family makes me endlessly proud. Thank you!

Table of Contents

Chapter I
General Introduction

I.1. Instabilities of Protein Pharmaceuticals

Stability during the entire lifecycle of a protein pharmaceutical is a prerequisite for the tolerability, efficacy, and safety of the medical treatment, as physical as well as chemical alterations may lead to decreased drug activity, higher toxicity and moreover increase the risk of unwanted immunological reactions in the patient.[1-5]

This is highly relevant for biopharmaceutical development, as all stages from production (fermentation/expression, unfolding/refolding, purification, and formulation), over processing and fill-and-finish (material transfer, filtration/sterilization, filling, and possibly spray- or freeze-drying), to shipment, storage and administration to the patient have the potential to expose biopharmaceuticals to a multitude of external stress factors that jeopardize the stability and activity of the drug substance. These stress factors include, among others, changes in the solution pH and ionic strength, temperature variation including elevated temperatures and freeze-thaw cycles, as well as exposure to light, mechanical and interfacial stress (stirring, pumping, shaking, or pressurization).[6-9]

The numerous potential instabilities of a protein pharmaceutical can be separated in two major groups, namely chemical modifications (I.1.1) and physical changes (I.1.2). As a general classification, chemical instabilities comprise a versatile number of reactions in which the chemical composition of the primary structure is altered via formation or breakage of covalent bonds, whereas physical instabilities include changes in the proteins secondary or higher order (tertiary, quaternary) structure.[10] Besides this idealized grouping, it is to mention that all instabilities of a protein are highly interrelated and therefore can be formed of or lead to degradation pathways of other instability classifications. In the following, these groups will be addressed in more detail, while exemplary degradation pathways and connections thereof will be given and analytical approaches are presented.

I.1.1. Chemical Instabilities

Chemical instabilities occur by alteration and degradation of amino acid side chains and the peptide backbone under intermediate and long-term storage of biopharmaceuticals. The number of possible chemical reactions and degradation pathways is large and often highly depending on the amino acid sequence of the molecule of interest. Possible reactions include deamidation (mainly asparagine) and isomerization (aspartic acid), oxidation (sulfur atoms e.g. methionine and aromatic rings e.g. tryptophan), formation, breakage or exchange of disulfide bonds (cysteine/cystine), glycation (reducing sugars), deglycosilation and peptide backbone cleavage. The respective control strategy for these instabilities depends strongly on the underlying degradation mechanism and often includes pH and excipient adjustments in liquid protein formulations. However, also storage and handling conditions (temperature, light exposure) as well as the nature and quality of the chosen primary packaging material and the presence of trace amounts of impurities can have detrimental effects on chemical stability.[10-20]

Depending on the nature of the chemical instability present, the degraded protein exposes a changed hydrophobicity, polarity, mass, and/or charge. Moreover, aggregation and/or fragmentation can potentially be induced. Thus, separation, identification and quantification of chemical changes are preferably performed by the use of liquid chromatography (reversed phase- (RP-), or ion exchange- (IEX-) HPLC), electrophoresis and isoelectric focusing (capillary- (cGE or cIEF) or gel- (SDS- or IEF-PAGE) format) or mass spectrometry (MS).[21-26]

I.1.2. Physical Instabilities

The group of physical instabilities can be subdivided in protein conformational changes, colloidal interactions, surface and interfacial instabilities, as well as aggregate and precipitate/particle formation.[10,13,27] In the present work, the main focus lies on the determination and comparative evaluation of protein unfolding parameters used for the high-throughput screening of protein formulations. Furthermore, the interplay of conformational and colloidal stabilities will be discussed in the context of non-native protein aggregation and precipitation as degradation endpoint. Surface and interfacial stability, not being an integral part of our investigations, will consequently not be further introduced.

I.1.2.1. Conformational Instability

Conformational instabilities summarize alterations in the proteins secondary or higher order (tertiary/quaternary) structure, which are commonly described as protein unfolding or denaturation and have wide-ranging impacts on protein stability. Moreover, structural integrity of the labile native folded state is essential for biological activity and therefore efficacy of a biopharmaceutical drug.[7,10]

Conformational transitions between the completely folded/native conformation of a protein and completely unfolded/denatured states are termed folding and unfolding. The native folded state typically buries hydrophobic amino acid residues in the core of the protein, while hydrophilic moieties are exposed to the (aqueous) solvent. This is called the *hydrophobic effect*. Intramolecular interactions as van der Waals' forces, hydrophobic and ionic interactions, as well as hydrogen bonds stabilize the native conformation, whereas the unfolded state is strongly entropy driven. These opposing forces result in a small net thermodynamic stabilization of the folded state that corresponds to a minimum free energy. Thus, even small perturbation of the conformational stability, by e.g. temperature excursions, pH changes or salt addition, may mitigate the abovementioned intramolecular interactions, alter the three-dimensional structure and lead to partial or complete unfolding of the protein. In further consequence, protein unfolding creates aggregation-prone intermediates, which expose hydrophobic amino acid side chains (i.e. *hydrophobic patches* or *aggregation hot spots*) to the solvent and hence trigger protein aggregation via random intermolecular self-association. A higher conformational stability or Gibbs free energy of unfolding will in turn favor the native state in the unfolding equilibrium and reduce the number of unfolded, aggregation-prone species.[7,11,13,28-30] For several monoclonal antibodies (mAbs), mechanistic evidence is given that the aggregation-prone regions (APRs) that tend to interact via hydrophobic interaction upon unfolding are located in the antigen-binding fragments (Fab). Hence, the aggregation propensity of mAbs is highly dependent on the conformational stability of the Fab domains, rather than the least stable domain.[31-34]

The entirety of possible protein conformations (i.e. the conformational space) can be visualized and expressed by the use of the *folding funnel* model, which displays conformation ensembles in the overall folding energy landscape that reaches from the free energy minimum of the native conformation, over a multitude of folding/unfolding intermediate states (e.g. transition state ensembles), to the energy-rich unfolded states. Non-native aggregates, originating from intermolecular hydrophobic interactions form additional ensembles in the energy landscape, which can be appended to the folding funnel. In analogy to the native state, they feature additional free energy minima, which render non-native aggregation in biopharmaceuticals mostly irreversible.[35-38]

In basic research and industry practice, higher-order structural changes can be examined by using a variety of spectroscopic techniques as UV absorbance, intrinsic and extrinsic fluorescence emission spectroscopy (FES), near- and far-UV circular dichroism (CD), as well as Fourier-transform infrared (FTIR) and Raman spectroscopy. Moreover, differential scanning calorimetry (DSC) is frequently used to detect conformational changes upon thermal unfolding and furthermore directly provides thermodynamic readout parameters. In addition to these established analytical standard approaches, more detailed structural information can be obtained by using highly complex assays as small-angle X-ray scattering (SAXS) or hydrogen-deuterium exchange (HDX) with nuclear magnetic resonance (NMR) or mass spectrometry (MS) readout.[6,39-44]

I.1.2.2. Colloidal Instability

Colloidal instability describes an unwanted solution condition that is caused by electrostatic self-interaction of proteins. The balance between repulsive, neutral and attractive forces is strongly influenced by the formulation pH, which in turn dictates the net charge of the protein in solution. At the pH of the proteins isoelectric point (pI), the net charge approaches zero and the electrostatic repulsion between molecules is minimal. At pH values far away from the pI, proteins are highly and uniformly charged, which leads to intra- and intermolecular electrostatic repulsion. This increases the colloidal stability, but may induce aggregation via the unfolding mechanism described in section I.1.2.1. In consequence, the ionic strength and the addition of uncharged co-solutes generate a major impact on the manifestation of molecular interactions due to possible shielding of the interacting moieties. Moreover, non-uniform charge distribution can create dipolar interactions between molecules, which dramatically destabilize the system.[7,11,45-48]

The self-interaction propensity of a protein in solution can be estimated via its zeta potential, while interaction parameters as the osmotic second virial coefficient (B_{22}), or the diffusion interaction parameter k_D are used to characterize repulsive or attractive protein-protein interactions. Colloidal stability is favored at high (positive or negative) zeta potentials and positive (high) B_{22}/k_D values, both representing pronounced repulsive forces which inhibit the approximation and assembly of molecules.[7,11,45]

While the zeta potential of a protein in solution is usually determined by evaluating the electrophoretic mobility of the protein in combination with laser doppler velocimetry, several approaches based on light scattering (SLS and DLS), analytical ultracentrifugation (AUC) and self-interaction chromatography (SIC) exist to determine B_{22} and/or k_D.[48-55]

I.1.2.3. Aggregation

Protein aggregation and particle formation is the ubiquitous route of protein instability that can be described in general terms as the formation of multimeric species by self-association. Aggregation can occur for the native protein or result from a multitude of chemical and physical instabilities. Thus, protein aggregation may take many different shapes and numerous different classifications of aggregates exist in the literature. These mostly rely on the preceding degradation mechanism, the reversibility of aggregation, the conformation or solubility of aggregates, or simply the particle size and morphology.[7,8,56-61]

Focusing on the mechanisms of aggregation induced by physical instabilities, both colloidal and conformational changes are described to potentially foster aggregation. Whereas for colloidal interactions, changes in the solution properties (pH and salt concentration) and the interrelated charge alteration of the protein may promote association between structurally native molecules, conformational changes alter the native structure and hence form folding-intermediates that are presumably prone to aggregation. Consequently, the resulting aggregation pathways are termed native aggregation and non-native aggregation, depending on the structural integrity of the protein involved. While native aggregation is potentially reversible, non-native aggregation leads in many cases to irreversible aggregate formation.[45,50,57]

Following the Lumry-Eyring two-state irreversible denaturation model[62-66] that describes an aggregation mechanism from native monomers, which first undergo a reversible conformational change to aggregation-prone unfolded intermediates and in a second step irreversibly assemble to the aggregated state, the interplay and control

of conformational and colloidal stability are of great importance in order to effectively prevent the formation and growth of aggregation.[29,45,67,68]

In an orthogonal classification approach, the size-differentiation spans a wide range from soluble aggregates/oligomers (< 100 nm, i.e. dimer, trimer etc.), over sub-micron (100 – 1000 nm) and subvisible particles (1 – 100 µm) to visible particles (> 100 µm). For all classes, the nomenclature is highly irregular and differs from one field of research to another.[58,59] Depending on the size and nature of the aggregates/particles to be investigated and the specific interrogation, as for example separation, sizing, quantification, visualization, or discrimination based on the particulate nature, different analytical approaches are pursued. In practice, the aggregate and particle analytics applied are either used for direct sizing/counting or for indirect aggregation detection via characterization of the higher order structure (see section I.1.2.1). Beyond visual inspection according to the compendial standards for visible particles, methods based on light absorption or blockage (i.e. light obscuration (LO), turbidimetry/nephelopmetry, or optical density (OD)), microscopy (e.g. membrane microscopy or backgrounded membrane imaging (BMI)), flow imaging (e.g. micro-flow imaging (MFI)) or the coulter principle (coulter counter (CC)) are used for quantification and/or size determination of visible to sub-visible particles. In the sub-micron particle-range and for soluble aggregates, separation methods (e.g. size exclusion chromatography (SEC), analytical ultracentrifugation (AUC), field flow fractionation (FFF, e.g. AF4), SDS- or native PAGE, isoelectric focusing (IEF)) and light scattering (static and dynamic light scattering (SLS, DLS), nanoparticle tracking analysis (NTA)) predominate besides other more sophisticated approaches like electron- or atomic-force microscopy (AFM) and mass spectrometry (MS).[8,61,69-72]

I.2. Stabilization of Biopharmaceuticals in Solution

As outlined in section I.1, the stability, efficacy and safety of biopharmaceuticals in solution is predetermined by the intrinsic properties of the protein itself, namely the primary amino acid sequence, the higher-order structure conformation, and post-translational modifications.

During protein formulation development, extrinsic environmental factors are modified and optimized in order to enhance the physical and chemical stability of the protein in solution. These factors consist of basic formulation conditions like the protein concentration, pH value and ionic strength, as well as a long list of possible stabilizing excipients that includes besides others a variety of buffer salts, sugars, polyols, amino acids, polymers, and surfactants. The influences on the stability of protein pharmaceuticals are as versatile as the mechanisms of action and will be outlined in the following.[11,13,56,73]

The importance of the pH value for the stability of proteins is evident, as chemical and physical (conformational, colloidal and interfacial) stabilities are often directly dependent on the chosen formulation pH. The usually applicable operating range covers pH values between 3 and 10, while the majority of products is formulated in a narrower range between 5 and 7.[10,11,13,74,75] In most protein formulations, the pH is stabilized via buffering agents, while for high concentration protein formulations the buffering capacity of the protein itself can be utilized.[103,104]

However, the influence of ionic strength is less unambiguous and increasing the salt concentration can have stabilizing, destabilizing or neutral effects, mainly dependent on the prevalent colloidal stability properties, the composition of the protein, the pH, as well as the type and concentration of salt. This is due to electrostatic screening of intra- and intermolecular interactions by increased salt content and potential direct interactions with the protein. Under attractive intermolecular conditions, moderate salt addition stabilizes the protein in solution, while under repulsive conditions, molecular attraction can be provoked. An inverse effect can be derived for the de-/stabilization of intramolecular interactions.[11,13,14,50,76,77]

For formulation components and excipients there are many stabilization mechanisms assumed, which describe the interaction of excipients and proteins in solution, but only few are well established and generally accepted. A group of mechanisms termed *preferential interactions* rank among the best investigated and are described to enhance the conformational stability. Thereby, stabilization can on the one hand side be achieved by *preferential binding* of the excipient to the native state of the protein.

According to the Wyman linkage function[78], this binding leads to net-stabilization and a shift of the unfolding equilibrium towards the native state. On the other hand side, excipients can preferentially act as excluded solutes and not bind to proteins. This *preferential exclusion/hydration* mechanism was extensively investigated by Timasheff and coworkers[79-84]. Exclusion of the excipient from the vicinity of the protein increases the free energy of both, the native and the denatured state. Thereby, the native compact state is favored as the free-energy increase is larger for the solvent accessible unfolded state and therefore the free energy difference, i.e. free energy of unfolding, is enhanced. While preferential binding is the predominant stabilization mechanism for buffer salts and is also described for surfactants, polymers and cyclodextrins, non-specific preferential exclusion/hydration is known for many sugars, polyols and polymers.[9,10,13,74,85] Though, it is to mention that both mechanisms can also lead to unwanted stability effects. In some cases preferential binding favors the denatured state over the native state, which leads to conformational destabilization. Moreover, the thermodynamically unfavorable preferential exclusion not only enhances the free energy of unfolding, but at the same time decreases the free energy of association, which jeopardizes the colloidal stability an may promote protein self-assembly and aggregation.[10,13,85,86]

Surfactants are traditionally used to prevent proteins from interaction with hydrophobic interfaces (air-water, ice-water, container-water, etc.), which can lead to subsequent unfolding and aggregation. Thus, they are very efficient in stabilizing proteins from various stresses during manufacturing, shipment and handling. The primary mode of action is presumably direct competition with the protein for the interfacial assembly and adsorption, while direct binding to hydrophobic patches of the proteins and associated conformational and colloidal stabilization was reported as well.[85,87-92] The downside of non-ionic surfactant is their inherent instability against degradation by oxidation and hydrolysis, which in turn can induce protein aggregation under long-term storage.[93-96] As an alternative, β-cyclodextrin derivatives like hydroxypropyl-β-cyclodextrin (HP-ß-CD) showed comparable stabilization effects by weak direct interaction to the protein rather than by competitive interface displacement.[97,98]

In formulation practice, a detailed knowledge about the present prevailing degradation mechanism is a basic prerequisite for efficient screening designs. Moreover, the effect of excipient addition and the detailed underlying mode of action are often difficult to predict and the selection of excipients used for enhancing the protein stability is therefore mostly based on previous experience and tested in a try and error approach.

In a state-of-the-art formulation development approach, the colloidal and chemical stability is usually optimized first by screening a variety of different pH values, buffering agents and salt concentrations. In the next step, conformational and interfacial stability are improved by the addition of sugars, sugar alcohols and surfactants. Thereby, unfolding and aggregation during processing and storage can be reduced.[11,13,56]

Beyond that, rational additive selections by computational modelling or protein-excipient binding experiments are still rare[99-101] but should be pursued more often in the future, in order to increase the knowledge and understanding of the underlying stabilization principles and thus effectively prevent degradation.[102] Additional emergent stabilization approaches target the intrinsic protein stability already during candidate selection and protein engineering by introducing mutations or *in vitro* modifications in order to reduce the aggregation propensity or immunogenicity of the molecules from scratch.[103-110]

I.3. Analytical Approaches used for the Assessment of Protein Stabilities and Early Protein Formulation Screenings

In all stages of biopharmaceutical drug product development, many approaches are pursued in order to enhance the R&D productivity by early risk mitigation and developability assessment, which goes hand in hand with an overall reduction of the time and cost effort.[111]

During formulation development, the main attention lies on the search for fast approaches that surrogate the conventional candidate selection process by long-term stability testing under real-time conditions that match the intended storage period and temperature (usually up to 24 month at 2-8 °C). By establishing that, the number of possible formulation candidates can be narrowed down earlier and a lead formulation can be selected faster. The most established and ICH recommended alternatives are accelerated stability testing[112,113] at elevated temperature and relative humidity (r.h.) conditions (e.g. 25 °C/60% r.h. or 40 °C/75% r.h.), as well as short-term stress testing[6,114-116] (i.e. forced degradation) by temperature excursion, freeze-thawing, agitation, oxidation, light etc.. Both approaches can support formulation development by revealing stabilizing conditions, as well as degradation products and associated pathways in comparably short time of several months (e.g. one to six months) for accelerated stability testing down to several days (e.g. one day to one week) for short-term stress testing.

In order to further accelerate early formulation screenings and lead formulation selection, current development approaches focus on the predictive and comparative high-throughput determination of physical protein stabilities and aggregation pathways. By this means, a combination of colloidal and conformational stability parameters are determined for a large number of protein formulations. Subsequently, the results are used to derive stability trends and determine excipient combinations, which exhibit maximum overall stability and thus are progressed as lead formulation compositions. The variety of analytical techniques and assays used for such stability investigation are compiled in recent reviews[44,67,117-119]. In summary, colloidal stability is characterized via assessment of interaction parameters (k_D or B_{22}) as outlined in section I.1.2.2. Conformational stability is mainly determined by thermal ramp denaturation and calculation of onset- or midpoint-temperatures of unfolding ($T_{m,onset}$ or T_m) as stability indicative surrogate parameters. Traditionally, unfolding transitions are tracked by highly sensitive differential scanning calorimetry (µDSC)[40,120-122], which moreover allows for direct evaluation of thermodynamic parameters as the enthalpy (ΔH) and the

Gibbs free energy of unfolding (ΔG). A long-time established alternative to µDSC is based on circular dichroism (CD)[122-124] and exploits protein unfolding induced ellipticity changes over temperature. Differential scanning fluorimetry (DSF)[125-127], a recent thermal denaturation and thermal shift assay provides a much higher throughput and lower sample consumption. The technique is based on fluorescence enhancement of polarity or viscosity sensitive extrinsic fluorescence probes that are also applied to isothermal aggregate detection[128-131]. However, as it requires the addition of non-inherent formulation additives, it exhibits limitations in terms of excipient compatibility or protein concentration, depending on the chosen dye.[132,133] These restrictions are overcome with the recent development of high-throughput intrinsic fluorescence emission spectroscopy (FES) instrumentation that alongside thermal protein unfolding moreover enables the analysis of aggregation events via the associated/concomitant light scattering increase.[134-136] Likewise, high-throughput aggregation and precipitation screening can also be obtained by optical density (OD) or turbidity analysis. A long-time neglected alternative to thermal unfolding assays exists in chemical unfolding (i.e. isothermal chemical denaturation (ICD))[137-139], which uses titration series of chaotropic denaturants like Urea or GuHCl to calculate the unfolding midpoint concentration (C_m) or determine ΔG as stability indicators. ICD is frequently used in fundamental research but due to the low throughput and the unknown effect of formulation manipulation by the denaturant addition only sparsely applied to extensive formulation screenings. However, the throughput was much enhanced by the introduction of high-throughput instrumentation for analysis (FES or CD) and the developments in automated liquid handling, facilitating the labor intensive dilution series preparation. Moreover, ICD, typically leading to fully reversible unfolding, allows for more straightforward and precise thermodynamic evaluation than aggregation-prone thermal unfolding that may be driven by aggregation kinetics and lead to deviations from the models fitted to the unfolding curves. The validity and sensitivity of stability assessments in the presence of molar concentrations of chaotropic agents still needs to be thoroughly evaluated. An alternative approach to investigate physical protein stabilities by making use of chaotropic denaturants was recently proposed by Svilenov et al.[140]. There, the size increase of monoclonal antibodies after incubation and subsequent dilution from a denaturing agent was investigated and found to change with different denaturant concentrations and formulation compositions. The straightforward approach and good correlation to standard assays suggests further evaluation of this method in larger formulation screening sets.

A few mechanistic case studies are reported in the literature[45,50,68,141-144], which further investigate the impact of conformational changes and colloidal interactions on the overall aggregation propensity via high throughput screenings and stress testing. The outcome corroborates the importance and mutual dependency of both, repulsive electrostatic interactions and unfolding stability to support aggregation resistance and gather further insight in the underlying degradation mechanisms. Depending on the solution conditions, each degradation route can represent the rate limiting step for aggregation, which additionally underlines the high importance and far-reaching effect of the chosen formulation parameters.

However, the overarching question for all accelerated stability approaches lies in the correlation and predictive power of the analytical results compared to the real-time quiescent storage conditions. The prediction of real-time aggregation rates or aggregation propensities is very challenging, as aggregation typically does not follow Arrhenius-like behavior. [6,145-147] Some formulation screening case studies use colloidal and/or conformational stability investigations to rank biopharmaceutical formulations according to their physical stability and compare the results to stability studies. Thereby, the majority of correlations are drawn to accelerated stability conditions, while valuable systematic comparisons to real-time stability studies as presented by Youssef et al.[148] and Maddux et al.[149] are rare. The results are diverse, ranging from a majority of partly predictive studies[135,150-152] to some encouraging data sets showing a high overlap[148,149,153]. However, as learned from these studies, the correlation of accelerated stress conditions (e.g. 40 °C) to refrigerated conditions is often comparably weak or even worse. The reason for the excess of modest results might lie in the fact that protein degradation is a multifactorial process that needs to be examined by multiple approaches in order to gain a conclusive data set. Moreover, chemical changes as potential alternative degradation routes have to be kept in mind, which typically require longer timescales to establish and thus are only being covered subordinate by predictive stability approaches. In summary, the predictive power of high throughput screenings, as well as accelerated and stress studies needs so far to be assessed case by case and future development in this field is dependent on new analytical approaches overcoming current limitations and providing valuable insights in protein degradation pathways in order to aid the selection of stable formulations earlier.[151]

This thesis supports the quest for new orthogonal analytical approaches applicable for high-throughput stability assessments during early formulation screening. MicroScale Thermophoresis (MST) is used as a novel readout for thermal protein unfolding and aggregation assessments, as well as for rational excipient selection by protein-excipient binding analyses. Furthermore, a technique termed Thermo-Optical Protein Characterization (TOPC) is developed as a screening tool investigating non-native aggregation propensities within minutes by forced thermal degradation. All results are compared to state-of-the-art analytical approaches and assays in the field.

I.4. References

1. Filipe V, Jiskoot W, Basmeleh AH, Halim A, Schellekens H, Brinks V. 2012. Immunogenicity of different stressed IgG monoclonal antibody formulations in immune tolerant transgenic mice. mAbs 4(6):740-752.

2. Schellekens H. 2005. Factors influencing the immunogenicity of therapeutic proteins. Nephrology Dialysis Transplantation 20(suppl 6):vi3-vi9.

3. Schellekens H. 2003. Immunogenicity of therapeutic proteins. Nephrology Dialysis Transplantation 18(7):1257-1259.

4. Wang W, Singh SK, Li N, Toler MR, King KR, Nema S. 2012. Immunogenicity of protein aggregates - concerns and realities. International Journal of Pharmaceutics 431(1):1-11.

5. Ratanji KD, Derrick JP, Dearman RJ, Kimber I. 2014. Immunogenicity of therapeutic proteins: Influence of aggregation. Journal of Immunotoxicology 11(2):99-109.

6. Hawe A, Wiggenhorn M, van de Weert M, Garbe JHO, Mahler H-C, Jiskoot W. 2012. Forced degradation of therapeutic proteins. Journal of Pharmaceutical Sciences 101(3):895-913.

7. Chi E, Krishnan S, Randolph T, Carpenter J. 2003. Physical stability of proteins in aqueous solution: Mechanism and driving forces in nonnative protein aggregation. Pharmaceutical Research 20(9):1325-1336.

8. Mahler H-C, Friess W, Grauschopf U, Kiese S. 2009. Protein aggregation: Pathways, induction factors and analysis. Journal of Pharmaceutical Sciences 98(9):2909-2934.

9. Wang W, Nema S, Teagarden D. 2010. Protein aggregation—Pathways and influencing factors. International Journal of Pharmaceutics 390(2):89-99.

10. Manning M, Chou D, Murphy B, Payne R, Katayama D. 2010. Stability of protein pharmaceuticals: An update. Pharmaceutical Research 27(4):544-575.

11. Uchiyama S. 2014. Liquid formulation for antibody drugs. Biochimica et Biophysica Acta (BBA) - Proteins and Proteomics 1844(11):2041-2052.

12. Wang W, Singh S, Zeng DL, King K, Nema S. 2007. Antibody structure, instability, and formulation. Journal of Pharmaceutical Sciences 96(1):1-26.

13. Chi EY. 2016. Excipients used in biotechnology products. In: Koo OMY, Pharmaceutical Excipients: Properties, Functionality, and Applications in Research and Industry. John Wiley & Sons, Inc. p 145-198.

14. Wang W. 1999. Instability, stabilization, and formulation of liquid protein pharmaceuticals. International Journal of Pharmaceutics 185(2):129-188.

15. Torosantucci R, Schöneich C, Jiskoot W. 2014. Oxidation of therapeutic proteins and peptides: Structural and biological consequences. Pharmaceutical Research 31(3):541-553.

16. Kerwin BA, Remmele RL. 2007. Protect from light: Photodegradation and protein biologics. Journal of Pharmaceutical Sciences 96(6):1468-1479.

17. Cleland JL, Powell MF, Shire SJ. 1993. The development of stable protein formulations: A close look at protein aggregation, deamidation, and oxidation. Critical Reviews in Therapeutic Drug Carrier Systems 10(4):307-377.

18. Li S, Schöneich C, Borchardt RT. 1995. Chemical instability of protein pharmaceuticals: Mechanisms of oxidation and strategies for stabilization. Biotechnology and Bioengineering 48(5):490-500.

19. Pace AL, Wong RL, Zhang YT, Kao Y-H, Wang YJ. 2013. Asparagine deamidation dependence on buffer type, pH, and temperature. Journal of Pharmaceutical Sciences 102(6):1712-1723.

20. Wakankar AA, Borchardt RT. 2006. Formulation considerations for proteins susceptible to asparagine deamidation and aspartate isomerization. Journal of Pharmaceutical Sciences 95(11):2321-2336.

21. Reubsaet JLE, Beijnen JH, Bult A, van Maanen RJ, Marchal JAD, Underberg WJM. 1998. Analytical techniques used to study the degradation of proteins and peptides: Chemical instability. Journal of Pharmaceutical and Biomedical Analysis 17(6–7):955-978.

22. Vlasak J, Ionescu R. 2008. Heterogeneity of monoclonal antibodies revealed by charge-sensitive methods. Current Pharmaceutical Biotechnology 9(6):468-481.

23. Yang H, Zubarev RA. 2010. Mass spectrometric analysis of asparagine deamidation and aspartate isomerization in polypeptides. Electrophoresis 31(11):1764-1772.

24. Zhou S, Mozziconacci O, Kerwin BA, Schöneich C. 2013. Fluorogenic tagging methodology applied to characterize oxidized tyrosine and phenylalanine in an immunoglobulin monoclonal antibody. Pharmaceutical Research 30:1311-1327.

25. Diepold K, Bomans K, Wiedmann M, Zimmermann B, Petzold A, Schlothauer T, Mueller R, Moritz B, Stracke JO, Mølhøj M. 2012. Simultaneous assessment of Asp isomerization and Asn deamidation in recombinant antibodies by LC-MS following incubation at elevated temperatures. PLoS ONE 7(1):e30295.

26. Folzer E, Diepold K, Bomans K, Finkler C, Schmidt R, Bulau P, Huwyler J, Mahler H-C, Koulov AV. 2015. Selective oxidation of methionine and tryptophan residues in a therapeutic IgG1 molecule. Journal of Pharmaceutical Sciences 104(9):2824-2831.

27. Reubsaet JLE, Beijnen JH, Bult A, van Maanen RJ, Marchal JAD, Underberg WJM. 1998. Analytical techniques used to study the degradation of proteins and peptides: Physical instability. Journal of Pharmaceutical and Biomedical Analysis 17(6):979-984.

28. Pace CN, Shirley BA, McNutt M, Gajiwala K. 1996. Forces contributing to the conformational stability of proteins. The FASEB Journal 10(1):75-83.

29. Bajaj H, Sharma VK, Badkar A, Zeng D, Nema S, Kalonia DS. 2006. Protein structural conformation and not second virial coefficient relates to long-term irreversible aggregation of a monoclonal antibody and ovalbumin in solution. Pharmaceutical Research 23(6):1382-1394.

30. Wu H, Kroe-Barrett R, Singh S, Robinson AS, Roberts CJ. 2014. Competing aggregation pathways for monoclonal antibodies. FEBS Letters 588(6):936-941.

31. Garber E, Demarest SJ. 2007. A broad range of Fab stabilities within a host of therapeutic IgGs. Biochemical and Biophysical Research Communications 355(3):751-757.

32. Sahin E, Grillo AO, Perkins MD, Roberts CJ. 2010. Comparative effects of pH and ionic strength on protein–protein interactions, unfolding, and aggregation for IgG1 antibodies. Journal of Pharmaceutical Sciences 99(12):4830-4848.

33. Brummitt RK, Nesta DP, Chang L, Chase SF, Laue TM, Roberts CJ. 2011. Nonnative aggregation of an IgG1 antibody in acidic conditions: Part 1. Unfolding, colloidal interactions,

and formation of high-molecular-weight aggregates. Journal of Pharmaceutical Sciences 100(6):2087-2103.

34. Sahin E, Weiss WF, Kroetsch AM, King KR, Kessler RK, Das TK, Roberts CJ. 2012. Aggregation and pH–temperature phase behavior for aggregates of an IgG2 antibody. Journal of Pharmaceutical Sciences 101(5):1678-1687.

35. Dill KA, Chan HS. 1997. From Levinthal to pathways to funnels. Nature Structural & Molecular Biology 4:10-19.

36. Onuchic JN, Wolynes PG. 2004. Theory of protein folding. Current Opinion in Structural Biology 14(1):70-75.

37. Clark PL. 2004. Protein folding in the cell: Reshaping the folding funnel. Trends in Biochemical Sciences 29(10):527-534.

38. Hartl FU, Hayer-Hartl M. 2009. Converging concepts of protein folding in vitro and in vivo. Nature Structural & Molecular Biology 16:574-581.

39. Pace CN, Scholtz JM. 1997. Measuring the conformational stability of a protein. In: Creighton TE, Protein structure: A practical approach. Oxford University Press. p 299-321.

40. Johnson CM. 2013. Differential scanning calorimetry as a tool for protein folding and stability. Archives of Biochemistry and Biophysics 531(1–2):100-109.

41. Garidel P, Hegyi M, Bassarab S, Weichel M. 2008. A rapid, sensitive and economical assessment of monoclonal antibody conformational stability by intrinsic tryptophan fluorescence spectroscopy. Biotechnology Journal 3(9-10):1201-1211.

42. Sancho J. 2013. The stability of 2-state, 3-state and more-state proteins from simple spectroscopic techniques... plus the structure of the equilibrium intermediates at the same time. Archives of Biochemistry and Biophysics 531(1–2):4-13.

43. Tsytlonok M, Itzhaki LS. 2013. The how's and why's of protein folding intermediates. Archives of Biochemistry and Biophysics 531(1–2):14-23.

44. Temel DB, Landsman P, Brader ML. 2016. Orthogonal methods for characterizing the unfolding of therapeutic monoclonal antibodies: Differential scanning calorimetry, isothermal chemical denaturation, and intrinsic fluorescence with concomitant static light scattering. Methods in Enzymology 567:359-389.

45. Chi EY, Krishnan S, Kendrick BS, Chang BS, Carpenter JF, Randolph TW. 2003. Roles of conformational stability and colloidal stability in the aggregation of recombinant human granulocyte colony-stimulating factor. Protein Science 12(5):903-913.

46. Garidel P, Blume A, Wagner M. 2015. Prediction of colloidal stability of high concentration protein formulations. Pharmaceutical Development and Technology 20(3):367-374.

47. Jachimska B, Wasilewska M, Adamczyk Z. 2008. Characterization of globular protein solutions by dynamic light scattering, electrophoretic mobility, and viscosity measurements. Langmuir 24(13):6866-6872.

48. Lehermayr C, Mahler H-C, Mäder K, Fischer S. 2011. Assessment of net charge and protein-protein interactions of different monoclonal antibodies. Journal of Pharmaceutical Sciences 100(7):2551-2562.

49. Saluja A, Fesinmeyer RM, Hogan S, Brems DN, Gokarn YR. 2010. Diffusion and sedimentation interaction parameters for measuring the second virial coefficient and their utility as predictors of protein aggregation. Biophysical Journal 99(8):2657-2665.

50. Saito S, Hasegawa J, Kobayashi N, Tomitsuka T, Uchiyama S, Fukui K. 2013. Effects of ionic strength and sugars on the aggregation propensity of monoclonal antibodies: Influence of colloidal and conformational stabilities. Pharmaceutical Research 30(5):1263-1280.

51. Zhang J, Liu XY. 2003. Effect of protein-protein interactions on protein aggregation kinetics. The Journal of Chemical Physics 119(20):10972-10976.

52. Connolly BD, Petry C, Yadav S, Demeule B, Ciaccio N, Moore JM, Shire SJ, Gokarn YR. 2012. Weak interactions govern the viscosity of concentrated antibody solutions: High-throughput analysis using the diffusion interaction parameter. Biophysical Journal 103(1):69-78.

53. Le Brun V, Friess W, Bassarab S, Mühlau S, Garidel P. 2010. A critical evaluation of self-interaction chromatography as a predictive tool for the assessment of protein–protein interactions in protein formulation development: A case study of a therapeutic monoclonal antibody. European Journal of Pharmaceutics and Biopharmaceutics 75(1):16-25.

54. Quigley A, Heng J, Liddell J, Williams D. 2013. The accurate measurement of second virial coefficients using self-interaction chromatography: Experimental considerations. European Journal of Pharmaceutics and Biopharmaceutics 85(3):1103-1111.

55. Some D, Kenrick S. 2012. Characterization of protein-protein interactions via static and dynamic light scattering. In: Cai J, Wang RE, Protein interactions. InTechOpen. p 401-426.

56. Wang W. 2005. Protein aggregation and its inhibition in biopharmaceutics. International Journal of Pharmaceutics 289(1–2):1-30.

57. Philo JS, Arakawa T. 2009. Mechanisms of protein aggregation. Current Pharmaceutical Biotechnology 10(4):348-351.

58. Narhi LO, Schmit J, Bechtold-Peters K, Sharma D. 2012. Classification of protein aggregates. Journal of Pharmaceutical Sciences 101(2):493-498.

59. Joubert MK, Luo Q, Nashed-Samuel Y, Wypych J, Narhi LO. 2011. Classification and characterization of therapeutic antibody aggregates. Journal of Biological Chemistry 286(28):25118-25133.

60. Sharma VK, Kalonia DS. 2010. Experimental detection and characterization of protein aggregates. In: Wang W, Roberts CJ, Aggregation of therapeutic proteins. John Wiley & Sons, Inc. p 205-256.

61. Narhi LO, Corvari V, Ripple DC, Afonina N, Cecchini I, Defelippis MR, Garidel P, Herre A, Koulov AV, Lubiniecki T. 2015. Subvisible (2–100 μm) particle analysis during biotherapeutic drug product development: Part 1, considerations and strategy. Journal of Pharmaceutical Sciences 104:1899-1908.

62. Lumry R, Eyring H. 1954. Conformation changes of proteins. The Journal of Physical Chemistry 58(2):110-120.

63. Andrews JM, Roberts CJ. 2007. A Lumry-Eyring nucleated polymerization model of protein aggregation kinetics: 1. Aggregation with pre-equilibrated unfolding. The Journal of Physical Chemistry B 111(27):7897-7913.

64. Li Y, Roberts CJ. 2009. Lumry− Eyring nucleated-polymerization model of protein aggregation kinetics. 2. Competing growth via condensation and chain polymerization. The Journal of Physical Chemistry B 113(19):7020-7032.

65. Sanchez-Ruiz JM. 1992. Theoretical analysis of Lumry-Eyring models in differential scanning calorimetry. Biophysical Journal 61(4):921-935.

66. Roberts CJ. 2003. Kinetics of irreversible protein aggregation: Analysis of extended lumry−eyring models and implications for predicting protein shelf life. The Journal of Physical Chemistry B 107(5):1194-1207.

67. Chaudhuri R, Cheng Y, Middaugh CR, Volkin DB. 2014. High-throughput biophysical analysis of protein therapeutics to examine interrelationships between aggregate formation and conformational stability. The AAPS Journal 16(1):48-64.

68. Goldberg DS, Bishop SM, Shah AU, Sathish HA. 2011. Formulation development of therapeutic monoclonal antibodies using high-throughput fluorescence and static light scattering techniques: Role of conformational and colloidal stability. Journal of Pharmaceutical Sciences 100(4):1306-1315.

69. Narhi LO, Jiang Y, Cao S, Benedek K, Shnek D. 2009. A critical review of analytical methods for subvisible and visible particles. Current Pharmaceutical Biotechnology 10(4):373-381.

70. Den Engelsman J, Garidel P, Smulders R, Koll H, Smith B, Bassarab S, Seidl A, Hainzl O, Jiskoot W. 2011. Strategies for the assessment of protein aggregates in pharmaceutical biotech product development. Pharmaceutical Research 28(4):920-933.

71. Zölls S, Tantipolphan R, Wiggenhorn M, Winter G, Jiskoot W, Friess W, Hawe A. 2012. Particles in therapeutic protein formulations, part 1: Overview of analytical methods. Journal of Pharmaceutical Sciences 101(3):914-935.

72. Telikepalli SN, Kumru OS, Kalonia C, Esfandiary R, Joshi SB, Middaugh CR, Volkin DB. 2014. Structural characterization of IgG1 mAb aggregates and particles generated under various stress conditions. Journal of Pharmaceutical Sciences 103(3):796-809.

73. Akers MJ. 2002. Excipient–drug interactions in parenteral formulations. Journal of Pharmaceutical Sciences 91(11):2283-2300.

74. Zbacnik TJ, Holcomb RE, Katayama DS, Murphy BM, Payne RW, Coccaro RC, Evans GJ, Matsuura JE, Henry CS, Manning MC. 2017. Role of buffers in protein formulations. Journal of Pharmaceutical Sciences 106(3):713-733.

75. Goswami S, Wang W, Arakawa T, Ohtake S. 2013. Developments and challenges for mAb-based therapeutics. Antibodies 2(3):452-500.

76. Bickel F, Herold EM, Signes A, Romeijn S, Jiskoot W, Kiefer H. 2016. Reversible NaCl-induced aggregation of a monoclonal antibody at low pH: Characterization of aggregates and factors affecting aggregation. European Journal of Pharmaceutics and Biopharmaceutics 107:310-320.

77. Fesinmeyer RM, Hogan S, Saluja A, Brych SR, Kras E, Narhi LO, Brems DN, Gokarn YR. 2009. Effect of ions on agitation-and temperature-induced aggregation reactions of antibodies. Pharmaceutical Research 26(4):903-913.

78. Wyman Jr. J. 1964. Linked functions and reciprocal effects in hemoglobin: A second look. In: Anfinsen Jr. CB, Anson ML, Edsall JT, Richards FM, Advances in Protein Chemistry. Elsevier Inc. p 223-286.

79. Arakawa T, Timasheff SN. 1982. Stabilization of protein structure by sugars. Biochemistry 21(25):6536-6544.

80. Timasheff SN. 1993. The control of protein stability and association by weak interactions with water: How do solvents affect these processes? Annual Review of Biophysics and Biomolecular Structure 22(1):67-97.

81. Lee JC, Timasheff SN. 1981. The stabilization of proteins by sucrose. Journal of Biological Chemistry 256(14):7193-7201.

82. Arakawa T, Timasheff S. 1985. The stabilization of proteins by osmolytes. Biophysical Journal 47(3):411-414.

83. Timasheff SN. 1998. Control of protein stability and reactions by weakly interacting cosolvents: The simplicity of the complicated. In: Di Cera E, Linkage Thermodynamics of Macromolecular Interactions. Academic Press. p 355-432.

84. Arakawa T, Kita Y, Carpenter JF. 1991. Protein-solvent interactions in pharmaceutical formulations. Pharmaceutical Research 8(3):285-291.

85. Ohtake S, Kita Y, Arakawa T. 2011. Interactions of formulation excipients with proteins in solution and in the dried state. Advanced Drug Delivery Reviews 63(13):1053-1073.

86. Abbas SA, Sharma VK, Patapoff TW, Kalonia DS. 2012. Opposite effects of polyols on antibody aggregation: Thermal versus mechanical stresses. Pharmaceutical Research 29(3):683-694.

87. Randolph TW, Jones LS. 2002. Surfactant-protein interactions. In: Carpenter JF, Manning MC, Rational Design of Stable Protein Formulations. Springer. p 159-175.

88. Khan TA, Mahler H-C, Kishore RSK. 2015. Key interactions of surfactants in therapeutic protein formulations: A review. European Journal of Pharmaceutics and Biopharmaceutics 97, Part A:60-67.

89. Lee HJ, McAuley A, Schilke KF, McGuire J. 2011. Molecular origins of surfactant-mediated stabilization of protein drugs. Advanced Drug Delivery Reviews 63(13):1160-1171.

90. Bam NB, Cleland JL, Yang J, Manning MC, Carpenter JF, Kelley RF, Randolph TW. 1998. Tween protects recombinant human growth hormone against agitation-induced damage via hydrophobic interactions. Journal of Pharmaceutical Sciences 87(12):1554-1559.

91. Garidel P, Hoffmann C, Blume A. 2009. A thermodynamic analysis of the binding interaction between polysorbate 20 and 80 with human serum albumins and immunoglobulins: A contribution to understand colloidal protein stabilisation. Biophysical Chemistry 143(1–2):70-78.

92. Hoffmann C, Blume A, Miller I, Garidel P. 2009. Insights into protein–polysorbate interactions analysed by means of isothermal titration and differential scanning calorimetry. European Biophysics Journal 38(5):557-568.

93. Kerwin BA. 2008. Polysorbates 20 and 80 used in the formulation of protein biotherapeutics: Structure and degradation pathways. Journal of Pharmaceutical Sciences 97(8):2924-2935.

94. Kishore RS, Kiese S, Fischer S, Pappenberger A, Grauschopf U, Mahler H-C. 2011. The degradation of polysorbates 20 and 80 and its potential impact on the stability of biotherapeutics. Pharmaceutical Research 28(5):1194-1210.

95. Wang W, Ignatius AA, Thakkar SV. 2014. Impact of residual impurities and contaminants on protein stability. Journal of Pharmaceutical Sciences 103(5):1315-1330.

96. Martos A, Koch W, Jiskoot W, Wuchner K, Winter G, Friess W, Hawe A. 2017. Trends on analytical characterization of polysorbates and their degradation products in biopharmaceutical formulations. Journal of Pharmaceutical Sciences 106(7):1722-1735.

97. Serno T, Härtl E, Besheer A, Miller R, Winter G. 2013. The role of polysorbate 80 and HPβCD at the air-water interface of IgG solutions. Pharmaceutical Research 30(1):117-130.

98. Härtl E, Dixit N, Besheer A, Kalonia D, Winter G. 2013. Weak antibody–cyclodextrin interactions determined by quartz crystal microbalance and dynamic/static light scattering. European Journal of Pharmaceutics and Biopharmaceutics 85(3):781-789.

99. Veurink M, Stella C, Tabatabay C, Pournaras CJ, Gurny R. 2011. Association of ranibizumab (Lucentis®) or bevacizumab (Avastin®) with dexamethasone and triamcinolone acetonide: An in vitro stability assessment. European Journal of Pharmaceutics and Biopharmaceutics 78(2):271-277.

100. Veurink M, Westermaier Y, Gurny R, Scapozza L. 2013. Breaking the aggregation of the monoclonal antibody bevacizumab (Avastin®) by dexamethasone phosphate: Insights from molecular modelling and asymmetrical flow field-flow fractionation. Pharmaceutical Research 30(4):1176-1187.

101. Westermaier Y, Veurink M, Riis-Johannessen T, Guinchard S, Gurny R, Scapozza L. 2013. Identification of aggregation breakers for bevacizumab (Avastin®) self-association through similarity searching and interaction studies. European Journal of Pharmaceutics and Biopharmaceutics 85(3):773-780.

102. Kamerzell TJ, Esfandiary R, Joshi SB, Middaugh CR, Volkin DB. 2011. Protein-excipient interactions: Mechanisms and biophysical characterization applied to protein formulation development. Advanced Drug Delivery Reviews 63(13):1118-1159.

103. Dudgeon K, Rouet R, Kokmeijer I, Schofield P, Stolp J, Langley D, Stock D, Christ D. 2012. General strategy for the generation of human antibody variable domains with increased aggregation resistance. Proceedings of the National Academy of Sciences 109(27):10879-10884.

104. Geng SB, Cheung JK, Narasimhan C, Shameem M, Tessier PM. 2014. Improving monoclonal antibody selection and engineering using measurements of colloidal protein interactions. Journal of Pharmaceutical Sciences 103(11):3356-3363.

105. Hermeling S, Crommelin DA, Schellekens H, Jiskoot W. 2004. Structure-immunogenicity relationships of therapeutic proteins. Pharmaceutical Research 21(6):897-903.

106. Rouet R, Lowe D, Christ D. 2014. Stability engineering of the human antibody repertoire. FEBS Letters 588(2):269-277.

107. Lee CC, Perchiacca JM, Tessier PM. 2013. Toward aggregation-resistant antibodies by design. Trends in Biotechnology 31(11):612-620.

108. Ueda T. 2014. Next-generation optimized biotherapeutics - A review and preclinical study. Biochimica et Biophysica Acta (BBA) - Proteins and Proteomics 1844(11):2053-2057.

109. Seeliger D, Schulz P, Litzenburger T, Spitz J, Hoerer S, Blech M, Enenkel B, Studts JM, Garidel P, Karow AR. 2015. Boosting antibody developability through rational sequence optimization. mAbs 7(3):505-515.

110. van der Kant R, Karow-Zwick AR, Van Durme J, Blech M, Gallardo R, Seeliger D, Aßfalg K, Baatsen P, Compernolle G, Gils A, Studts JM, Schulz P, Garidel P, Schymkowitz J, Rousseau F. 2017. Prediction and reduction of the aggregation of monoclonal antibodies. Journal of Molecular Biology 429(8):1244-1261.

111. Zurdo J. 2013. Developability assessment as an early de-risking tool for biopharmaceutical development. Pharmaceutical Bioprocessing 1(1):29-50.

112. ICH Guideline Q1A(R2). Available at: https://www.ich.org/fileadmin/Public_Web_Site/ICH_Products/Guidelines/Quality/Q1A_R2/Step4/Q1A_R2__Guideline.pdf. Accessed: January 5, 2019.

113. ICH Guideline Q5C. Available at: https://www.ich.org/fileadmin/Public_Web_Site/ICH_Products/Guidelines/Quality/Q5C/Step4/Q5C_Guideline.pdf. Accessed: January 5, 2019.

114. Chan CP. 2016. Forced degradation studies: Current trends and future perspectives for protein-based therapeutics. Expert Review of Proteomics 13(7):651-658.

115. Nowak C, K. Cheung J, M. Dellatore S, Katiyar A, Bhat R, Sun J, Ponniah G, Neill A, Mason B, Beck A, Liu H. 2017. Forced degradation of recombinant monoclonal antibodies: A practical guide. mAbs 9(8):1217-1230.

116. Tamizi E, Jouyban A. 2016. Forced degradation studies of biopharmaceuticals: Selection of stress conditions. European Journal of Pharmaceutics and Biopharmaceutics 98:26-46.

117. Samra HS, He F. 2012. Advancements in high throughput biophysical technologies: Applications for characterization and screening during early formulation development of monoclonal antibodies. Molecular Pharmaceutics 9(4):696-707.

118. Razinkov VI, Treuheit MJ, Becker GW. 2013. Methods of high throughput biophysical characterization in biopharmaceutical development. Current Drug Discovery Technologies 10(1):59-70.

119. Senisterra GA, Finerty Jr PJ. 2009. High throughput methods of assessing protein stability and aggregation. Molecular BioSystems 5(3):217-223.

120. Bruylants G, Wouters J, Michaux C. 2005. Differential scanning calorimetry in life science: Thermodynamics, stability, molecular recognition and application in drug design. Current Medicinal Chemistry 12(17):2011-2020.

121. Freire E. 1995. Differential Scanning Calorimetry. In: Shirley BA, Protein Stability and Folding: Theory and Practice. Humana Press. p 191-218.

122. Vermeer AW, Norde W. 2000. The thermal stability of immunoglobulin: Unfolding and aggregation of a multi-domain protein. Biophysical Journal 78(1):394-404.

123. Li CH, Nguyen X, Narhi L, Chemmalil L, Towers E, Muzammil S, Gabrielson J, Jiang Y. 2011. Applications of circular dichroism (CD) for structural analysis of proteins: qualification of near- and far-UV CD for protein higher order structural analysis. Journal of Pharmaceutical Sciences 100(11):4642-4654.

124. Benjwal S, Verma S, Röhm KH, Gursky O. 2006. Monitoring protein aggregation during thermal unfolding in circular dichroism experiments. Protein Science 15(3):635-639.

125. He F, Hogan S, Latypov RF, Narhi LO, Razinkov VI. 2010. High throughput thermostability screening of monoclonal antibody formulations. Journal of Pharmaceutical Sciences 99(4):1707-1720.

126. Ericsson UB, Hallberg BM, DeTitta GT, Dekker N, Nordlund P. 2006. Thermofluor-based high-throughput stability optimization of proteins for structural studies. Analytical Biochemistry 357(2):289-298.

127. Niesen FH, Berglund H, Vedadi M. 2007. The use of differential scanning fluorimetry to detect ligand interactions that promote protein stability. Nature Protocols 2:2212-2221.

128. Hawe A, Filipe V, Jiskoot W. 2010. Fluorescent molecular rotors as dyes to characterize polysorbate-containing IgG formulations. Pharmaceutical Research 27(2):314-326.

129. Hawe A, Sutter M, Jiskoot W. 2008. Extrinsic fluorescent dyes as tools for protein characterization. Pharmaceutical Research 25(7):1487-1499.

130. He F, Phan DH, Hogan S, Bailey R, Becker GW, Narhi LO, Razinkov VI. 2010. Detection of IgG aggregation by a high throughput method based on extrinsic fluorescence. Journal of Pharmaceutical Sciences 99(6):2598-2608.

131. Li Y, Mach H, Blue JT. 2011. High throughput formulation screening for global aggregation behaviors of three monoclonal antibodies. Journal of Pharmaceutical Sciences 100(6):2120-2135.

132. Menzen T, Friess W. 2013. High-throughput melting-temperature analysis of a monoclonal antibody by differential scanning fluorimetry in the presence of surfactants. Journal of Pharmaceutical Sciences 102(2):415-428.

133. Ablinger E, Leitgeb S, Zimmer A. 2013. Differential scanning fluorescence approach using a fluorescent molecular rotor to detect thermostability of proteins in surfactant-containing formulations. International Journal of Pharmaceutics 441(1):255-260.

134. Qi W, Zeng Y, Orgel S, Francon A, Kim JH, Randolph TW, Carpenter JF, Middaugh CR. 2014. Preformulation study of highly purified inactivated polio vaccine, serotype 3. Journal of Pharmaceutical Sciences 103(1):140-151.

135. Brader ML, Estey T, Bai S, Alston RW, Lucas KK, Lantz S, Landsman P, Maloney KM. 2015. Examination of thermal unfolding and aggregation profiles of a series of developable therapeutic monoclonal antibodies. Molecular Pharmaceutics 12(4):1005-1017.

136. Garidel P. 2012. Right angle light scattering protein thermostability screening: From research to development. Spectroscopy Europe 24(1):13-18.

137. Freire E, Schön A, Hutchins BM, Brown RK. 2013. Chemical denaturation as a tool in the formulation optimization of biologics. Drug Discovery Today 18(19–20):1007-1013.

138. Alexander CG, Wanner R, Johnson CM, Breitsprecher D, Winter G, Duhr S, Baaske P, Ferguson N. 2014. Novel microscale approaches for easy, rapid determination of protein stability in academic and commercial settings. Biochimica et Biophysica Acta (BBA) - Proteins and Proteomics 1844(12):2241-2250.

139. Svilenov H, Markoja U, Winter G. 2018. Isothermal chemical denaturation as a complementary tool to overcome limitations of thermal differential scanning fluorimetry in predicting physical stability of protein formulations. European Journal of Pharmaceutics and Biopharmaceutics 125:106-113.

140. Svilenov H, Gentiluomo L, Friess W, Roessner D, Winter G. 2018. A New Approach to Study the Physical Stability of Monoclonal Antibody Formulations—Dilution From a Denaturant. Journal of Pharmaceutical Sciences 107(12):3007-3013.

141. Kim N, Remmele RL, Liu D, Razinkov VI, Fernandez EJ, Roberts CJ. 2013. Aggregation of anti-streptavidin immunoglobulin gamma-1 involves Fab unfolding and competing growth pathways mediated by pH and salt concentration. Biophysical Chemistry 172:26-36.

142. Chou DK, Krishnamurthy R, Manning MC, Randolph TW, Carpenter JF. 2012. Physical stability of albinterferon-α2b in aqueous solution: Effects of conformational stability and colloidal stability on aggregation. Journal of Pharmaceutical Sciences 101(8):2702-2719.

143. Menzen T, Friess W. 2014. Temperature-ramped studies on the aggregation, unfolding, and interaction of a therapeutic monoclonal antibody. Journal of Pharmaceutical Sciences 103(2):445-455.

144. Wang T, Kumru OS, Yi L, Wang YJ, Zhang J, Kim JH, Joshi SB, Middaugh CR, Volkin DB. 2013. Effect of ionic strength and pH on the physical and chemical stability of a monoclonal antibody antigen-binding fragment. Journal of Pharmaceutical Sciences 102(8):2520-2537.

145. Weiss WF, Young TM, Roberts CJ. 2009. Principles, approaches, and challenges for predicting protein aggregation rates and shelf life. Journal of Pharmaceutical Sciences 98(4):1246-1277.

146. Roberts CJ, Das TK, Sahin E. 2011. Predicting solution aggregation rates for therapeutic proteins: Approaches and challenges. International Journal of Pharmaceutics 418(2):318-333.

147. Wang W, Roberts CJ. 2013. Non-Arrhenius protein aggregation. The AAPS Journal 15(3):840-851.

148. Youssef AMK, Winter G. 2013. A critical evaluation of microcalorimetry as a predictive tool for long term stability of liquid protein formulations: Granulocyte colony stimulating factor (GCSF). European Journal of Pharmaceutics and Biopharmaceutics 84(1):145-155.

149. Maddux NR, Iyer V, Cheng W, Youssef AM, Joshi SB, Volkin DB, Ralston JP, Winter G, Middaugh CR. 2014. High throughput prediction of the long-term stability of pharmaceutical macromolecules from short-term multi-instrument spectroscopic data. Journal of Pharmaceutical Sciences 103(3):828-839.

150. Goldberg DS, Lewus RA, Esfandiary R, Farkas DC, Mody N, Day KJ, Mallik P, Tracka MB, Sealey SK, Samra HS. 2017. Utility of high throughput screening techniques to predict stability of monoclonal antibody formulations during early stage development. Journal of Pharmaceutical Sciences 106(8):1971-1977.

151. Thiagarajan G, Semple A, James JK, Cheung JK, Shameem M. 2016. A comparison of biophysical characterization techniques in predicting monoclonal antibody stability. mAbs 8(6):1088-1097.

152. Shi S, Liu J, Joshi SB, Krasnoperov V, Gill P, Middaugh CR, Volkin DB. 2012. Biophysical characterization and stabilization of the recombinant albumin fusion protein sEphB4–HSA. Journal of Pharmaceutical Sciences 101(6):1969-1984.

153. Burton L, Gandhi R, Duke G, Paborji M. 2007. Use of microcalorimetry and its correlation with size exclusion chromatography for rapid screening of the physical stability of large pharmaceutical proteins in solution. Pharmaceutical Development and Technology 12(3):265-273.

Chapter II
Aim and Outline of the Thesis

The overall aim of this thesis is to develop and qualify MicroScale Thermophoresis as a versatile and reliable tool for the high-throughput analysis and stability prediction of protein pharmaceuticals. The application of MST targets three major challenges and objectives in the early stage development of liquid protein formulations: (i) unfolding stability, (ii) aggregation propensity, and (iii) protein-excipient interactions. These investigations simplify the workflow of formulation scientists by reducing the almost infinitely large number of possible formulation candidates already in early development phases. Moreover, thermophoresis potentially delivers new insights in physical stability changes and protein-excipient interactions, which would help to understand the underlying degradation and interaction mechanisms and to derive a protein-specific stabilization strategy.

At first, an introduction to the fundamentals of MST is given (Chapter III) and the measurement principles, as well as standard terms are outlined for a better understanding of the following method and assay development phase (Chapter IV). Therein, the focus is on the construction and validation of multiple MST-based prototype measurement setups and assays suited for the abovementioned tasks in formulation development. Besides high precision and throughput, label- and immobilization-free protein analysis was a prerequisite. Moreover, routine approaches for straightforward data analysis and first proof-of-principle results from the prototype instruments are presented. In the following, the prototype setups are continuously improved and the implemented assays are tested and extended along several protein stability and formulation screening case studies. These include the investigation of model proteins (Chapter VI), drug candidates (Chapter V and Chapter VIII) as well as therapeutic biopharmaceuticals (Chapter VII). In order to work out the strengths and weaknesses of the developed methods and investigate the stability and interaction paradigms of the respective protein in greater detail, the results of the thermophoresis approaches are comprehensively benchmarked with established analytical methods and alternative assays for the respective analyses. In an overall summary and conclusion (Chapter IX), the results of the unfolding and aggregation investigations, forced degradation studies and protein-excipient interactions are reflected in order to derive a final estimation of the utility of thermophoresis-based formulation development approaches.

Chapter III
MicroScale Thermophoresis (MST)

III.1. Fundamentals of Thermophoresis

When a temperature gradient is applied to a macromolecular aqueous solution or a colloidal suspension, a heat transport is evoked and molecules start to migrate directed in the gradient.[1-3] This connection between a flow of heat and a flow of molecules along a temperature gradient is called *thermophoresis*, *thermodiffusion* or the *Ludwig-Soret effect*.[4,5]

The molecules experience, additional to the ubiquitous Brownian motion, a steady drift velocity (v_T), depending linearly on the size of the thermal gradient (∇T) and the thermophoretic mobility, or in other words the thermal diffusion coefficient (D_T) which acts as proportionality constant and hence is no diffusion coefficient in the proper meaning of the word (Equation 1).[6,7] The resulting mass flow (J) derives from the interplay of the Brownian diffusion coefficient (D) and D_T(Equation 2).[2,8,9]

$$v_T = -D_T \nabla T \qquad \text{[Equation 1]}$$

$$J = J_D - J_{DT} = -D\nabla c - cD_T\nabla T \qquad \text{[Equation 2]}$$

Since the thermal diffusion is compensated by ordinary mass diffusion a steady state is created. In the absence of convection, the steady-state concentration gradient (∇c) is only dependent on the Soret coefficient (S_T) and the size of the temperature gradient (∇T) (Equation 3). Therefore, the Soret coefficient determines the magnitude of thermophoretic mobility in the steady-state (Equation 4).[3,4,6]

$$\nabla \mathrm{c} = -\mathrm{c}\, \mathrm{S_T} \nabla \mathrm{T} \qquad \text{[Equation 3]}$$

$$\mathrm{S_T} = \frac{\mathrm{D_T}}{\mathrm{D}} \qquad \text{[Equation 4]}$$

The orientation of the thermophoretic motion, respectively the sign of D_T differs from one investigated system to another and is not yet predictable. While most biological samples show a directed movement towards the cold, termed *thermophobic* motion, there are examples of molecules displaying a flow along the temperature gradient, showing a *thermophilic* behavior. The Soret coefficient is, according to a positive D_T, by definition positive for thermophobic molecules.[2,10]

Together with the presence of a local thermodynamic equilibrium, as established by Duhr and Braun[9], the Soret coefficient equals the negative entropy (S) of the particle-solvent system (Equation 5). Taken the contributions of the temperature-sensitive entropy of water hydration and the entropy of the ionic shielding into account, which constitute the major influence to the particle entropy in water, the expression adds up to Equation 6 with σ_{eff} being the effective charge per surface area, s_{hyd} the hydration entropy, ε the dielectric constant and β its temperature derivative. Considering the term, the Soret coefficient (S_T) is therefore linearly dependent on the particle surface (A) and the Debye length (λ_{DH}).[1,6,11]

$$S_T = -\frac{S}{kT} \qquad \text{[Equation 5]}$$

$$S_T = \frac{A}{kT}\left(-s_{hyd} + \frac{\beta\sigma_{eff}^2}{4\varepsilon\varepsilon_0 T}\right) \times \lambda_{DH} \qquad \text{[Equation 6]}$$

Since thermophoresis is the connection of the thermophoretic mobility (D_T) and the diffusion coefficient (D), it is mainly dependent on global changes in size, charge and the solvation entropy of the molecule, as long as the buffer conditions are maintained constant.[4,11,12]

This indicates that changes in the extent and the direction of the thermophoretic movement should allow for the detection of unfolding, aggregation and binding events of a biopharmaceutical drug, being the main scopes of our investigations.

III.2. Measurement Setup and Readout

The all-optical measurement setup for MicroScale Thermophoresis, a technology developed at the group of Prof. D. Braun at the biophysics department of the LMU, which was further improved and later commercialized by the university spin-off company NanoTemper Technologies GmbH, is schematically represented in Figure 1. In this approach, a moderately focused IR-laser (1480 nm), which is strongly absorbed by water, is used to generate a local, precise and steep temperature gradient in the focal volume of glass capillaries containing the protein sample. This temperature increase results in thermophoretic movement of molecules which can be tracked label- and immobilization free via the intrinsic fluorescence of aromatic amino acids (mainly tryptophan and tyrosine[13,14]) that is excited by a UV-LED (280 nm). The combination of the IR-laser coupled into the same optical path as the excitation/detection unit ensures co-localization of temperature increase and fluorescence detection.[4,11,12,15-17]

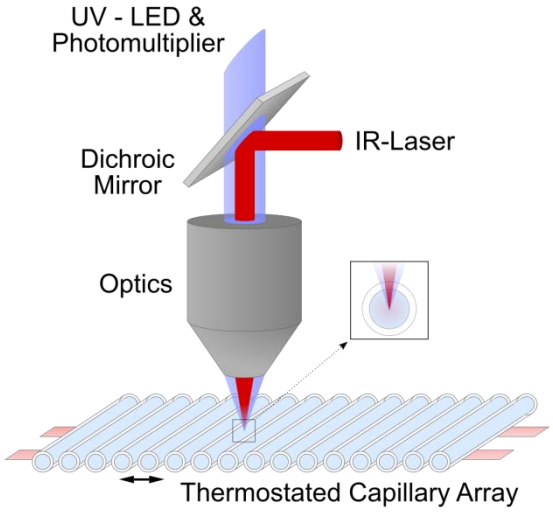

Figure 1: MicroScale Thermophoresis measurement setup.

Because the local temperature of the solution in the laser spot is only increased around 2-6 K on a micrometer scale and therefore moderate temperature gradients are used, the setup fulfills the requirements to apply the laws of a local thermodynamic equilibrium.[1,6,18]

The recorded changes in fluorescence over time (i.e. fluorescence timetrace) can be divided in six different phases, distinguished by their respective timescales and their characteristic fluorescence signals dependent on the IR-Laser heating (Figure 2).[4]

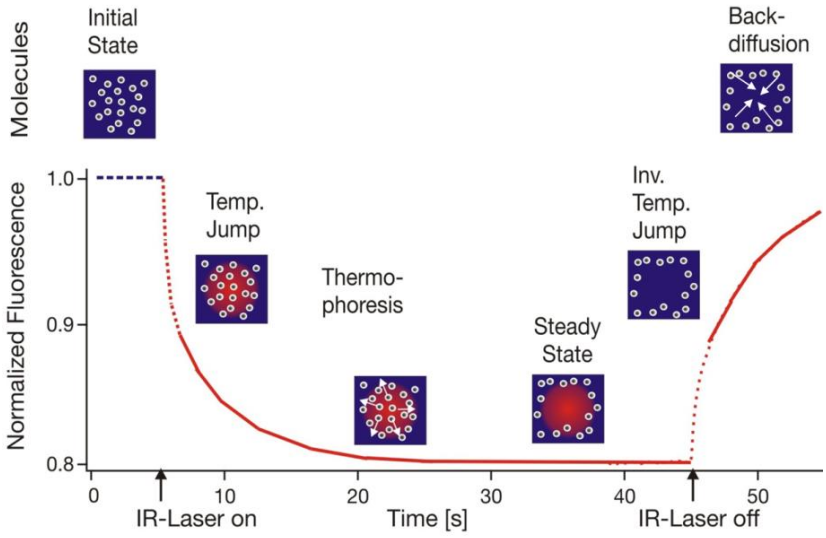

Figure 2: Typical MST timetrace, generated by measuring and normalizing intrinsic fluorescence over time subject to IR-laser input. Figure copied from Jerabek-Willemsen et al.[4]

In the *initial state* before laser heating, all molecules are subject to omnipresent undirected Brownian motion, resulting in a uniform fluorescence readout. After switching on the IR-laser, the temperature in the solution is increased and two effects are induced which can be easily separated by their distinctive timescales. Within approximately 50 ms, an exponential decrease in intrinsic fluorescence is present, which is called *temperature jump*. This event is based on temperature induced changes in the local surrounding of the fluorophores (aromatic amino acids) and does not rely on molecular motion yet. On the slower timescale of diffusion, *thermophoresis* sets in only after more than 1 s and changes the fluorescence signal because of the molecular depletion from the heated spot. In contrast to the temperature jump, which is sensitive to changes in the local properties, thermophoresis is a probe of the global surface changes. After a timescale of 10 to 30 seconds, thermal diffusion and ordinary diffusion average out, which leads to a *steady-state* distribution of molecules. After a steady-state is reached, the infrared-laser is turned off, and the sample cooling evokes an *inverted temperature jump* before the molecules undergo *pure mass diffusion* in order to undo the concentration imbalance and reestablish a uniform distribution.[1,4,11,12]

III.3. Data Evaluation

The abovementioned phases of a MST timetrace are used for the calculation of the MST parameters thermophoresis, temperature jump, as well as the combination of both. All parameters can be determined from the thermophoretic signal by evaluating the concentration (= fluorescence) ratio of a timescale after the event (*hot*) and a timescale before the event (*cold*)[1], which is expressed through the normalized fluorescence (F_{norm}), given in permille. Moreover, as deduced in section III.1, the change in concentration is linearly related to the Soret coefficient, because the alterations in temperature and concentration are small compared to the initial values (Equation 7).[4,12]

$$\mathrm{F_{norm}} = \frac{\mathrm{F_{hot}}}{\mathrm{F_{cold}}} \equiv \frac{\mathrm{c_{hot}}}{\mathrm{c_{cold}}} = \mathrm{e}^{-\mathrm{S_T}\Delta\mathrm{T}} \qquad \text{[Equation 7]}$$

By variation of the moment in time at which F_{cold} and F_{hot} are measured, it is possible to distinguish between thermophoresis, the temperature jump, or the combination of both. Furthermore, intrinsic fluorescence can be evaluated from the raw initial fluorescence (Figure 3).[4]

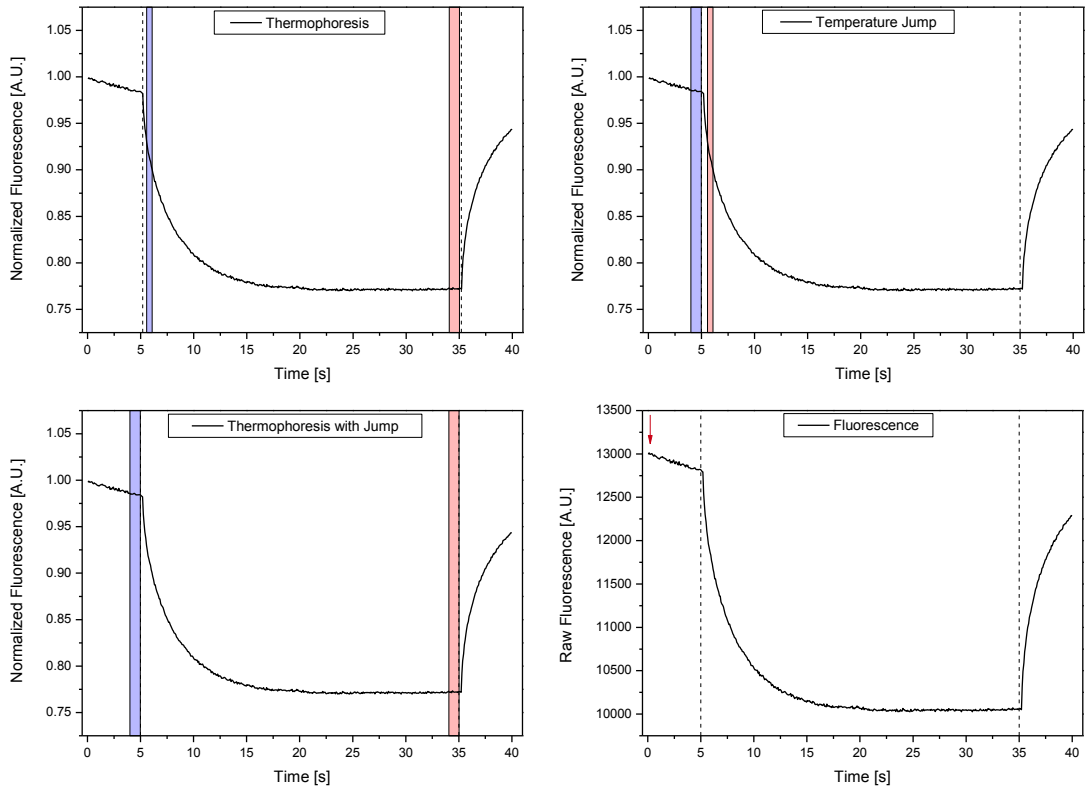

Figure 3: Exemplary cursor settings of hot (red bars) and cold (blue bars) for the evaluation of thermophoresis (left – top), temperature jump (top – right), and thermophoresis with jump (bottom – left). Moreover, intrinsic fluorescence can be evaluated from the raw initial fluorescence, as indicated by the red arrow (bottom – right).

III.4. Protein-Excipient Interaction Analysis by using MicroScale Thermophoresis (MST)

The well-established standard application of MST is the analysis of all kinds of biomolecular interactions, ranging from ion- or small molecule-protein interactions, over protein-protein, protein-DNA or protein-RNA interactions to assays investigating multi-component complexes as liposomes or ribosomes. This wide range of interactions is possible, as MST is not dependent on binding-induced size changes, which is a benefit over alternative approaches as fluorescence correlation spectroscopy (FCS) or surface plasmon resonance (SPR).[4,12,16]

Moreover, the MST assay is fully immobilization-free and can be performed either label-free by evaluating the intrinsic fluorescence of aromatic amino acid residues, or by the use of an extrinsic dye, covalently attached to one of the binding partners. Whereas the label-free approach that we use in our studies has the advantage of measuring the native system without any dye artifacts (e.g. the steric hindrance of the fluorescent tag on the binding site), extrinsic fluorescent dyes enable the measurement in biological media (blood, serum, milk etc.) which can be of high interest for compound screenings under *in vivo* conditions.[1,19-21]

The quantification of an interaction is usually set up as a titration experiment using multiple concentration ratios of the binding partners. Therefore, the concentration of the fluorescent binding partner is held constant and the amount of unlabeled binding partner is varied in a serial dilution from sub-stoichiometric concentrations to concentrations at least 10 times above the expected equilibrium dissociation constant (K_d) so that a saturation of all binding sites is ensured. By plotting the concentration of the added binding partner on a logarithmic scale against the change in the normalized fluorescence (ΔF_{norm}), or the in the initial fluorescence, a sigmoidal binding curve is generated from which the biomolecular interaction can be easily quantified from the transition between the plateaus for the totally unbound (baseline) and the totally bound state (saturation). Typically, ΔF_{norm} is calculated between the initial state and the steady-state of thermophoresis, while in some cases also the T-jump and/or the backdiffusion can indicate binding events and may be taken into account for binding analysis. It is often also possible to receive distinguishable fluorescence values if thermophoresis is not able to reach a steady-state within the measurement time, due to the slow diffusion.[1,4]

For the analysis of protein-excipient interactions, UV-LED and IR-laser settings were adjusted for each system, in order to get a satisfactory high initial fluorescence signal and thermophoretic depletion. The cursor settings for the evaluation of the MST parameters were kept constant and are given as a starting time and timeframe length for both the cold (blue) and the hot (red) region (Table 1). Additionally, intrinsic fluorescence was evaluated from the raw initial fluorescence emission.

Table 1: Data evaluation settings for determining the protein-excipient interactions by using MST, given in relation to the start of fluorescence measurement.

MST parameter	Cold start [s]	Cold length [s]	Hot start [s]	Hot length [s]
Temperature jump	4.55	0.97	6.18	0.52
Thermophoresis	6.18	0.52	34.50	0.97
Thermophoresis with jump	4.55	0.97	34.50	0.97

III.5. References

1. Wienken CJ, Baaske P, Rothbauer U, Braun D, Duhr S. 2010. Protein-binding assays in biological liquids using microscale thermophoresis. Nature Communications 1:100.

2. Iacopini S, Piazza R. 2003. Thermophoresis in protein solutions. Europhysics Letters 63(2):247-253.

3. Piazza R. 2008. Thermophoresis: Moving particles with thermal gradients. Soft Matter 4(9):1740-1744.

4. Jerabek-Willemsen M, Wienken CJ, Braun D, Baaske P, Duhr S. 2011. Molecular interaction studies using microscale thermophoresis. Assay and Drug Development Technologies 9(4):342-353.

5. Wiegand S. 2004. Thermal diffusion in liquid mixtures and polymer solutions. Journal of Physics: Condensed Matter 16(10):R357.

6. Duhr S, Braun D. 2006. Why molecules move along a temperature gradient. Proceedings of the National Academy of Sciences 103(52):19678-19682.

7. Piazza R, Parola A. 2008. Thermophoresis in colloidal suspensions. Journal of Physics: Condensed Matter 20(15):153102 (153118pp).

8. Piazza R, Iacopini S, Triulzi B. 2004. Thermophoresis as a probe of particle-solvent interactions: The case of protein solutions. Physical Chemistry Chemical Physics 6(7):1616-1622.

9. Duhr S, Braun D. 2006. Thermophoretic depletion follows boltzmann distribution. Physical Review Letters 96(16):168301.

10. Iacopini S, Rusconi R, Piazza R. 2006. The “macromolecular tourist": Universal temperature dependence of thermal diffusion in aqueous colloidal suspensions. The European Physical Journal E 19(1):59-67.

11. Reineck P, Wienken CJ, Braun D. 2010. Thermophoresis of single stranded DNA. Electrophoresis 31(2):279-286.

12. Baaske P, Wienken CJ, Reineck P, Duhr S, Braun D. 2010. Optical thermophoresis for quantifying the buffer dependence of aptamer binding. Angewandte Chemie International Edition 49(12):2238-2241.

13. Garidel P, Hegyi M, Bassarab S, Weichel M. 2008. A rapid, sensitive and economical assessment of monoclonal antibody conformational stability by intrinsic tryptophan fluorescence spectroscopy. Biotechnology Journal 3(9-10):1201-1211.

14. Teale FW, Weber G. 1957. Ultraviolet fluorescence of the aromatic amino acids. Biochemical Journal 65(3):476-482.

15. Zillner K, Jerabek-Willemsen M, Duhr S, Braun D, Langst G, Baaske P. 2012. Microscale thermophoresis as a sensitive method to quantify protein: nucleic acid interactions in solution. In: Kaufmann M, Klinger C, Functional Genomics Methods in Molecular Biology (Methods and Protocols). Springer. p 241-252.

16. Jerabek-Willemsen M, André T, Wanner R, Roth HM, Duhr S, Baaske P, Breitsprecher D. 2014. Microscale thermophoresis: Interaction analysis and beyond. Journal of Molecular Structure 1077:101-113.

17. Duhr S, Arduini S, Braun D. 2004. Thermophoresis of DNA determined by microfluidic fluorescence. The European Physical Journal E 15(3):277-286.

18. Braun D, Libchaber A. 2002. Trapping of DNA by thermophoretic depletion and convection. Physical Review Letters 89(18):188103.

19. Lippok S, Seidel SA, Duhr S, Uhland K, Holthoff HP, Jenne D, Braun D. 2012. Direct detection of antibody concentration and affinity in human serum using microscale thermophoresis. Analytical Chemistry 84(8):3523-3530.

20. Seidel SA, Dijkman PM, Lea WA, Jerabek-Willemsen M, Lazic A, Joseph JS, Srinivasan P, Baaske P, Simeonov A, Katritch I. 2012. Microscale thermophoresis quantifies biomolecular interactions under previously challenging conditions. Methods 59(3):301-315.

21. Seidel SA, Wienken CJ, Geissler S, Jerabek-Willemsen M, Duhr S, Reiter A, Trauner D, Braun D, Baaske P. 2012. Label-free microscale thermophoresis discriminates sites and affinity of protein-ligand binding. Angewandte Chemie International Edition 51(42):10656-10659.

Chapter IV
Method and Assay Development

In the course of this thesis, two methods for the characterization of protein stabilities have been developed, implemented, and thoroughly tested in comparison with benchmark methods and assays used in the respective field of interest. Technical implementation and prototype setup have been performed by NanoTemper Technologies GmbH (Munich, Germany). Both developed methods including all prototype instruments share the same origin in label-free IR-laser induced MicroScale Thermophoresis (MST) technology and instrumentation (Chapter III).

In section IV.1, we describe the major development steps in order to utilize MicroScale Thermophoresis (MST) for unfolding and aggregation investigations of biopharmaceuticals. Therefore, a prototype setup was developed and steadily optimized in terms of enhanced automation as well as focusing and tempering accuracy. Moreover, the parameters for a stepped thermal ramp assay are discussed and an exemplary data evaluation is presented.

A second approach is presented in section IV.2. There a method named thermo-optical protein characterization (TOPC) was developed in order to combine classical forced degradation investigations with simultaneous unfolding, aggregation and precipitation analysis. This measurement approach distinguishes itself from standard MST experiments by a significantly enhanced IR-laser power applied. Apart from thermophoretic depletion, this modification is primarily implemented in order to rapidly heat up the samples by water absorption to temperatures above the respective protein melting temperature. Thus, forced protein aggregation is evoked, which can be evaluated by intrinsic fluorescence.

IV.1. Unfolding and Aggregation Investigations by using MicroScale Thermophoresis (MST)

IV.1.1. Measurement Setup

The determination of highly comparable and reproducible unfolding and aggregation parameters required several modifications of standard label-free MST measurement setups as the Monolith NT.LabelFree instrument (Figure 1, NanoTemper Technologies GmbH, Munich, Germany). Besides an overall extended accessible temperature range from ambient to 90 °C and highly precise temperature adjustment via a thermostated sample tray, the exact determination of capillary positions over the measurement time had to be guaranteed. These goals have been stepwise accomplished and improved during the development of three consecutive prototype generations (Table 2).

The goal of extending the maximum obtainable temperature range from 45 °C to ≥ 90 °C was already reached with a modified power adapter in the 1st generation prototype and continued ever since. Additionally, thermal equilibration and homogeneity throughout all samples had to be ensured at every temperature step. Before the measurement of the first sample, this was achieved by setting an initial delay of 15 minutes at the starting temperature.

In the 1st prototype setup, an additional delay of 600 s was used after each stepwise temperature increase, which could be shortened by 90% for the 2nd and was made redundant for the 3rd prototype. This drastic reduction was established by first equipping the initially grooved aluminum sample tray (1st gen) with a temperature preserving lid (2nd gen). In the 3rd generation setup, the sample tray was replaced by a continuous silicon wafer, while the lid was adopted. The main advantage of a continuous tray is the full contact to the measurement region of the capillaries which allows for most precise and immediate temperature control. In order to preclude a mutual interference of the samples investigated, a capillary distance of 4.5 mm, matching the well-to-well spacing of a 384-well plate, was maintained for all array configurations.

The focusing accuracy was increased by performing a capillary scan to determine the exact horizontal-/x-position of each capillary on the tray during the initial equilibration time. From the second generation prototype onwards, additionally the exact vertical-/y-position was measured for every capillary at each temperature step to correct for thermal expansion and agitation over the measurement time.

Last, a precise dual-LED system was implemented in the 3rd generation prototype, replacing the former single wavelength detection, which covered only one relatively broad spectral range (330-380 nm). The measurement of two independent wavelengths (330 and 350 nm) extended the readout options of the MST parameters additionally and allowed for selecting the thermophoretic melting curves displaying the unfolding transition most clearly. Furthermore, this feature was used for the measurement of spectral shifts occurring during the unfolding transition of the protein[1].

Table 2: Overview of the three prototype generations developed for the determination of predictive unfolding and aggregation markers by using a stepped thermal ramp assay.

Parameter	1st generation	2nd generation	3rd generation
Capillary array	Al-tray	Al-tray with lid	Si-wafer/array
Temperature range	20-90 °C	20-90 °C	15-95 °C
Temperature readout	Manual (PT100)	Automatic	Automatic
Temperature precision	Low	Medium	High
Equilibration delay	600 s	60 s	0 s
Detection wavelength(s)	355 ± 25 nm	355 ± 25 nm	330 & 350 nm
Capillary detection	x-scan	x- and y-scans	x- and y-scans

Parallel to developing the measurement prototype, the material and coating of the glass capillaries have been improved for our purposes and a convenient and effective sealing method has been developed. The initially used borosilicate glass capillaries (NT.LabelFree Capillaries) have been replaced by fused silica capillaries (NT.LabelFree Zero Background Capillaries) which drastically reduced the background fluorescence/capillary auto-fluorescence, which increased the measurement sensitivity and enabled the precise measurement of minute changes in protein conformation or aggregation events even at low protein concentrations. Furthermore, the standard treated capillaries were refined with an improved coating (MST premium coating) during the method development activities, in order to prevent sample adsorption to the inner capillary surface. The measurement of melting curves for up to 16 formulations in parallel made an effective and tight sealing of the capillary ends necessary in order to exclude changes in the protein concentration by solvent evaporation. This was realized in a first step by sealing the capillaries with wax and further optimized by the use of liquid dip gum. The details on the sealing modifications are given in section VI.2.1.1 where the influence of capillary closure is elaborated by using the thermophoretic melting curves of human serum albumin.

IV.1.2. Measurement Assay and Parameters

Our main goal was to derive relevant short-term stability parameters, which can be used for high-throughput prediction, differentiation and ranking of multiple proteins or formulations already in an early development stage. For this purpose, a stepped thermal ramp scanning assay was implemented, re-measuring MST over a set temperature range in defined temperature steps. Figure 4 displays the normalized fluorescence readout for all MST measurements in an exemplary data set, ranging from 35 °C to 75 °C in 1 °C steps. At every temperature increase, which is adjusted by heating up the capillary array, intrinsic fluorescence was recorded for 20 seconds in total. During this timeframe, initial fluorescence was tracked for 5 seconds, before the IR-laser was turned on and the subsequent temperature jump followed by the thermophoretic movement, both generated by the IR-laser induced temperature increase, were measured. 10 seconds later, equilibrium between thermal diffusion and ordinary mass diffusion was reached and the laser was turned off again. Immediately, the solution exhibits an inverse temperature jump and a subsequent back diffusion of molecules which were tracked for additional 5 seconds.[2]

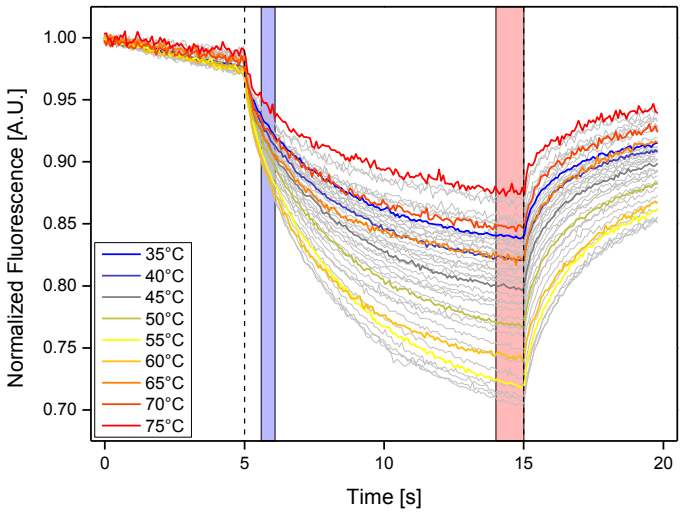

Figure 4: Intrinsic fluorescence timetraces measured by MST. For ease of identification, the fluorescence timetraces of each 5 °C step were highlighted in color. The area between the dashed lines represents the 10 s laser on time. The cursor positions used for calculation of the thermophoresis values are indicated by the blue (cold region) and red (hot region) bar. (Note: the original fluorescence timetraces of this measurement show a delay of 0.4 seconds to the theoretical laser-on time of 5 s, which has been corrected for this graph)

The two fundamental measurement parameters of MST, namely LED- and IR-laser-Power, were individually adapted for each protein examined, in order to perform all measurements at optimal tailor-made conditions. The UV-LED used for fluorescence excitation at a wavelength of 280 ± 20 nm was set to the lowest possible intensity which allowed for a reduction of potential photo-bleaching effects during multiple sample measurement but still ensured an intermediate to high starting fluorescence level above the background fluorescence level. To realize this tradeoff, also the photomultiplier recording the fluorescence emission was slightly adapted within the dynamic range of the system. Likewise, the IR-laser intensity had to fulfill a compromise between high thermophoretic depletion, resulting in an enhanced signal to noise ratio, and a low local temperature increase of the sample, otherwise potentially disturbing the native properties of the system and creating measurement artifacts.[3]

IV.1.3. Data Evaluation

After an intrinsic fluorescence timetrace at each single temperature step was measured, thermophoresis and/or temperature jump values were calculated as described in section III.3 and III.4, by using the cursor settings given in Table 3. It is to mention that the exact time point of laser activation on the absolute time scale varied marginally between the different prototype generations. Therefore, appropriate settings have been determined for exemplary timetraces on each instrument individually and are given in the appendix as entered in the software (IV.3). Additionally to the three MST derived parameters (thermophoresis, t-jump and thermophoresis with t-jump), intrinsic fluorescence can be evaluated from the raw initial fluorescence emission.

Table 3: Data evaluation settings for the three MST parameters, given in relation to the moment of laser activation. The settings for the cold and the hot region frame the respective parameter.

MST parameter	Cold start [s]	Cold end [s]	Hot start [s]	Hot end [s]
Temperature jump	-1.0	0.0	0.6	1.1
Thermophoresis	0.6	1.1	9.0	10.0
Thermophoresis with jump	-1.0	0.0	9.0	10.0

Obtaining one data point value per temperature gives us the possibility to plot a chart of signal over temperature, termed melting curve (Figure 5). In all unfolding and aggregation measurements, thermophoresis and/or t-jump melting curves showed one or more distinct peaks upon protein unfolding which were assigned as apparent melting temperatures (T_m). In order to evaluate a melting point for each protein formulation, the single data points of the melting curve were smoothed and interpolated before the peak positions were calculated. For the intrinsic fluorescence data, the unfolding transitions are sigmoid curves which are analyzed by calculating the first derivative curve, which is in the following smoothed and interpolated before the peak temperatures are determined.

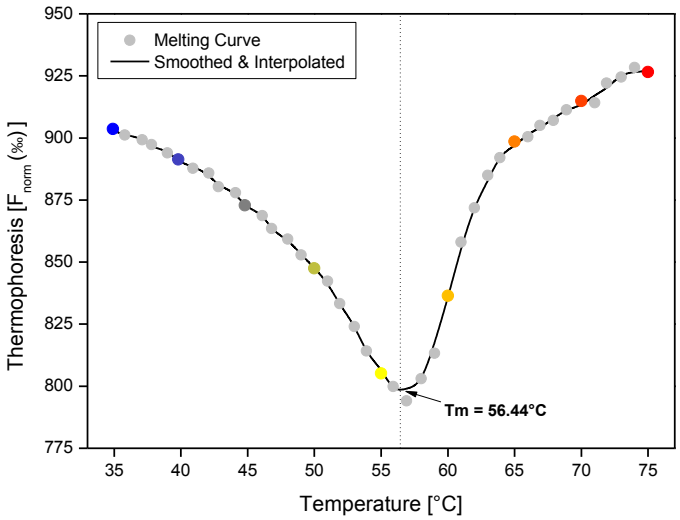

Figure 5: Exemplary thermophoresis melting curve including smoothing and interpolation of the data points as well as evaluation of the apparent melting temperature (T_m).

IV.2. Forced Degradation Studies by using Thermo-Optical Protein Characterization (TOPC)

IV.2.1. Measurement Setup

The simultaneous forced thermal degradation of protein formulations and detection of changes in the intrinsic fluorescence was implemented in a prototype setup for thermo-optical protein characterization (TOPC, Figure 6, NanoTemper Technologies GmbH, Munich, Germany). In our approach, thermal stress was generated by using an enhanced intensity IR-laser (1480 nm), which is strongly absorbed by water and allows for rapid heat stressing of up to 16 protein formulations pulled up into glass capillaries. Resultant changes in the intrinsic tryptophan fluorescence were detected at a wavelength of 355 ± 25 nm over time and assigned to biomolecular stability events as unfolding, aggregation and precipitation. For each protein investigated, the IR-laser power, as well as the LED power and the detection timeframe were individually adapted.

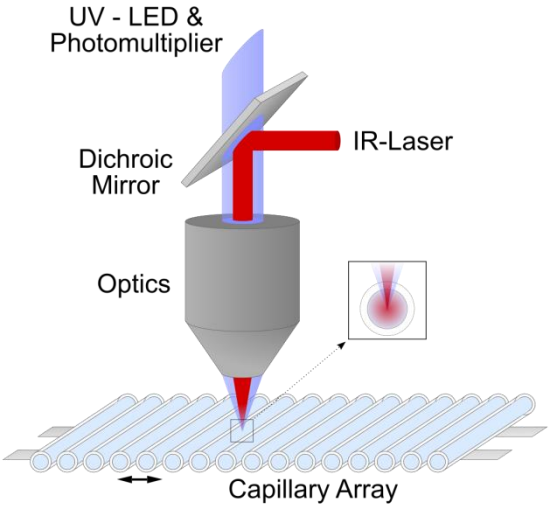

Figure 6: Measurement setup for thermo-optical protein characterization. The protein formulations are pulled up in glass capillaries and positioned on a capillary array. The strong IR-laser is via a dichroic mirror directly focused into the center of the respective capillary to rapidly heat up the solution. Meanwhile, protein unfolding, aggregation and precipitation events are tracked via intrinsic tryptophan fluorescence.

Parts of this section have been published under: Wanner R, Breitsprecher D, Duhr S, Baaske P, Winter G 2017. Thermo-Optical Protein Characterization for Straightforward Preformulation Development. Journal of Pharmaceutical Sciences 106(10):2955-2958.

IV.2.2. Raw Data Interpretation

Figure 7 exemplarily displays one set of time-resolved fluorescence measurements during forced thermal degradation, covering thee different formulations of the same mAb. The fluorescence timetrace of every single experiment can be divided into different sections which are explained in the following. After 5 seconds of initial fluorescence, the IR-laser is turned on and rapidly heats up the focal volume of the investigated protein formulation. The steep temperature increase leads to a pronounced temperature jump, thermophoretic depletion and immediate thermal protein denaturation. The respective unfolding transition could be seen within 15 seconds after turning on the high-power IR-laser by a more or less pronounced peak in fluorescence emission. Subsequently, the timetraces spread and establish a distinct aggregation and precipitation pattern, indicated by the respective fluorescence level and the occurrence of periodic fluctuations in the fluorescence signal. Based on a publication by Mast and Braun[4], we attribute these observations to the concurrence of laser-induced convective flow and accumulation of protein particles. After 155 seconds, the laser input is terminated, the samples cool down and the fluorescence signal reacts with a rapid increase. This observation is on the one hand side attributed to the increasing quantum yield at lower temperatures and on the other hand side to the backdiffusion of depleted molecules to the focal area. The final fluorescence level is therefore related to the amount of protein particles (aggregates and precipitates) generated during the measurement.

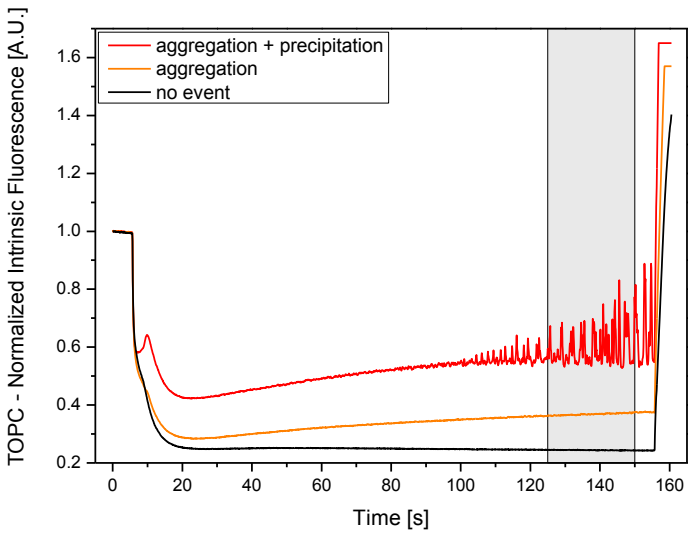

Figure 7: Signal types from thermo-optical protein characterization.

IV.2.3. Data Evaluation

From the raw TOPC curves, a representative timeframe is chosen (Figure 7 – grey area) and the fluorescence level, as well as the scattering are evaluated in terms of mean fluorescence values and standard deviation (Figure 8). This allows for a ranking of aggregation and precipitation propensities among different formulations. In this example, the formulation that showed neither aggregation nor precipitation induced events upon heating for 150 seconds is described with the lowest mean and standard deviation levels. Increased mean fluorescence intensities are observed for the formulations forming soluble aggregates under heat stressing. Furthermore, the level of fluorescence intensity clearly distinguishes the aggregating samples from each other and reveals the highest aggregation propensity for the formulation displayed in red. Last, the scattering of the intrinsic fluorescence timetrace that yields in an increased standard deviation value is also clearly enhanced for this formulation compared to the other two. This is attributed to the induction of large, insoluble aggregates that did not occur under the ‘black’ and ’orange’ formulation conditions.

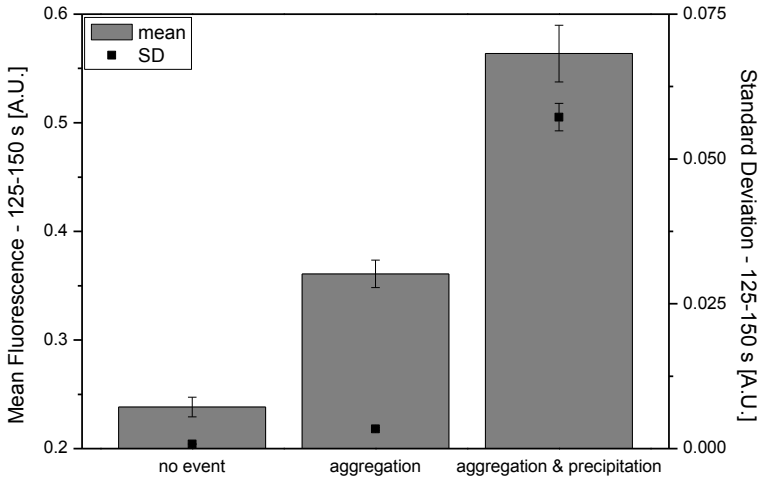

Figure 8: Data evaluation of mean fluorescence values and the standard deviation in the timeframe from 125 to 150 s within the TOPC measurements. The error bars express the standard deviation from triplicate measurements.

IV.2.4. Proof-of-Principle

In order to further strengthen our concept of combining purely IR-laser induced stress testing with simultaneous intrinsic fluorescence evaluation, additional proof-of-principle investigations have been performed. First, the influence of different concentrations on the TOPC readout was investigated by using a mAb formulation showing neither aggregation nor precipitation events. In Figure 9 (left), the respective raw fluorescence traces at 0.1, 0.2, 0.3, 0.4, and 0.5 mg/ml are given, which show the expected concentration dependent fluorescence offset but expose a highly comparable and parallel progression without the manifestation of any events arising from colloidal instabilities. This comparability is even more evident in the normalized plot (right), where all data points are displayed in relation to the initial fluorescence value and a perfect overlay of all concentrations is achieved. These findings underline the feasibility of normalization between varying initial fluorescence values which could occur due to pH or excipient variations in extensive formulation screenings.

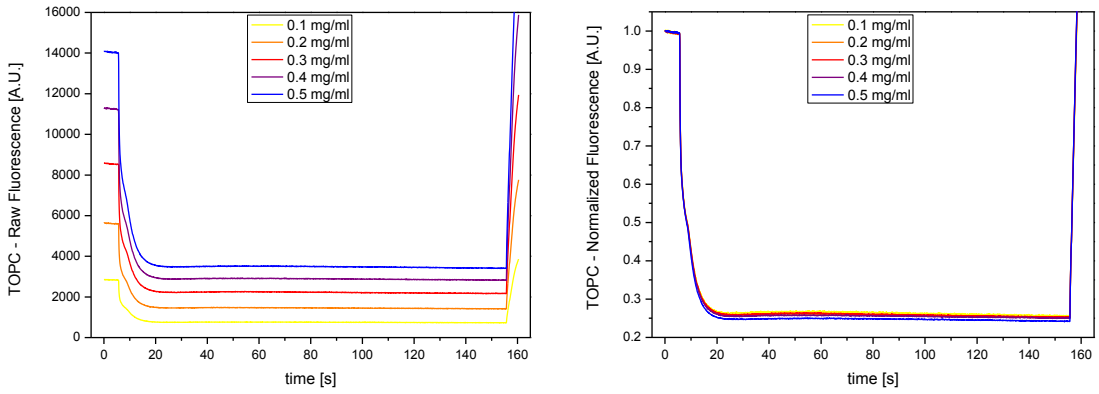

Figure 9: Raw (left) and normalized (right) fluorescence traces at different protein concentrations for the formulation not exposing aggregation or precipitation events (Formulation 1).

Following this, the results were compared to a formulation with very high aggregation and precipitation propensity (Figure 10). Here, a completely different picture was apparent, showing strong differences in aggregation and especially precipitation levels. Stepwise decreasing the mAb concentration from 0.5 to 0.1 mg/ml, the onset of precipitation spikes was first shifted to later timescales, which was accompanied by a considerable decrease in scattering intensity (left). At the same time, also soluble aggregation, derived from the intrinsic fluorescence level is decreased, what is most prominent at 0.1 and 0.2 mg/ml and easiest derived from the normalized illustration (right).

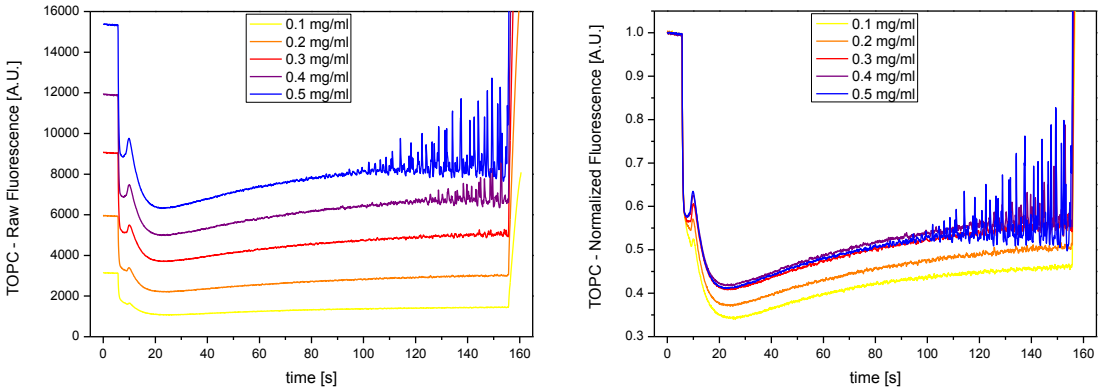

Figure 10: Raw (left) and normalized (right) fluorescence traces at different protein concentrations for the formulation exposing pronounced aggregation and precipitation events (Formulation 2).

A summarizing data evaluation of the concentration effects on the TOPC measurements is given in Figure 11. Formulation 1, showing neither aggregation nor precipitation events, was not influenced by the protein concentration. Consequently, the mean fluorescence, as well as the standard deviation evaluation was constant over changing concentrations. However, the aggregating and precipitating Formulation 2 was strongly influenced by changes in the protein content, as higher concentrations led to an accumulation of soluble protein aggregates, reflected in increasing mean fluorescence values, and insoluble precipitates, which lead to a strong increase of timetrace scattering and standard deviation values. This discrepancy on the influence of protein content is attributed to the concentration dependency of aggregation and precipitation and will in the upcoming measurements be addressed with the interplay of protein concentration and the IR-laser heating rates.

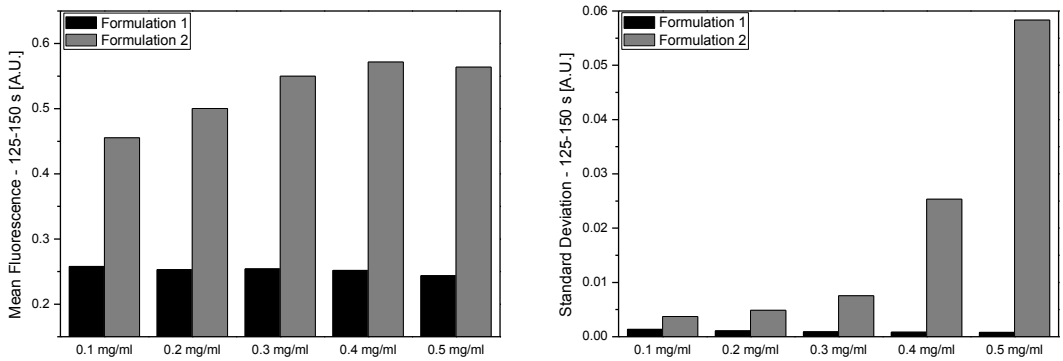

Figure 11: Concentration influence on the fluorescence intensity readout.

In order to elaborate in more detail on the influence of IR-laser heating we conducted additional measurements. In the TOPC setup, the extent of temperature increase and as well the heating rates are predominantly influenced by (i) the capillary diameter and (ii) the IR-laser intensity, which were both investigated.

In the first experiment, a formulation showing a pronounced unfolding peak as well as extended precipitation under continuous laser heating was filled in capillaries of different inner diameters ranging from 320 – 800 µm. As Figure 12 clearly depicts, the capillary diameter has a large effect on the timescales and extent of unfolding, aggregation and precipitation. With reducing capillary diameter, the amount of water absorbing the IR-laser radiation in the focal volume and at the same time the convective transport mixing the material within the capillary decreases. In summary, these two effects led to a faster and more complete unfolding of the protein (right). On the other hand side, aggregation and precipitation was found to be more pronounced with increasing focal volumes (left), which is a result of the larger amount of protein material in the measurement area and the extended exchange with the surrounding volume. The convection cycle generated during a persistent measurement leads to the accumulation of molecules periodically flowing through the focus, a phenomenon well described by Braun and Libchaber[5,6]. As a conclusion of this pre-test, we decided to proceed with capillaries of 500 µm inner diameter in order to combine a complete unfolding of the molecule and a pronounced aggregation and precipitation.

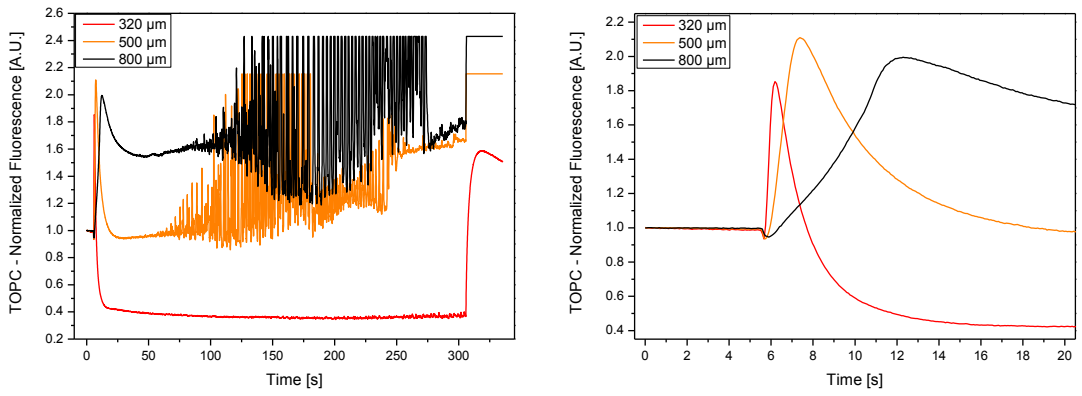

Figure 12: Comparative studies on the influence of the capillary inner diameter on unfolding , aggregation and precipitation during TOPC. Three different diameters were tested, which are shown in red (320 µm), orange (500 µm) and black (800 µm).

In the second experiment targeting the influence of the heating rates during TOPC, the IR-laser power was varied between 114% and 341% (Figure 13). Identical to the investigations on the inner diameters, a strong effect on conformational and aggregation stability was observed. Higher laser intensities lead to higher final temperatures within the capillary and faster heating rates. This causes a faster and more complete unfolding of the protein (right). The influence on the precipitation tendency however seems to be non-linear (left). Whereas both, the low (114%) and the high (341%) IR-laser power led to fluctuations in the fluorescence signal with rather small amplitudes, the medium setting (227%) exposes a very high scattering signal. However, taking a closer look at the results, additional changes in the scattering frequency are observed, which seem to follow a more linear behavior over increasing laser heating when compared to the scattering amplitudes. While the frequency of fluorescence timetrace scattering is expected to be proportional to the speed of particles flowing through the focal volume, the amplitude should increase with either a higher number of particles or a larger particle size. Consequently, our hypothesis to the observations with varying laser powers is the following. At the lowest laser intensity, incomplete unfolding leads to a low number of particles generated which are periodically flowing through the focal volume. After increasing the laser power to the medium value, unfolding is complete, a higher particle concentration is found and consequently the amplitude increases. At the highest IR-laser setting, the amount of particles generated is identical but the amplitude decreased. This is attributed to a constant increase of the convection speed over increasing laser input promoting the particle exchange with the surrounding out-of-focus volume which keeps the amplitude low, when the frequency is maximal. Defaults settings for TOPC analysis will be fixed to medium IR-laser intensities (227%), while fine adjustment for every single protein to be investigated will enable the conduction of TOPC measurements with highest information content on aggregation and precipitation propensities and clearly distinguish between stable and unstable formulations.

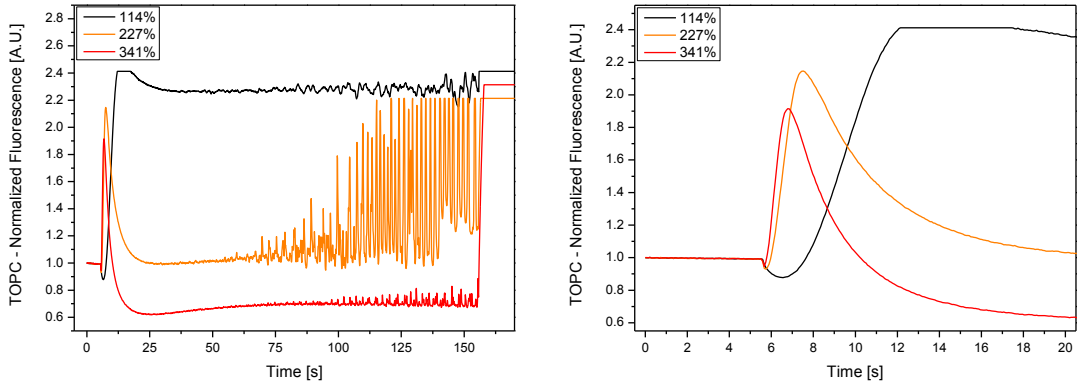

Figure 13: Comparative studies on the influence of the IR-laser power on unfolding, aggregation and precipitation during TOPC. Three different settings were tested, which are shown in red (341%), orange (227%) and black (114%). The percentage given in the figure legend corresponds to the IR-laser power.

The concept presented in this method and assay development section is in the following benchmarked against conventional stress testing approaches and predictive stability screenings to prove the assumptions made from the observations under IR-laser heating.

IV.3. Appendix

Table 4: MST data evaluation settings for the 1st generation prototype unfolding and aggregation measurements, given in relation to the start of fluorescence measurement.

MST parameter	Cold start [s]	Cold length [s]	Hot start [s]	Hot length [s]
Temperature jump	3.80	1.00	5.40	0.50
Thermophoresis	5.40	0.50	13.80	1.0
Thermophoresis with jump	3.80	1.00	13.80	1.0

Table 5: MST data evaluation settings for the 2nd generation prototype unfolding and aggregation measurements, given in relation to the start of fluorescence measurement.

MST parameter	Cold start [s]	Cold length [s]	Hot start [s]	Hot length [s]
Temperature jump	4.40	0.97	5.96	0.52
Thermophoresis	5.96	0.52	14.46	0.97
Thermophoresis with jump	4.40	0.97	14.46	0.97

Table 6: MST data evaluation settings for the 3rd generation prototype unfolding and aggregation measurements, given relative to the moment of laser activation. Note: For the 3rd generation prototype instrument and the MO.AffinityAnalysis software, the cursor settings are given as *region start* and *region end* in relation to the time point of laser activation. Moreover, the cursor settings for t-jump and thermophoresis slightly differ from the 1st and 2nd generation prototypes. However, in the data presented, only thermophoresis with jump has been evaluated that complies with the previous data evaluations.

MST parameters	Cold start [s]	Cold end [s]	Hot start [s]	Hot end [s]
Temperature jump	-1.00	0.00	0.50	1.50
Thermophoresis	1.00	2.00	8.96	9.96
Thermophoresis with jump	-1.00	0.00	8.96	9.96

IV.4. References

1. Garidel P, Hegyi M, Bassarab S, Weichel M. 2008. A rapid, sensitive and economical assessment of monoclonal antibody conformational stability by intrinsic tryptophan fluorescence spectroscopy. Biotechnology Journal 3(9-10):1201-1211.

2. Baaske P, Wienken CJ, Reineck P, Duhr S, Braun D. 2010. Optical thermophoresis for quantifying the buffer dependence of aptamer binding. Angewandte Chemie International Edition 49(12):2238-2241.

3. Alexander CG, Wanner R, Johnson CM, Breitsprecher D, Winter G, Duhr S, Baaske P, Ferguson N. 2014. Novel microscale approaches for easy, rapid determination of protein stability in academic and commercial settings. Biochimica et Biophysica Acta (BBA) - Proteins and Proteomics 1844(12):2241-2250.

4. Mast CB, Braun D. 2010. Thermal trap for DNA replication. Physical Review Letters 104(18):188102.

5. Braun D, Libchaber A. 2002. Trapping of DNA by thermophoretic depletion and convection. Physical Review Letters 89(18):188103.

6. Braun D, Libchaber A. 2004. Thermal force approach to molecular evolution. Physical Biology 1(1):1-8.

Chapter V
Engineered Antibody Derivatives

The sales of monoclonal antibody (mAb) drugs have been tremendously increasing over the past years. Together with novel antibody scaffolds like antigen-binding fragments (Fab), single-chain variable fragments (scFv), antibody-drug-conjugates (ADC), and bispecific antibodies (BsMAb), they represent the largest and fastest growing markets the biopharmaceutics industry with hundreds of drug candidates in the development pipelines. But not only innovative engineered antibody drugs are on the rise, also the first biosimilar antibody products have recently been approved.[1-7]

Structurally, mAbs are complex Y-shaped multi-domain biomolecules forming a tetrameric structure with a molecular weight of 150 kDa. Each IgG antibody consist of two identical light chains (50 kDa each) and two identical heavy chains (25 kDa each). Moreover, the structure can be divided in a (constant) Fc (CH2 and CH3) and a Fab (with variable CDRs) region, which substantially control the overall protein stability.[8-10]

The case study presented in this section is targeting the influences of chemical derivation on the conformational and aggregation stability of monoclonal antibodies (mAbs). As provided by the supplier, the antibodies investigated tend to aggregate during unfolding. While the unfolding of the Fc part at lower temperatures is known to be reversible, Fab unfolding at elevated temperatures remains irreversible and the expected ranking in terms of their non-native aggregation stability is Ab3, Ab4, Ab1, Ab2, sorted from high to low. Thus, properties of the Fab domain dictate the aggregation stability of the antibodies. This influence of the mAb variable region on the aggregation propensity is often described in literature and referred to aggregation-prone regions (APRs) that might be exposed during Fab unfolding.[9,11-14] Comparing Ab3 and Ab4 as well as Ab1 and Ab2, the modification reduces the aggregation stability. As the modified and the unmodified antibodies share the same Fab part each, the conformational stability of Fab unfolding remains unchanged.

V.1. Materials and Methods

V.1.1. Materials

The antibodies and antibody derivatives used in this study were kindly donated by Sanofi S.A. (Vitry-sur-Seine, France). An overview of the drug product (DP) materials including protein concentration and the composition of the used formulation buffers is given in Table 7. The molecular weight of all the proteins is in the range of 150 kDa.

Table 7: Overview of the drug products used in the antibody derivatives study.

Material	Concentration [mg/ml]	Formulation composition
Ab1 (native/naked Ab)	10.1	50 mM potassium phosphate, 50 mM NaCl, 2 mM EDTA, pH 6.6
Ab2 (modified Ab1)	5.2	10 mM acetate, 3.75% mannitol, 2.5% sucrose, 0.005% polysorbate 80, pH 5.5*
Ab3 (native/naked Ab)	5.3	PBS
Ab4 (modified Ab3)	10.8	10 mM histidine, pH 5.5

* the percentages are given in w/V

The study was conducted with DP material diluted in phosphate buffered saline (PBS). Therefore, 10-fold concentrated PBS stock solution pH 7.4 was diluted to 1-fold with deionized water. Thereafter, the four different drug products were centrifuged for at least 5 min at minimum 13000 rpm and subsequently volumetrically diluted with 1x PBS to a concentration of 1 mg/ml each. In consequence, ~ 5 or ~ 10-fold dilutions at mixture pH values between 5.5 and 7.4 were received, depending on the starting concentration and pH value of the stock DP material.

Table 8: Overview of the materials used in the antibody derivatives study.

Material	Supplier	Art.-number	Lot-number
Roti®-Stock 10x PBS	Carl Roth GmbH & Co KG, Karlsruhe, Germany	1058.1	423206137
Water AnalaR Normapur®	VWR International, Radnor, PA, USA	102927G	-

V.1.2. Unfolding and Aggregation Investigations

V.1.2.1. MicroScale Thermophoresis (MST)

The 1st generation stepped thermal ramp prototype setup (NanoTemper Technologies GmbH, Munich, Germany) was introduced in the course of feasibility studies for the execution of predictive unfolding and aggregation studies by using MST. In our assay, fluorescence excitation LED Power was set to 50% while an IR-laser MST Power of 20% was used. In order to guarantee for temperature homogeneity on the tray, an increased delay of 600 s was used after each temperature increase. The overall measurement runtime was reduced by using an elevated starting temperature of 58 °C and increasing the temperature of the capillary tray up to 88 °C in 1 °C steps. This shortened temperature range covered all expected unfolding transitions and the aggregation event of the antibodies investigated.

Furthermore, a control experiment monitoring potential influences of multiple IR-laser and UV-LED input on the thermophoretic behavior of the sample was performed. Therefore, the LED- and MST-settings from the stepped thermal ramp assay were retained, but on the contrary, the temperature was kept at a base temperature of 30 °C. In order to obtain an increased resolution of potential signal changes, the delay between two measurements was decreased to 305 s. In parallel, the overall analysis time was extended to almost 8.5 hours by setting a 43-fold measurement of each sample on a full tray load containing 15 capillaries. LabelFree UI software version 2.1.31 (NanoTemper Technologies) was used for performing the MST experiment, while the thermophoresis values for each sample and temperature step have been calculated by using NT Analysis software version 1.5.41 (NanoTemper Technologies). For both measurements, NT.LabelFree Standard Treated Capillaries (NanoTemper Technologies) were used.

In the revised 2nd generation prototype setup, the unfolding and aggregation experiment was repeated for all antibody variants. NT Control software version 2.1.31 (NanoTemper Technologies) was used to conduct the stepped thermal ramp assay by increasing the ambient temperature from 50 °C to 90 °C in 1 °C steps. The LED Power was set to 10% (PMT = 700 V) while an MST Power of 20% was used. With the reconstructed capillary tray all around enclosing the capillaries the equilibration time could be reduced to 60 s at each temperature step. In order to minimize sample evaporation during the temperature cycle, both capillary ends of the NT.LabelFree Standard Treated Capillaries (NanoTemper Technologies) were sealed with wax and nail polish.

NT Analysis Software Version 1.5.41 (NanoTemper Technologies GmbH) was used to derive thermophoresis values for each temperature step, before aggregation onset temperatures ($T_{agg\ onset}$) for the aggregation spikes in the resulting thermophoresis melting curves were calculated using Origin 8G software (OriginLab Corp., Northampton, MA, USA). The $T_{agg\ onset}$ was defined as the temperature, where the slope of the aggregation event reaches 10% of its maximum. For data evaluation, the first derivative curve was calculated, smoothed (Savitzky-Golay, polynomial order 1, points of the window 3) and interpolated (cubic spline, 6001 points between 30 °C and 90 °C). Afterwards, the temperature value exceeding 10% of the maximal slope was determined as $T_{agg\ onset}$.

V.1.2.2. Dynamic Light Scattering (DLS)

Dynamic light scattering (DLS) was measured at an angle of 173° by using a Zetasizer Nano ZS (Malvern Instruments Ltd, Malvern, UK). Protein particle growth due to aggregation and precipitation after forced thermal degradation was evaluated via the mean intensity of the main peak. Therefore, Ab3 was diluted to 0.1 mg/ml with placebo buffer and subsequently heat-stressed in 2 ml conical micro-centrifuge tubes (VWR International LLC) for 10 min using a ThermoMixer Comfort (Eppendorf AG, Hamburg, Germany). The eight temperatures investigated (40, 60, 70, 75, 80, 82, 85 and 90 °C) were chosen from the progression of the unfolding and aggregation curve by thermophoresis (Figure 14). After cooling down to room temperature and overnight storage at 2-8 °C, the measurements were carried out in triplicates using disposable semi-micro PMMA cuvettes (Brand GmbH & Co. KG, Wertheim, Germany).

V.1.2.3. Intrinsic Fluorescence Emission Spectroscopy (intrinsic FES)

V.1.2.3.1. Cuvette fluorimeter (Jasco FP-8300)

A fluorescence spectrometer (FP-8300) equipped with a water thermostated 4-position cell changer (FCT-816) (both Jasco Deutschland GmbH, Pfungstadt, Germany) was used for reference measurements of stepped thermal unfolding by using intrinsic tryptophan fluorescence. 50 µL protein formulation was carefully pipetted in ultra-micro cell quartz cuvettes (Hellma GmbH & Co. KG, Muellheim, Germany). The solution was overlaid with 500 µL paraffin oil and the cuvette was closed with the provided plastic plug to minimize evaporation. Excitation was performed at 280 ± 2.5 nm and the emission was recorded in the range of 300-380 nm given a bandwidth of 5 nm.
A temperature ramp from 30 °C to 90 °C was executed, measuring a full fluorescence spectrum of the given range in 1 °C steps. The photomultiplier (PMT) voltage was set to 490 V, which guaranteed high initial fluorescence levels, and the excitation path was opened only for the measurements, minimizing photo-bleaching to the recording times of the spectra.
In order to obtain apparent melting temperatures (T_m) from the intrinsic fluorescence emission, the ratio of 350/330 nm was evaluated. The raw data were differentiated (1st derivative), smoothed (Savitzky-Golay, polynomial order 1, points of the window 5), interpolated (cubic spline, 6001 points between 30 °C and 90 °C) and the local maximum was analyzed using the included Impulse Analyzer tool (Origin 8G, OriginLab Corp., Northampton, MA, USA).

V.1.2.3.2. nano Differential Scanning Fluorimetry (Prometheus NT.48)

A Prometheus NT.48 prototype instrument (NanoTemper Technologies) was used for reference measurements of linear thermal unfolding by using intrinsic tryptophan fluorescence. In order to save sample material all samples have been diluted to 0.5 mg/ml with PBS 1X pH 7.4 and subsequently loaded into NT.LabelFree Standard Treated Capillaries (NanoTemper Technologies) by pure capillary force. Sample evaporation from the capillaries at elevated temperatures was reduced by sealing both ends with liquid dip gum (Capillary Sealing Paste, NanoTemper Technologies). A temperature ramp from 30 °C to 100 °C was executed using a slope of 1 °C/min, while intrinsic protein fluorescence was measured continuously at the emission wavelengths of 330 nm and 350 nm.

A preliminary data analysis script (NanoTemper Technologies) was used to evaluate the raw data and assess the intrinsic fluorescence emission ratio of 350 nm/330 nm over increasing temperatures. Origin 8G (OriginLab Corp., Northampton, MA, USA) was used to calculate apparent melting temperatures (T_m) from the respective melting curves. Therefore, the single curves were smoothed (Savitzky-Golay, polynomial order 1, points of the window 15) and differentiated (1st derivative). After another smoothing step (Savitzky-Golay, polynomial order 1, points of the window 25), the data points were interpolated (cubic spline, 6001 points between 30 °C and 90 °C) and the local maximum was determined by using the included Impulse Analyzer tool.

V.1.2.3.3. Capillary fluorimeter (Optim 1000)

An Optim 1000 instrument (Avacta Analytical Ltd, Wetherby, UK, now Unchained Labs, Pleasanton, CA, USA) was used for a comparative linear thermal unfolding and aggregation study. The samples were pipetted in the capillaries of a 9 µl micro-cuvette array (MCA), which were tightly closed with the provided silicone seals using a MCA frame. Using the Optim Client software V1.5.4 (Avacta Analytical) the temperature was linearly increased from 20 °C to 90 °C in a rate of 1 °C per minute, while a hold time of 1 s was used at each well for recording of the fluorescence spectrum. An excitation wavelength of 266 nm was used to induce deep UV intrinsic fluorescence, setting a slit width of 100 µm and an exposure time of 1000 ms. Fluorescence emission was recorded from 249 to 504 nm using a center wavelength of approximately 380 nm. For data evaluation, the fluorescence ratio of 350/330 nm was chosen and unfolding temperatures (T_m) were automatically calculated by the Optim Analysis software V2.0.4 (Avacta Analytical). If necessary, melting temperatures were re-adjusted according to the maxima of the 1st derivative fluorescence curves.

V.1.2.4. Static Light Scattering (SLS)

Additionally to intrinsic fluorescence (section V.1.2.3.3), static light scattering intensity was evaluated from the Optim 1000 measurement for the UV laser at 266 nm. Therefore, the 90° light scattering values at 266 ± 5 nm were plotted over temperature and the aggregation onset temperatures ($T_{agg\ onset}$) were evaluated by using the Optim Analysis software V2.0.4 (Avacta Analytical). For calculation, a Heaviside step function was applied to the 1st derivative curve of static light scattering and the temperature corresponding to the 10% value of the maximum was determined.

V.2. Results and Discussion

V.2.1. Unfolding and Aggregation Investigations

V.2.1.1. MicroScale Thermophoresis (MST)

Figure 14 displays an example of the thermophoresis readout over temperatures for the unfolding and aggregation assay. For clarity and ease of detailed evaluation, the thermophoresis values over temperatures are only demonstrated exemplarily for Ab3, the supposedly most stable antibody in the study. With increasing temperatures, two clear events were detectable, overlaying well for the three capillaries investigated. First, a very broad halo shaped peak at ~ 70 °C is apparent which can be attributed to the early unfolding of the Fc part. The unfolding transition is followed by a remarkably sharp peak at ~ 80 °C, which to our hypothesis corresponds to nascent protein aggregation and precipitation that seems to superimpose the Fab unfolding transition completely.

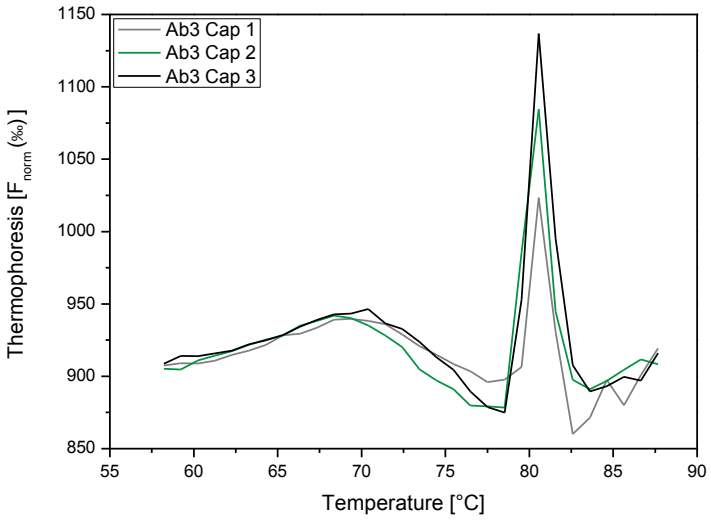

Figure 14: Thermophoresis of Ab3 over temperature exhibits protein unfolding and aggregation (n = 3).

The results of the thermal unfolding and aggregation measurements were verified by a control experiment targeting the stability of the protein under repetitive IR-laser and UV-LED input but without an increase in temperature (Figure 15). The aim of the experiment was to exclude influences of the measurement principle itself and thus strengthen the validity of MST based unfolding and aggregation detection as a prerequisite of successful assay development. The depletion of molecules and therefore the calculated thermophoresis values remained stable in the course of 43 consecutive measurements of the four antibody variants over more than 8.5 hours. This indicates that neither unfolding nor aggregation occurred in the MST setup over time, proving that influences by LED- and IR-radiation are negligible.

Furthermore, distinct differences in the thermophoretic depletion of the two unmodified antibodies (Ab1 and Ab3) were noticeable, allowing for immediate differentiation of the native molecules. Derivation did not drastically change the thermophoretic behavior and therefore the molecule-pairs yield in analogous behavior. These observations match the underlying principles and dependencies of thermophoresis, which state that the movement of a molecule in a temperature gradient is altered by changes in its charge, size or hydration shell.[15] Transferring this theory to our current data set, the two unmodified antibodies (Ab1 and Ab3) differ significantly, while the derivation was only very minimally and showed no influence on the thermophoretic readout.

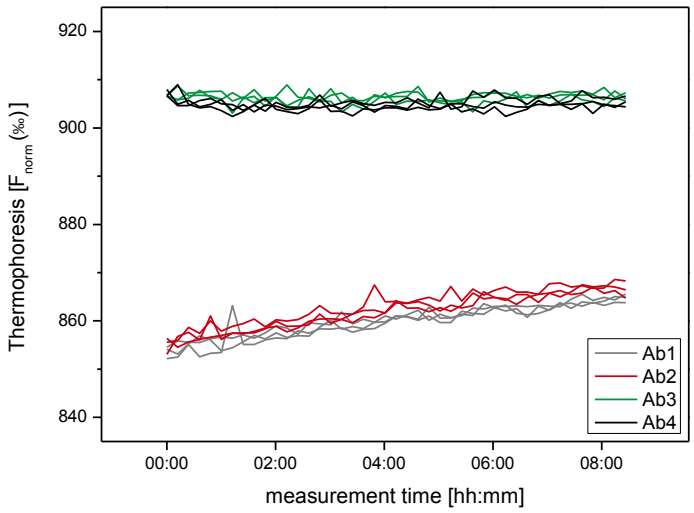

Figure 15: Stability of the thermophoretic depletion of the two antibodies (Ab1 and Ab3) and respective antibody-derivatives (Ab2 and Ab4) to repetitive IR-laser and UV-LED-radiation over time (n ≥ 3).

In the 2nd generation prototype setup, the unfolding and aggregation experiment of all antibody variants was repeated (Figure 16). As elaborately described in section IV.1, this revised experimental setup allows for automatic temperature readout at each step, enhanced and repetitive focusing accuracy, including the correction for thermal expansion, as well as faster thermal equilibration times by using an improved capillary tray. The thermophoresis results illustrate that a clustering of the molecules is possible with one look at the curves. In other words, unfolding of the Fc part of the mAb, as well as protein aggregation, which is potentially induced by Fab unfolding, appears earlier for Ab1 and Ab2. Therefore, Ab3 and Ab4 are considerably more stable in terms of conformational and aggregation stability. Moreover, derivation seems to slightly destabilize the unfolding of the Fc part and prepone the onset temperature of aggregation.

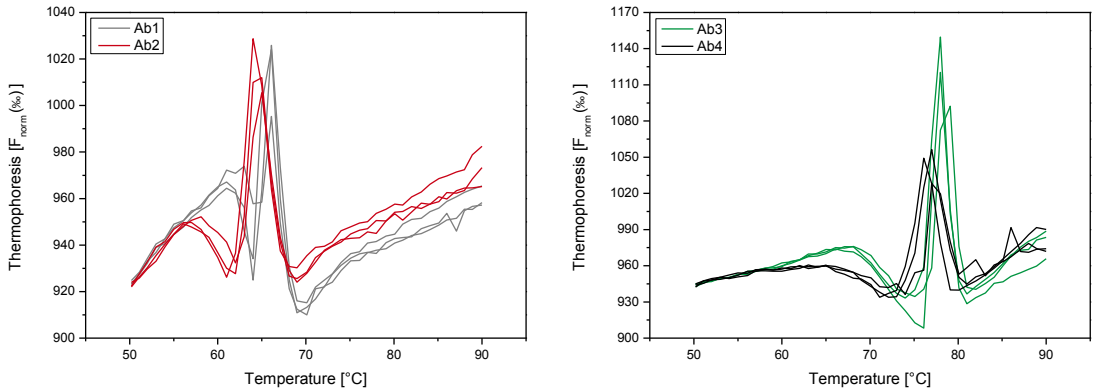

Figure 16: Thermal unfolding and aggregation measurements of Ab1/2 (left) and Ab3/4 (right).

In order to further evaluate the non-native aggregation behavior, we continued the investigation by calculating definite aggregation onset temperatures ($T_{agg\ onset}$) for the thermophoresis evaluation. Therefore, the $T_{agg\ onset}$ was defined as the temperature, where the slope of the aggregation peak exceeds 10% of its maximum. With this definition, aggregation is visualized easiest in the first derivative curve of thermophoresis (Figure 17 – left). Inspecting the raw data as well as comparing the calculated $T_{agg\ onset}$ values (Figure 17 – right) confirms the preliminary conclusions. Ab3 and Ab4 show a higher aggregation stability compared to Ab1 and Ab2. Moreover, derivation promotes protein aggregation and consequently shifts the calculated $T_{agg\ onset}$ to lower temperatures. With these results, the non-native aggregation stability ranking provided by the supplier was confirmed.

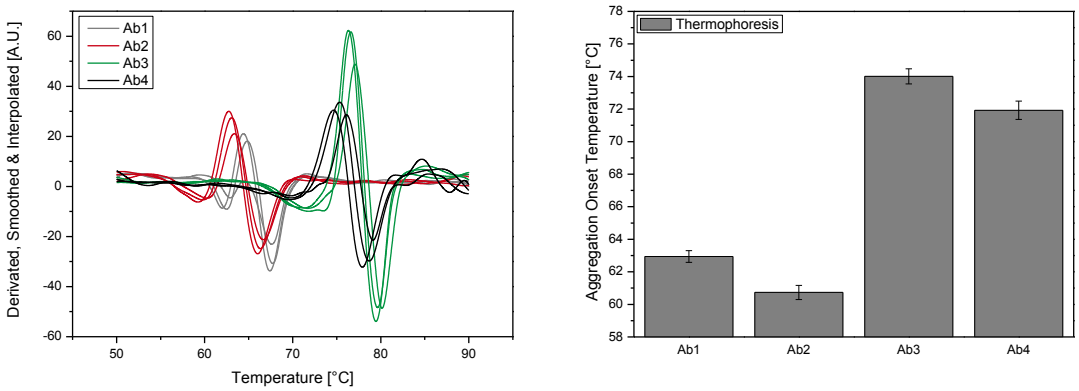

Figure 17: Aggregation onset determination. Left: Smoothed and interpolated first derivative curves of thermophoresis for Ab1 (grey), Ab2 (red), Ab3 (green) and Ab4 (black). Right: Calculated $T_{agg\ onset}$ values (n = 3).

V.2.1.2. Dynamic Light Scattering (DLS)

Dynamic light scattering (DLS) was measured after incubation at elevated temperatures in order to examine the temperature induced aggregation and thereby strengthen our aggregation hypothesis derived from the pronounced sharp peak in thermophoresis (Figure 14). Due to the large sample consumption for external incubation and sample analysis, this benchmark method was only investigated for Ab3. The DLS results exhibit an increase in size distribution over temperature with an onset above 75 °C. Moreover, the area of the main peak is decreasing for the samples ≥ 85 °C, which indicates an enhanced polydispersity due to the generation of multiple aggregate species. These findings are in very good agreement with the thermal unfolding and aggregation measurements by using MST, and confirm the detection of protein aggregates which was observed in the steep rise of thermophoresis values. Additionally, the onset of increasing particle sizes above 75 °C determined by DLS corresponds well to the calculated onset temperature by thermophoresis (74 °C).

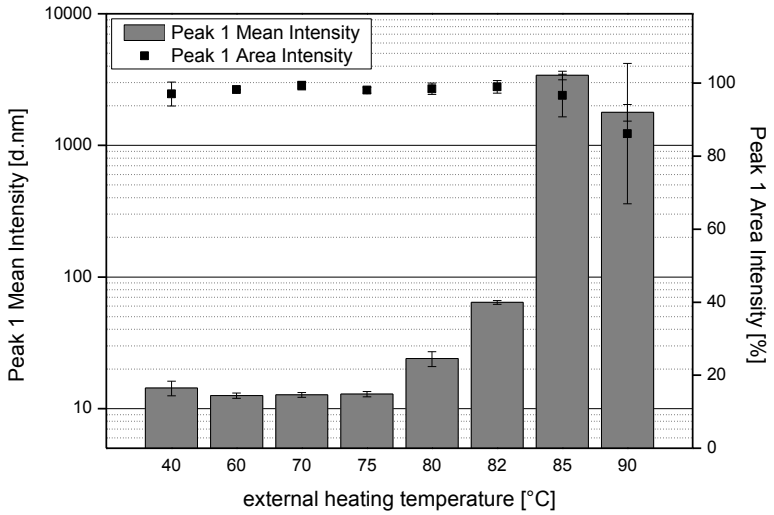

Figure 18: Dynamic light scattering (DLS) of Ab3 after external heating of the samples for 10 minutes (n = 3).

V.2.1.3. Intrinsic Fluorescence Emission Spectroscopy (intrinsic FES)

A comparative protein unfolding study by fluorescence emission spectroscopy (FES) was conducted by the use of three fluorimeters, differing in the data acquisition setup, sample volume, and throughput. One cuvette based spectrofluorimeter (Jasco FP-8300) and two capillary fluorimeters (Optim 1000 and Prometheus NT.48) were investigated, while for all methods the intrinsic fluorescence emission ratio of 350/330 nm was evaluated. Exemplary melting curves from the Prometheus NT.48 measurements are displayed in Figure 19.

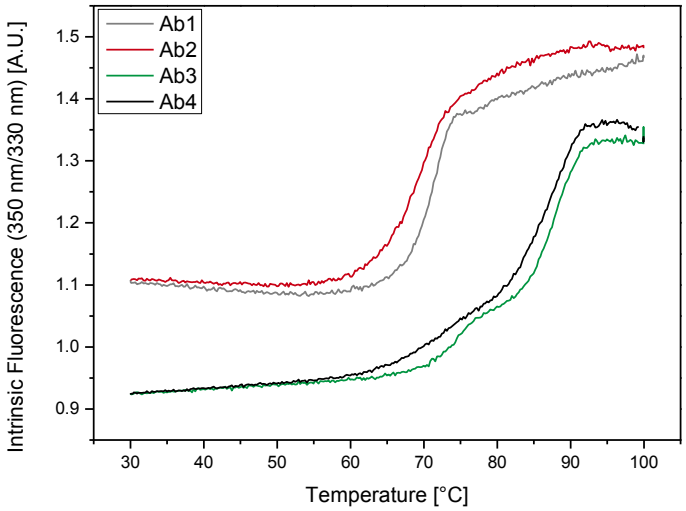

Figure 19: Exemplary melting curves for intrinsic fluorescence by nanoDSF.

The head to head comparison of the derived Tm values for all systems yields in a consistent ranking of conformational stabilities among each other and in comparison to the thermophoresis results (Figure 20 – left). In all fluorescence measurements, the unmodified Ab3 turned out to be the most stable molecule in the screening, while the native Ab1 was substantially less stable. Derivation of both antibodies (Ab3 and Ab1) showed a negative effect on conformational stability, resulting in lower T_m values. This trend is also consistent for the additional unfolding transition (T_m1) that could be resolved for Ab3 and Ab4 (Figure 20 – left, white striped columns). A positive offset of approximately 5 °C was detected for all melting temperatures derived from the Prometheus NT.48 prototype measurements, showing no effect on the overall stability trend and the excellent correlation of the T_m2 values among the methods (Figure 20 – right). The offset can be attributed to an inaccurate temperature calibration in this early prototype stage that was corrected in later versions.

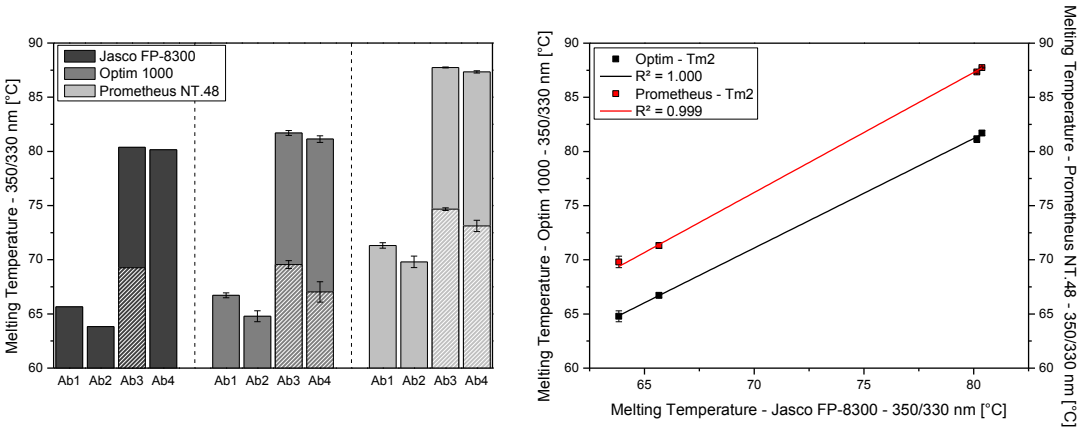

Figure 20: Comparison and correlation of the melting temperatures by intrinsic FES. Left: Comparison of melting temperatures by fluorescence emission ratio (350 nm/330 nm) for Ab1-Ab4 using a cuvette based fluorimeter (Jasco FP-8300, n=1, black) and two capillary fluorimeters (Optim 1000, n=4, dark grey and Prometheus NT.48, n=3, light grey). Right: Correlation of the determined T_m2 values.

V.2.1.4. Static Light Scattering (SLS)

The aggregation phenomenon identified in the thermophoresis melting curves and the thereof derived $T_{agg\ onset}$ values of all antibodies and antibody derivatives were validated by comparative static light scattering measurements. Figure 21 (left) displays the scattering intensities at a wavelength of 266 nm over temperature. All investigated drug products show strong temperature dependent aggregation, which is reflected in increasing light scattering intensities. Furthermore, sample precipitation was indicated by in reverse decreasing values. While the scattering peak intensities are very comparable between the samples, aggregation onset temperatures differ distinctly. The derived aggregation onset pattern (Figure 21 – right) is congruent with the thermophoresis evaluation, identifying Ab3/Ab4 as the couple with the higher aggregation temperatures and confirming the negative effect of derivation on stability in both cases.

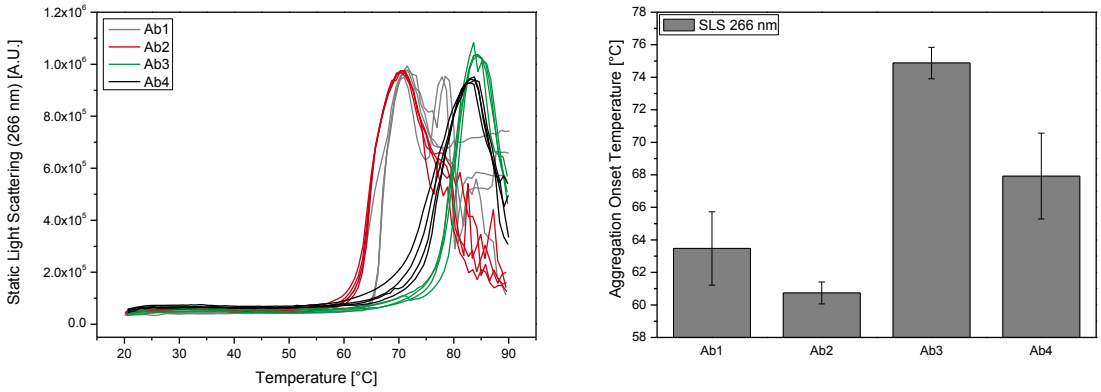

Figure 21: Static light scattering at 266 nm. Left: SLS curve comparison over temperature for Ab1 (grey), Ab2 (red), Ab3 (green) and Ab4 (black). Right: Corresponding $T_{agg\ onset}$ values (n=4).

V.3. Summary and Conclusions

In this case study, we were able to correlate events detected in thermophoresis melting curves to protein unfolding transitions and non-native aggregation of single antibody domains, qualifying MST as a predictive marker for conformational protein stability and aggregation propensity.

Broad, halo shaped peaks in thermophoresis could be allocated to protein melting transitions. Thereby, MST showed an advanced resolution of unfolding events in comparison to intrinsic fluorescence evaluation, revealing the early transition of Fc parts (T_m1) for all investigated antibodies. In contrast, FES was merely able to resolve the unfolding for the Fc parts of the most stable DPs Ab3 and Ab4 (Figure 19). In consequence, thermophoresis offers an additional stability indicator, being crucial for storage at typically low temperatures.

Very sharp peaks in thermophoresis melting curves were found to coincide with an increase in size distribution over temperature measured by DLS and aggregation onset temperatures evaluated from increasing SLS intensities at elevated temperatures. Thus, MST was capable of sensitively detecting protein aggregation, showing lower standard deviations for replicate measurements compared to reference techniques.

Advantages of the MST approach over established methods were the low material consumption by minimal sample volumes and concentrations, as well as the high sensitivity and throughput of MST. Moreover, MST showed sensitivity to unfolding and aggregation events, which on the contrary limited the detection of unfolding transitions in the presence of aggregation events. For the methods evaluating changes in intrinsic fluorescence, aggregation was not observed and the detection of unfolding events was not impacted by simultaneous aggregation.

Evaluating the global picture and the interplay of conformational and aggregation stability, our study revealed a high comparability and coincidence of Fab unfolding and protein aggregation events. This concurrence strengthens the hypothesis of APRs, present in the Fab region, being exposed during protein unfolding and consequently induce colloidal protein-protein interactions which result in irreversible protein aggregation and precipitation.

V.4. References

1. Ecker DM, Jones SD, Levine HL. 2015. The therapeutic monoclonal antibody market. mAbs 7(1):9-14.

2. Carter PJ. 2011. Introduction to current and future protein therapeutics: A protein engineering perspective. Experimental Cell Research 317(9):1261-1269.

3. Goswami S, Wang W, Arakawa T, Ohtake S. 2013. Developments and challenges for mAb-based therapeutics. Antibodies 2(3):452-500.

4. Elvin JG, Couston RG, van der Walle CF. 2013. Therapeutic antibodies: Market considerations, disease targets and bioprocessing. International Journal of Pharmaceutics 440(1):83-98.

5. Beck A, Goetsch L, Dumontet C, Corvaïa N. 2017. Strategies and challenges for the next generation of antibody-drug conjugates. Nature Reviews Drug Discovery 16(5):315-337.

6. Uchiyama S. 2014. Liquid formulation for antibody drugs. Biochimica et Biophysica Acta (BBA) - Proteins and Proteomics 1844(11):2041-2052.

7. Beck A. 2011. Biosimilar, biobetter and next generation therapeutic antibodies. mAbs 3(2):107-110.

8. Rosati S, Yang Y, Barendregt A, Heck AJ. 2014. Detailed mass analysis of structural heterogeneity in monoclonal antibodies using native mass spectrometry. Nature Protocols 9(4):967-976.

9. Wu H, Kroe-Barrett R, Singh S, Robinson AS, Roberts CJ. 2014. Competing aggregation pathways for monoclonal antibodies. FEBS Letters 588(6):936-941.

10. Bork P, Holm L, Sander C. 1994. The immunoglobulin fold: Structural classification, sequence patterns and common core. Journal of Molecular Biology 242(4):309-320.

11. Brummitt RK, Nesta DP, Chang L, Chase SF, Laue TM, Roberts CJ. 2011. Nonnative aggregation of an IgG1 antibody in acidic conditions: Part 1. Unfolding, colloidal interactions, and formation of high-molecular-weight aggregates. Journal of Pharmaceutical Sciences 100(6):2087-2103.

12. Roberts CJ, Das TK, Sahin E. 2011. Predicting solution aggregation rates for therapeutic proteins: Approaches and challenges. International Journal of Pharmaceutics 418(2):318-333.

13. Wang X, Singh SK, Kumar S. 2010. Potential aggregation-prone regions in complementarity-determining regions of antibodies and their contribution towards antigen recognition: A computational analysis. Pharmaceutical Research 27(8):1512-1529.

14. Wang X, Das TK, Singh SK, Kumar S. 2009. Potential aggregation prone regions in biotherapeutics: A survey of commercial monoclonal antibodies. mAbs 1(3):254-267.

15. Duhr S, Braun D. 2006. Why molecules move along a temperature gradient. Proceedings of the National Academy of Sciences 103(52):19678-19682.

Chapter VI
Human Serum Albumin (HSA)

In this case study, a small pH screening of the model protein HSA was prepared in PBS to further develop thermal unfolding and aggregation investigations by using MST and to perform the first feasibility study of thermo-optical protein characterization (TOPC). First, the influence of different pH values on shape changes and shifts in thermophoresis and t-jump melting curves was examined and compared. The derived pH effects on the thermal unfolding as well as aggregation stability of HSA were then benchmarked by intrinsic tryptophan fluorescence and static light scattering measurements. Additionally, the sample set was used to evaluate different approaches for an effective prevention of solvent evaporation in the MST setup, setting the stage for more extensive formulation screenings. For TOPC, the consequences of high power IR-laser heating were inspected for the different formulation pH values and confronted with the results of the unfolding and aggregation investigations.

VI.1. Materials and Methods

VI.1.1. Materials

Human serum albumin (HSA) is a 66 kDa model protein that has been extensively used in fundamental research including folding and unfolding studies. The molecule contains only one single tryptophan residue at position 214 that will be used to investigate the unfolding and aggregation behavior in dependency of the solution pH in various analytical setups and serve as a reference standards for prototype and assay modifications.[1-4]

An overview of materials used in this study can be found in Table 9.

Table 9: Overview of materials used in the HSA study.

Material	Supplier	Art.-number	Lot-number
Albumin from human serum (HSA), essentially fatty-acid free	Sigma Aldrich, St. Louis, MO, USA	A3782-5G	107K75651
Roti-Stock 10x PBS	Carl Roth GmbH & Co KG, Karlsruhe, Germany	1058.1	423206137
Water AnalaR Normapur	VWR International, Radnor, PA, USA	102927G	-

VI.1.2. Formulations

A phosphate buffered saline (PBS) 10x stock solution was diluted to 1x with deionized water and the pH values were adjusted to the target pH values of 6.0, 6.5, 7.0 and 7.5 by titration using NaOH or HCl respectively for each placebo solution. The pH values were measured by using a HI83141 pH-meter, equipped with a HI1230 electrode (Hanna Instruments Deutschland GmbH, Voehringen, Germany). Subsequently, essentially fatty-acid free Human Serum Albumin (HSA) was dissolved in the freshly prepared placebo solutions. After complete dissolution, the protein concentration was measured by absorbance using a NanoPhotometer P330 instrument equipped with and a NanoPhotometer P-Class Submicroliter Cell (Implen GmbH, Munich, Germany) and an extinction coefficient of $\varepsilon(HSA)=0.531\ ml*mg^{-1}*cm^{-1}$ (at 279 nm)[3]. Subsequently, the concentration was adjusted to 0.75 mg/ml each by dilution with the respective placebo buffer. The formulations were aliquoted and stored at - 80 °C upon usage. After thawing and equilibration at room temperature, the samples were centrifuged for at least 5 min at 15000 rpm to remove insoluble aggregates potentially induced by the freeze-thaw cycle.

VI.1.3. Unfolding and Aggregation Investigations

VI.1.3.1. MicroScale Thermophoresis (MST)

MST was used for predictive unfolding and aggregation studies by using the 2nd generation prototype setup (NanoTemper Technologies GmbH, Munich, Germany). The temperature was increased from 30 °C to 90 °C in 1 °C steps. Fluorescence excitation LED Power was set to 2% (PMT=780 V), while an MST Power of 20% was used. These settings optimize the signal to noise ratio while photo-bleaching effects can be reduced by minimal excitation LED intensities. NT.LabelFree Zero Background Standard Treated Capillaries (NanoTemper Technologies) were used exclusively to reduce the fluorescence background/capillary auto-fluorescence and therefore increase measurement sensitivity.

For the pH screening experiment, the capillaries were closed with sealing wax (NanoTemper Technologies) on one side to reduce sample evaporation during the temperature cycle. In order to achieve a more effective capillary sealing, additional measurements were performed under the use of liquid dip gum (Capillary Sealing Paste, NanoTemper Technologies) applied to both capillary ends.

The measurements were performed by using NT Control software version 2.1.31, while NT Analysis software version 1.5.41 (NanoTemper Technologies) was used to calculate thermophoresis and t-jump values for each temperature step. Subsequently, Origin 8G (OriginLab Corp., Northampton, MA, USA) was used to calculate melting temperatures (T_m) for the respective melting curves of both data evaluations by smoothing (Savitzky-Golay, polynomial order 1, points of the window 3), interpolation (cubic spline, 6001 points between 30 °C and 90 °C) and local minimum analysis using the included Impulse Analyzer tool.

VI.1.3.2. Intrinsic Fluorescence Emission Spectroscopy (intrinsic FES)

A fluorescence spectrometer (FP-8300) equipped with a water thermostated 4-position cell changer (FCT-816) (both Jasco Deutschland GmbH, Pfungstadt, Germany) was used for reference measurements of stepped thermal unfolding by using intrinsic tryptophan fluorescence. 50 µL protein formulation was carefully pipetted in ultra-micro cell quartz cuvettes (Hellma GmbH & Co. KG, Muellheim, Germany). The solution was overlaid with 500 µL paraffin oil and the cuvette was closed with the provided plastic plug to minimize evaporation. Excitation was performed at 280 ± 2.5 nm and the emission was recorded in the range of 300 nm to 380 given a bandwidth of 5 nm. A temperature ramp from 30 °C to 90 °C was executed, measuring a full fluorescence spectrum of the given range in 1 °C steps. The PMT voltage was set to 540 V, which guaranteed high initial fluorescence levels, and the excitation path was opened only for the measurements, minimizing photo-bleaching to the recording times of the spectra.
In order to obtain apparent melting temperatures (T_m), intrinsic fluorescence emission was evaluated in the range from 330 nm to 380 nm. The raw data were differentiated (1st derivative), smoothed (Savitzky-Golay, polynomial order 1, points of the window 3), interpolated (cubic spline, 6001 points between 30 °C and 90 °C) and the local minimum was analyzed using the Impulse Analyzer tool (Origin 8G, OriginLab Corp., Northampton, MA, USA).

VI.1.3.3. Static Light Scattering (SLS)

An Optim 1000 instrument (Avacta Analytical Ltd, Wetherby, UK, now Unchained Labs, Pleasanton, CA, USA) was used for a comparative linear thermal aggregation study. The samples were pipetted in the capillaries of a 9 µl micro-cuvette array (MCA), which were tightly closed with the provided silicone seals using a MCA frame. The temperature was linearly increased from 15 °C to 90 °C in a rate of 1 °C per minute. Between 30 °C and 90 °C, static light scattering intensity was plotted over temperature and the aggregation onset temperatures ($T_{agg\ onset}$) were evaluated for 90° light scattering at 266 ± 5 nm by using the Optim Analysis software V2.0.4 (Avacta Analytical). For calculation, a Heaviside step function was applied to the 1st derivative curve of static light scattering and the temperature corresponding to the 10% value of the maximum was determined.

VI.1.3.4. Thermo-Optical Particle Characterization (TOPC)

TOPC was used for predictive thermal aggregation studies by IR-laser induced stress testing. The fluorescence excitation LED power was set to 2% (PMT=780 V) and heat stress was applied by using an IR-laser power of 170%. Changes in intrinsic fluorescence were detected for 175 s in total. After recording initial fluorescence for 5 s, the effects of the IR-laser input were tracked for 150 s. Subsequently, the laser was turned off again and backdiffusion was measured for additional 20 s.

In order to complement the observations and conclusions during TOPC with a well-known assay, a standard MST experiment at a laser power of 45% was appended by using the same pre-stressed samples. The resulting MST timetraces were compared in regards of abnormalities in the curve shapes.

All measurements were performed in singlicates at an ambient assay temperature of 25°C by exclusively using NT.LabelFree Zero Background Standard Treated Capillaries (NanoTemper Technologies). NT Control software version 2.1.31 was used to perform the measurements, while the intrinsic fluorescence timetraces were normalized, exported and MST as well as T-Jump values were calculated by using NT Analysis software version 1.5.41 (both NanoTemper Technologies).

The TOPC experiments were analyzed by calculating mean values and standard deviations for all formulations in the timeframe between 125 and 150 s. All calculations and data plotting were performed with Origin 8G software (OriginLab Corp., Northampton, MA, USA).

VI.2. Results and Discussion

VI.2.1. Unfolding and Aggregation Investigations

VI.2.1.1. MicroScale Thermophoresis (MST)

Thermal unfolding and aggregation investigations were performed in order to further qualify MST for this application, by optimizing the assay and comparing the results to benchmark methods as well as orthogonal approaches. The resulting T-jump (Figure 22 – left) as well as thermophoresis (Figure 22 – right) values were found to change dramatically with increasing temperatures, leading to melting curves with pronounced and broad negative peaks. These peaks were assigned to the single thermal unfolding event of HSA.[2,5] Moreover, changing the formulation pH value led to shifts in the unfolding peaks for both evaluations suggesting the detection of a stabilizing/destabilizing effect. In detail, decreasing pH values lead to a temperature increase of the peak position and consequently higher apparent T_m values. This effect corresponds to increasing conformational stability with decreasing pH values.

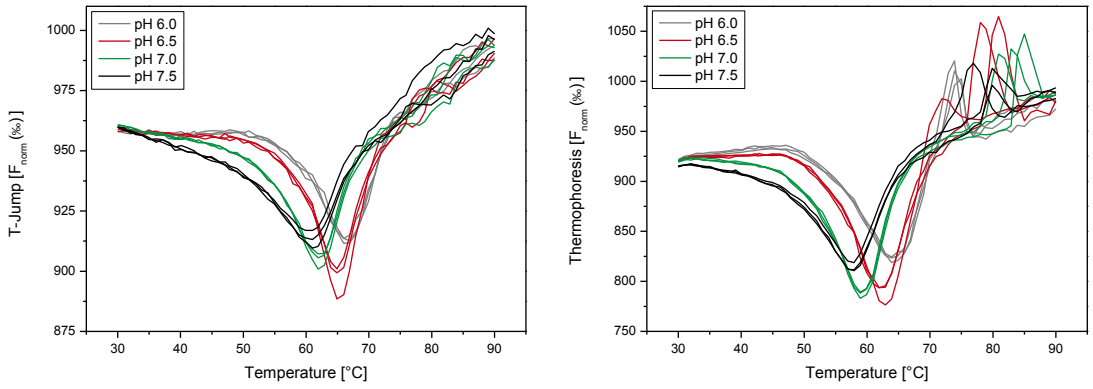

Figure 22: Melting curves by t-jump (left) and thermophoresis (right) for the HSA pH screening. pH 6.0 (grey), 6.5 (red), 7.0 (green) and 7.5 (black) (n=3).

Figure 23 displays the T_m analysis of the negative peaks for the t-jump and thermophoresis evaluation, confirming the inspection from the raw data curves with highest conformational stability at pH 6.0. Furthermore, this illustration exhibits a temperature difference between the T_m values determined by t-jump and thermophoresis in the order of 2-3 °C. This divergence fits in direction and extent to the expected temperature increase induced by the IR-laser, leading to earlier unfolding, e.g. lower T_m values, for the thermophoresis evaluation.

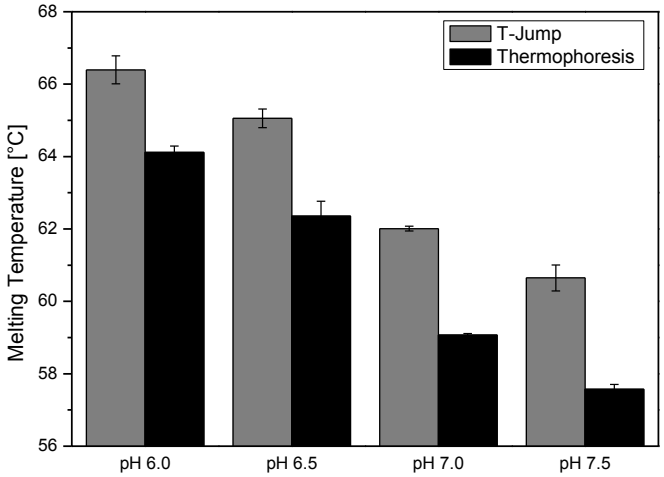

Figure 23: Melting temperatures (T_m) for the thermophoresis and for the t-jump data evaluations.

Evaluating the thermophoresis/t-jump melting curves (Figure 22) in more detail, another observation becomes apparent: In contrast to the t-jump results, thermophoresis melting curves show further, very sharp peaks at temperatures above the melting transition, additionally indicating non-native protein aggregation and/or precipitation. Accordingly, this clustering of single molecules affects the overall protein structure including the hydration shell, but not the direct surrounding of the single tryptophan moiety, remaining the t-jump values unchanged. At a closer look it is noticeable that at pH 6.0, the peaks for the different capillaries investigated occur simultaneously immediate after unfolding, while the appearance of additional peaks for the other pH values happens rather diffused and random mostly at higher temperatures. Our hypothesis on the random aggregation events visible at the higher pH values comprises solvent evaporation from the capillaries at elevated temperatures. The associated concentration increase might lead to molecular crowding and occasional protein aggregation, depending on the extent of solvent loss. The observance that the aggregation signal at pH 6.0 appears earlier and synchronized for all capillaries, leads to a different conclusion. In contrast to the evaporation aggregation at pH 6.5-7.5, aggregation at pH 6.0 seems to be independent of evaporation and might be of intrinsic origin. In consequence, low pH values would lead to increased conformational stability but decreased colloidal stability.

In order to further classify the evaporation and aggregation effects visible in the melting curves of the pH screening, an alternative sealing procedure was evaluated. Liquid dip gum applied to both capillary ends was tested in a head-to-head comparison with sealing by wax on one side. Both, pH 6.0 and pH 7.5 were investigated scrutinizing the prevention of evaporation and the nature of aggregation in parallel. Figure 24 elucidates that the peak for pH 7.5 completely vanishes by the change from wax to gum sealing. This suggests an effective hindrance of sample evaporation and inhibition of concentration dependent aggregation. At pH 6.0 the capillary sealing has evidently no effect on the peak formation and thus aggregation occurs concentration- and evaporation-independent. These findings confirm our hypothesis of aggregation and precipitation being favored at low pH conditions.

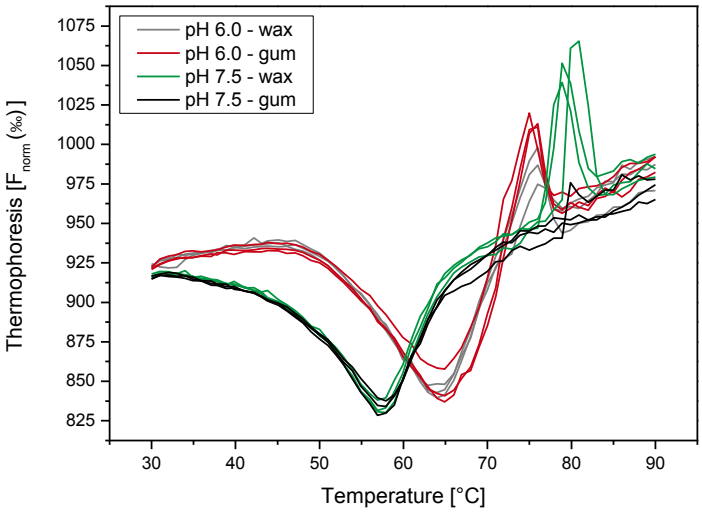

Figure 24: Thermophoresis melting curves for comparison of capillary closure by liquid dip gum at both sides vs. sealing by wax at one side (n=3).

An additional control experiment was performed proving the effective capillary sealing by liquid dip gum (Figure 25) The measurement represents the worst case scenario of a full capillary tray load (16 capillaries) combined with 300 seconds equilibration time at each temperature, leading to an extended total runtime of 15 hours. It impressively proves that the aggregation peaks in thermophoresis vanish under capillary closure by liquid dip gum for all eight capillaries, underlying the effective inhibition of evaporation and the consequent hindering of up-concentration and aggregation.

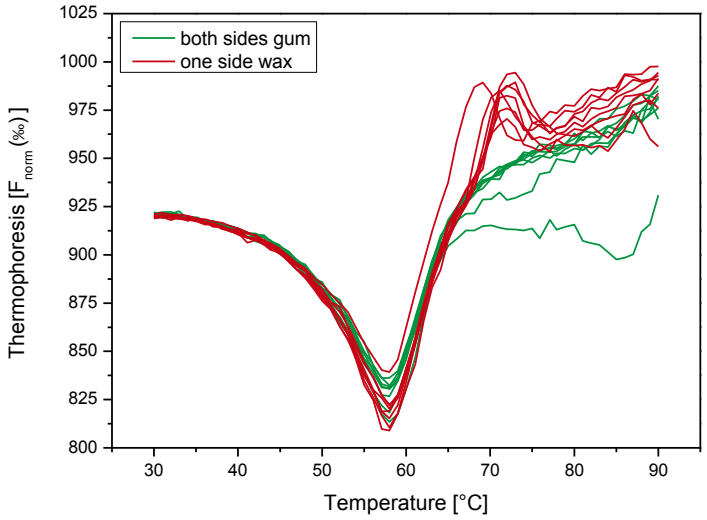

Figure 25: Head-to-head comparison of capillary closure by liquid dip gum at both sides vs. sealing wax at one side (n=8).

VI.2.1.2. Intrinsic Fluorescence Emission Spectroscopy (intrinsic FES)

The unfolding event of HSA followed by intrinsic tryptophan fluorescence measured in a standard cuvette fluorimeter is rather weak, showing one negative sigmoid unfolding transition (Figure 26). These findings are in contrast to the distinct peak shaped thermophoresis and t-jump melting curves in section VI.2.1.1. However, the resulting T_m values show a comparable trend of increasing unfolding temperatures when reducing the pH value, which results in the highest conformational stability for HSA at pH 6.0 (Figure 27). Moreover, the unfolding curve for HSA at pH 6.0 by intrinsic fluorescence shows a drop in fluorescence at approximately 80 °C that does not occur for higher pH values (Figure 26). This emission decrease is attributed to strong protein aggregation, leading to precipitation and consequently removal of sample material from the optical path. Therefore, the fluorimeter data confirm the stability ranking by t-jump and thermophoresis, identifying pH 6.0 as the optimum in terms of conformational stability but entailing the highest risk for non-native protein aggregation at temperatures above the melting point.

Overall, the data quality of the fluorescence measurements is comparable to MST, while the sample consumption of the cuvette fluorimeter is ~ 5-fold and the analysis time per sample is approximately 30% higher. Another argument for the MST approach is that it is parallelizable for analyzing up to 16 samples in parallel whereas standard fluorimeters are often limited to 4 or maximum 8 sample holders.

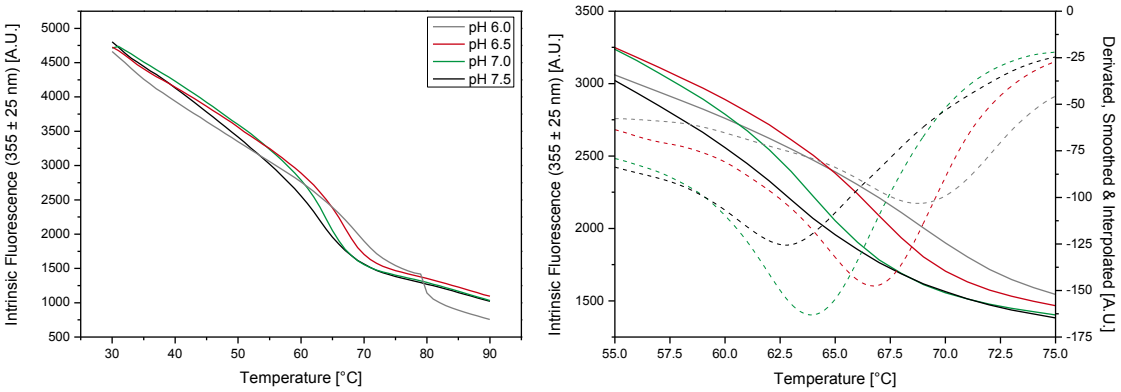

Figure 26: Melting curves of HSA by using intrinsic fluorescence (n=1). Left: Full view melting curves for HSA in PBS pH 6.0 (grey), 6.5 (red), 7.0 (green) and 7.5 (black). Right: Zoom of melting curves (lines) and corresponding smoothed and interpolated first derivative functions (dotted lines).

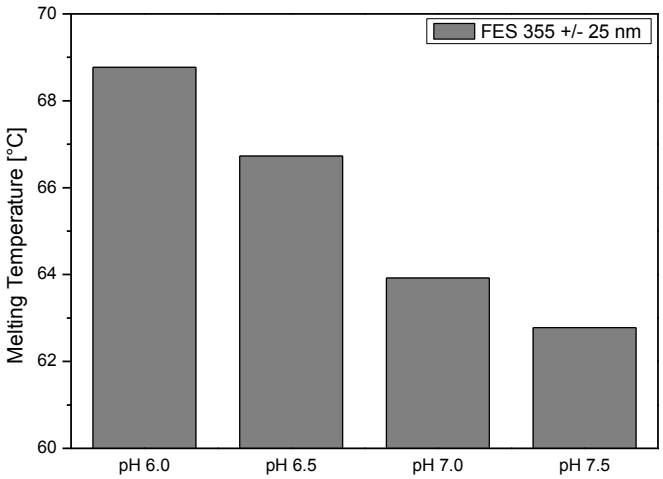

Figure 27: Melting temperatures (Tm) for intrinsic fluorescence (355 ± 25 nm).

The evaluation of initial intrinsic fluorescence over temperatures from the pH screening experiment in the MST setup (Figure 28) furthermore strengthens the assumption of increasing aggregation instabilities at low pH values due to an additional fluorescence decrease at temperatures above 70 °C which is potentially caused by precipitation of sample material. These observations are in very good alignment with the intrinsic fluorescence curves measured in the cuvette based fluorimeter.

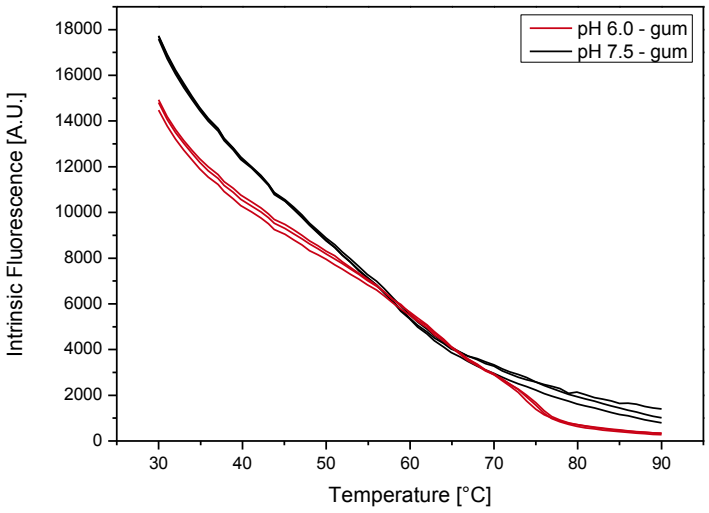

Figure 28: Intrinsic fluorescence melting curves for comparison of capillary closure by liquid dip gum at both sides vs. sealing by wax at one side.

VI.2.1.3. Static Light Scattering (SLS)

Static light scattering measurements were carried out in order to validate the presumption of decreasing aggregation stabilities at lower pH values. Aggregation was detected at all four pH values, while a steeper slope in light scattering was found at lower pH values (Figure 29 – left) what leads to overall increased integrated light scattering values (Figure 29 – right). Therefore, SLS fully confirms the previously described pH dependent aggregation.

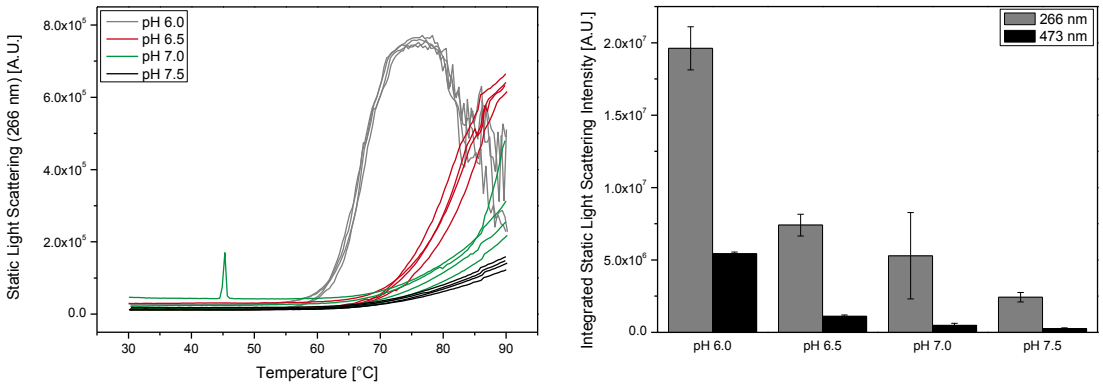

Figure 29: Static light scattering (SLS) at 266 nm of 0.75 mg/ml HSA in PBS. Left: SLS comparison over temperatures at pH 6.0 (grey), 6.5 (red), 7.0 (green) and 7.5 (black). Right: Corresponding integrated static light scattering intensities.

At the same time, the apparent aggregation onset temperatures are similar for pH 6.5 to 7.5 and differ only for pH 6.0 where scattering increases earlier (Figure 30). Moreover, this formulation shows distinct precipitation at temperatures above ~ 75 °C which is observable in the declining scattering at higher temperatures. This is congruent with the emerging extra peak in the thermophoresis and t-jump melting curves as well as signal loss for the fluorescence measurements.

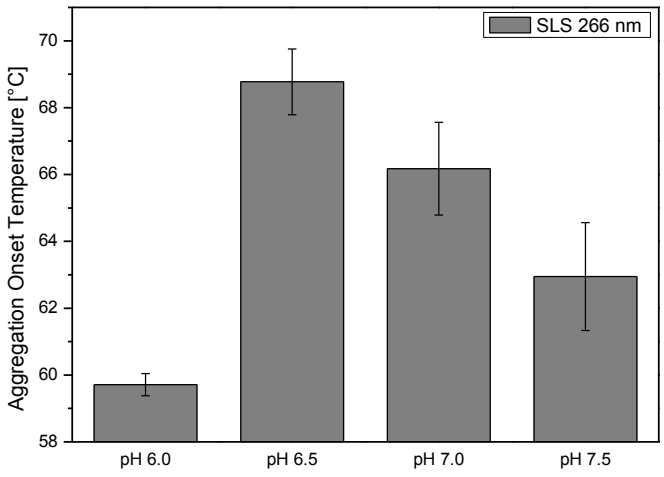

Figure 30: Aggregation onset temperatures for static light scattering at 266 nm.

VI.2.2. Forced Degradation Studies

Orthogonal forced degradation studies were performed in order to underline the consistent findings from the thermal unfolding and aggregation screening. Figure 31 and Figure 32 display the normalized intrinsic fluorescence timetraces recorded within the TOPC experiments for the HSA pH screening. Large differences in the curve shapes are apparent with changing pH values. While the formulations at pH 7.5 and pH 7.0 show neither pronounced aggregation, nor precipitation indicating events under IR-laser heating, the formulations at pH 6.5 and especially at pH 6.0 are affected by heat stressing. For pH 6.5, a slight increase in fluorescence is registered that suggests the accumulation of protein aggregates in the focal area, without formation of insoluble precipitating particles. Furthermore, a much steeper increase is apparent for HSA at pH 6.0 that is, at later timescales, superimposed by a rise in fluorescence scattering. Accordingly, these observations are indicating the emergence of an even larger aggregate fraction or larger sized particles that precipitate under constant temperature input. Moreover, the deposition of precipitated material within the capillary additionally causes higher fluorescence levels after laser shutdown and backdiffusion of molecules.

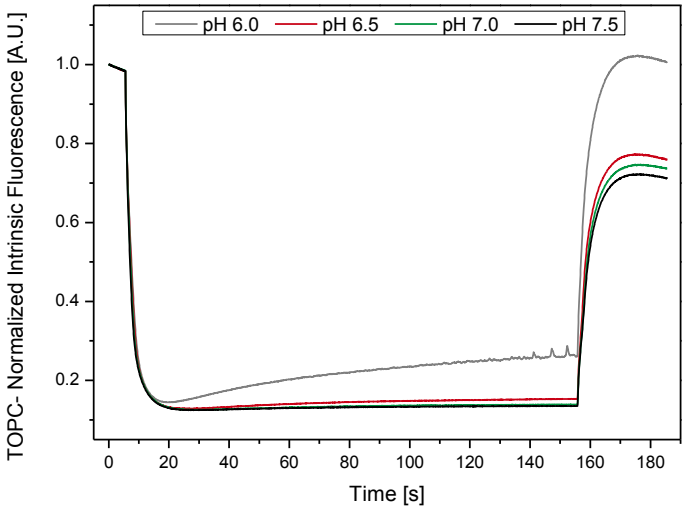

Figure 31: Normalized intrinsic fluorescence signal over time for thermo-optical protein characterization (TOPC) within the HSA pH screening.

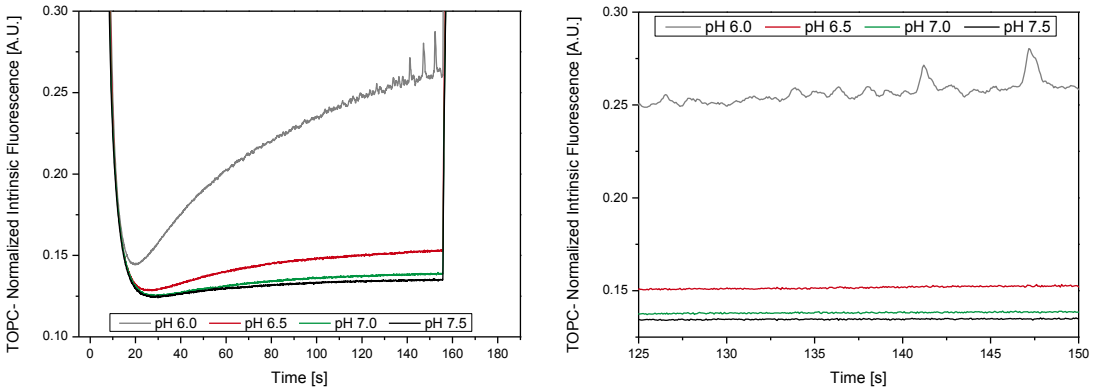

Figure 32: Zoom-in of the TOPC curves to highlight the differences in fluorescence level and scattering (left) and the timeframe between 125 and 150 s which was used for analysis (right).

The observations from the raw data are confirmed by analysis of mean fluorescence and standard deviation values in the timeframe of 125-150 s (Figure 33). Again, soluble aggregates are anticipated to enhance the mean fluorescence values while the formation of insoluble aggregates increases the standard deviation. Unsurprisingly, the HSA formulation at pH 6.0 exhibits the highest values in both evaluations, what underlines the intense pH dependent aggregation and precipitation. Increasing the pH to 6.5 stabilizes the protein widely and only a slightly increased fluorescence level and standard deviation is observed. Among the higher pH values 7.0 and 7.5, the stability to heat exposure reaches a plateau and only marginal differences remain.

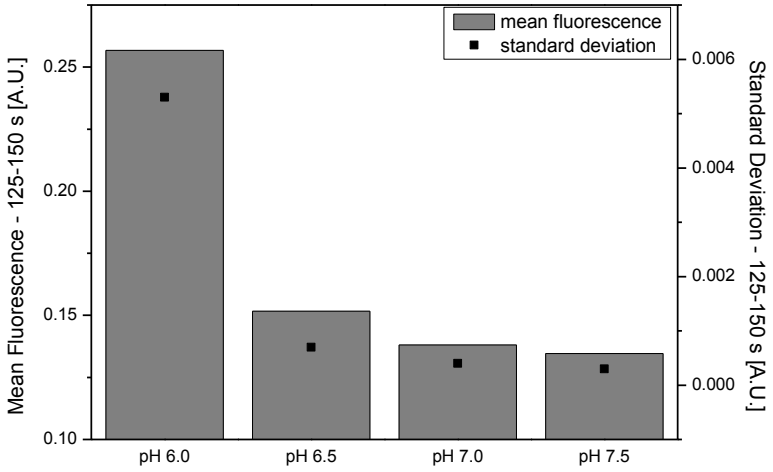

Figure 33: TOPC data analysis of mean fluorescence and standard deviation in the measurement timeframe between 125 and 150 s.

Subsequently to the TOPC measurement, the same samples/capillaries were re-investigated by means of a standard MST experiment (Figure 34). MST measurements with analogous settings were executed for the stepped thermal unfolding and aggregation investigations (Figure 22), which resulted in highly comparable thermophoresis and t-jump values between all investigated formulations at the starting temperature of 30 °C. As expected, the MST timetraces after thermal stressing in the TOPC setup show substantial deviations between the different pH values. For the formulation at pH 6.0, an overall reduced thermophoretic depletion combined with a non-exponential timetrace is obtained. Also in standard MST, this observation can be attributed to the presence of protein aggregates periodically flowing through the focal volume.[6] In comparison to the TOPC experiment, the particulate flow occurs at a drastically reduced frequency, as the convective transport is reduced at the decreased IR-laser power and heating rate.[7-9] Furthermore, a higher thermophoresis value was also obtained for pH 6.5, but the timetrace was found to be perfectly exponential and thus the absence of insoluble aggregates/particles was indicated. At pH 7.0 and pH 7.5 the protein was not affected by thermal stress and the MST timetraces remained unchanged.

In conclusion, MST analysis of pre-stressed or stored samples can be used as additional measure of protein integrity and quality, when compared to unstressed or fresh samples. An identical application for a purely intrinsic fluorescence based instrument has been recently implemented by NanoTemper Technologies with the introduction of the Tycho NT.6. Instead of MST, this system measures the fluorescence ratio of 350 nm/330 nm and evaluates changes in the initial value (ratio) and the signal amplitude (Δ ratio) of a thermal unfolding scan.

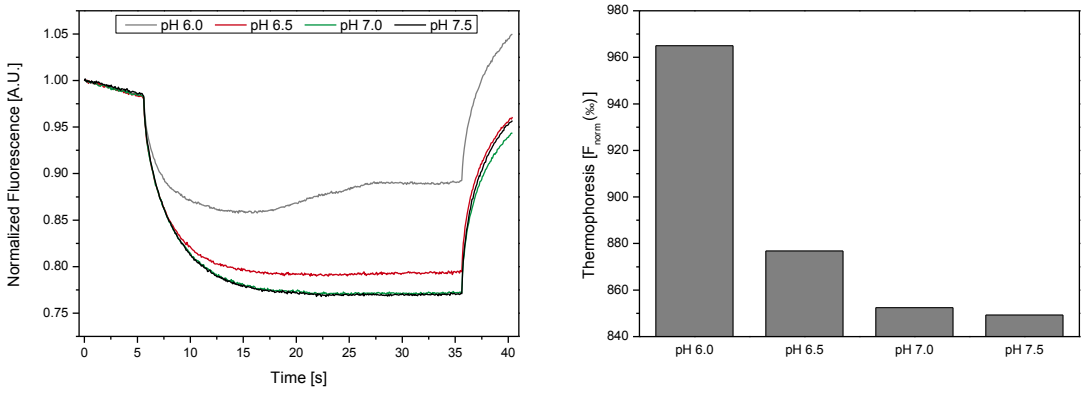

Figure 34: Standard MST measurement of the samples pre-stressed within the TOPC experiment. Left: Normalized MST timetraces. Right: Data analysis of the parameters thermophoresis and t-jump.

VI.3. Summary and Conclusions

MST and TOPC were able to reveal changes in conformational protein characteristics as well as aggregation stability facilitating a rapid stability profiling for an exemplary pH screening setup of HSA.

Thermal unfolding and aggregation investigations by using MST revealed an accurate stability profiling, analyzing up to 16 conditions in parallel with a sample volume of only 10 µl each. By contrast, the benchmark measurement of intrinsic fluorescence by using the Optim 1000 instrument exposed a very high noise level, which made the evaluation of unfolding temperatures with this setup impossible. In comparison to a standard cuvette based fluorimeter, our measurement approach required substantially lower sample volumes and generated a higher throughput, as in detail demonstrated within our publication about isothermal chemical denaturation investigations by intrinsic fluorescence[10]. Moreover, the generated stability rankings by MST and FES were found to be highly comparable (Figure 35) yielding a positive effect of lower pH values on the unfolding stability of HSA.

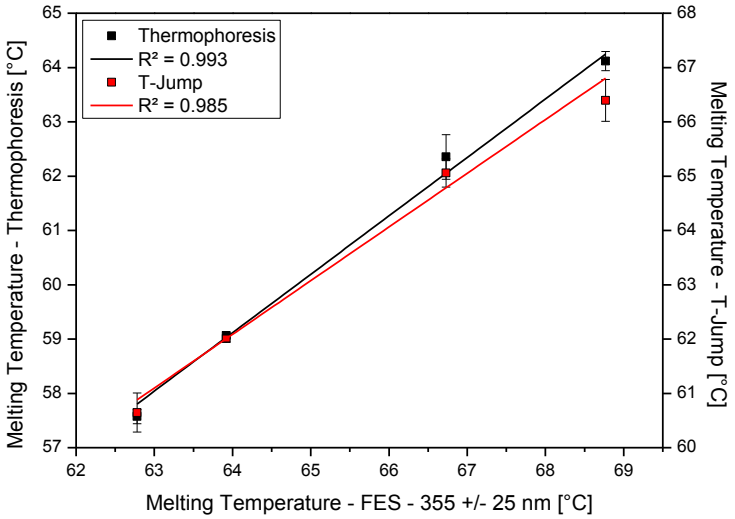

Figure 35: Correlation of melting temperatures from intrinsic fluorescence with thermophoresis (black dots and line) and t-jump (red dots and line).

Additionally, changes in non-native protein aggregation and/or precipitation were indicated by the occurrence of additional spikes in thermophoresis data evaluation. This assumption was confirmed by a prominent decrease in intrinsic fluorescence emission above melting temperature, not occurring for the formulations between pH 6.5 and 7.5 and therefore probably being related to molecular precipitation.

Finally, static light scattering displayed strongest aggregation for pH 6.0 and additional precipitation at temperatures above ~ 75 °C.

Particularly with regard to future more extended and time consuming formulation screenings, an effective capillary sealing technique was implemented by the use of liquid dip gum that prevents sample evaporation from the capillaries for hours, even at elevated temperatures.

Furthermore, TOPC and subsequent MST analysis revealed considerable differences between the pH values investigated. While the formulations at pH 7.5 and pH 7.0 remain stable under continuous laser input, fluorescence values and timetrace scattering increases over time for pH 6.5 and especially for pH 6.0. These events are attributed to the formation of soluble aggregates and precipitates flowing through the measurement focus. With these results, the trend in colloidal stability received from the thermal unfolding and aggregation studies was confirmed, increasing the aggregation and precipitation propensity with decreasing pH values.

In summary, model protein and formulations were well chosen because an inversely proportional stability trend was received for conformational and colloidal stability. In real formulation practice, these results would demand for a compromise between lowest aggregation propensity at high pH and highest thermal stability at low pH.

VI.4. References

1. Moriyama Y, Ohta D, Hachiya K, Mitsui Y, Takeda K. 1996. Fluorescence behavior of tryptophan residues of bovine and human serum albumins in ionic surfactant solutions: A comparative study of the two and one tryptophan(s) of bovine and human albumins. Journal of Protein Chemistry 15(3):265-272.

2. Barone G, Giancola C, Verdoliva A. 1992. DSC studies on the denaturation and aggregation of serum albumins. Thermochimica Acta 199:197-205.

3. Product Information Sheet - Albumin, human. Available at: https://www.sigmaaldrich.com/content/dam/sigma-aldrich/docs/Sigma/Product_Information_Sheet/a3782pis.pdf. Accessed: February 18, 2018.

4. Wetzel R, Becker M, Behlke J, Billwitz H, Bohm S, Ebert B, Hamann H, Krumbiegel J, Lassmann G. 1980. Temperature behaviour of human serum albumin. European Journal of Biochemistry 104(2):469-478.

5. Farruggia B, Picó GA. 1999. Thermodynamic features of the chemical and thermal denaturations of human serum albumin. International Journal of Biological Macromolecules 26(5):317-323.

6. Jerabek-Willemsen M, Wienken CJ, Braun D, Baaske P, Duhr S. 2011. Molecular interaction studies using microscale thermophoresis. Assay and Drug Development Technologies 9(4):342-353.

7. Duhr S, Arduini S, Braun D. 2004. Thermophoresis of DNA determined by microfluidic fluorescence. The European Physical Journal E 15(3):277-286.

8. Duhr S, Braun D. 2006. Why molecules move along a temperature gradient. Proceedings of the National Academy of Sciences 103(52):19678-19682.

9. Braun D, Libchaber A. 2002. Trapping of DNA by thermophoretic depletion and convection. Physical Review Letters 89(18):188103.

10. Alexander CG, Wanner R, Johnson CM, Breitsprecher D, Winter G, Duhr S, Baaske P, Ferguson N. 2014. Novel microscale approaches for easy, rapid determination of protein stability in academic and commercial settings. Biochimica et Biophysica Acta (BBA) - Proteins and Proteomics 1844(12):2241-2250.

Chapter VII
Recombinant human Granulocyte Colony Stimulating Factor (rh-GCSF)

Recombinant human granulocyte colony stimulating factor (rh-GCSF) is a recombinant human cytokine, which stimulates the production and maturation of granulocytes, as well as their release to the blood circulation. rh-GCSF has several applications in the treatment of neutropenia and is for example used after a chemotherapeutic cancer treatment in order to increase the recovery rate and to prevent bacterial and fungal infections.[1-3] On the market, GCSF is available as recombinant human drug (Filgrastim)[4] and in PEGylated form (Pegfilgrastim)[5], for which the half-life is increased to enable an administration once a day. Besides the originator drugs, multiple biosimilars are available.

In this case study, a formulation screening investigating the effect of pH, the presence or absence of buffer salts, and the impact of different concentrations of a polysorbate and a cyclodextrin is presented. The different formulations were investigated in unfolding and aggregation studies by using MST and the results were compared to commonly used gold standard techniques like intrinsic and extrinsic fluorescence, calorimetry and light scattering. Furthermore, forced degradation studies were carried out by using TOPC and a comparative conventional stress testing approach, which was combined with turbidity and light obscuration readouts.

Apart from the formulation screening, MST binding studies were performed between rh-GCSF and various cyclodextrins as well as the non-ionic surfactant pluronic F-127. The observed interactions were verified by evaluating the stability consequences by nanoDSF and SLS.

VII.1. Materials and Methods

VII.1.1. rh-GCSF

Recombinant human Granulocyte Colony Stimulating Factor (rh-GCSF) was a gift from Wacker Biotech GmbH (Jena, Germany). The growth hormone stock solution was formulated at a concentration of 4 mg/ml in 10 mM sodium acetate buffer pH 3.9 with 5% sorbitol and 0.004% polysorbate 80. The E.coli expressed protein lacks glycosylation and consists of 174 amino acids, including two tryptophan residues in position 58 and 118. The theoretical molar mass sums up to 18.8 kDa, with an isoelectric point (pI) of 6.1.[1,6,7]

VII.1.2. Excipients and Reagents

An overview of excipients and reagents used in the formulation screening can be found in Table 10, while Table 11 summarized all materials used for the protein-excipient interaction investigations. The sodium hydroxide and hydrochloric acid standard solutions used for pH adjustment were of analytical grade. All given pH values were adjusted by titration to a precision of ± 0.02. Highly purified water (ELGA Purelab, ELGA LabWater, Celle, Germany, now Veolia Water Technologies GmbH) was used exclusively for all preparation steps.

Table 10: Overview of excipients and reagents used for the rh-GCSF formulation screening.

Material	Supplier	Art.-number	Lot-number
Tween 80 (Polysorbate)	Merck KGaA, Darmstadt, Germany	8.17061.1000	K38539861 827
Hydroxy-Propyl-beta-Cyclodextrin (HP-β-CD, Cavasol W7 HP Pharma)	Wacker Chemie AG, Burghausen, Germany	60012210	73B014
Citric acid, anhydrous	Hermes Arzneimittel GmbH, Großhesselohe, Germany	Raw material sample	9300900
Acetic acid, glacial	LMU central supply CUP	CAS: 64-19-7	-

Table 11: Overview of excipients and reagents used for the rh-GCSF-excipient interaction study.

Material	Supplier	Art.-number	Lot-number
Acetic acid, glacial	LMU central supply CUP	CAS: 64-19-7	-
Sodium dihydrogen phosphate dihydrate	Applichem GmbH, Darmstadt, Germany	A1939,1000	0A006917
Alpha-Cyclodextrin (α-CD)	CycloLab R&D Ltd, Budapest, Hungary	CY-1001	CYL-2322
Beta-Cyclodextrin (β-CD, Cavamax W7 Pharma)	Wacker Chemie AG, Burghausen, Germany	60006994	70P255
Hydroxy-Propyl-beta-Cyclodextrin (HP-β-CD, Cavasol W7 HP Pharma)	Wacker Chemie AG, Burghausen, Germany	60012210	73B012
Methyl-beta-Cyclodextrin (M-β-CD, Cavasol W7 M Pharma)	Wacker Chemie AG, Burghausen, Germany	60007006	71P019
Sulfobutyl-Ether-beta-Cyclodextrin (Captisol SBE-β-CD Sodium Salt)	CyDex Inc, Lenexa, KS, USA	-	NC-04A-05009
Gamma-Cyclodextrin (γ-CD)	CycloLab R&D Ltd, Budapest, Hungary	CY-3001	CYL-1815
Maltoheptaose	CycloLab R&D Ltd, Budapest, Hungary	CY-4004	CYL-2217/2
Sodium Chloride (NaCl)	Carl Roth GmbH & Co KG, Karlsruhe, Germany	9265.1	-
Pluronic F-127	NanoTemper Technologies GmbH, Munich, Germany	-	-

VII.1.3. Formulations

The protein stock solution was adjusted to pH 3.5 by titration and then dialyzed to highly diluted hydrochloric acid solution (pH 3.5) in order to remove the buffer salt and the excipients, while ensuring an acid solution pH. The dialysis was performed at 2-8 °C in three steps of 4 liter medium each, by using Slide-A-Lyzer dialysis cassettes (2000 MWCO, 12-30 ml capacity, Thermo Scientific, Rockford, IL, USA). The extensive dialysis protocol consisted of two hours dialysis, 1st buffer exchange, two hours dialysis, 2nd buffer exchange and overnight dialysis, which ensured a dialysis time of 20 hours in total. Afterwards, the solution was split into three batches and the pH values of the solutions were adjusted to pH 4.0, 4.5 and 5.0 by titration using HCl or NaOH respectively. Subsequently the respective batches were diluted to twelve different formulations (Table 12) using highly purified water, buffer and excipient stock solutions. After preparation, the pH values of the single formulations were checked

again and adjusted when necessary. The protein formulations were filtrated using 0.22 µm Millex® GV PVDF syringe filter units (Merck Millipore Ltd., Tullagreen, Ireland). For each formulation, a reference solution missing the protein was prepared accordingly, which was filtrated using 0.2 µm cellulose acetate sterile syringe filters (VWR International LLC, Radnor, PA, USA). The pH adjustments were performed by using an MP220 pH meter, equipped with an InLab Expert pH electrode (Mettler-Toledo, Greifensee, Switzerland). Protein concentrations were determined by using UV spectroscopy measured with a NanoDrop2000 instrument (Thermo Scientific, Wilmington, USA) and an extinction coefficient of $\varepsilon_{280\,nm}$=0.86 ml*mg^{-1}*cm^{-1}.[1,6,8] All samples and references were aliquoted in 2 ml conical micro-centrifuge tubes (VWR International LLC, Radnor, PA, USA) with minimum headspace to reduce mechanical stress during sample handling and were stored at 2-8 °C upon preparation. An identical, randomized order was used for all analyses, in order to exclude potential storage and measurement time effects on the determined stability parameters.

Table 12: Overview of the formulations prepared for the rh-GCSF formulation screening.

ID	GCSF [mg/ml]	Buffer system	pH	Tween 80 [%]	HP-β-CD [%]
F1	0.2	-	4.0	0.005	-
F2	0.2	-	4.0	0.05	-
F3	0.2	-	4.0	-	1.0
F4	0.2	-	4.0	-	5.0
F5	0.2	-	4.5	0.005	-
F6	0.2	-	4.5	0.05	-
F7	0.2	-	4.5	-	1.0
F8	0.2	-	4.5	-	5.0
F9	0.2	-	5.0	0.005	-
F10	0.2	-	5.0	0.05	-
F11	0.2	20 mM citrate	4.5	0.005	-
F12	0.2	20 mM acetate	4.5	0.005	-

VII.1.4. Further Preparations

In the course of the protein-excipient interaction study, stock solutions of the different excipients were prepared as stated in Table 13. Thereby, all excipients were weighed into 10 ml volumetric flasks with an accuracy of ± 0.1 mg to the respective target weight. The excipients were then dissolved in the chosen buffer by vortexing and the volume was filled ad 10 ml with buffer after completely dissolving the substance. Additional to the 20 mM acetate buffer pH 4.0 without salt, two buffer variants including 15 mM and 3 M NaCl were prepared in order to investigate the salt dependency of the rh-GCSF-excipient interactions. For investigating the rh-GCSF binding to surfactants, a 5% pluronic F-127 stock solution in water was provided by NanoTemper Technologies, which was pre-diluted in in 20 mM acetate buffer pH 4.0 to a concentration of 4%.

Table 13: Overview of the excipient stock solutions prepared for the rh-GCSF protein-excipient binding studies.

Stock solution	Target weight [g]	Buffer system		
		20 mM acetate pH 4.0	20 mM phosphate pH 4.0	20 mM phosphate pH 7.0
15 mM α-CD	0.1459	x	x	-
15 mM β-CD	0.1703	x	x	-
15 mM HP-β-CD	0.2100	x	x	x
150 mM HP-β-CD	2.1000	x	-	x
15 mM M-β-CD	0.1965	x	x	-
15 mM SBE-β-CD	0.2138	x	x	x
150 mM SBE-β-CD	2.1380	x	-	x
15 mM γ-CD	0.1946	x	x	-
15 mM Maltoheptaose	0.1730	x	x	-
15 mM NaCl	0.0088	x	-	-
3 M NaCl	1.7532	x	-	-

x = solution prepared; - = solution not prepared

Subsequently, the previously dialyzed rh-GCSF material (0) was pre-diluted to working solutions (WS) of 20 µM in the three buffer systems used. After dilution, the pH values were checked and adjusted if necessary. The pH adjustments were performed by using a HI83141 pH-meter, equipped with a HI1230 electrode (Hanna Instruments Deutschland GmbH, Voehringen, Germany). In the next step, a 1:1 serial dilution of the excipient stock solution was prepared in the respective assay buffer under

thorough homogenization by pipetting up and down several times. Afterwards an equal amount of the rh-GCSF WS was added in order to reach a final protein concentration of 10 µM for all dilution steps. All dilution steps were performed at 4 °C on ice. After final homogenization, the samples were centrifuged for 10 min (15000 g, 4 °C) in order to remove larger aggregates.

VII.1.5. Unfolding and Aggregation Investigations

VII.1.5.1. MicroScale Thermophoresis (MST)

MST was used for predictive unfolding and aggregation studies in a stepped thermal ramp setup by using the 2nd generation prototype setup (NanoTemper Technologies GmbH, Munich, Germany). Therefore, the temperature was increased from 30 °C to 90 °C in 1 °C steps. Fluorescence excitation LED Power was set to 15% (PMT=810 V) using an MST Power of 20%. NT.LabelFree Zero Background Standard Treated Capillaries (NanoTemper Technologies) were used exclusively and sealed with liquid dip gum (Capillary Sealing Paste, NanoTemper Technologies) at both capillary ends. In order to exclude effects from prolonged thermal history of capillaries at the end of the sample tray, all samples were measured in quadruplicates by executing four consecutive runs in a randomized order with fresh capillaries each.

The measurements were performed by using NT Control software version 2.1.31, while NT Analysis software version 1.5.41 (NanoTemper Technologies) was used to calculate thermophoresis and t-jump values for each temperature step. Melting temperatures (T_m) for the respective melting curves of both data evaluations were calculated by smoothing (Savitzky-Golay, polynomial order 1, points of the window 3), interpolation (cubic spline, 6001 points between 30 °C and 90 °C) and local maximum analysis using the included Impulse Analyzer tool (Origin 8G, OriginLab Corp., Northampton, MA, USA).

VII.1.5.2. Fluorescence Emission Spectroscopy (FES)

VII.1.5.2.1. Nano Differential Scanning Fluorimetry (nanoDSF)

A Prometheus NT.48 prototype instrument (NanoTemper Technologies GmbH, Munich, Germany) was used for reference measurements of linear thermal unfolding by intrinsic tryptophan fluorescence. A temperature ramp was executed from 30 °C to 90 °C by using a slope of 1 °C/min. An LED Power of 15% was used to induce intrinsic protein fluorescence which was continuously collected at 330 nm and 350 nm, enabling a data density of ≥ 11 data points per °C. All samples have been analyzed in

four subsequent runs using NT.LabelFree Zero Background Standard Treated Capillaries (NanoTemper). Evaporation of the sample material from the capillaries at elevated temperatures was reduced by sealing both ends with liquid dip gum (Capillary Sealing Paste, NanoTemper Technologies).

In order to obtain melting temperatures (T_m) from the intrinsic fluorescence emission, the intensities of the single wavelengths at 330 nm and 350 nm as well as the ratio of 350/330 nm was calculated and evaluated over temperatures. Calculation of the fluorescence values was conducted by using a customized Python(x,y) script (software version 2.7.6.0) before T_m values were determined with a hard-coded NT.Analysis tool (both NanoTemper Technologies).

VII.1.5.2.2. Intrinsic Fluorescence Emission Spectroscopy (intrinsic FES)

An Optim 1000 instrument (Avacta Analytical Ltd, Wetherby, UK, now Unchained Labs, Pleasanton, CA, USA) was used for a comparative linear thermal unfolding and aggregation study. The samples were pipetted in the capillaries of a 9 µl micro-cuvette array (MCA), which were tightly closed with the provided silicone seals using a MCA frame. Using the Optim Client software V1.5.4 (Avacta Analytical), all formulations were measured in quadruplicates by performing three consecutive runs with 1 MCA (=16 capillaries) each. Thereby, the capillary positions of the formulations within the MCA were changed in each run to avoid error carryover. Before each measurement, the thermostat temperature was set to 30 °C for a pre-scanning delay of 15 min. Following this equilibration time, the temperature was linearly increased from 30 °C to 90 °C in a rate of 1 °C per minute, while a hold time of 1 s was used at each well for recording of the fluorescence spectrum. An excitation laser wavelength of 266 nm was used to induce deep UV intrinsic fluorescence, setting a slit width of 100 µm and an exposure time of 1000 ms. Fluorescence emission was recorded from 249 to 504 nm using a center wavelength of approximately 380 nm. For data evaluation, the ratio of 350 nm/330 nm was chosen and unfolding temperatures (T_m) were automatically calculated by the Optim Analysis Software V2.0.4 (Avacta Analytical). If necessary, melting temperatures were re-adjusted according to the maxima of the 1st derivative fluorescence curves.

VII.1.5.2.3. Differential Scanning Fluorimetry (DSF)

Differential Scanning Fluorimetry (DSF) was used for reference measurements of linear thermal unfolding by evaluating changes in the extrinsic fluorescence of SYPRO orange (SO) and 9-(2,2-dicyanovinyl)julolidine (DCVJ).

SYPRO Orange Protein Gel Stain was purchased as a 5000x concentrated stock solution (SS) in DMSO (Sigma Aldrich, St. Louis, MO, USA). First, the SS was diluted with highly purified water (HPW) to a working solution (WS) of 21x. Subsequently, 20 µl protein formulation or placebo reference respectively was provided in the wells of a skirted 96-well microplate (Biometra GmbH, Goettingen, Germany) and 1 µl WS was spiked in and thoroughly mixed. The resulting final volume per well was 21 µl with a SO concentration of 1x. For each formulation 8 wells were prepared, 6 with protein material and 2 with the respective placebo reference. To prevent evaporation and ensure proper filling of each without air bubbles, the well plate was covered with self-adhesive optical sealing film (Biometra) and centrifuged at 2000 g for 2 minutes.

The unfolding experiment was conducted using a qTower 2.2 UV instrument (Analytik Jena AG, Jena, Germany). After an initial equilibration time of 15 minutes at 30 °C, the temperature was stepwise increased to 90 °C following a scan rate of 1° C/min and a measurement interval of 1 per °C. An excitation wavelength of 490 nm was used, while the fluorescence emission of SO was collected at 580 nm by using the corresponding channel of the instrument at a gain of 5. At each temperature, three repetitive measurements were performed.

Before melting temperatures (T_m) were evaluated, the placebo reference measurements were subtracted from the verum melting curves, in order to exclude effects from buffer background fluorescence. Subsequently, the background subtracted data were differentiated (1^{st} derivative), smoothed (Savitzky-Golay, polynomial order 1, points of the window 5), interpolated (cubic spline, 6001 points between 30 °C and 90 °C) and the local maximum was analyzed using the included Impulse Analyzer tool (Origin 8G, OriginLab Corp., Northampton, MA, USA).

9-(2,2-dicyanovinyl)julolidine (DCVJ) was purchased as solid powder from Sigma Aldrich (St. Louis, MO, USA) and diluted in DMSO to a stock solution (SS) of 210 mM. This SS was further diluted to a 2.1 mM working solution (WS) with HPW. Subsequently, the WS was spiked to rh-GCSF Formulation 1 in different proportions and thoroughly mixed, yielding final concentrations between 10 and 500 µM DCVJ. The wells of a Thermo-Fast 96 PCR Detection Plate (Thermo Scientific, Loughborough, UK) were filled with 21 µl of each preparation and sealed with

Adhesive Sealing Sheets (Thermo Scientific, Loughborough, UK). The well plate was centrifuged for 2 minutes at 2000 g to ensure filling without air bubbles.

A 7300 real-time PCR system (Applied Biosystems, Foster City, CA, USA) was used for the unfolding experiment. After an initial equilibration time of 15 minutes at the starting temperature of 30 °C, the temperature was stepwise increased to 90 °C following a scan rate of 1° C/min and a measurement interval of 1 per °C. A tungsten-halogen lamp was used for fluorescence excitation, while the emission was recorded at ~ 520 nm using the detection filter A. For conducting the measurement, a 7300 System SDS Software version 1.3.1 (Applied Biosystems, Foster City, CA, USA) was used.

VII.1.5.3. Differential Scanning Micro-Calorimetry (µDSC)

A VP-DSC microcalorimeter (MicroCal Inc., Northampton, MA, USA, now Malvern Instruments Ltd, Malvern, UK) was used for comparative thermal unfolding studies. The placebo and verum formulations were degassed for approximately 5 min by using a ThermoVac vacuum pump (MicroCal) in order to remove potential air bubbles from the samples. Subsequently, 550 µl of the placebo reference was injected by using a 2.5 ml gastight Hamilton syringe (Hamilton Company, Reno, NV, USA) at 25 °C before the verum material was injected accordingly. A temperature up-scan was performed from 30 °C to 90 °C by performing a slope of 60 °C/h. A pre-scan thermostat of 15 minutes was set at the starting temperature to ensure thermal equilibration. During the measurement, a filtering period of 1 second was set without a feedback mode/gain, while the chamber pressure was checked to be ≥ 22 psi. After each run, the cells were cooled down to 30 °C again.

Between two sample runs, a cleaning routine was performed by heating up a 50% (V/V) nitric acid solution under the same conditions as the samples, but using a scan rate of 90 °C/min and no pre-scan thermostat. Afterwards, a solution of 1% (w/V) sodium dodecyl sulfate (SDS) (Merck KGaA, Darmstadt, Germany) in HPW was used to flush each cell for 30 seconds, followed by a thorough rinse with 100 ml water per cell.

The data evaluation was performed by the Origin DSC data analysis software (Origin 7 SR2, OriginLab Corp., Northampton, MA, USA) and MicroCal VPViewer2000 version 1.4.10 (MicroCal). The thermograms were normalized by subtracting a baseline measured by water vs. water scans to exclude device parameters and instrumental effects. Afterwards, the endothermic peaks indicating protein unfolding events (T_m) were determined using the included Peak Picking Tool.

VII.1.5.4. Static Light Scattering (SLS)

Additionally to intrinsic fluorescence (section VII.1.5.2.2), static light scattering intensity over temperature was evaluated from the Optim 1000 measurement for the UV laser at 266 nm and the blue laser at 473 nm. Therefore, 90° light scattering values were plotted over temperature and aggregation onset temperatures ($T_{agg\ onset}$) were evaluated for 266 nm and 473 nm, given a bandwidth of 5 nm each, by using the Optim Analysis software V2.0.4 (Avacta Analytical). For calculation, the software applied a Heaviside step function to the 1st derivative curve of static light scattering and the temperature corresponding to the 10% value of the maximum was determined automatically.

VII.1.6. Forced Degradation Studies

VII.1.6.1. Thermo-Optical Particle Characterization (TOPC)

TOPC was used for predictive thermal aggregation studies by IR-laser induced stress testing. The fluorescence excitation LED power was set to 15% (PMT=810 V) and heat stress was applied by using an IR-laser power of 227%. Changes in intrinsic fluorescence were detected for 185 s in total. After recording the initial fluorescence for 5 s, the laser was turned on and the effects of the IR-laser input were tracked for 150 s, before the laser was turned off again and backdiffusion was measured for additional 30 s.

All measurements were performed in singlicates following a fixed random order of formulations at an ambient assay temperature of 25°C by exclusively using NanoTemper LabelFree MST Premium Coated Zero Background Capillaries (NanoTemper Technologies GmbH) in order to avoid measurement artifacts from sample binding to the capillaries and capillary auto-fluorescence.

NT Control software version 2.1.31 was used to perform the measurements, while the intrinsic fluorescence timetraces were normalized and exported by using NT Analysis software version 1.5.41 (both NanoTemper Technologies). The TOPC experiments were analyzed by calculating mean values and standard deviations for all formulations in the timeframe between 100 and 125 s. All calculations and data plotting were performed with Origin 8G software (OriginLab Corp., Northampton, MA, USA).

VII.1.6.2. Conventional Stress Testing

All formulations were heat- and shake-stressed in 2 ml conical micro-centrifuge tubes (VWR International LLC, Radnor, PA, USA) by using a filling volume of 1 ml. Heat stress was applied for 10 minutes at 75 °C (after 15 minutes for temperature equilibration) using a ThermoMixer Comfort (Eppendorf AG, Hamburg, Germany). Horizontal shaking was performed for 30 minutes in a Mixer 5432 (Eppendorf AG, Hamburg, Germany) at 1450 ± 30 rpm as stated by the manufacturer. As a reference, one aliquot of each sample was stored at 4 °C for the same time.

VII.1.6.2.1. Turbidimetry

A Dr. Lange Nephla Turbidimeter (Hach-Lange, Duesseldorf, Germany) was used for measuring the turbidity of the native and stressed protein formulations. All samples were diluted 1:10 with filtered placebo buffer and subsequently 2 ml of each sample was filled in a glass cuvette. Turbidity was determined as 90° scattered light (860 nm) in Formazin Nephelometric Units (FNU). The measurement was carried out in singlicates.

VII.1.6.2.2. Light Obscuration

A PAMAS SVSS instrument (PAMAS GmbH, Rutesheim, Germany) was used for measuring the turbidity of the native and stressed protein formulations. Before analysis, all samples were diluted 1:10 with filtered placebo buffer. The samples were analyzed in three sub-runs with a total analysis volume of 0.3 ml. In between two sample measurements, the system was purged with highly purified water and one water measurement was performed to check the cleanliness of the system. The particle concentration is given in particles ≥ 1 µm per ml under consideration of the dilution factor.

VII.1.7. Protein-Excipient Interaction Analysis

VII.1.7.1. MicroScale Thermophoresis (MST)

MST was used for protein-excipient binding studies of rh-GCSF to cyclodextrins and pluronic F-127. All measurements were performed on a Monolith NT.LabelFree instrument (NanoTemper Technologies) by using a MST Power of 20%. The Fluorescence excitation LED Power was set individually for each measurement series in order to get a satisfactory high fluorescence signal. For the binding studies of rh-GCSF to cyclodextrins, the excitation power was set to 20% for the measurements in 20 mM acetate pH 4 and 20 mM phosphate pH 4, while for 10 mM phosphate pH 7 it was decreased to 7%. A value of 10% was chosen for the rh-GCSF interaction studies with pluronic-F127 in 20 mM acetate buffer pH 4. NT.LabelFree Zero Background MST Premium Coated Capillaries (NanoTemper Technologies GmbH) were used exclusively and the measurements were carried out at ambient room temperature. Only for the binding studies with pluronic F-127, the temperature was varied between 22 and 37 °C in 5 °C steps.

The measurements were performed by using NT Control software version 2.1.31, while NT Analysis software version 1.5.41 (NanoTemper Technologies) was used to calculate thermophoresis and intrinsic fluorescence values for each excipient concentration and compute equilibrium dissociation constants (K_d) by fitting a Boltzmann-function to the respective data. Plotting of the data was performed by using Origin 8G software (OriginLab Corp., Northampton, MA, USA).

VII.1.7.2. Nano Differential Scanning Fluorimetry (nanoDSF)

A Prometheus NT.48 instrument (NanoTemper Technologies GmbH, Munich, Germany) was used for linear thermal unfolding measurements of the protein-excipient dilution series. A temperature ramp was executed from 15 °C to 95 °C in a slope of 1 °C/min, while protein fluorescence was continuously collected at 330 nm and 350 nm. The fluorescence excitation power was set individually for each measurement series in order to get a satisfactory high fluorescence signal. For the binding studies of rh-GCSF to cyclodextrins, the excitation power was set to 40% (medium sensitivity) for the measurements in 20 mM acetate pH 4 and 20 mM phosphate pH 4. A value of 15% (medium sensitivity) was chosen for the rh-GCSF interaction studies with pluronic-F127 in 20 mM acetate buffer pH 4. All titration steps have been analyzed in singlicate runs by using NT.LabelFree Zero Background MST Premium Coated Capillaries (NanoTemper Technologies).

In order to obtain melting temperatures (T_m) from the intrinsic fluorescence emission, the intensities of the single wavelengths at 330 nm and 350 nm as well as the ratio of 350/330 nm was calculated and evaluated over temperatures by using NT.Prometheus Control software version 1.11 (NanoTemper Technologies).

VII.1.7.3. Static Light Scattering (SLS)

An Optim 1000 instrument (Avacta Analytical Ltd, Wetherby, UK, now Unchained Labs, Pleasanton, CA, USA) was used for a comparative linear thermal aggregation study of the protein-excipient dilution series. As this method is very sensitive to low concentrations of aggregates in solution, all buffer and excipient solutions were sterile filtrated using 0.2 µm cellulose acetate sterile syringe filters (VWR International, Darmstadt, Germany). The protein solution was filtrated using 0.22 µm Millex GV PVDF syringe filter units (Merck Millipore Ltd., Tullagreen, Ireland). After filtration, the dilution series was prepared and the samples were pipetted in the capillaries of a 9 µl micro-cuvette array (MCA), which were tightly closed with the provided silicone seals using a MCA frame. The temperature was linearly increased from 15 °C to 95 °C in a rate of 1 °C per minute, after maintaining the starting temperature of 15 °C for 15 minutes in order to guarantee temperature equilibration. The static light scattering intensity was evaluated and plotted over temperature for 90° light scattering at 266 ± 5 nm by using the Optim Analysis software V2.0.4 (Avacta Analytical).

VII.2. Results and Discussion

VII.2.1. Unfolding and Aggregation Investigations

VII.2.1.1. MicroScale Thermophoresis (MST)

The melting curves of all twelve rh-GCSF formulations (see page 85) showed pronounced positive peaks for the evaluations of thermophoresis (Figure 36 – left), temperature jump (Figure 36 – right) and the combination of both (data not shown). Moreover, those peaks were found to shift in temperature, depending on the respective formulation composition and were therefore assigned as apparent unfolding temperatures (T_m) and used to rank the formulations in terms of conformational stability (Figure 37). In the T_m comparison, a strong influence of pH was found, with a more stable protein conformation at lower pH values. Additionally, HP-β-CD containing formulations showed higher melting temperatures compared to preparations including polysorbate 80. The stabilizing effect of HP-β-CD was independent of the concentration used, while higher polysorbate contents resulted in slightly decreased T_m values, especially at low pH values. The use of citrate (F11) and acetate (F12) as buffering agents at pH 4.5 resulted in negative effects on the API stability compared to the unbuffered solution at the same pH (F5). While acetate lowered the T_m only by 2-3 °C to a value being comparable to the results of the unbuffered solution at pH 5.0 (F9), citrate showed a T_m decreased of ~ 6 °C and ranks as the most instable formulation in the screening. Overall, the evaluation of t-jump alone did result in smaller amplitudes for the unfolding transition compared to the thermophoresis and the combined evaluations. Consequently, this led to a lower signal-to-noise ratio and a reduced precision for the fitting of the peak maxima.

A clear effect on aggregation stability in terms of an individual aggregation signal could not be derived from the raw unfolding curves, although it is noticeable that the curve shape after the unfolding transition is identical for all formulations in the t-jump melting curves (Figure 36 – right), but differs for the different pH values in the thermophoresis evaluation (Figure 36 – left). Thereby, the formulations at low pH values (F1-F4, green lines) show polymorphous, scattering and overall decreasing progressions, which changes at higher pH values and under the usage of buffering agents (F5-F12, grey & red lines) to rather uniform, straight and ascending trending.

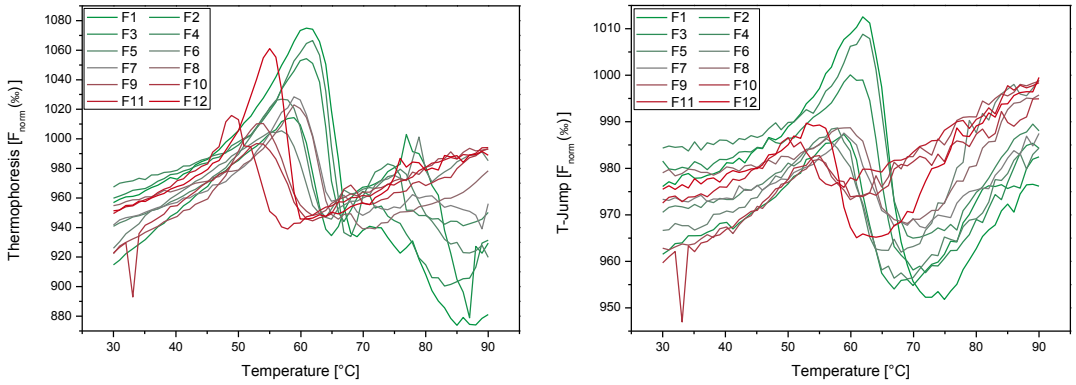

Figure 36: Melting curves by thermophoresis (left) and t-jump (right) within the rh-GCSF formulation screening (n=1).

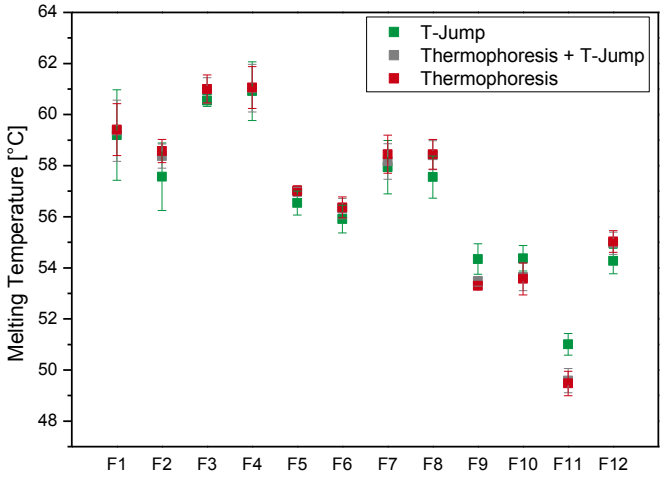

Figure 37: Melting temperatures determined for T-Jump (green squares), Thermophoresis (red squares) and Thermophoresis including T-Jump (grey squares) within the rh-GCSF study (n=4).

These results are put into context with the literature, where manifold studies targeting the conformational and aggregation stability of rh-GCSF can be found.[8-16] These precisely confirm the high relevance of the pH value and the buffer system, which was derived from the MST results, accordingly describing an increased conformational stability and aggregation resistance at acidic pH values of pH 4.0 or less. Moreover, the stability of rh-GCSF was in all cases highest for the formulations without any added buffer salt. In buffered formulations, acetate, phosphate, and glutamate provided improved stabilities compared to citrate and succinate. Additionally, a stabilizing effect is reported for sugars[13,17] and polysorbate[4,18], while high salt concentration destabilize[7,16,19]. By analogy, the marketed originator products are formulated in sodium acetate buffer containing sorbitol and polysorbate[20,21].

Furthermore, mechanistic studies on the irreversible aggregation of rh-GCSF are available, elucidating this process in greater detail.[7,10,17,19,22,23] Summarizing these investigations, the aggregation cascade can be divided in two major, equally relevant steps. Initially, aggregation is induced by slight conformational expansion within the native state ensemble, which in the following leads to colloidal interactions and irreversible aggregation. Depending on the solution conditions, the rate-limiting step can be either the conformational change (depending on the free energy of unfolding (ΔG_{unf})) or the colloidal interaction (depending on the osmotic second virial coefficient (B_{22})). This widely explains the importance of colloidal factors like pH and ionic strength, preventing or favoring attractive interactions, as well as conformational stabilizers like sugar or sugar alcohols, which promote structurally compact conformations by direct interaction or preferential exclusion.

In our case, the colloidal stability seems to be rate-limiting, as increasing the pH and/or the ionic strength has a much higher stability effect than the addition of HP-β-CD. Moreover, the addition of polysorbate did not have a pronounced effect on the thermal stability. This is in alignment with the results of the studies by Bam et al.[24] and Youssef et al.[14], who both refer to interfacial stabilization potentially playing an inferior role in thermal denaturation.

VII.2.1.2. Fluorescence Emission Spectroscopy (FES)

Comparative measurements benchmarking the results of the thermophoretic melting curves were carried out by using intrinsic and extrinsic fluorescence emission spectroscopy.

While two independent measurement setups evaluating intrinsic fluorescence (NanoTemper Prometheus NT.48 and Avacta Optim 1000) showed distinct unfolding transitions, independent of the type and concentration of excipients used for the formulations, extrinsic fluorescence performed worse (Figure 39).

The interaction of the hydrophobic excipient Tween and the reporter dye Sypro Orange is well described in literature and leads to a concentration dependent increased background fluorescence emission, reducing the extent of fluorescence increase during protein unfolding.[25-27] In our thermal unfolding experiments (Figure 38 – left), this interference was negligible for the formulations containing 0.005% Tween 80 (F1, 5, 9, 11 and 12) but very pronounced at an 10-fold increased surfactant concentration of 0.05% (F2, 6, 10). There, the unfolding transition was completely superimposed, making a T_m determination impossible. Moreover, a concentration independent interference was found for formulations containing HP-β-CD in the range of 1% to 5%, where overall fluorescence levels were comparable to the other formulations, but still no unfolding induced fluorescence increase was detected. This observance might as well be caused by hydrophobic interactions between the SO and the hydrophobic cavity of β-cyclodextrin[28], which prevent the dye molecules from binding to the exposed hydrophobic sites (AA residues) upon unfolding of rh-GCSF.

The molecular rotor DCVJ is used to measure melting curves in the presence of polysorbates as the quantum yield/fluorescence increase following the decrease of rotational freedom during protein unfolding is not impacted by surfactants.[25,29,30] However, our data indicate that higher protein concentrations are required, so that none of the used dye concentrations showed an unfolding transition (Figure 38 – right).

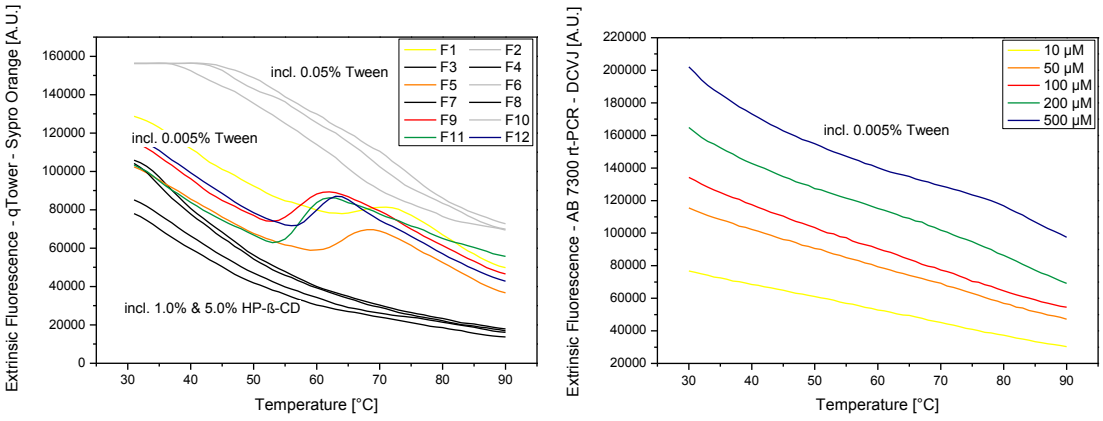

Figure 38: Melting curves for DSF by using extrinsic fluorescence emission of sypro orange (left) and DCVJ (right). Both data sets are displayed as raw data before background subtraction. (n=1)

In the T_m data evaluation (Figure 39), the trending towards lower conformational stability at increased pH values was confirmed by both intrinsic fluorescence assays, as well as DSF using SO as extrinsic fluorescence probe. Furthermore, for the comparison of the buffer-free (F5), citrate-buffered (F11) and acetate-buffered (F12) formulation, a consistent and pronounced destabilization by citrate was found, whereas the absence of buffer salt was beneficial over acetate in Prometheus FES and qTower DSF, while the T_m values of the two formulations were comparable in Optim FES. Results on the influence of different excipient concentrations (polysorbate and HP-β-CD) on the conformational stability could only be achieved by intrinsic fluorescence, as the above described dye interactions in DSF make an evaluation impossible. However, the impact was not fully identical among the intrinsic methods and the different pH values studied, showing individual trends towards stabilization as well as destabilization at higher concentrations. Moreover, both excipients contributed equally to the overall formulation stability, not indicating a definite benefit from polysorbate over cyclodextrin or vice versa. Remarkably, the increased resolution of the Prometheus data compared to the benchmark methods (> 11 data points/°C compared to ≤ 1 data point/°C) resulted in a minimal replicate deviation and an additional pre-melting transition for F2, explaining the large inter-assay variance for this formulation. Additionally, it is to mention that the spectral shift in intrinsic fluorescence from 330 nm to 350 nm was found to be much weaker compared to the changes in single wavelength fluorescence emission. For this reason, the evaluation was performed at 330 nm (Prometheus) and for fluorescence intensity (Optim), respectively.

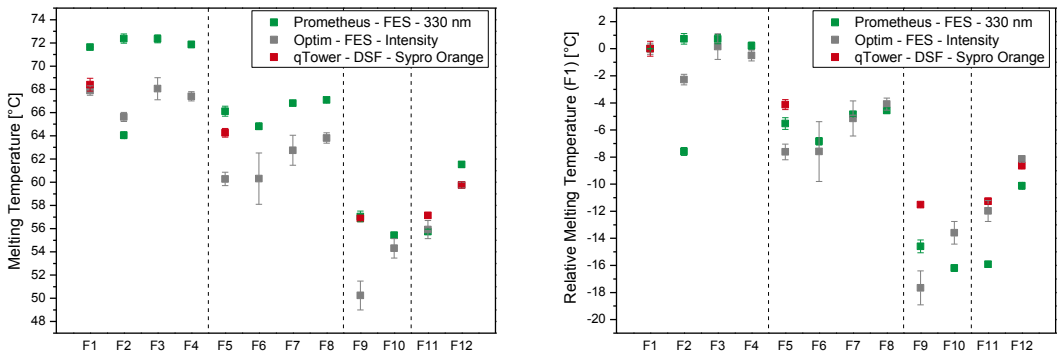

Figure 39: Comparison of absolute (left) and relative (right) melting temperatures (T_m) by using intrinsic (green and grey squares) as well as extrinsic (red squares) fluorescence emission spectroscopy. The dashed lines indicate the steps between pH 4.0 (F1-F4), pH 4.5 (F5-F8), pH 5.0 (F9-F10), and pH 4.5 with buffering agent (F11-F12).

Figure 40 shows the correlation of intrinsic fluorescence with extrinsic fluorescence as well as both intrinsic fluorescence methods among each other. The clear pH effect on the conformational stability is producing strongly correlating data for the comparison of intrinsic fluorescence by Prometheus and evaluable formulations for extrinsic fluorescence by Sypro Orange measured in the qTower rt-PCR system. However, the discussed variations for the influence of the excipients and their different concentrations led to a slightly lowered correlation between the two intrinsic fluorescence methods.

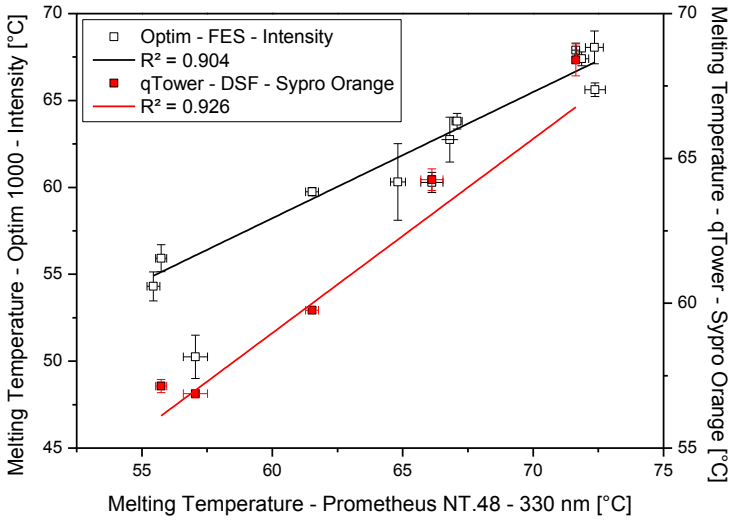

Figure 40: Correlation of intrinsic fluorescence emission at 330 nm by using Prometheus NT.48 with intrinsic fluorescence intensity by Optim 1000 (black squares and line) and extrinsic fluorescence by Sypro Orange measured in a qTower rt-PCR device (red squares and line).

VII.2.1.3. Differential Scanning Micro-Calorimetry (µDSC)

The obtained µDSC data do not show the pronounced influence of pH on the thermal stability of rh-GCSF, which was previously described for the other methods investigated and in the literature. In our experiments, a minor tendency towards conformational destabilization by increasing the pH value was only visible between pH 4.0 (F1 – F4) and pH 4.5 (F5 - F8). Further neutralization of the pH to 5.0 did not have a remarkable effect. The most pronounced destabilization determined by using µDSC was caused by the change from an unbuffered (F5) to a citrate (F11) or acetate (F12) buffered formulation, which led to an immense decrease of the T_m by ~ 10 °C. This is in agreement with earlier investigations by Youssef[31], who evaluated the predictive power of µDSC measurements of rh-GCSF and received a comparably weak influence of pH on the unfolding temperature evaluated by µDSC. Moreover,

high standard deviations were found for most of the performed replicate measurements, what makes a clear differentiation of conformational stabilities among the different formulations difficult. These large variances might be caused by the low protein concentration used and the associated low self-buffering capacity, potentially leading to pH changes upon storage. Furthermore, the substantially higher sample consumption, compared to all other methods investigated, made the analysis of different aliquots necessary.

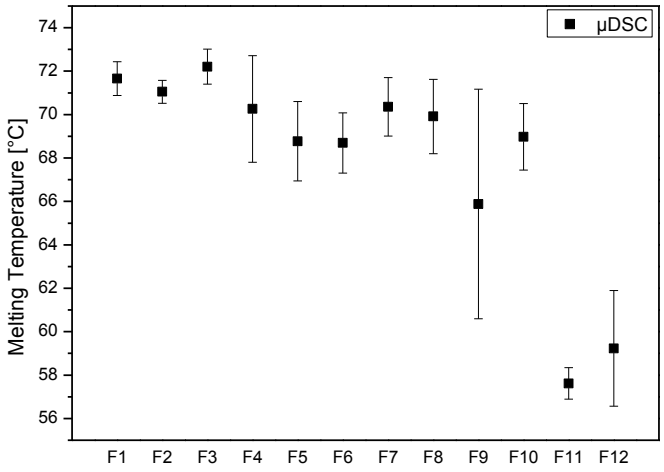

Figure 41: Melting temperatures for differential scanning calorimetry within the rh-GCSF formulation screening (n≥3).

VII.2.1.4. Static Light Scattering (SLS)

Aggregation stability investigated by static light scattering distinguished most clearly between stabilizing and destabilizing formulation conditions, which yielded in a very distinct stability trending over pH values. The raw data evaluation at 266 nm (Figure 42 – left) not only differentiates between aggregation propensities by the scattering onset temperature (Figure 42 – right), but moreover between the underlying aggregation rates by the progression of the overall scattering intensity. Both aggregation markers indicate a higher stability at pH 4.0 (F1-F4), showing (i) highest $T_{agg\ onset}$ values and (ii) comparably moderate slopes leading to low scattering plateaus below 200000 A.U.. Interestingly, F2 and less pronounced F1 (dark grey and black lines) seem to establish only intermediate plateaus followed by a second aggregation onset at temperatures > 75 °C (F2) and > 85 °C (F1). However, a second aggregation onset did not occur when Tween 80 was replaced by HP-β-CD (F3+4), independent of the cyclodextrin concentration.

On the contrary, formulations at pH 4.5 and 5.0 aggregate at lower temperatures and exhibit steep increases as well as high scattering intensities. Whereas the $T_{agg\ onset}$ is strongly dependent on the formulation pH (except of F11 – 20 mM citrate, pH 4.5), the slope and the overall scattering intensities are found to be comparable between the two pH levels. Regarding the different buffer systems at pH 4.5, the unbuffered formulation (F5) and acetate buffer (F12) perform comparable, while citrate buffer (F11) is considerable less stable and ranks among the unbuffered formulations at pH 5.0 (F9+F10).

The influence of Tween 80 and HP-β-CD as formulation excipients was comparable, showing a slight trend towards higher $T_{agg\ onset}$ values for increased concentrations and for the cyclodextrin over the polysorbate.

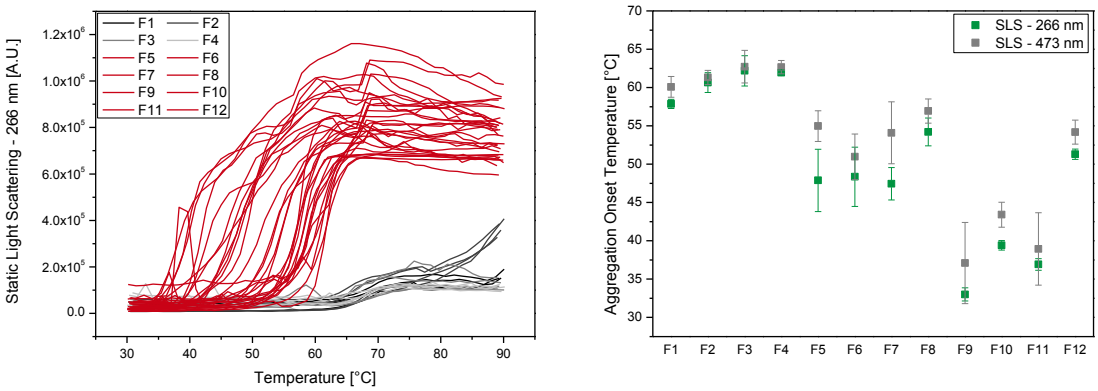

Figure 42: Static light scattering for rh-GCSF formulation screening (n=4). Left: Raw data for SLS at 266 nm over temperature. Right: Comparison of the determined $T_{agg\ onset}$ values at 266 nm and 473 nm.

VII.2.1.5. Comparison and Evaluation of MST as a Tool for Unfolding and Aggregation Investigations

Within the rh-GCSF formulation screening, MST was able to achieve a matching and well correlating conformational stability ranking compared to intrinsic fluorescence based benchmark methods (Figure 43) and indicated several advantages over microcalorimetry and extrinsic fluorescence. Furthermore, a very high coincidence was found for the comparison with literature data regarding the stability dependencies on the formulation pH, the presence or absence of buffering agents as well as stabilizers. On the contrary, microcalorimetry performed imperfect in the low concentration range used, what resulted in a low signal-to-noise ratio for the single thermograms and large standard deviations for the respective T_m values obtained.

Extrinsic fluorescence was investigated by using two different dyes, Sypro Orange and DCVJ, both exposing drawbacks compared to intrinsic fluorescence and thermophoresis. On the one hand side, DSF under the use of SO was able to identify congruent unfolding events for the formulations containing 0.05% Tween 80, but did not expose any unfolding transition at higher polysorbate concentrations as well as for cyclodextrin containing formulations. On the other hand side, DCVJ that is described to facilitate measurements in the presence of polysorbates was found to require increased protein concentrations as no unfolding event was detected for any of the formulations and different dye concentrations investigated.

However, in retrospect it must be stated that the selection of formulations was non-optimal. A lot of unbuffered formulations in a rather low protein concentration were used. This has not only the disadvantage that the measurements are in all methods close to the detection limit but moreover that the self-buffering capacity of the protein is very weak. This leads to a rather instable system that shows large aliquot to aliquot variations (µDSC) and potential pH shifts upon pulling up or pipetting the solution into acid capillary glass (MST, Optim and Prometheus).

Aggregation stability, determined as the onset temperature of light-scattering increase, showed the most differentiated results between stable and unstable formulations and was found to be highly impacted by the unfolded state of the protein, as both stability readouts show a similar trending and explicit as well a high overall correlation between the calculated T_m and $T_{agg\ onset}$ values.

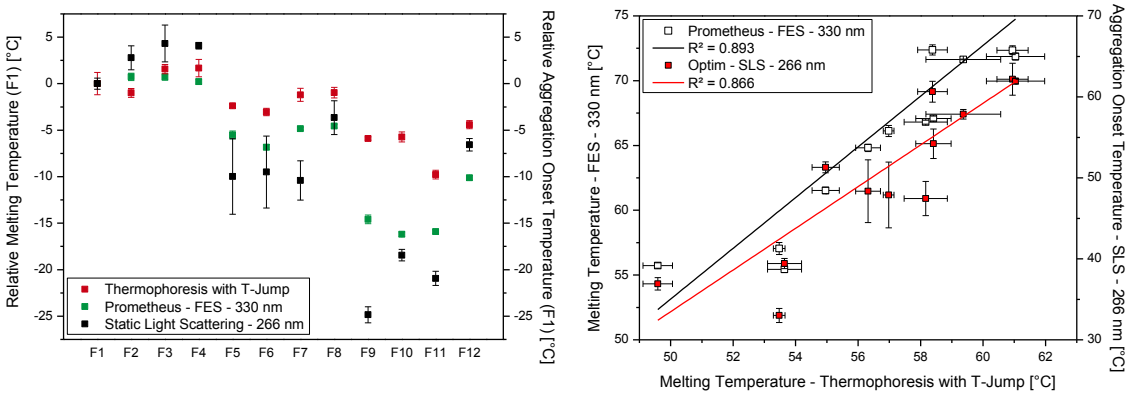

Figure 43: Benchmarking of thermophoresis with t-jump (T_m) with fluorescence emission spectroscopy (T_m) and static light scattering ($T_{agg\ onset}$). Left: Comparison of relative melting as well as aggregation onset temperatures. Right: Correlation of conformational stability and aggregation parameters.

VII.2.2. Forced Degradation Studies

VII.2.2.1. Thermo-Optical Protein Characterization (TOPC)

In addition to the unfolding and aggregation studies using MST (VII.2.1), TOPC was investigated for the twelve different rh-GCSF formulations (see page 85) in order to further investigate the dependencies of the aggregation stability with the orthogonal approach of forced degradation. The results are displayed in Figure 44 as raw (left) and normalized (right) intrinsic fluorescence signal over time. As visible from the raw signal, the initial fluorescence values of the different formulations vary widely, with F10, F2, and F6 showing the highest, while F3 is showing the lowest fluorescence values. This fluorescence difference is attributable to the addition of excipients, which either show a concentration dependent auto-fluorescence or increase the fluorescence of the protein. In our case, mainly Tween 80 at the high concentration level of 0.05% leads to a fluorescence increase. This excipient related fluorescence change seems not to be stability indicative, as e.g. the pH value had a much larger influence in the unfolding and aggregation studies. Moreover, it impedes the data evaluation of the mean fluorescence levels from the normalized fluorescence values, which is normally performed in order to compensate for differences in protein concentration. However, by evaluating the raw fluorescence curves, after 100 s of laser input, the fluorescence difference of F2 and F3 – two of the initially most distant formulations – was reduced from ~ 12.000 to ~925 A.U.. Moreover, for the majority of formulations, a stability profiling comparable to the unfolding and aggregation assay is obtained that underlines the strong pH dependence of rh-GCSF aggregation stability.

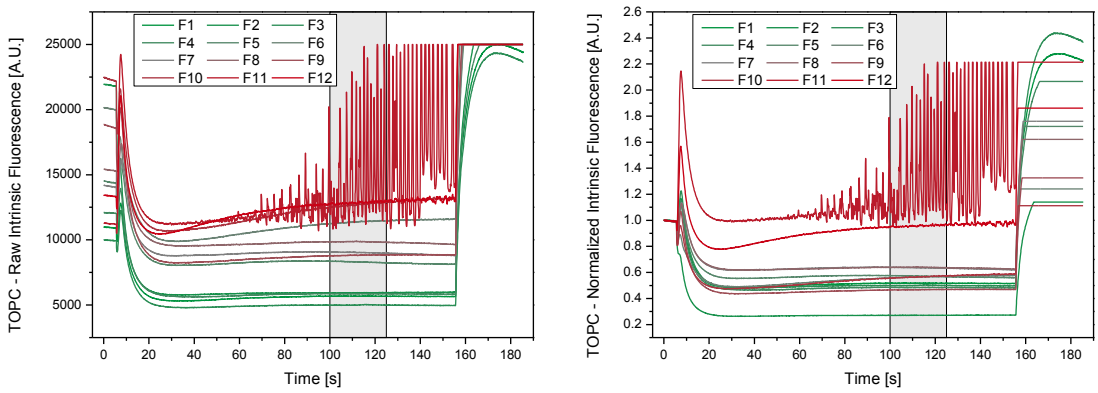

Figure 44: TOPC raw (left) and normalized (right) intrinsic fluorescence over time within the rh-GCSF formulation screening. The area between the horizontal bars (grey background) indicates the timeframe of the measurement that was used for further evaluation. (n=1)

The results of the mean fluorescence and standard deviation evaluation from the raw intrinsic fluorescence values in the timeframe between 100 and 125 s are displayed in Figure 45. In comparison of the formulations, a clear stepwise progressing trend was detectable with increasing mean fluorescence and standard deviations from pH 4.0 (F1-F4) to pH 4.5 (F5-F8). However, for the next step to pH 5.0 (F9 and F10) this trend was less clear, with F9 showing a comparable stability to the formulations at pH 4.5 and only F10 exposing increased fluorescence and scattering levels.

Another strong influence was detected for concentration changes of the excipients. While increasing concentrations of Tween 80 (F1 to F2, F5 to F6, F9 to F10) led to a higher aggregation and precipitation propensity, increasing concentrations of HP-β-CD (F3 to F4 and F7 to F8) tended to stabilize the system.

The buffered formulation compositions F12 (20 mM acetate) and especially F11 (20 mM citrate) showed increased baseline scattering, which is transferrable to enhanced aggregation and precipitation, when compared to the other formulations at pH 4.5 (F5-F8). The strong precipitation for F11 led to enormous scattering amplitudes, caused by the generation of very large particle sizes or concentrations. In comparison to the next lower scattering sample (F10), the standard deviation of F11 was more than 30-fold higher.

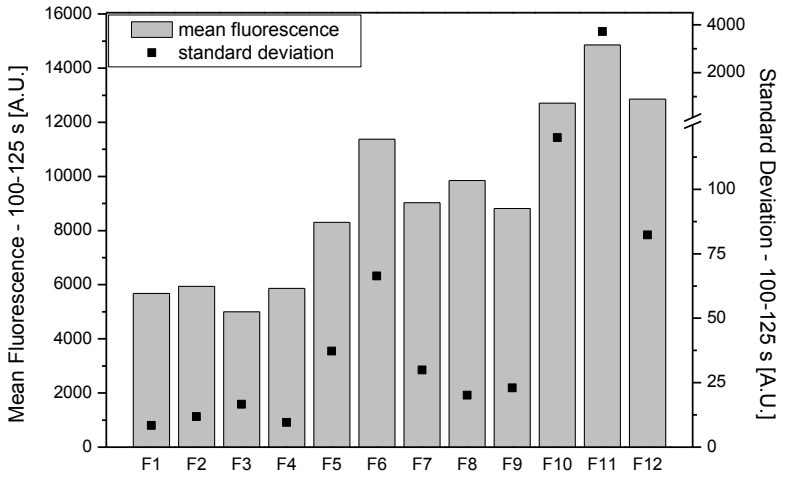

Figure 45: Mean fluorescence and standard deviation analysis from the raw intrinsic fluorescence values of the TOPC experiment in the timeframe between 100 and 125 s. (n=1)

VII.2.2.2. Conventional Stress Testing

VII.2.2.2.1. Turbidimetry

As an orthogonal conventional approach to elucidate the processes during TOPC and to test the rh-GCSF stability upon forced degradation, turbidity measurements were conducted after horizontal shaking or intensive heat exposure (Figure 46).

The turbidity after heat stressing confirms the previously derived stability ranking with a distinct stability dependency on the formulation pH and the presence or absence of buffering agents. Consequently, the formulations with a pH value of 4.0 (F1-F4) showed a very high aggregation resistance with only a minor change of the sample turbidity by a factor of two, when compared to a reference sample stored at 4 °C. This factor grows to around 25-fold at pH 4.5 and to around 60-fold at pH 5.0. The addition of buffer salts (F11 and F12) furthermore increased the aggregation and precipitation in comparison to the unbuffered formulation of the same pH (F5-F8). This effect was most pronounced for the citrate buffered formulation (F11), where the highest visible turbidity, but also severe precipitation with high sedimentation velocities was observed. Due to the colloidal instability of this sample, it was excluded from the turbidity analysis and was plotted only for illustrative reasons.

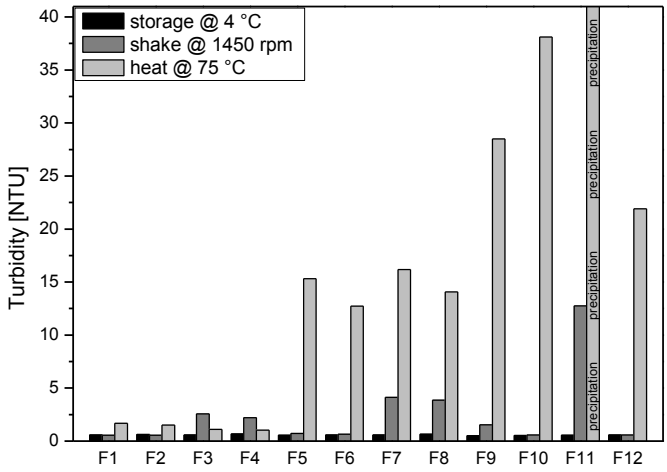

Figure 46: Turbidity measurements of the heat (light grey) and shake (dark grey) stressed rh-GCSF formulations in comparison to unstressed reference formulations (black). F11 showed severe precipitation after heat stress and was excluded from the measurements. The respective bar was marked with precipitation and was included to the plot for illustrative reasons only. (n=1)

Strong shaking of the formulations with consecutive turbidity analysis of the samples however resulted in a different turbidity ranking. Here, besides F9 and F11, the formulations containing HP-β-CD (F3, F4, F7, and F8) showed the highest turbidity values. Whereas the increased turbidity of F9 and F11 after shaking is likely to be a valid indicator of the agitation stability, the influence of HP-β-CD on the turbidity after shaking, but not after heating is not expected. It might in parts be a true effect, especially due to the larger increase at higher pH, but could also be caused by the stabilization of air bubbles in solution during this specific stressing procedure, which can lead to an increased turbidity.

VII.2.2.2.2. Light Obscuration

Light obscuration analysis was performed in order to determine the concentration increase of sub-visible particles in solution after forced degradation.

The majority of control samples stored at 4 °C showed very low particle concentrations ≤ 5,000 particles/ml (1-200 µm), while the particle counts for some of the HP-β-CD containing formulations were arbitrarily higher and reached values up to 20,000 particles/ml (1-200 µm) for F3 (pH 4.0, 1% HP-β-CD) and F4 (pH 4.0, 5% HP-β-CD). In contrast to the shaking stress samples, this deviation was not fully consistent after heat stressing, which could be caused by the elimination of air bubbles during the heating cycle and would further support the abovementioned air bubble-hypothesis. The detection of air bubbles is expected for the light obscuration setup as well, as the system is not able to distinguish between proteinaceous particles and air bubbles blocking the light before reaching the detector.

The particle analysis after shaking stress precisely confirms the picture gathered from the turbidity measurements that however differs widely from the TOPC results. Again, F9, F11 and the CD containing formulations (F3, F4, F7, and F8) show the largest increase of particles in the µm-range. The fact that the particle content of F9 shows a substantial increase that is not observed for F10, while both formulations differ only in the concentration of the included polysorbate, indicates the stabilizing effect of the surfactant at a concentration of 0.05% but not at 0.005%. By contrast, the protein did not show any instability at lower pH levels (pH 4.0 and pH 4.5), independent of the surfactant concentration.

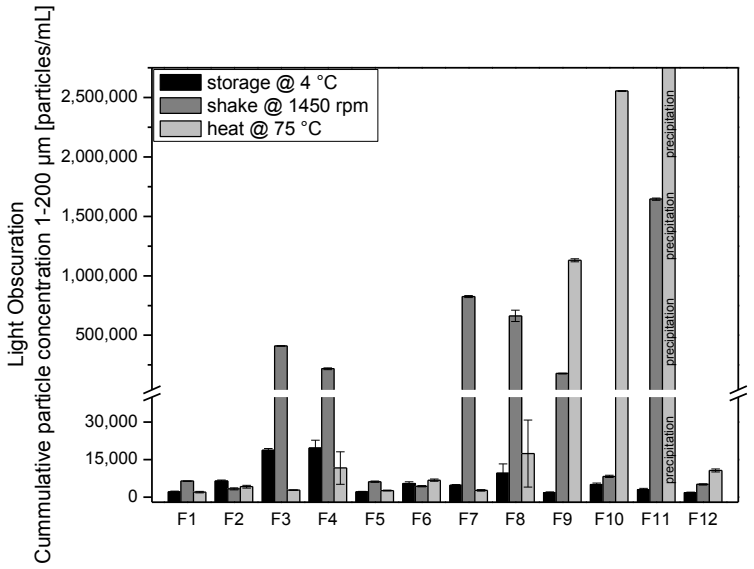

Figure 47: Light obscuration measurements of the heat (light grey) and shake (dark grey) stressed rh-GCSF formulations in comparison to unstressed reference formulations (black). F11 showed severe precipitation after heat stress and was excluded from the measurements. The respective bar was marked with precipitation and was included to the plot for illustrative reasons only. (n=3)

For the heating stress samples, only F9 and F10 (both pH 5.0) showed increased particle concentrations. These results are so far congruent with the TOPC assay and the turbidity determination that these formulations showed a considerably reduced aggregation stability when compared to the formulations at lower pH values. However, a differentiation between the lower pH values pH 4.0 (F1-F4) and pH 4.5 (F5-F8) could not be resolved in the particle measurement, whereas TOPC and turbidity analysis detected a clear difference between the two groups. Surprisingly, also the particle concentration of F12 (20 mM acetate pH 4.5) was not substantially increased after heat exposure. Yet, the turbidity measurements after forced degradation and the TOPC showed considerably increased values and pointed towards an increase in particulate matter. For F11 (20 mM citrate pH 4.5) that showed severe precipitation, potentially very high particle counts would have been observed. Though, the sample was excluded from the light obscuration analysis in order to not block the fluidics of the system and was plotted only for illustrative reasons.

However, it is to mention that the chosen heat stress conditions (storage at 75 °C) deviate from standard forced degradation approaches, where incubation usually is executed below the melting temperature of the protein. In our case, we wanted to mimic the condition during TOPC, where full denaturation of the protein is reached before aggregation is induced.

VII.2.2.3. Comparison and Evaluation of TOPC as a Tool for Predictive Forced Degradation Studies

The aim of the study presented was to promote two different aspects of the establishment and evaluation of TOPC as a tool for predictive aggregation studies. On the one hand side, more detailed information about the stress characteristics during the TOPC analysis should be achieved. On the other hand side, the TOPC results should be benchmarked against conventional forced degradation approaches and thermal unfolding and aggregation screenings in order to strengthen the validity of the assay. In principle, continuous IR-laser input mainly applies heat stress, but also shear stress could be induced. In our assay, heating is achieved due to IR-laser absorption by water, while shear stress occurs due to particle migration and mixing by convective molecular flow within the temperature gradient. Consequently, we covered both parts of the study by comparing the TOPC results to two different forced degradation strategies, (i) heat exposure and (ii) shaking stress.

In conclusion, with TOPC we were able to distinguish between formulations in terms of different aggregation and precipitation propensities. The TOPC results were closely reflected by heat stressing, almost perfectly matching the turbidity increase after external forced degradation and widely confirmed by the stability ranking gathered from sub-visible particle determination. On the contrary, shaking stress was found to play a tangential role for the conditions during IR-laser exposure (Table 14).

Table 14: Comparison of the TOPC results with conventional stress testing. Results for each evaluation were normalized between 0 (low) and 100 (high). The not determined results for the heat stressed and precipitating F11* are displayed for illustrative reasons only and were arbitrarily set to 125% of the maximum value observed.

ID	TOPC (mean)	TOPC (SD)	Turbidity (heat)	LO (heat)	Turbidity (shake)	LO (shake)
F1	5.0	1.0	1.5	0.0	0.1	0.2
F2	6.6	0	1.1	0.1	0	0
F3	0	3.0	0.2	0.0	16.5	24.8
F4	6.5	0.6	0	0.3	13.6	13.1
F5	33.4	4.0	32.0	0.0	1.5	0.2
F6	71.3	5.3	26.2	0.2	0.8	0.1
F7	45.2	7.5	33.9	0.0	29.3	50.1
F8	49.6	9.6	29.2	0.5	27.1	40.2
F9	70.8	9.9	61.5	36.9	8.0	10.6
F10	100	24.1	83.0	83.3	0.2	0.3
F11	96.4	100	100*	100*	100	100
F12	93.6	16.8	46.7	0.3	0.2	0.1

VII.2.3. Protein-Excipient Interaction Analysis

VII.2.3.1. Binding Studies with Cyclodextrins

VII.2.3.1.1. MicroScale Thermophoresis (MST)

The binding curves obtained for the MST measurement of rh-GCSF with three different cyclodextrins (α-CD, β-CD, and γ-CD), three β-CD derivatives (HP-β-CD, SBE-β-CD, and M-β-CD), and a negative control (maltoheptaose) in 20 mM acetate buffer pH 4.0 are shown in Figure 48 (thermophoresis) and Figure 49 (intrinsic fluorescence). For both evaluations, an interaction with rh-GCSF is only apparent for SBE-β-CD, while all other cyclodextrins including the different modifications of β-CD and maltoheptaose did not show any concentration dependent change neither in thermophoresis, nor in intrinsic fluorescence evaluation. Interestingly, the interaction between SBE-β-CD and rh-GCSF evaluated by thermophoresis revealed a non-expected curve shape, that deviates from the ideal sigmoidal progression and indicates a superposition by a second effect at cyclodextrin concentrations between 58.59 and 937.5 µM. This interference is reflected by a spontaneous decrease in thermophoretic depletion (i.e. increase in F_{norm} [‰]). However, the intrinsic fluorescence analysis did not show pronounced alterations in the binding curves, but only a broader deviation of the single titration points from the ideal curve progression in the same concentration range. Removing the thermophoresis evaluation data points in the area of the adverse effect (Figure 48 – right), the interaction between SBE-β-CD and rh-GCSF was fitted with a K_d of 6.68 µM as mean value of triplicate measurements (Table 15). On the other hand side, intrinsic fluorescence yields a highly comparable value of 7.30 µM without the necessity of removing data points (Figure 49 – right and Table 16). Due to the sulfobutylether residues, SBE-β-CD that was used as sodium salt with a strong negative net charge is the only ionic excipient investigated. rh-GCSF is positively charged at the assay pH of 4.0, having an isoelectric point of 6.1.[19] This suggests the presence of an ionic interaction beyond the theory of cyclodextrins' hydrophobic cavity interacting with solvent exposed hydrophobic amino acid residues of the protein[32-34].

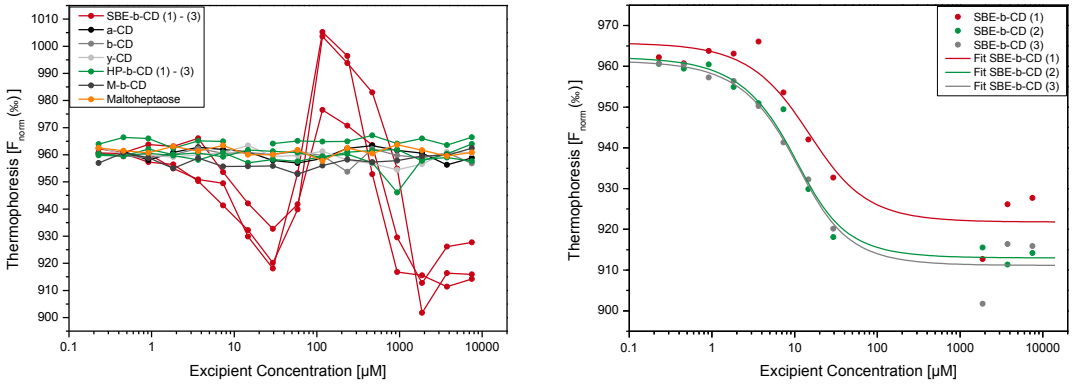

Figure 48: Thermophoresis binding studies of rh-GCSF to cyclodextrins in 20 mM acetate buffer pH 4.0. Left: Interaction screening of rh-GCSF to various cyclodextrins and maltoheptaose as a reference. Right: K_d fit of the interaction between rh-GCSF and SBE-β-CD. Before fitting the protein-excipient binding, the titration points showing the additional phase between 58.59 and 937.5 µM SBE-β-CD have been removed.

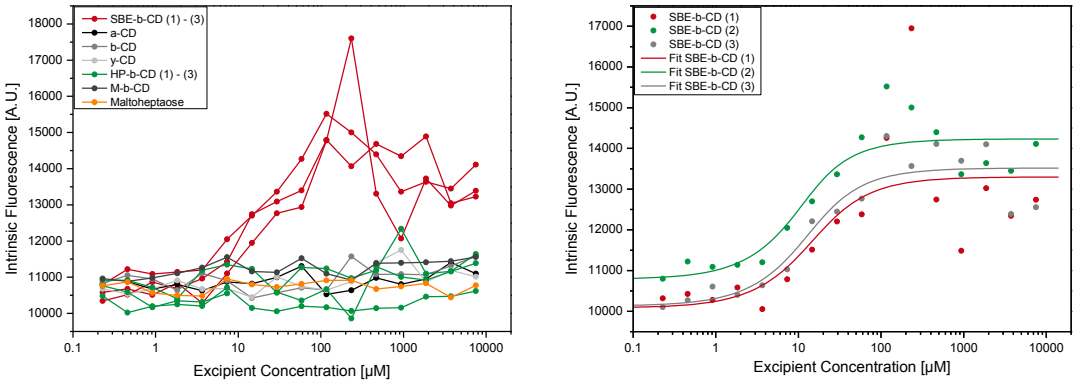

Figure 49: Intrinsic fluorescence binding studies of rh-GCSF to cyclodextrins in 20 mM acetate buffer pH 4.0. Left: Interaction screening of rh-GCSF to various cyclodextrins and maltoheptaose as a reference. Right: K_d fit of the interaction between rh-GCSF and SBE-β-CD.

In order to characterize the interaction of SBE-β-CD and rh-GCSF in more detail and to elucidate the interaction mechanism, additional measurements were performed while adding 7.5 mM NaCl (1:1 ratio with SBE-β-CD) and 75 mM NaCl (10:1 ratio with SBE-β-CD) to the assay buffer. This alteration interferes with potential ionic interactions by shielding of the charged residues, what in consequence would lead to a weakening or complete suppression of the interaction. The thermophoresis results of this study can be found in Figure 50 and Table 15, while the intrinsic fluorescence evaluation is shown in Figure 51 and Table 16. Salt addition changed the binding characteristics as anticipated and shifts the K_d towards higher SBE-β-CD concentrations. For the thermophoresis data evaluation, the initial K_d of 6.68 µM

increased in the first step to 10.5 µM (7.5 mM NaCl) and in the second step to 602 µM (75 mM NaCl). At the same time, the adverse binding effect, being apparent under NaCl free conditions, vanished and the overall binding amplitude between unbound and bound declined. These findings substantiate the existence of a protein-excipient binding and serve as another evidence of an interaction quenching by NaCl. The respective K_d values for intrinsic fluorescence raised from 7.30 µM, over 31.4 µM (7.5 mM NaCl), to 651 µM (75 mM NaCl). However, an amplitude change was not observed for fluorescence. In total, these finding strengthen our hypothesis of ionic attraction driving the interaction between SBE-β-CD and rh-GCSF.

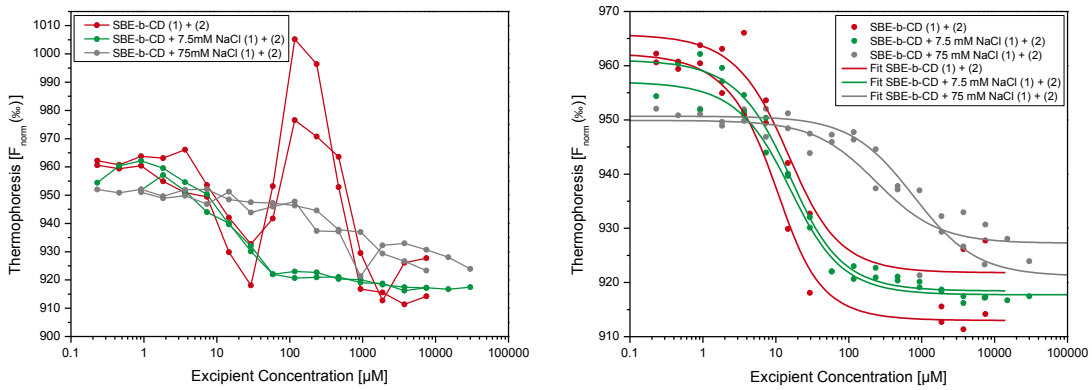

Figure 50: Thermophoresis binding studies of rh-GCSF to SBE-β-CD in 20 mM acetate buffer pH 4.0 in the presence and absence of sodium chloride. Left: interaction screening of rh-GCSF to SBE-β-CD under the presence of 7.5 mM and 75 mM NaCl. Right: K_d fit of the interaction between rh-GCSF and SBE-β-CD. Before fitting the protein-excipient binding in the absence of NaCl, the titration points showing the additional phase between 58.59 and 937.5 µM SBE-β-CD have been removed.

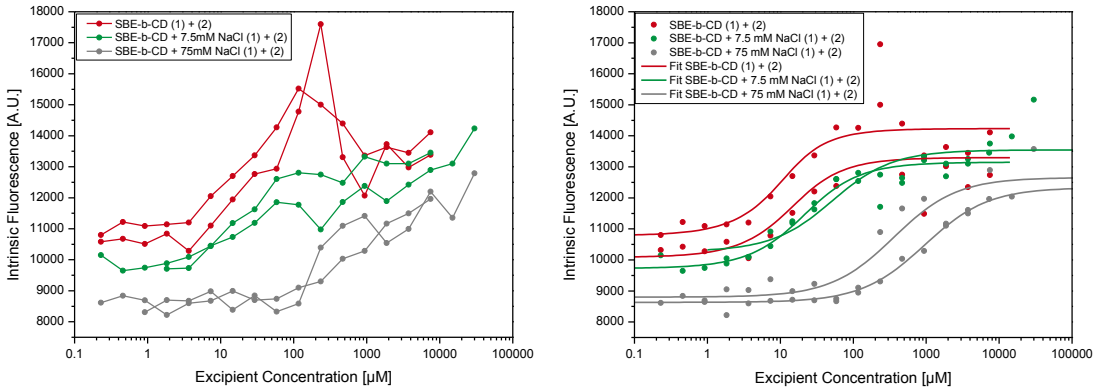

Figure 51: Intrinsic fluorescence binding studies of rh-GCSF to SBE-β-CD in 20 mM acetate buffer pH 4.0 in the presence and absence of sodium chloride. Left: interaction screening of rh-GCSF to SBE-β-CD under the presence of 7.5 mM and 75 mM NaCl. Right: K_d fit of the interaction between rh-GCSF and SBE-β-CD.

Table 15: K_d comparison for the interaction between SBE-β-CD and rh-GCSF in 20 mM acetate buffer pH 4.0 measured by thermophoresis in the presence and absence of sodium chloride. Computed K_d values for single experiments are given including the fitting error, while for mean K_d values, the standard deviation of the included experiments is presented.

Experiment name	Computed K_d [µM]	Unbound [‰]	Bound [‰]	Amplitude [‰]
SBE-β-CD + 0.0 mM NaCl (1)	9.61 ± 0.828	965.76	921.80	-43.96
SBE-β-CD + 0.0 mM NaCl (2)	4.98 ± 0.359	962.25	912.99	-49.26
SBE-β-CD + 0.0 mM NaCl (3)	5.45 ± 0.258	961.34	911.16	-50.18
Mean + 0.0 mM NaCl	**6.68 ± 2.55**	**963.12**	**915.32**	**-47.80**
SBE-β-CD + 7.5 mM NaCl (1)	10.4 ± 0.5	961.06	918.43	-42.63
SBE-β-CD + 7.5 mM NaCl (2)	10.6 ± 0.5	957.00	917.73	-39.27
Mean + 7.5 mM NaCl	**10.5 ± 0.1**	**959.03**	**918.08**	**-40.95**
SBE-β-CD + 75 mM NaCl (1)	770 ± 38	950.68	921.18	-29.50
SBE-β-CD + 75 mM NaCl (2)	233 ± 42	949.91	927.25	-22.66
Mean + 75 mM NaCl	**502 ± 380**	**950.30**	**924.22**	**-26.08**

Table 16: K_d comparison for the interaction between SBE-β-CD and rh-GCSF in 20 mM acetate buffer pH 4.0 measured by intrinsic fluorescence. Computed K_d values for single experiments are given including the fitting error, while for mean K_d values, the standard deviation of the included experiments is presented.

Experiment name	Computed K_d [µM]	Unbound [A.U.]	Bound [A.U.]	Amplitude [A.U.]
SBE-β-CD + 0.0 mM NaCl (1)	9.27 ± 2.30	10083.29	13299.92	3216.63
SBE-β-CD + 0.0 mM NaCl (2)	5.19 ± 0.61	10786.59	14233.27	3446.68
SBE-β-CD + 0.0 mM NaCl (3)	7.44 ± 0.86	10128.45	13519.41	3390.96
Mean + 0.0 mM NaCl	**7.30 ± 2.04**	**10332.78**	**13684.20**	**3351.42**
SBE-β-CD + 7.5 mM NaCl (1)	16.0 ± 0.9	9726.46	13149.68	3423.22
SBE-β-CD + 7.5 mM NaCl (2)	46.7 ± 8.6	10269.40	13545.14	3275.74
Mean + 7.5 mM NaCl	**31.4 ± 21.7**	**9997.93**	**13347.41**	**3349.48**
SBE-β-CD + 75 mM NaCl (1)	948 ± 38	8633.09	12329.17	3696.08
SBE-β-CD + 75 mM NaCl (2)	354 ± 56	8802.26	12654.94	3852.68
Mean + 75 mM NaCl	**651 ± 420**	**8717.68**	**12492.06**	**3774.38**

Additionally, the rh-GCSF-excipient binding studies in 20 mM acetate buffer pH 4.0 were extended to a different buffer system (20 mM phosphate buffer pH 4.0) and an altered buffer pH value (20 mM phosphate buffer pH 7.0).

In accordance to our previous findings, SBE-β-CD also showed a thermophoresis (Figure 52) as well as an intrinsic fluorescence (Figure 53) binding signal in the phosphate buffer with identical pH. Furthermore, neither fluorescence, nor thermophoresis changes were observed when varying the concentration for any of the other cyclodextrins (α-CD, β-CD, and γ-CD), β-CD derivatives (HP-β-CD and M-β-CD), and the negative control (maltoheptaose) in the range of 0.23 to 7500 µM. In detailed consideration of the binding affinities of SBE-β-CD to rh-GCSF in 20 mM phosphate buffer pH 4.0 (Table 17), differences between the thermophoresis and the fluorescence evaluation as well as the parameters determined for 20 mM acetate buffer pH 4.0 become apparent. The K_d values determined in the phosphate buffer are generally higher as in the acetate buffer. In the case of intrinsic fluorescence, the affinity in phosphate buffer is around 300 µM higher than for acetate. As we recently

learned, this could be caused by an increased salt concentration due to the titration of the sodium dihydrogen phosphate buffer to a pH value as low as 4.0. However, the NaCl content needed for the actual K_d-shift would be substantial and is not expected for this pH adjustment. Moreover, the differences between the two MST evaluations (thermophoresis and intrinsic fluorescence) are increased. One possible explanation for the high fluorescence K_d of 307 µM could be the non-optimal curve fitting. Nevertheless, when the data points for the five lowest SBE-β-CD concentrations are removed, the fitted binding curve experiences the most extreme shift to lower affinities, but the computed K_d would only be decreased to 181 µM (data not shown). Moreover, in the literature, a very similar binding affinity of 365 µM was reported for the binding of SBE-β-CD to rh-GCSF in exactly the same assay buffer.[35] This information increases the confidence in the values generated by intrinsic fluorescence despite the problematic curve fitting and rather disputes the conclusions for thermophoresis, which resulted in an almost perfect fit but should in general be evaluated with care when the underlying fluorescence values are changing over the concentration range investigated.

As a final point, the results received for the interaction assay in 20 mM phosphate buffer pH 7.0 reinforce the assumptions of an ion-ion binding mechanism between SBE-β-CD and rh-GCSF, which were based on the opposing charges of the binding partners at pH 4.0 and the influence of increased salt concentrations. As shown in Figure 54, the interaction is completely inhibited when increasing the assay pH from 4.0 to 7.0. This drastic change is effected by charge inversion of the former positively charged rh-GCSF to an overall negatively charged molecule.[19] Thus, an ionic binding to the highly negatively charged sulfobutylether-β-cyclodextrin is hindered.

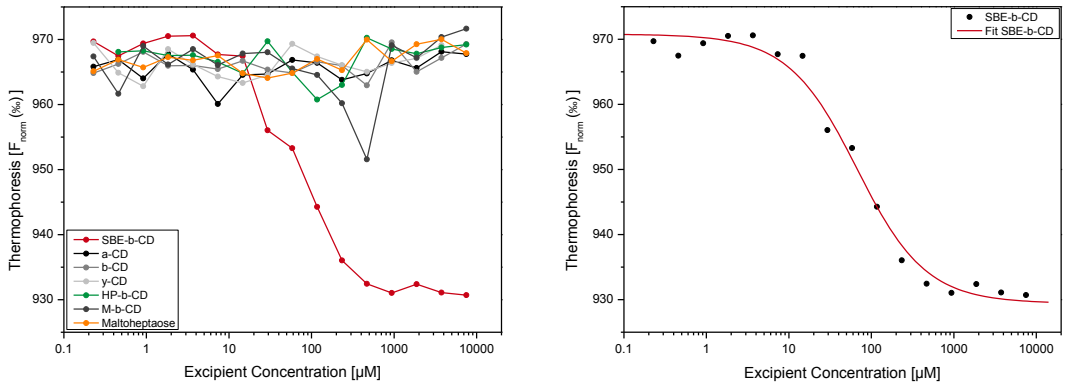

Figure 52: Thermophoresis binding studies of rh-GCSF to cyclodextrins in 20 mM phosphate buffer pH 4.0. Left: interaction screening of rh-GCSF to various cyclodextrins and maltoheptaose as a reference. Right: K_d fit of the interaction between rh-GCSF and SBE-β-CD.

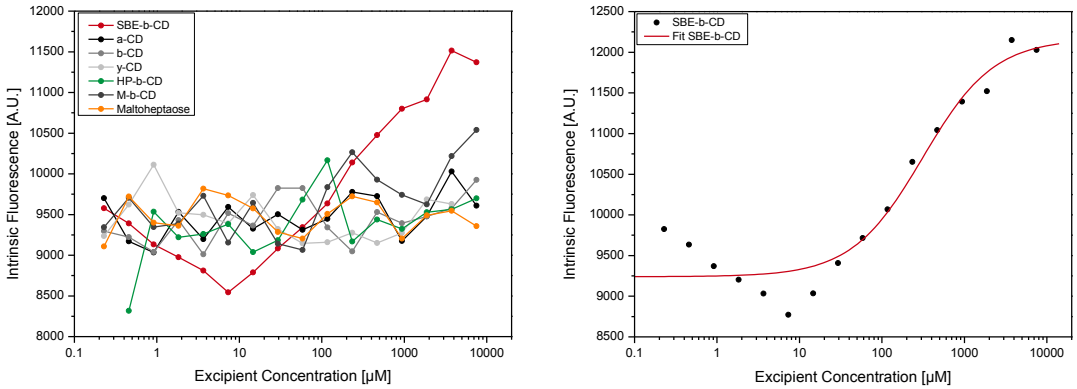

Figure 53: Intrinsic fluorescence binding studies of rh-GCSF to cyclodextrins in 20 mM phosphate buffer pH 4.0. Left: interaction screening of rh-GCSF to various cyclodextrins and maltoheptaose as a reference. Right: K_d fit of the interaction between rh-GCSF and SBE-β-CD.

Table 17: K_d comparison for the interaction between SBE-β-CD and rh-GCSF in 20 mM phosphate buffer pH 4.0 measured by thermophoresis and intrinsic fluorescence. Computed K_d values are given including the fitting error.

Experiment name	Computed K_d [µM]	Unbound [‰ / A.U.]	Bound [‰ / A.U.]	Amplitude [‰ / A.U.]
SBE-β-CD (Thermophoresis)	61.9 ± 2.9	970.79	929.43	-41.36
SBE-β-CD (Intr. Fluorescence)	307 ± 20	9239.94	12166.80	2926.86

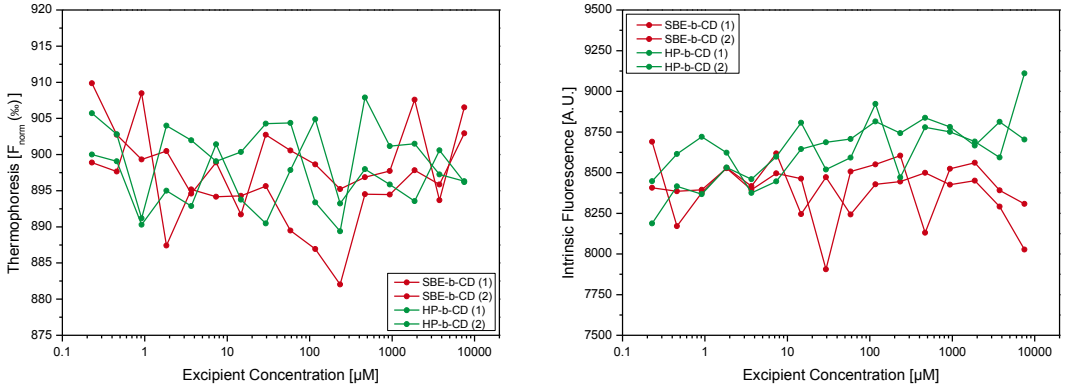

Figure 54: Binding studies of rh-GCSF to SBE-β-CD and HP-β-CD in 20 mM phosphate buffer pH 7. Head-to-head comparison of the thermophoresis (left) and intrinsic fluorescence (right) data evaluation.

VII.2.3.1.2. Nano Differential Scanning Fluorimetry (nanoDSF)

Subsequent to the protein-excipient binding analysis by MST, the prepared titration series were reused for a thermal unfolding stability screening in dependence of the cyclodextrin concentration. Thus, for every titration step an unfolding scan was performed and changes in the unfolding curves, as well as the respective melting temperatures were evaluated from the intrinsic fluorescence emission at 350 nm in order to track binding induced changes in the conformational stability of rh-GCSF.

Figure 55 shows the unfolding screening of rh-GCSF in 20 mM acetate buffer pH 4.0 while changing the concentration of SBE-β-CD (top – left) and HP-β-CD (top – right) between 0.23 and 7500 µM. Additionally, the influence of 7.5 mM NaCl (bottom – left) and 75 mM NaCl (bottom – right) on the SBE-β-CD binding to rh-GCSF was tested. The evaluated melting temperatures of this study are plotted and compared in Table 18 and Figure 56. While the first derivative melting curves of rh-GCSF and the corresponding melting temperatures remained unchanged for increasing concentrations of HP-β-CD, enormous differences were observed for µM to mM concentrations of SBE-β-CD. At nM concentrations of SBE-β-CD, the unfolding transitions are still congruent with the melting curves in the absence of an excipient (data not shown) and under addition of HP-β-CD. However, from the low µM range onwards, the transition shifts towards lower temperatures and additionally a second, less stable conformation occurs. At SBE-β-CD concentrations above 7.32 µM, the initial transition vanishes completely and is fully replaced by the alternative melting point. Hence, a drastic destabilization of rh-GCSF is present in the presence of SBE-β-CD, shifting the T_m from ~ 67.5 °C to a minimum of 42.8 °C at a SBE-β-CD concentration of 117.2 µM. These results are in perfect agreement with unfolding studies reported by Serno[35], where a destabilization by more than 10 °C was induced by the addition of 10 mM SBE-β-CD, while an identical concentration of HP-β-CD did not have any effect on the conformational stability when compared to a reference formulation. In conclusion, the destabilization under increasing cyclodextrin concentrations match the previously characterized binding event between the excipient and the protein where 50% of the molecules were bound at low µM concentrations. Moreover, the SBE-β-CD concentration at which the minimum melting temperature was observed coincides with the peak of the superimposed thermophoresis event.

Under addition of 7.5 mM sodium chloride to the assay buffer, the initial melting transition is shifted towards lower temperatures and the additional unfolding peak appears at higher temperatures, therefore the events converge. At an increased concentration of 75 mM NaCl, this trend is furthermore strengthened and the differences between the two states coalesce. In summary, NaCl destabilizes the initial native state but stabilizes the additional appearing conformation. Whereas the colloidal destabilization of rh-GCSF under increased salt concentration is a well described effect[7,16,19], the latter mentioned stabilization of the transition with lower conformational stability can be explained by a weakening of the detrimental SBE-β-CD interaction to rh-GCSF at excess concentrations of salt, as it was already described in section VII.2.3.1.1.

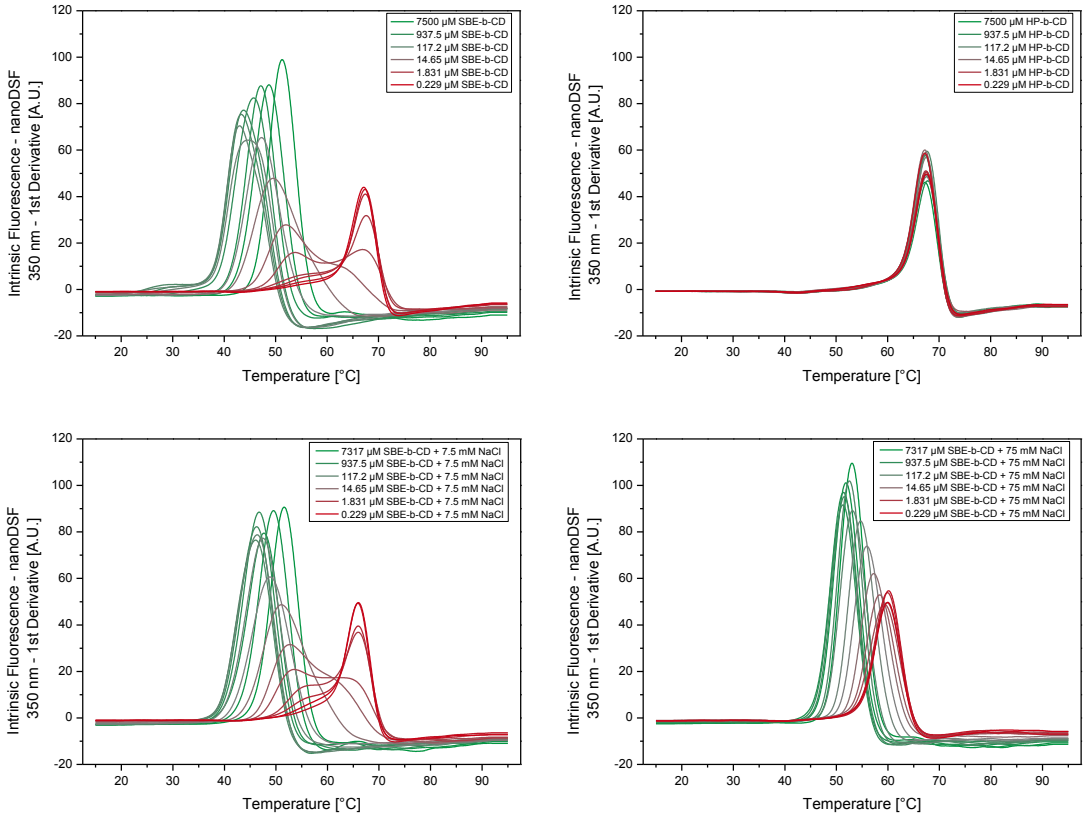

Figure 55: Thermal unfolding studies of the dilution series of SBE-β-CD (top – left) and HP-β-CD (top – right) to rh-GCSF in 20 mM acetate buffer pH 4.0. Additionally, the unfolding curves for the titration of SBE-β-CD in the presence of 7.5 mM NaCl (bottom – left) and 75 mM NaCl (bottom – right) is shown. The color code corresponds to different cyclodextrin concentrations and changes from green over grey to red with progressing dilution.

Table 18: Melting temperature comparison of the rh-GCSF thermal unfolding studies in 20 mM acetate buffer pH 4.0 at different concentrations of HP-β-CD and SBE-β-CD (including 0.0, 7.5 and 75 mM NaCl).

Excipient concentration [µM]	Melting temperature - nanoDSF – 350 nm [°C]					
	HP-β-CD	SBE-β-CD		SBE-β-CD + 7.5 mM NaCl		SBE-β-CD + 75 mM NaCl
	T_m	T_m1	T_m2	T_m1	T_m2	T_m
0.229	67.6	-	67.2	-	66.1	60.0
0.458	67.3	-	67.5	-	66.0	60.1
0.916	67.6	-	67.5	56.1	66.1	59.9
1.831	67.5	-	67.7	55.7	66.1	59.8
3.662	67.3	53.7	66.9	53.4	64.0	59.3
7.324	67.6	51.9	62.8	52.6	62.1	58.3
14.65	67.3	49.5	-	51.0	-	57.2
29.30	67.6	47.2	-	48.8	-	55.9
58.59	67.6	43.8	-	47.5	-	54.7
117.2	67.6	42.8	-	46.4	-	53.1
234.4	67.7	43.1	-	46.2	-	52.5
468.8	67.4	43.5	-	46.3	-	51.5
937.5	67.3	45.8	-	46.7	-	51.3
1875	67.8	47.1	-	47.7	-	51.4
3750	67.6	48.7	-	49.5	-	51.8
7500	67.3	51.3	-	51.6	-	53.0

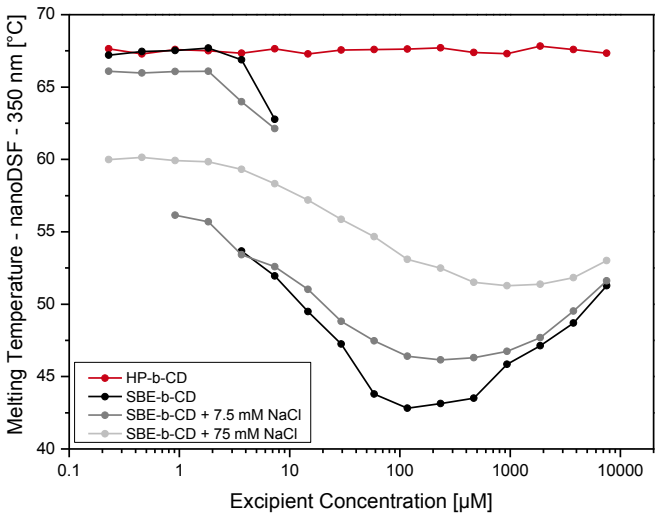

Figure 56: Melting temperature evaluation of the rh-GCSF thermal unfolding studies in 20 mM acetate buffer pH 4.0 at different concentrations of HP-β-CD and SBE-β-CD (including 0.0, 7.5 and 75 mM NaCl). For SBE-β-CD without NaCl and with 7.5 mM NaCl, two melting points were detected, which co-occurr for 2-4 SBE-β-CD concentrations between 0.916 and 7.32 µM SBE-β-CD.

The melting curve comparison was continued with the binding studies in 20 mM phosphate buffer pH 4.0 (Figure 57) and 20 mM phosphate buffer pH 7.0 (data not shown). When changing the buffer system from acetate to phosphate while maintaining the buffer pH at 4.0, a comparable destabilization becomes apparent with increasing concentrations of SBE-β-CD. Moreover, HP-β-CD addition did again not have any impact on the evaluated unfolding temperatures. Nevertheless, it is worth to mention that the T_m values in the phosphate buffer for all HP-β-CD and for the neglegibly low SBE-β-CD concentrations are around 4 °C lower when compared to the acetate buffer. Moreover, the T_m decrease is less pronounced under influence of SBE-β-CD. Thus, the conformational stability rather compares to the acetate buffer with an increased ionic strength, which also would fit very good to the higher K_d values measured in the phosphate buffer system. Overall, the trends received for 20 mM phosphate buffer pH 4.0 are very comparable to 20 mM acetate buffer pH 4.0.

For 20 mM phosphate buffer pH 7.0, no change in melting temperature was observed for both, the SBE- and HP-β-CD titration. That confirms the lack of any measurable interaction under these conditions. Furthermore, the apparent T_m values for both excipients range around 57.5 °C, what corresponds to another destabilization by 6 °C in comparison to 20 mM phosphate buffer pH 4.0 and an overall reduction by 10 °C compared to the initial 20 mM acetate buffer at pH 4.0.

These results substantiate the presence of an ionic interaction between SBE-β-CD and rh-GCSF under acidic assay conditions, shifting the T_m values to lower temperatures and therefore destabilizing the protein conformation. Moreover, again no interaction of HP-β-CD to surface exposed aromatic amino acid residues was observed, which is described to preferentially occur for the unfolded state[36,37] and thus expected to lower the apparent melting temperature.

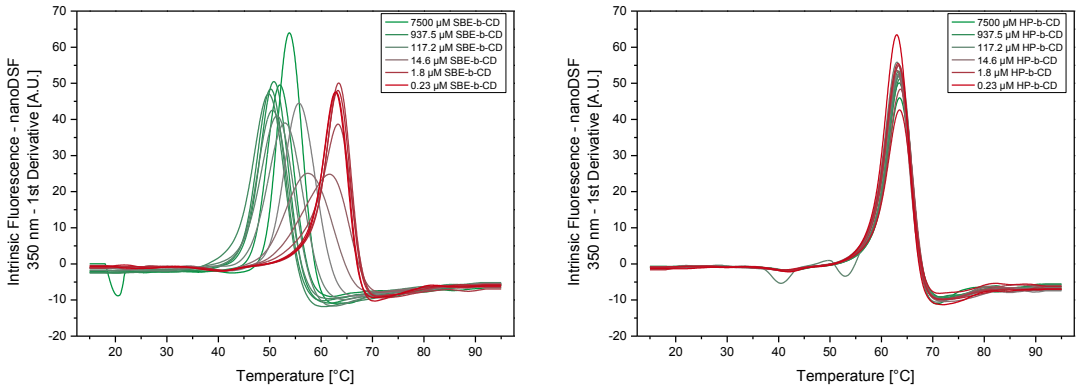

Figure 57: Thermal unfolding studies of the dilution series of SBE-β-CD (left) and HP-β-CD (right) to rh-GCSF in 20 mM phosphate buffer pH 4.0. The color code corresponds to different cyclodextrin concentrations and changes from green over grey to red with progressing dilution.

VII.2.3.1.3. Static Light Scattering (SLS)

Aggregation propensity as the other half of thermal stability investigations was studied to complete the rh-GCSF-cyclodextrin binding analysis. Since unfolding stability was already drastically reduced by the addition of SBE-β-CD, there is reason to presume a negative effect on the tendency to aggregate. Aggregation stability was investigated for the excipient-buffer combinations from former measurements by using static light scattering in a linear thermal ramp assay.

For the dilution series of HP-β-CD to rh-GCSF in 20 mM acetate buffer pH 4.0 (Figure 58 – right) and 20 mM phosphate buffer pH 4.0 (Figure 59 – right) only minor aggregation was observed, starting in the temperature range of the respective unfolding events (see VII.2.3.1.2) and not showing any difference between changing concentration levels of the cyclodextrins. Nevertheless, the absolute amplitude of aggregation is larger for the phosphate buffer what indicates the generation of an increased number or size of particles.

For SBE-β-CD (Figure 58 – left and Figure 59 – left), aggregation sets in immediately after initiating the temperature increase for both buffer systems. Moreover, earlier aggregation onsets and overall increased scattering levels are seen for higher cyclodextrin concentrations. At this immense instability, a difference between the two buffer salts was not identified.

The aggregation propensities derived from the type of cyclodextrin used are in very good aggreement with previous investigations by Serno[35], where the addition of HP-β-CD effectively supressed rh-GCSF aggregation during agitation, freeze-thawing and storage stability studies, while SBE-β-CD even showed adverse stability effects.

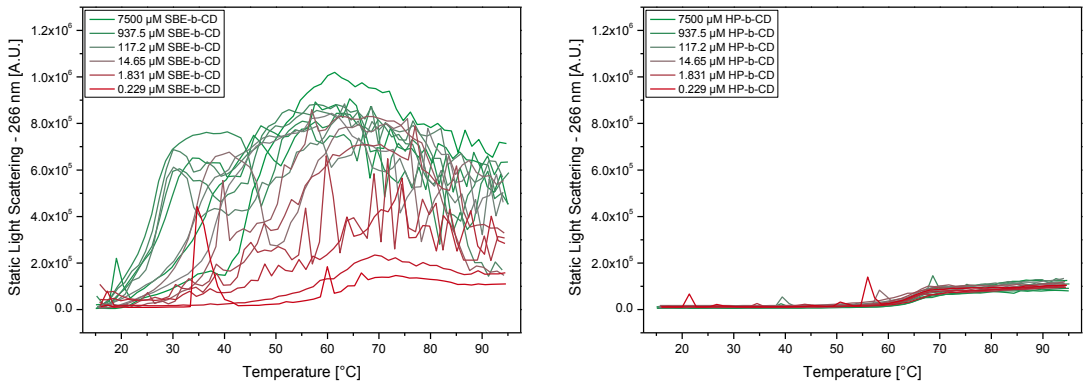

Figure 58: Thermal aggregation studies of the dilution series of SBE-β-CD (left) and HP-β-CD (right) to rh-GCSF in 20 mM acetate buffer pH 4.0. The color code corresponds to different cyclodextrin concentrations and changes from green over grey to red with progressing dilution.

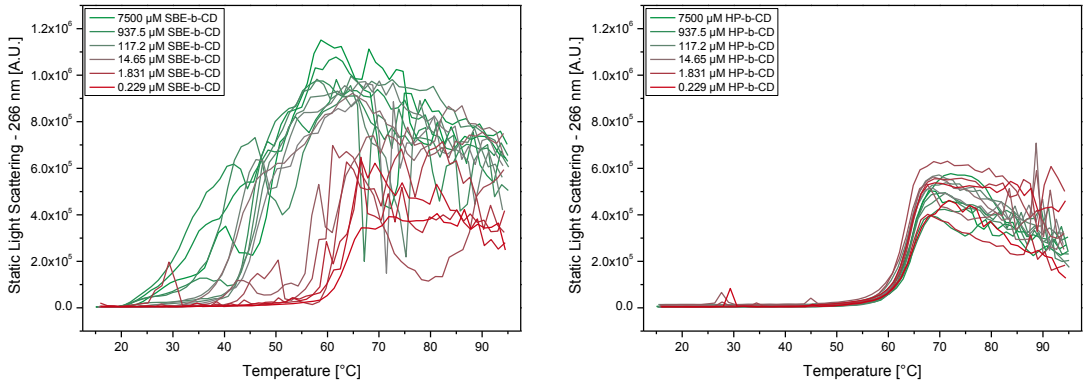

Figure 59: Thermal aggregation studies of the dilution series of SBE-β-CD (left) and HP-β-CD (right) to rh-GCSF in 20 mM phosphate buffer pH 4.0. The color code corresponds to different cyclodextrin concentrations and changes from green over grey to red with progressing dilution.

VII.2.3.2. Binding Studies with Surfactants

Additional binding studies were used to examine the interaction of rh-GCSF with monomeric surfactant molecules or incorporation into micellar structures. Elucidating the interaction mechanism between the protein of interest and surfactants can simplify the development of stable formulations that minimize interfacial degradation.[38-40] For our investigations, Pluronic F-127, an amphiphilic triblock copolymer consisting of ethylene oxide and propylene oxide units, was chosen over other more commonly used non-ionic group members like polysorbate 20 or 80, as it does not show intrinsic auto-fluorescence in the concentration range used and is also FDA approved for parenteral administration.[41-43]

VII.2.3.2.1. MicroScale Thermophoresis (MST)

Figure 60 shows the intrinsic fluorescence (left) and thermophoresis (right) values for a broad range of pluronic F-127 concentrations titrated to rh-GCSF. The assay was performed in 20 mM acetate buffer pH 4.0 under variation of the temperature.

At an assay temperature of 22 °C only a minor fluorescence increase at the highest surfactant concentrations was observed. However, when changing the assay temperature to 27 °C, the quantum yield increases drastically from pluronic concentrations above 0.1%. Moreover, this immense increase was found to be also highly temperature dependent, as the onset of the increase in fluorescence is shifted to lower concentrations when the temperature is further increased. In our assay, the maximal temperature of 37 °C decreases the onset concentration to approximately 0.01%. These findings indicate rather the formation of micelles and incorporation of rh-GCSF than a simple 1:1 binding between monomeric pluronic and rh-GCSF. In this theory, the strong temperature dependence observed is explained by the characteristics of pluronic F-127 micellization, being highly temperature dependent in the range investigated[44]. Consequently, the spontaneous increase in fluorescence would be caused by the encapsulation of rh-GCSF into the hydrophobic core of the micelles. Intrinsic protein fluorescence by aromatic amino acids (mainly Trp and Tyr) is known to be very sensitive to changes in the local environment of the fluorophores and might increase upon transition from the aqueous, hydrophilic solution to the hydrophobic environment within the core of a micelle.[45,46]

For thermophoresis, the measurement data have to be interpreted with great care as variations in the underlying fluorescence signal can lead to evaluation artifacts. In detail, the thermophoresis evaluation would be biased by a high fluorescence increase in terms of enhanced thermophoretic depletion and consequent decrease in the thermophoresis values. Therefore, only data points at which the fluorescence was not increased were taken into account for analysis. At low concentrations of pluronic F-127, the thermophoresis signal is constant for all temperatures investigated. With increasing surfactant concentrations a rise in the thermophoresis signal is observed. Comparing the increases in thermophoresis and fluorescence at 22 and 27 °C, thermophoresis already changes at lower surfactant concentrations. This deviation might be caused by the IR-laser induced heating of the sample, which potentially is enough to exceed the critical micelle temperature (CMT) and therefore allow the in-situ formation of micelles during the measurement. This would also explain the rapid thermophoresis increase, as a micelle formation induced fluorescence increase during the measurement would lead to a pseudo decrease in thermophoretic depletion or even negative thermophoresis and a consequential increase in thermophoresis values. In conclusion, incorporation into pluronic F-127 micelles is assumed, while for this application the fluorescence readout is less ambiguous than thermophoresis, which inevitably induces an IR-laser temperature increase.

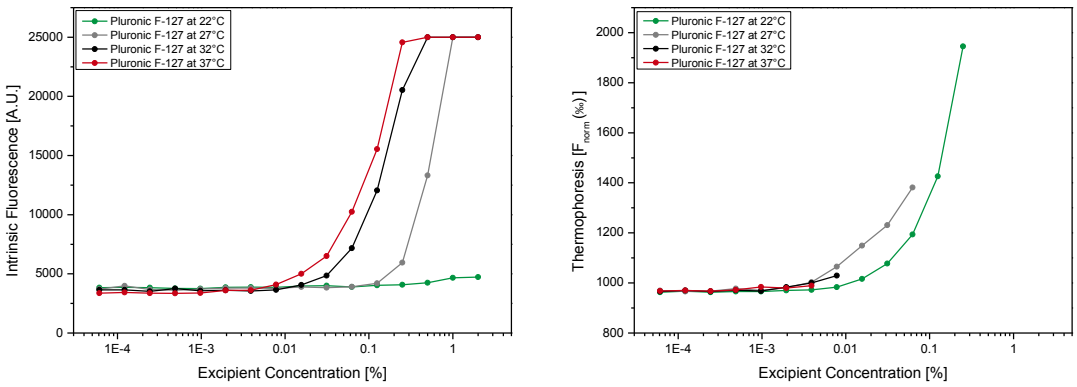

Figure 60: rh-GCSF binding studies with pluronic F-127 in 20 mM acetate buffer pH 4.0 at different temperatures evaluated by intrinsic fluorescence (left) and thermophoresis (right).

VII.2.3.2.2. Nano Differential Scanning Fluorimetry (nanoDSF)

Thermal protein unfolding analysis by intrinsic fluorescence analysis (nanoDSF) was used to get a broader picture of the fluorescence changes over temperature for every single titration step. In Figure 61 the fluorescence emission (left) as well as the first derivative curves (right) of rh-GCSF with varying concentrations of pluronic F-127 are shown as a function of the temperature. For very low concentrations of Pluronic F-127 (red lines) there is an increase in the fluorescence observed only when the protein unfolds at around 67 °C. When the surfactant concentration exceeds 0.002%, a fluorescence increase at above 40 °C prior to the melting temperature appears and the fluorescence traces split from the uniform unfolding curves. Further, the size of the unfolding peak in the first derivative curve decreases and another event at lower temperatures emerges. From concentrations of 0.125% onwards, the fluorescence at lower temperatures is drastically increased and the melting event is not visible any longer. Overall, a combination of temperature and concentration dependence is observed in this measurement, as at high concentrations the large fluorescence increase occurs at lower temperatures compared to lower concentrations of pluronic F-127. A formation of micelles at pluronic concentrations above 0.125% is likely, as the reported critical micelle concentration (CMC) values of pluronic F-127 at ambient temperatures are in a broad range of 0.1 to 2%, with generally decreasing concentrations being reported at increasing temperatures.[44,47-49] Moreover, the fluorescence intensity increase is purely related to the intrinsic fluorescence of rh-GCSF as comparable temperature ramp studies performed with pure pluronic dilution series in the absence of rh-GCSF did result in very low fluorescence values (below 250 A.U.), without any fluorescence peaks/increases over the whole temperature range (data not shown).

In conclusion, a formation of micelles and incorporation of rh-GCSF molecules under the present measurement conditions is hypothesized and additional studies investigating CMC values in the presence of the protein with orthogonal techniques would give further insight in the underlying mechanisms.

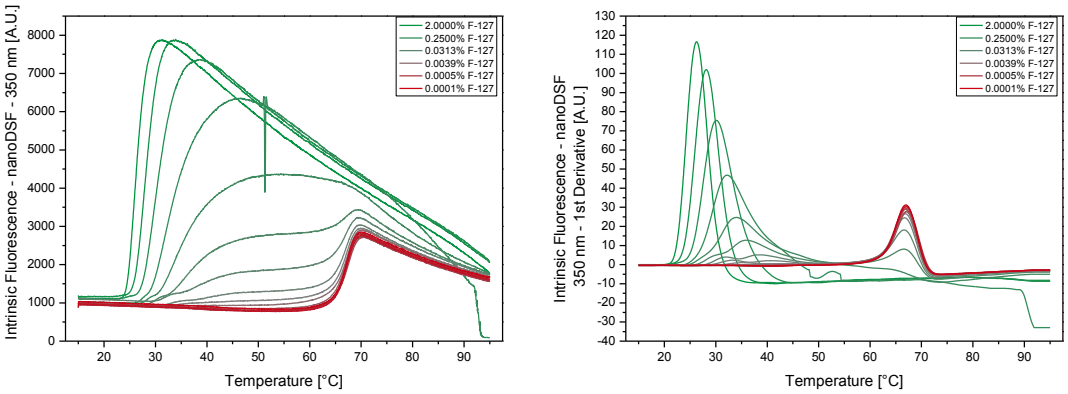

Figure 61: Thermal unfolding studies of the dilution series of pluronic F-127 to rh-GCSF in 20 mM acetate buffer pH 4.0 by nanoDSF evaluated at 350 nm (left) and the first derivative plot (right). The color code corresponds to different pluronic F-127 concentrations and changes from green over grey to red with progressing dilution of the surfactant.

VII.2.3.3. Comparison and Evaluation of MST as a Tool for Protein-Excipient Interaction Analysis

Protein-excipient interaction analyses by MST, as exemplarily studied for the binding of cyclodextrins and pluronic F-127 to rh-GCSF, were found to provide valuable insights into the molecular stabilization and destabilization mechanisms in protein formulations.

Within the interaction screening of various cyclodextrins, MST measurements conclusively distinguished between binding and non-binding variants. Moreover, influences of the formulation pH, the buffering agent and added salt on the protein-excipient interaction between SBE-β-CD and rh-GCSF were revealed. In the following, the determined interactions were confirmed by analyzing the stability consequences via thermal unfolding and aggregation studies, which led to a pronounced destabilization of rh-GCSF for increasing concentrations of SBE-β-CD.

Furthermore, incorporation of rh-GCSF into the hydrophobic core of micelles upon reaching the CMC or the CMT was indicated via MST and nanoDSF studies. All gathered results and derived trends were found to correlate well with literature data, making MST a valid and with great justice accepted tool for the screening of all kinds of biomolecular interactions.

VII.3. Summary and Conclusions

In the case study presented, the stability of twelve rh-GCSF formulations was assessed as resistance towards unfolding and aggregation in a stepped thermal ramp assay by using MST and an innovative forced degradation approach by using TOPC. Stability trends were derived for the formulation pH, as well as the addition of polysorbate, HP-β-CD, and buffering agents. The derived trends for protein unfolding as well as aggregation propensity were benchmarked with orthogonal approaches for the determination of physical stabilities.

In summary, the unfolding and aggregation propensity of rh-GCSF was found to consistently increase with increasing pH values and in the presence of buffer salts, which is in very good alignment with the comprehensive literature and patent database available. Thermal unfolding and aggregation evaluated by MST, as well as forced degradation by using TOPC showed several advantages over conventional approaches, being unaffected by the excipients tested and very low in material and time consumption. This could be beneficial for cost-efficient early formulation selections by screening of a large number of solution conditions under high material scarcity and time pressure.

Furthermore, rh-GCSF-excipient interactions were investigated for cyclodextrins and pluronic F-127 via MST binding titrations. Interactions between rh-GCSF and cyclodextrins were detected and quantified under variation of the buffer salt, ionic strength and the solution pH. Moreover, the stability consequences of protein-excipient binding were investigated. For pluronic F-127, the presence and mode of interaction between rh-GCSF and the surfactant were assessed.

Among the list of cyclodextrins investigated, protein-excipient binding was merely detected for rh-GCSF and SBE-β-CD. The binding mechanism was characterized as ionic interaction between the negatively charged excipient and the positively charged protein. Consequently, salt addition weakened and changing the formulation pH to neutral inhibited the interaction. Stability investigations by using nanoDSF and SLS confirmed the interaction and rendered the ion-pairing detrimental for unfolding and aggregation stability. Investigation of the interaction between rh-GCSF and pluronic F-127 resulted in prominent and strongly temperature and concentration dependent fluorescence effects, which indicate interaction and protein incorporation into micelles.

Taken all aspects together, MST and TOPC are suggested for greater applicability in straightforward, material and time saving stability investigations as well as rational excipient selections in the early phases of protein formulation development.

VII.4. References

1. Brems DN. 2002. The kinetics of G-CSF folding. Protein Science 11(10):2504-2511.

2. Metcalf D. 1985. The granulocyte-macrophage colony-stimulating factors. Science 229(4708):16-22.

3. Shochat E, Rom-Kedar V, Segel LA. 2007. G-CSF Control of neutrophils dynamics in the blood. Bulletin of Mathematical Biology 69(7):2299-2338.

4. Herman AC, Boone TC, Lu HS. 2002. Characterization, formulation, and stability of Neupogen® (filgrastim), a recombinant human granulocyte-colony stimulating factor. In: Pearlman R, Wang YJ, Formulation, Characterization, and Stability of Protein Drugs: Case Histories. Springer. p 303-328.

5. Piedmonte DM, Treuheit MJ. 2008. Formulation of Neulasta® (pegfilgrastim). Advanced Drug Delivery Reviews 60(1):50-58.

6. Kolvenbach CG, Elliott S, Sachdev R, Arakawa T, Narhi LO. 1993. Characterization of two fluorescent tryptophans in recombinant human granulocyte-colony stimulating factor: Comparison of native sequence protein and tryptophan-deficient mutants. Journal of Protein Chemistry 12(2):229-236.

7. Chi E, Krishnan S, Randolph T, Carpenter J. 2003. Physical stability of proteins in aqueous solution: Mechanism and driving forces in nonnative protein aggregation. Pharmaceutical Research 20(9):1325-1336.

8. Narhi LO, Kenney WC, Arakawa T. 1991. Conformational changes of recombinant human granulocyte-colony stimulating factor induced by pH and guanidine hydrochloride. Journal of Protein Chemistry 10(4):359-367.

9. Hinderer W, Lubenau H. 2015. Method of treatment using stable liquid formulation of G-CSF. US Patent US 8,946,161 B2. Biogenerix GmbH. Available at: https://patents.google.com/patent/US8946161B2/en. Accessed: October 14, 2018

10. Raso SW, Abel J, Barnes JM, Maloney KM, Pipes G, Treuheit MJ, King J, Brems DN. 2005. Aggregation of granulocyte-colony stimulating factor in vitro involves a conformationally altered monomeric state. Protein Science 14(9):2246-2257.

11. Michaelis U, Rudolph R, Winter G, Woog H. 1999. Aqueous pharmaceutical preparations of G-CSF with a long shelf life. US Patent 5,919,757. Boehringer Mannheim GmbH. Available at: https://patents.google.com/patent/US5919757A/en. Accessed: October 14, 2018

12. Zbacnik TJ, Holcomb RE, Katayama DS, Murphy BM, Payne RW, Coccaro RC, Evans GJ, Matsuura JE, Henry CS, Manning MC. 2017. Role of buffers in protein formulations. Journal of Pharmaceutical Sciences 106(3):713-733.

13. Ablinger E, Hellweger M, Leitgeb S, Zimmer A. 2012. Evaluating the effects of buffer conditions and extremolytes on thermostability of granulocyte colony-stimulating factor using high-throughput screening combined with design of experiments. International Journal of Pharmaceutics 436(1):744-752.

14. Youssef AMK, Winter G. 2013. A critical evaluation of microcalorimetry as a predictive tool for long term stability of liquid protein formulations: Granulocyte colony stimulating factor (GCSF). European Journal of Pharmaceutics and Biopharmaceutics 84(1):145-155.

15. Ricci MS, Sarkar CA, Fallon EM, Lauffenburger DA, Brems DN. 2003. pH dependence of structural stability of interleukin-2 and granulocyte colony-stimulating factor. Protein Science 12(5):1030-1038.

16. Boone TC, Kenney WC. 1992. Stabilized hydrophobic protein formulations of G-CSF. US Patent 5,104,651. Amgen Inc. Available at: https://patents.google.com/patent/US5104651A/en. Accessed: October 14, 2018

17. Krishnan S, Chi EY, Webb JN, Chang BS, Shan D, Goldenberg M, Manning MC, Randolph TW, Carpenter JF. 2002. Aggregation of granulocyte colony stimulating factor under physiological conditions: Characterization and thermodynamic inhibition. Biochemistry 41(20):6422-6431.

18. Johnston TP. 1996. Adsorption of recombinant human granulocyte colony stimulating factor (rhG-CSF) to polyvinyl chloride, polypropylene, and glass: effect of solvent additives. PDA Journal of Pharmaceutical Science and Technology 50(4):238-245.

19. Chi EY, Krishnan S, Kendrick BS, Chang BS, Carpenter JF, Randolph TW. 2003. Roles of conformational stability and colloidal stability in the aggregation of recombinant human granulocyte colony-stimulating factor. Protein Science 12(5):903-913.

20. Product Information Neupogen. Available at: https://www.gelbe-liste.de/produkte/Neupogen-30-Mio-E-300-g-1-0-ml_112372. Accessed: October 1, 2018.

21. Product Information Neulasta. Available at: https://www.gelbe-liste.de/produkte/Neulasta-6-mg-Injektionsloesung_363101#! Accessed: October 1, 2018.

22. Thirumangalathu R, Krishnan S, Brems DN, Randolph TW, Carpenter JF. 2006. Effects of pH, temperature, and sucrose on benzyl alcohol-induced aggregation of recombinant human granulocyte colony stimulating factor. Journal of Pharmaceutical Sciences 95(7):1480-1497.

23. Banks DD, Zhang J, Siska CC. 2014. Relationship between native-state solubility and non-native aggregation of recombinant human granulocyte colony stimulating factor: Practical implications for protein therapeutic development. Molecular Pharmaceutics 11(10):3431-3442.

24. Bam NB, Cleland JL, Yang J, Manning MC, Carpenter JF, Kelley RF, Randolph TW. 1998. Tween protects recombinant human growth hormone against agitation-induced damage via hydrophobic interactions. Journal of Pharmaceutical Sciences 87(12):1554-1559.

25. Menzen T, Friess W. 2013. High-throughput melting-temperature analysis of a monoclonal antibody by differential scanning fluorimetry in the presence of surfactants. Journal of Pharmaceutical Sciences 102(2):415-428.

26. Ablinger E, Leitgeb S, Zimmer A. 2013. Differential scanning fluorescence approach using a fluorescent molecular rotor to detect thermostability of proteins in surfactant-containing formulations. International Journal of Pharmaceutics 441(1):255-260.

27. Samra HS, He F. 2012. Advancements in high throughput biophysical technologies: Applications for characterization and screening during early formulation development of monoclonal antibodies. Molecular Pharmaceutics 9(4):696-707.

28. Del Valle EMM. 2004. Cyclodextrins and their uses: A review. Process Biochemistry 39(9):1033-1046.

29. Hawe A, Filipe V, Jiskoot W. 2010. Fluorescent molecular rotors as dyes to characterize polysorbate-containing IgG formulations. Pharmaceutical Research 27(2):314-326.

30. Hawe A, Sutter M, Jiskoot W. 2008. Extrinsic fluorescent dyes as tools for protein characterization. Pharmaceutical Research 25(7):1487-1499.

31. Youssef AMK. 2010. Systematic studies to correlate microcalorimetry with stability studies on liquid formulations of various protein drugs. Dissertation. Ludwig-Maximilians-Universität München. Available at: https://edoc.ub.uni-muenchen.de/11623/1/Ahmed_Moustafa_Kamal_Youssef_Mohamed.pdf. Accessed: October 14, 2018.

32. Davis ME, Brewster ME. 2004. Cyclodextrin-based pharmaceutics: Past, present and future. Nature Reviews Drug Discovery 3:1023-1035.

33. Horský J, Pitha J. 1994. Inclusion complexes of proteins: Interaction of cyclodextrins with peptides containing aromatic amino acids studied by competitive spectrophotometry. Journal of Inclusion Phenomena and Molecular Recognition in Chemistry 18(3):291-300.

34. Otzen DE, Knudsen BR, Aachmann F, Larsen KL, Wimmer R. 2002. Structural basis for cyclodextrins' suppression of human growth hormone aggregation. Protein Science 11(7):1779-1787.

35. Serno T. 2010. Inhibition of therapeutic protein aggregation by cyclodextrins. Dissertation. Ludwig-Maximilians-Universität München. Available at: https://edoc.ub.uni-muenchen.de/13125/1/Serno_Tim.pdf. Accessed: October 14, 2018.

36. Cooper A. 1992. Effect of cyclodextrins on the thermal stability of globular proteins. Journal of the American Chemical Society 114(23):9208-9209.

37. Cooper A, Lovatt M, Nutley MA. 1996. Energetics of protein-cyclodextrin interactions. Journal of Inclusion Phenomena and Molecular Recognition in Chemistry 25(1-3):85-88.

38. Khan TA, Mahler H-C, Kishore RSK. 2015. Key interactions of surfactants in therapeutic protein formulations: A review. European Journal of Pharmaceutics and Biopharmaceutics 97, Part A:60-67.

39. Lee HJ, McAuley A, Schilke KF, McGuire J. 2011. Molecular origins of surfactant-mediated stabilization of protein drugs. Advanced Drug Delivery Reviews 63(13):1160-1171.

40. Randolph TW, Jones LS. 2002. Surfactant-protein interactions. In: Carpenter JF, Manning MC, Rational Design of Stable Protein Formulations. Springer. p 159-175.

41. Chiappetta DA, Sosnik A. 2007. Poly (ethylene oxide)–poly (propylene oxide) block copolymer micelles as drug delivery agents: Improved hydrosolubility, stability and bioavailability of drugs. European Journal of Pharmaceutics and Biopharmaceutics 66(3):303-317.

42. Domínguez-Delgado CL, Fuentes-Prado E, Escobar-Chávez JJ, Vidal-Romero G, Rodríguez-Crus I, Díaz-Torres R. 2016. Chitosan and Pluronic® F-127: Pharmaceutical applications. In: Mishra MK, Encyclopedia of Biomedical Polymers and Polymeric Biomaterials. Taylor & Francis. p 1513-1535.

43. Sezgin Z, Yüksel N, Baykara T. 2006. Preparation and characterization of polymeric micelles for solubilization of poorly soluble anticancer drugs. European Journal of Pharmaceutics and Biopharmaceutics 64(3):261-268.

44. Bohorquez M, Koch C, Trygstad T, Pandit N. 1999. A study of the temperature-dependent micellization of pluronic F127. Journal of Colloid and Interface Science 216(1):34-40.

45. Ghisaidoobe A, Chung S. 2014. Intrinsic tryptophan fluorescence in the detection and analysis of proteins: A focus on förster resonance energy transfer techniques. International Journal of Molecular Sciences 15(12):22518-22538.

46. Teale FW, Weber G. 1957. Ultraviolet fluorescence of the aromatic amino acids. Biochemical Journal 65(3):476-482.

47. Linse P, Malmsten M. 1992. Temperature-dependent micellization in aqueous block copolymer solutions. Macromolecules 25(20):5434-5439.

48. Gao Q, Liang Q, Yu F, Xu J, Zhao Q, Sun B. 2011. Synthesis and characterization of novel amphiphilic copolymer stearic acid-coupled F127 nanoparticles for nano-technology based drug delivery system. Colloids and Surfaces B: Biointerfaces 88(2):741-748.

49. Singh V, Khullar P, Dave PN, Kaur N. 2013. Micelles, mixed micelles, and applications of polyoxypropylene (PPO)-polyoxyethylene (PEO)-polyoxypropylene (PPO) triblock polymers. International Journal of Industrial Chemistry 4:12.

Chapter VIII
Monoclonal Antibody (mAb)

Antibodies and antibody derivatives have already been introduced in Chapter V as they make up the most prominent group of marketed biopharmaceutical drug products, showing a very high efficacy and low adverse effects.[1]

Due to this high relevance, an extended formulation screening investigating the stability of another monoclonal antibody (mAb) is presented in this chapter. In a pH pre-screening, the influence of different pH values on protein unfolding and aggregation parameters is targeted. The second step consists of a set of eleven formulations that is used to additionally determine the stability dependence on different buffer salts and various formulation excipients such as sugars, polyols, salt and polysorbate. For both steps, the lead formulation (10 mM phosphate, pH 6.0), as well as the overall pH range and excipient selection were adapted from previous investigations on the same antibody[2]. Using these screening sets, the capability of MST and TOPC as valuable tools in drug product development is investigated. Our results for thermal unfolding and aggregation stability are compared to a variety of benchmark methods as intrinsic and extrinsic fluorescence emission spectroscopy, static and dynamic light scattering, as well as differential scanning calorimetry. Furthermore, chemical unfolding is investigated as an emerging technology in the field of protein formulation development.[3,4] The TOPC results are benchmarked with a conventional forced degradation approach, followed by visual inspection, dynamic light scattering and turbidity readout.

Additionally to the formulation screening, the mAb is undertaken interaction analyses by using MST. Three different cyclodextrins as well as two β-CD derivatives are used to investigate the interaction mechanism and to derive stability consequences of protein-excipient binding in dependence of the formulation pH.

Parts of this chapter have been published under: Wanner R, Breitsprecher D, Duhr S, Baaske P, Winter G 2017. Thermo-Optical Protein Characterization for Straightforward Preformulation Development. Journal of Pharmaceutical Sciences 106(10):2955-2958.

VIII.1. Materials and Methods

VIII.1.1. mAb

The monoclonal antibody (mAb) used in this study was kindly donated by Roche Diagnostics GmbH (Penzberg, Germany). The IgG subtype protein stock solution was formulated at a concentration of 18.65 mg/ml in 10 mM phosphate buffer, pH 6.4.

VIII.1.2. Excipients and Reagents

An overview of excipients and buffer salts used in the formulation screening can be found in Table 19. During formulation preparation, stock solutions of all listed substances were prepared in HPW and used for the formulation compounding. In Table 20 all materials used for the further preparation during chemical unfolding and protein-excipient interaction investigations are summarized. The sodium hydroxide and hydrochloric acid standard solutions used for pH adjustment were of analytical grade. All given pH values were adjusted by titration to a precision of ± 0.02. Highly purified water (ELGA Purelab, ELGA LabWater, Celle, Germany, now Veolia Water Technologies GmbH) was used exclusively for all preparation steps.

Table 19: Overview of excipients and buffer salts used for the mAb formulation screenings.

Material	Supplier	Art.-number	Lot-number
Tween 80 (Polysorbate)	Merck KGaA, Darmstadt, Germany	8.17061.1000	K38539861 827
D(-)-Sorbitol	Merck KGaA, Darmstadt, Germany	1.07759.0100	L58065059 829
Sucrose	Südzucker AG, Plattling, Germany	Raw material sample	L 115210300
Glycerol	AppliChem GmbH, Darmstadt, Germany	A4443,1000	3J008408
Sodium chloride	VWR International BVBA, Leuven, Belgium	27810.295	12J150047
Hydroxy-Propyl-beta-Cyclodextrin (HP-β-CD, Cavasol W7 HP Pharma)	Wacker Chemie AG, Burghausen, Germany	60012210	73B012
Sodium dihydrogen phosphate dihydrate	Applichem GmbH, Darmstadt, Germany	A1939,1000	0A006917
L-Histidine monohydrochloride monohydrate	Sigma Aldrich, St. Louis, MO, USA	H4036-1KG	068K8310
Succinic acid	Merck KGaA, Darmstadt, Germany	1.00682.0250	K33027682 434

Table 20: Overview of excipients and reagents used for chemical denaturation and the mAb-excipient interaction study.

Material	Supplier	Art.-number	Lot-number
Guanidine hydrochloride (GuHCl)	Sigma Aldrich, St. Louis, MO, USA	G4505-100G	071M5429V
Sodium dihydrogen phosphate dihydrate	Applichem GmbH, Darmstadt, Germany	A1939,1000	0A006917
Alpha-Cyclodextrin (α-CD)	CycloLab R&D Ltd, Budapest, Hungary	CY-1001	CYL-2322
Beta-Cyclodextrin (β-CD, Cavamax W7 Pharma)	Wacker Chemie AG, Burghausen, Germany	60006994	70P255
Hydroxy-Propyl-beta-Cyclodextrin (HP-β-CD, Cavasol W7 HP Pharma)	Wacker Chemie AG, Burghausen, Germany	60012210	73B012
Sulfobutyl-Ether-beta-Cyclodextrin (Captisol SBE-β-CD Sodium Salt)	CyDex Inc, Lenexa, KS, USA	-	NC-04A-05009
Gamma-Cyclodextrin (γ-CD)	CycloLab R&D Ltd, Budapest, Hungary	CY-3001	CYL-1815

VIII.1.3. Formulations

For the preparation of the pH pre-screening, the protein stock solution was prediluted to 15.0 mg/ml with 10 mM phosphate buffer, pH 5.0, before it was further diluted to the final concentration of 0.5 mg/ml with the respective 10 mM phosphate reference buffers, ranging from pH 4.0 to 6.2 in steps of 0.2. Afterwards, the samples were adjusted to the desired pH values by titration using HCl/NaOH to an accuracy of ± 0.01 and sterile filtrated using 0.22 µm Millex GV PVDF syringe filter units (Merck Millipore Ltd., Tullagreen, Ireland). The buffer references were filtrated using sterile syringe filters with a 0.2 µm cellulose acetate membrane (VWR International LLC, Radnor, PA, USA).

Table 21: Overview of the formulations prepared for the mAb pH pre-screening.

ID	mAb [mg/mL]	Buffer system	pH
pH 4.0, ..., pH 6.2	0.5	10 mM phosphate	4.0, 4.2, 4.4, ..., 6.0, 6.2

For the subsequent formulation excipient screening, the protein stock solution was dialyzed in three batches to phosphate, histidine, and succinate buffer, each in a concentration of 10 mM at pH 6.0. All dialyses were performed at 2-8 °C in three steps of 4 liter dialysis buffer each by using Slide-A-Lyzer dialysis cassettes (10000 MWCO,

0.5-3 ml (His & Suc) and 3-12 ml (Pho) capacity, Thermo Scientific, Rockford, IL, USA). The extensive dialysis protocol consisted of two hours dialysis, 1st buffer exchange, two hours dialysis, 2nd buffer exchange and overnight dialysis, which ensured a dialysis time of 20 hours in total. Afterwards, the pH values were checked and, if necessary, adjusted to pH 6.0 by titration, using HCl or NaOH respectively. After measuring the resulting protein content and pre-adjustment of the concentration to 15.0 mg/ml in the respective dialysis buffer, the protein batches were diluted to 11 different formulations (see Table 22) by using highly purified water, as well as the respective excipient and buffer stock solutions. After preparation, the pH value of every formulation was checked again and adjusted when needed. The protein formulations were filtrated using 0.22 µm Millex® GV PVDF syringe filter units (Merck Millipore Ltd., Tullagreen, Ireland). For each formulation a reference solution missing the protein was prepared accordingly, which was filtrated using 0.2 µm cellulose acetate sterile syringe filters (VWR International LLC, Radnor, PA, USA). The pH adjustments were performed by using an MP220 pH meter, equipped with an InLab Expert pH electrode (Mettler-Toledo, Greifensee, Switzerland). The given protein concentrations were determined by using UV spectroscopy measured with a NanoDrop2000 instrument (Thermo Scientific, Wilmington, USA) and using an extinction coefficient of $\varepsilon_{280\ nm}$=1.499 mL*mg^{-1}*cm^{-1}. After compounding, all formulations were stored at 2-8 °C.

Table 22: Overview of the formulations prepared for the mAb excipient screening.

ID	mAb [mg/mL]	Buffer system	pH	Excipient (% in m/V)
F1	0.5	10 mM phosphate	4.2	-
F2	0.5	10 mM phosphate	5.0	-
F3	0.5	10 mM phosphate	6.0	-
F4	0.5	10 mM histidine	6.0	-
F5	0.5	10 mM succinate	6.0	-
F6	0.5	10 mM phosphate	6.0	0.05% Tween 80
F7	0.5	10 mM phosphate	6.0	5% sorbitol
F8	0.5	10 mM phosphate	6.0	5% sucrose
F9	0.5	10 mM phosphate	6.0	2.5% glycerol
F10	0.5	10 mM phosphate	6.0	150 mM NaCl
F11	0.5	10 mM phosphate	6.0	1% HP-β-CD

An identical, randomized formulation order was used for all analyses, in order to exclude potential storage and measurement time effects on the determined stability parameters.

VIII.1.4. Further Preparations

For the examination of isothermal chemical protein denaturation (ICD) in the course of the mAb formulation screening, all formulations were prepared in a dilution series of guanidine hydrochloride (GuHCl). Therefore, GuHCl was dissolved in the respective placebo buffers to a concentration of 6.25 mol/l and the pH values of the resulting stock solutions were readjusted to the formulation pH with a precision of ± 0.01. The pH adjustments were performed by using an MP220 pH meter, equipped with an InLab Expert pH electrode (Mettler-Toledo, Greifensee, Switzerland). At the same time, the residual mAb stock solutions (SS) from dialysis performed within the formulation screening were pre-diluted in dialysis buffer to working solutions (WS) of 10 mg/ml. For the preparation of the dilution series, different amounts of GuHCl-containing and GuHCl-free placebo buffers were mixed and the resulting solution was thoroughly homogenized by vortexing. Afterwards, an appropriate amount of the respective mAb WS was spiked in to reach a final protein of 0.5 mg/ml, before all compounded solutions were mixed by gentle pipetting. The final protein and excipient concentrations match the formulation conditions used for the thermal denaturation assays and allow for direct head-to-head comparison of the results. Finally, all samples were equilibrated for 14 hours at room temperature to reach full equilibration of the unfolding reactions. An overview of the pipetting scheme and the resulting GuHCl concentration steps is given in Table 23.

Table 23: GuHCl concentration steps and pipetting scheme for the chemical unfolding titrations.

Sample ID	GuHCl [M]	10 mg/ml mAb WS [µl]	Placebo [µl]		Total volume [µl]
			0 M GuHCl	6.25 M GuHCl	
1	0.000	5.00	95.00	0.00	100.00
2	0.250	5.00	91.00	4.00	100.00
3	0.500	5.00	87.00	8.00	100.00
4	0.750	5.00	83.00	12.00	100.00
5	1.000	5.00	79.00	16.00	100.00
6	1.125	5.00	77.00	18.00	100.00
7	1.250	5.00	75.00	20.00	100.00
8	1.375	5.00	73.00	22.00	100.00
9	1.500	5.00	71.00	24.00	100.00
10	1.625	5.00	69.00	26.00	100.00
11	1.750	5.00	67.00	28.00	100.00
12	1.875	5.00	65.00	30.00	100.00
13	2.000	5.00	63.00	32.00	100.00
14	2.125	5.00	61.00	34.00	100.00
15	2.250	5.00	59.00	36.00	100.00
16	2.375	5.00	57.00	38.00	100.00
17	2.500	5.00	55.00	40.00	100.00
18	2.625	5.00	53.00	42.00	100.00
19	2.750	5.00	51.00	44.00	100.00
20	2.875	5.00	49.00	46.00	100.00
21	3.000	5.00	47.00	48.00	100.00
22	3.125	5.00	45.00	50.00	100.00
23	3.250	5.00	43.00	52.00	100.00
24	3.375	5.00	41.00	54.00	100.00
25	3.500	5.00	39.00	56.00	100.00
26	3.625	5.00	37.00	58.00	100.00
27	3.750	5.00	35.00	60.00	100.00
28	3.875	5.00	33.00	62.00	100.00
29	4.000	5.00	31.00	64.00	100.00
30	4.250	5.00	27.00	68.00	100.00
31	4.500	5.00	23.00	72.00	100.00
32	4.750	5.00	19.00	76.00	100.00
33	5.000	5.00	15.00	80.00	100.00

In the course of the protein-excipient interaction study, stock solutions of the different excipients were prepared as stated in Table 24. Thereby, all excipients were weighed into 10 ml volumetric flasks with an accuracy of ± 0.1 mg to the respective target weight. The excipients were then dissolved in the chosen buffer by vortexing and the volume was filled ad 10 ml with buffer after completely dissolving the substance.

Table 24: Overview of the excipient stock solutions prepared for the mAb protein-excipient binding studies.

Stock solution	Target weight [g]	Buffer system	
		10 mM phosphate pH 4.2	10 mM phosphate pH 6.0
15 mM α-CD	0.1459	x	x
15 mM β-CD	0.1703	x	x
15 mM HP-β-CD	0.2100	x	x
120 mM HP-β-CD	1.6800	x	-
15 mM SBE-β-CD	0.2138	x	x
240 mM SBE-β-CD	3.4207	x	-
15 mM γ-CD	0.1946	x	x

x = solution prepared; - = solution not prepared

Subsequently, the previously dialyzed mAb material in 10 mM phosphate buffer pH 6.0 (VIII.1.3) was pre-diluted to working solutions (WS) of 1 mg/ml in the two buffer systems used. In the next step, a 1:1 serial dilution of the cyclodextrin stock solution was prepared in the respective assay buffer under thorough homogenization by pipetting up and down several times. Afterwards an equal amount of the mAb WS was added in order to reach a final protein concentration of 0.5 mg/ml for all dilution steps. All dilution steps were performed at 4 °C on ice. After final homogenization, the samples were centrifuged for 10 min (15000 g, 4 °C) in order to remove larger aggregates.

VIII.1.5. Unfolding and Aggregation Investigations

VIII.1.5.1. MicroScale Thermophoresis (MST)

The second and third generation prototype instruments (NanoTemper Technologies GmbH, Munich, Germany) have been used for predictive unfolding and aggregation studies within the mAb stability screenings. For both measurement setups a stepped thermal ramp assay was carried out by increasing the temperature from 30 °C to 90 °C in 1 °C steps and recording a thermophoresis timetrace at each step. Therefore, overall low, instrument specific UV-LED powers of 1% (2nd gen, PMT=780 V) and 2% (3rd gen, dual LED, medium sensitivity) were used respectively. NT.LabelFree Zero Background MST Premium Coated Capillaries (NanoTemper Technologies GmbH) were used exclusively in order to exclude measurement artifacts from protein binding to the capillary surface. Furthermore, liquid dip gum (Capillary Sealing Paste, NanoTemper Technologies) was applied at both capillary ends to effectively prevent sample evaporation during the temperature ramp.

Preceding the thermophoretic analysis of the stability screenings, the measurement parameters were optimized to allow for a high signal to noise ratio and a clear detection of both unfolding transitions. Thereby, the 2nd generation prototype was used to examine the influence of differently strong thermophoretic driving forces on the resulting melting curves. This was achieved by a stepwise increase of the IR-laser power from 5% to 40%. NT Control software version 2.1.31 and NT Analysis software version 1.5.41 (both NanoTemper Technologies) were used for carrying out the MST measurements and calculating the thermophoresis values for each temperature step.

Considering the results from this IR-laser experiment, the 3rd generation prototype was operated at an optimal intermediate laser power of 10%. Equipped with a dual-LED system, the system was used to measure initial intrinsic fluorescence and the three thermophoretic parameters (thermophoresis, t-jump, and thermophoresis with t-jump) at four different fluorescence readouts. These are the single fluorescence emission wavelengths at 330 nm and 350 nm, as well as the ratio of 350 nm/330 nm and the mean value of the two wavelengths. Eventually, thermophoresis with t-jump was determined as the most suitable thermophoretic parameter and the fluorescence readout wavelength at 350 nm was found beneficial. The above described settings were used for all following thermal unfolding and aggregation measurements in the course of the stability screenings.

For both, the pH and the formulation screening, all samples were measured repetitively by using a customized measurement script and executing at least four

consecutive runs in a randomized order with fresh capillaries each. In this way, effects from a prolonged thermal history of capillaries at the end of the sample tray could be excluded. After the measurement, MO.AffinityAnalysis software version 0 (NanoTemper Technologies) was used to calculate the values for thermophoresis with t-jump at 350 nm for each temperature step. The resulting melting curves exposed two unfolding transition peaks for each formulation which were assigned as apparent melting temperatures (T_m). Both values were calculated by smoothing (Savitzky-Golay, polynomial order 1, points of the window 5), interpolation (cubic spline, 6001 points between 30 °C and 90 °C) and local maximum analysis (Impulse Analyzer) of the melting curves by using Origin software version 8G (OriginLab Corp., Northampton, MA, USA).

VIII.1.5.2. Fluorescence Emission Spectroscopy (FES)

VIII.1.5.2.1. Nano Differential Scanning Fluorimetry (nanoDSF)

A Prometheus NT.48 instrument (NanoTemper Technologies GmbH) was used to measure protein melting temperatures (T_m) and the reversibility of protein unfolding for both stability screenings. Therefore, two consecutive temperature up-scans from 30 °C to 90 °C in a linear ramp of 1 °C/min were performed each. Between the two up-scans, a controlled temperature down-scan from 90 °C to 30 °C at a scan rate of 1 °C/min was performed for the pH pre-screening, while for the formulation screening the samples were equilibrated at 30 °C after the first heating cycle as fast as possible. An initial delay of 15 min at 30 °C before the first and second measurement was set for both experiments to ensure temperature equilibration among the samples. In the formulation screening a fluorescence excitation power of 10% (medium sensitivity) was set for the 1st up-scan, which was decreased to 40% (low sensitivity) in the 2nd up-scan. In the case of the pH screening a LED power of 75% (low sensitivity) was used for both measurements. Measurements were carried out in quadruplicates by using NT.LabelFree Zero Background MST Premium Coated Capillaries (NanoTemper Technologies) which were sealed with liquid gum (Capillary Sealing Paste, NanoTemper Technologies) on both capillary ends to prevent evaporation during the prolonged temperature cycle.

For all temperature up-scans, T_m values were calculated by evaluating the inflection points in the shift of tryptophan fluorescence from 330 nm to 350 nm using NT.Prometheus Control software version 1.11 (NanoTemper Technologies). Unfolding reversibility was stated for the samples, again showing an unfolding transition in the second temperature up-scan.

In an orthogonal approach, isothermal chemical protein denaturation was measured and the unfolding denaturant concentration (C_m) at the inflection points of the obtained unfolding curves was determined. Therefore, one discovery scan was performed to for each formulation, measuring all 33 concentration steps in one run. For all measurements, the temperature of the capillary array was set to 25 °C and a fluorescence excitation power of 70% (low sensitivity) was used. Measurements were carried out in singlicates by using NT.LabelFree Zero Background Standard Treated Capillaries (NanoTemper Technologies GmbH).

The shift in tryptophan fluorescence from 330 nm to 350 nm was evaluated by using NT.Prometheus Control software version 1.11 (NanoTemper Technologies GmbH) and calculating the ratio of 350 nm to 330 nm for each capillary. Afterwards, unfolding curves were plotted and the respective concentrations of GuHCl (C_m) at the inflection points were calculated by using Origin 8G software (OriginLab Corp., Northampton, MA, USA). For the determination of C_m values, the unfolding curves were differentiated (1st derivative), interpolated (cubic spline, 501 points between 0 M and 5 M GuHCl) and the local maxima were analyzed using the included Impulse Analyzer tool.

VIII.1.5.2.2. Intrinsic Fluorescence Emission Spectroscopy (Intrinsic FES)

An Optim 1000 instrument (Avacta Analytical Ltd, Wetherby, UK, now Unchained Labs, Pleasanton, CA, USA) was used for a comparative linear thermal unfolding and aggregation study. The samples were pipetted in the capillaries of a 9 µl micro-cuvette array (MCA), which were tightly closed with the provided silicone seals using a MCA frame. Using the Optim Client software V1.5.4 (Avacta Analytical), all formulations were measured at least 4 times by performing three consecutive runs with 1 MCA (=16 capillaries) each. Before each measurement, the thermostat temperature was set to 30 °C for a pre-scanning delay of 15 min. Following, the temperature was linearly increased from 30 °C to 90 °C in a rate of 1 °C per minute, while a hold time of 1 s was used at each well for recording of the fluorescence spectrum. An excitation laser wavelength of 266 nm was used to induce deep UV intrinsic fluorescence, setting a slit width of 100 µm and an exposure time of 1000 ms. Fluorescence emission was recorded from 249 to 504 nm using a center wavelength of approximately 380 nm. For data evaluation, the ratio of 350 nm/330 nm was chosen and unfolding temperatures (T_m) were automatically calculated by the Optim Analysis Software V2.0.4 (Avacta Analytical). If necessary, melting temperatures were re-adjusted according to the maxima of the 1st derivative fluorescence curves.

VIII.1.5.2.3. Differential Scanning Fluorimetry (DSF)

In the formulation screening, differential scanning fluorimetry (DSF) was used for reference measurements of linear thermal unfolding by evaluating changes in the extrinsic fluorescence of SYPRO® orange (SO) and 9-(2,2-dicyanovinyl)julolidine (DCVJ).

SYPRO® Orange Protein Gel Stain was purchased as a 5000x concentrated stock solution (SS) in DMSO (Sigma Aldrich, St. Louis, MO, USA). First, the SS was diluted with highly purified water (HPW) to a working solution (WS) of 21x. Subsequently, 20 µl protein formulation or placebo reference respectively was provided in the wells of a skirted 96-well microplate (Biometra GmbH, Goettingen, Germany) and 1 µl WS was spiked in and thoroughly mixed. The resulting final volume per well was 21 µl with a SO concentration of 1x. For each formulation 8 wells were prepared, 6 with protein material and 2 with the respective placebo reference. To prevent evaporation and ensure proper filling of each without air bubbles, the well plate was covered with self-adhesive optical sealing film (Biometra) and centrifuged at 2000 g for 2 minutes.

The unfolding experiment was conducted using a qTower 2.2 UV instrument (Analytik Jena AG, Jena, Germany). After an initial equilibration time of 15 minutes at 30 °C, the temperature was stepwise increased to 90 °C following a scan rate of 1° C/min and a measurement interval of 1 per °C. An excitation wavelength of 490 nm was used, while the fluorescence emission of SO was collected at 580 nm by using the corresponding channel of the instrument at a gain of 5. At each temperature, three repetitive measurements were performed.

Before melting temperatures (T_m) were evaluated, the placebo reference measurements were subtracted from the verum melting curves, in order to exclude effects from buffer background fluorescence. Subsequently, the background subtracted data were differentiated (1st derivative), smoothed (Savitzky-Golay, polynomial order 1, points of the window 5), interpolated (cubic spline, 6001 points between 30 °C and 90 °C) and the two local maxima were analyzed using the included Impulse Analyzer tool (Origin 8G, OriginLab Corp., Northampton, MA, USA).

9-(2,2-dicyanovinyl)julolidine (DCVJ) was purchased as solid powder from Sigma Aldrich (St. Louis, MO, USA) and diluted in DMSO to a stock solution (SS) of 210 mM. This SS was further diluted to a 2.1 mM working solution (WS) with HPW. A dilution series of seven mAb concentrations ranging from 0.1 mg/ml to 15 mg/ml was prepared in 10 mM phosphate buffer at pH 5.0 by using protein stock solution material. Subsequently, 20 µl protein formulation or respective placebo reference was provided in the wells of a MicroAmp® optical 96-well reaction plate (Applied Biosystems, Foster

City, CA, USA) and 1 µl DCVJ WS was spiked in and thoroughly mixed. The resulting final volume per well was 21 µl with a DCVJ concentration of 100 µM. For each dilution and the placebo reference, four wells were prepared. The filled wells were sealed with optical adhesive film (Applied Biosystems, Foster City, CA, USA) and the plate was centrifuged for 2 minutes at 2000 g to ensure filling without air bubbles.

A 7300 real-time PCR system (Applied Biosystems, Foster City, CA, USA) was used for the unfolding experiment. After an initial equilibration time of 15 minutes at the starting temperature of 30 °C, the temperature was stepwise increased to 90 °C following a scan rate of 1° C/min and a measurement interval of 1 per °C. A tungsten-halogen lamp was used for fluorescence excitation, while the emission was recorded at ~ 520 nm using the detection filter A. For conducting the measurement, a 7300 System SDS Software version 1.3.1 (Applied Biosystems, Foster City, CA, USA) was used.

For data analysis, Origin 8G software (OriginLab Corp., Northampton, MA, USA) was used. For all verum formulation melting curves, the reference baseline of 10 mM phosphate buffer pH 5.0 was subtracted. Afterwards, the extrinsic fluorescence readout curves were differentiated (1st order), smoothed (polynomial order 1, points 5) and interpolated (cubic spline, 6001 data points between 30 °C and 90 °C). T_m values were determined by selecting the two local maxima by using the included Impulse Analyzer tool.

VIII.1.5.3. Differential Scanning Micro-Calorimetry (µDSC)

A VP-DSC microcalorimeter (MicroCal Inc., Northampton, MA, USA, now Malvern Instruments Ltd, Malvern, UK) was used for comparative thermal unfolding studies. The placebo and verum formulations were degassed for approx. 5 min by using a ThermoVac vacuum pump (MicroCal) in order to remove potential air bubbles from the samples. Subsequently, 550 µl of the placebo reference was injected using a 2.5 ml gastight Hamilton syringe (Hamilton Company, Reno, NV, USA) at 25 °C before the verum material was injected accordingly. A temperature up-scan was performed from 30 °C to 90 °C by performing a slope of 60 °C/h. A pre-scan thermostat of 15 minutes was set at the starting temperature to ensure thermal equilibration. During the measurement, a filtering period of 1 second was set without a feedback mode/gain, while the chamber pressure was checked to be ≥ 22 psi. After each run, the cells were cooled down to 30 °C again. Sample analysis was performed at least in triplicates for each formulation.

Between two sample runs, a cleaning routine was performed by heating up a 50% (V/V) nitric acid solution under the same conditions as the samples, but using a scan rate of 90 °C/min and no pre-scan thermostat. Afterwards, a solution of 1% (w/V) sodium dodecyl sulfate (SDS) (Merck KGaA, Darmstadt, Germany) in HPW was used to flush each cell for 30 seconds, followed by a thorough rinse with 100 ml water per cell.

The data evaluation was performed by the Origin DSC data analysis software (Origin 7 SR2, OriginLab Corp., Northampton, MA, USA) and MicroCal VPViewer2000 version 1.4.10 (MicroCal). The thermograms were normalized by subtracting a baseline measured by water vs. water scans to exclude device parameters and instrumental effects. Afterwards, the endothermic peaks indicating protein unfolding events (T_m) were determined using the included Peak Picking tool.

VIII.1.5.4. Static Light Scattering (SLS)

Additionally to intrinsic fluorescence (section VIII.2.1.2.2), static light scattering intensity over temperature was evaluated from the Optim 1000 measurement for the UV laser at 266 nm and the blue laser at 473 nm. Therefore, 90° light scattering values were plotted over temperature and aggregation onset temperatures ($T_{agg\ onset}$) were evaluated for 266 nm and 473 nm, given a bandwidth of 5 nm each, by using the Optim Analysis software V2.0.4 (Avacta Analytical). For calculation, the software applied a Heaviside step function to the 1st derivative curve of static light scattering and the temperature corresponding to the 10% value of the maximum was determined automatically. Formulations that showed no increase in light scattering over the complete temperature up-scan were assigned and displayed with a theoretical value above 90 °C.

VIII.1.6. Forced Degradation Studies

VIII.1.6.1. Thermo-Optical Particle Characterization (TOPC)

TOPC was used for predictive thermal aggregation studies by IR-laser induced stress testing for the pH pre-screening and the formulation screening. The fluorescence excitation LED power was set to 10% (PMT=825 V, pH screening) and 20% (PMT=780 V, formulation screening) and heat stress was applied by using an IR-laser power of 341%. Changes in intrinsic fluorescence were detected for 160 s in total. After recording the initial fluorescence for 5 s, the laser was turned on and the effects of the IR-laser input were tracked for 150 s, before the laser was turned off again and backdiffusion was measured for additional 5 s.
In order to test the repeatability of the assay, the measurements of the pH screening were performed in triplicates by performing three independent consecutive runs, while for the formulation screening only singlicates were analyzed. All measurements were performed in a fixed random order of formulations at an ambient assay temperature of 25°C by exclusively using NanoTemper LabelFree MST Premium Coated Zero Background Capillaries (NanoTemper Technologies GmbH) in order to avoid measurement artifacts from sample binding to the capillaries and capillary auto-fluorescence.
NT Control software version 2.1.31 was used to perform the measurements, while the intrinsic fluorescence timetraces were normalized and exported by using NT Analysis software version 1.5.41 (both NanoTemper Technologies). The TOPC experiments were analyzed by calculating mean values and standard deviations for all formulations in the timeframe between 125 and 150 s. All calculations and data plotting were performed with Origin 8G software (OriginLab Corp., Northampton, MA, USA).

VIII.1.6.2. Conventional Stress Testing

All formulations were heat-stressed in 2 ml conical micro-centrifuge tubes (VWR International LLC, Radnor, PA, USA) at 80 °C for 10 minutes (after 15 minutes for temperature equilibration) using a ThermoMixer Comfort (Eppendorf AG, Hamburg, Germany). As a reference, one aliquot of each sample was stored at 4 °C for the same time.

VIII.1.6.2.1. Dynamic Light Scattering (DLS)

Dynamic Light Scattering was measured using a Zetasizer Nano ZS (Malvern Instruments GmbH, Herrenberg, Germany). The Z-Average diameters of the native

and stressed protein formulations were evaluated to detect protein particle growth due to thermal aggregation and precipitation after the forced degradation. The measurements were carried out in triplicates using disposable semi-micro PMMA cuvettes (Brand GmbH & Co. KG, Wertheim, Germany).

VIII.1.6.2.2. Turbidimetry

A Dr. Lange Nephla Turbidimeter (Hach-Lange, Duesseldorf, Germany) was used for measuring the turbidity of the native and stressed protein formulations. 2 ml of each sample were filled in a glass cuvette and turbidity was determined as 90° scattered light (860 nm) in Formazin Nephelometric Units (FNU). The measurement was carried out in minimum triplicates by turning the cuvette and measuring turbidity again.

VIII.1.6.2.3. Visual Inspection

The heat stressed and native samples of the pH pre-screening were additionally visually inspected in the turbidimetry cuvettes using an inspection cabinet. Pictures were taken with a Nikon D5300 digital camera (Nikon Inc., Tokyo, Japan).

VIII.1.7. Protein-Excipient Interaction Analysis

VIII.1.7.1. MicroScale Thermophoresis (MST)

MST was used for protein-excipient binding studies of the mAb to cyclodextrins. All measurements were performed on a Monolith NT.LabelFree instrument (NanoTemper Technologies) by using a fluorescence excitation LED Power of 7% and a MST Power of 20%. These settings were selected in order to get a satisfactory high initial fluorescence signal and thermophoretic depletion. NT.LabelFree Zero Background MST Premium Coated Capillaries (NanoTemper Technologies GmbH) were used exclusively and the measurements were carried out at ambient room temperature.
The measurements were performed by using NT Control software version 2.1.31, while NT Analysis software version 1.5.41 (NanoTemper Technologies) was used to calculate thermophoresis and intrinsic fluorescence values for each excipient concentration and compute equilibrium dissociation constants (K_d) by fitting a Boltzmann-function to the respective data. Plotting of the data was performed by using Origin 8G software (OriginLab Corp., Northampton, MA, USA).

VIII.1.7.2. Nano Differential Scanning Fluorimetry (nanoDSF)

A Prometheus NT.48 instrument (NanoTemper Technologies GmbH, Munich, Germany) was used for linear thermal unfolding measurements of the protein-excipient dilution series. A temperature ramp was executed from 15 °C to 95 °C in a slope of 1 °C/min, while protein fluorescence was continuously collected at 330 nm and 350 nm. The fluorescence excitation power was set to 30% (low sensitivity) in order to get a satisfactory high fluorescence signal. All titration steps have been analyzed in singlicate runs by using NT.LabelFree Zero Background MST Premium Coated Capillaries (NanoTemper Technologies).
In order to obtain melting temperatures (T_m) from the intrinsic fluorescence emission, the intensities of the single wavelengths at 330 nm and 350 nm as well as the ratio of 350/330 nm was calculated and evaluated over temperatures by using NT.Prometheus Control software version 1.11 (NanoTemper Technologies).

VIII.2. Results and Discussion

VIII.2.1. Unfolding and Aggregation Investigations

VIII.2.1.1. MicroScale Thermophoresis (MST)

Prior to executing the pH pre-screening and the formulation excipient screening, a detailed investigation on two major influence factors of thermophoretic melting curves was performed and the measurement settings were optimized for clear detection and an improved signal to noise ratio of both unfolding events. In this pre-test, the dependency of the melting curves on (i) the MST/IR-laser power and (ii) the fluorescence readout was investigated.

Figure 62 and Figure 63 display melting curves by thermophoresis for F1 (10 mM phosphate, pH 4.2) and F3 (10 mM phosphate, pH 6.0) measured at different MST powers. For both examples, the expected increase in thermophoretic depletion at higher laser intensities was apparent at the starting temperature of 30 °C. Increasing the laser intensity on the one hand side improves the signal to noise ratio for the individual timetraces, but on the other hand side, increases the temperature in the focal area and therefore the perturbation of the system in the same way. In order to focus on the laser power effects on the shape of the melting curves and to correct for the depletion amplitude, we normalized all melting curves for the further analysis. Formulation 1 (Figure 62 – right) displays a clear laser power effect on the formation of melting transitions. Whereas at a low MST power of 5% only one peak was detected (T_m1), an additional peak shoulder at higher temperatures (T_m2) emerges when using 10% laser power that grows substantially during increasing laser intensities until its intensity outweighs the first peak for the highest laser powers of 30% and 40%. Taken this together, we observed a clear shift of the peak intensities in the MST melting curves from T_m1 to T_m2 with increasing laser intensities. For the lead formulation F3 (Figure 63 – right), however, a similar effect could only be hypothesized when, increasing the laser power from 5% to 10%, a second transition appears. All other laser settings did not resolve both transitions, maybe due to the higher proximity and potential overlapping of the unfolding events at the increased pH value that is also apparent for the 10% MST power curve. Consequently, the MST/IR-laser power was fixed to an intensity of 10% for all following measurements. This setting will allow for full resolution of both unfolding transitions from pH 4.2 to pH 6.0, a moderate perturbation of the solution and a suitable signal to noise ratio for both, the single MST timetraces as well as the resulting melting curve.

With regard to our previously described mAb unfolding and aggregation studies by using MST (V.1.2.1) and many differential scanning microcalorimetry investigations of mAbs reported in the literature[5-10], the first unfolding transition (T_m1) detected is presumably attributed to the unfolding of the CH2 domain localized within the Fc fragment. The second and most prominent melting event (T_m2) that is often associated with nascent protein aggregation and emerges in our case with increasing IR-laser intensities is caused by Fab unfolding. Heat denaturation of the CH3 domain is often found to be conformationally most stable, but due to the low intensity hard to separate from the Fab event. Therefore this transition either appears last, or is only detectable as a small shoulder and only evaluable by deconvolution of the unfolding signal.

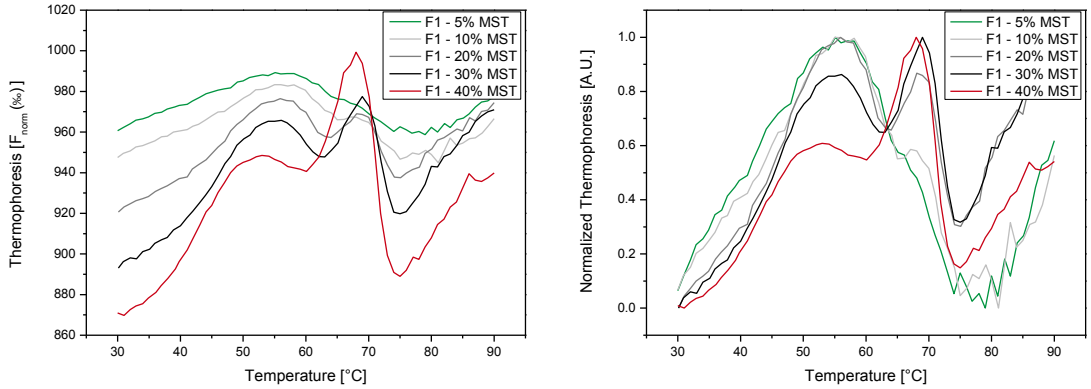

Figure 62: Dependence of the thermophoresis melting curves on the IR-laser (MST) power for Formulation 1 (10 mM phosphate, pH 4.2). Left: Absolute thermophoresis versus temperature. Right: Normalized thermophoresis versus temperature.

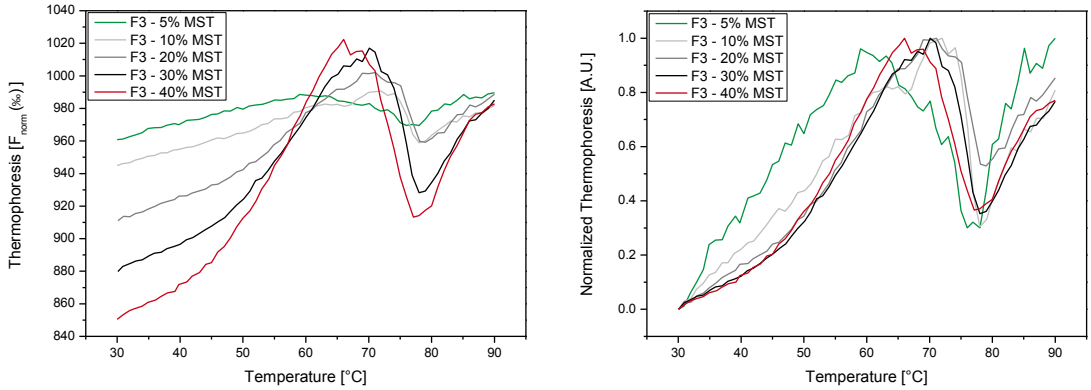

Figure 63: Dependence of the thermophoresis melting curves on the IR-laser (MST) power for Formulation 3 (10 mM phosphate, pH 6.0). Left: Absolute thermophoresis versus temperature. Right: Normalized thermophoresis versus temperature.

Implemented with the dual-LED system in the 3rd prototype instrument, the detection of intrinsic fluorescence emission at two independent wavelengths (330 nm and 350 nm) was enabled. This development leads to the possibility of interpreting four different fluorescence modes in the evaluation of initial intrinsic fluorescence as well as thermophoresis and t-jump melting curves. The full melting curve comparison of all evaluations combined with all fluorescence readouts is given in Figure 64. In contrast to the HSA melting curves discussed in section VI.2.1.1, where the thermophoresis and t-jump melting curves both showed uniform negative unfolding peaks, the mAb behaved completely different. In the single wavelength inspection, the t-jump values (Figure 64 – top – left) showed a stepwise decrease over increasing temperatures that was hardly influenced by the evaluation wavelength. This minor wavelength dependence led to a very high noise level in the calculated fluorescence ratio (350 nm/330 nm) that though indicated the two transition steps which could be assigned to the separate unfolding events of individual antibody domains (T_m1 & T_m2). For the melting curves by thermophoresis (Figure 64 – top – right), the fluorescence emission at 330 nm showed only one small unfolding peak (T_m2), while the readout at 350 nm exhibited both transitions additionally with a higher resolution (T_m1 & T_m2). Consequently, this clear difference in wavelengths induced a similar curve progression for the fluorescence ratio calculated by 350 nm/330 nm. The evaluation of thermophoresis with t-jump at 350 nm combines the stepwise signal decrease from the t-jump, the two peak-shaped unfolding transitions from the thermophoresis plots and moreover enhances the signal to noise ratio, especially for the smaller first transition (T_m1). Thus, we proceeded with these settings for the data analysis of the pH pre-screening and the formulation excipient screening.

As the evaluation of intrinsic fluorescence melting curves of mAbs is well described in literature[11-14] and in our assay the fluorescence readout might be influenced by the repetitive UV-LED and IR-laser radiation, we will not go into any greater detail at this point and refer to the standalone fluorescence evaluations of the two mAb screenings discussed in section VIII.2.1.2.

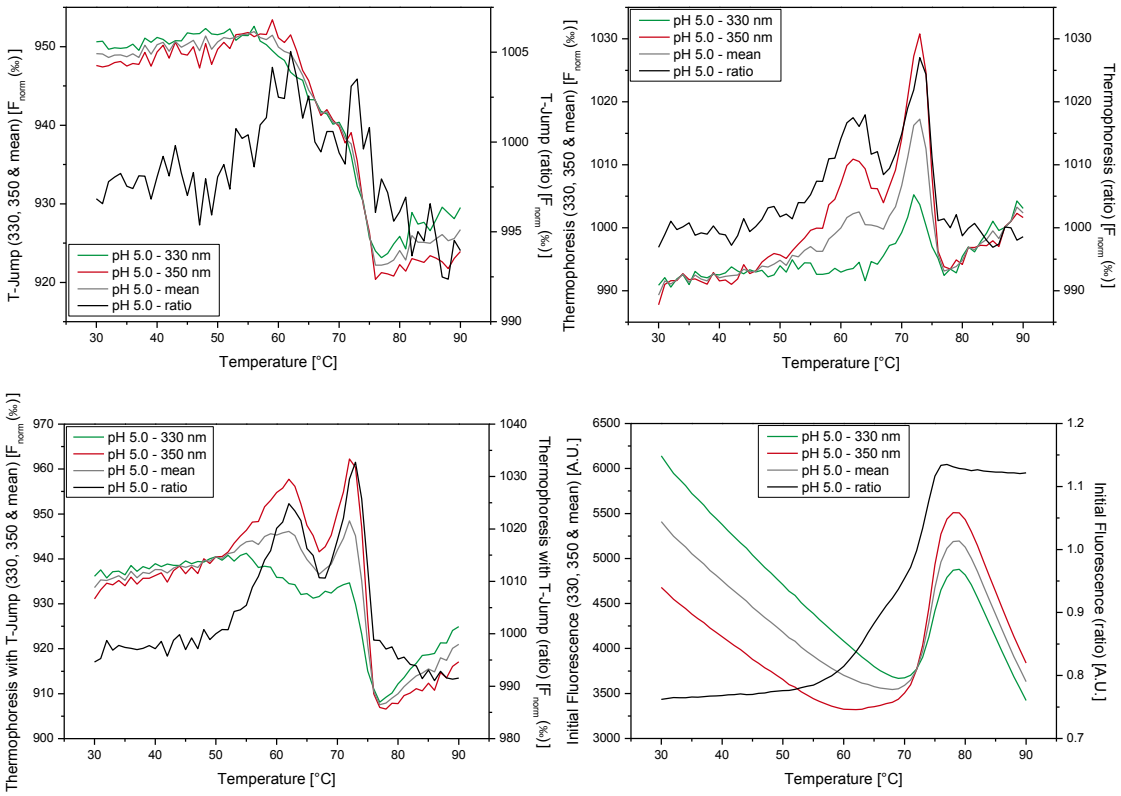

Figure 64: Comparison of the four different fluorescence readouts (330 nm, 350 nm, mean 330 nm + 350 nm, and ratio 350 nm/330 nm) measurable with the 3rd generation prototype instrument for the t-jump (top – left), thermophoresis (top – right), thermophoresis with t-jump (bottom – left), and initial fluorescence (bottom – right) melting curves. The exemplary curves are given for Formulation 2 (10 mM phosphate, pH 5.0).

Figure 65 shows exemplary melting curves for the method selected above within the pH pre-screening of the mAb formulated in 10 mM phosphate buffer. For all pH values, two distinct melting peaks were obtained that shift to higher temperatures with increasing pH values. This observation was confirmed by the T_m evaluation (Figure 66 – left) and results in an enhanced conformational stability with increasing pH that was found to be stronger for the first unfolding transition (T_m1). In the raw data, an additional very sharp aggregation peak was visible from pH 5.4 on that shifted towards lower temperatures with increasing pH values and disturbed the T_m2 determination above pH 5.6 and also the T_m1 value at pH 6.2. For further development steps, this emerging aggregation would require a compromise between minimum aggregation propensity and a high unfolding stability. As the aggregation peak appears first at a pH value of 5.4 and the increase in conformational stability is strongest between pH 4.0 and pH 5.0, an intermediate pH value of 5.0 or 5.2 is proposed as an optimized lead formulation from this study.

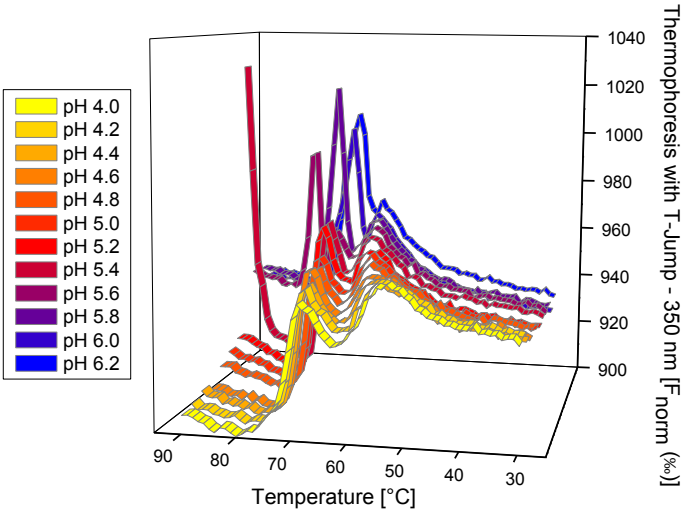

Figure 65: Exemplary melting curves for thermophoresis with t-jump at 350 nm for the pH pre-screening (Run 2 of 4).

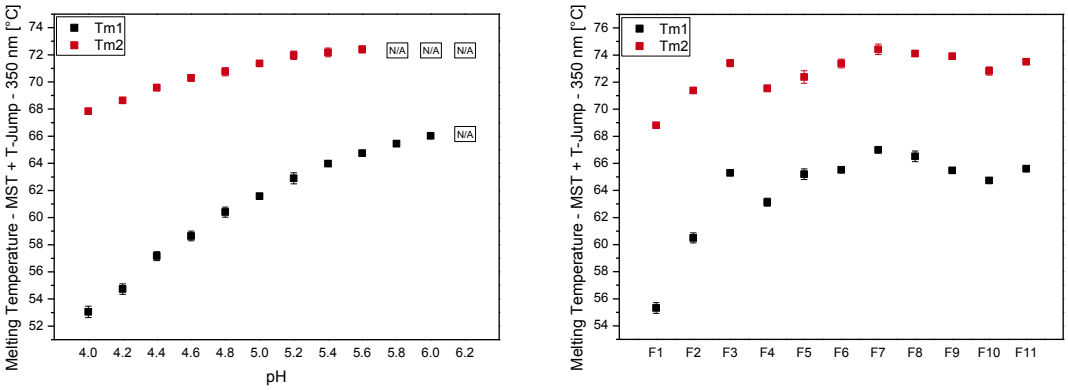

Figure 66: Melting temperatures for the pH pre-screening (left, n≥3) and the excipient screening (right, n=5) determined by thermophoresis with t-jump at 350 nm. Within the pH pre-screening, the T_m1 value at pH 6.2 as well as the T_m2 values at pH 5.8-6.2 were (partially) superimposed by an additional aggregation peak and were consequently excluded from the illustration.

The excipient screening, additionally targeting the mAb thermal stability dependent on different buffer salts as well as formulation excipients is based on the 10 mM phosphate buffered solution at pH 6.0 as a lead formulation (F3), which was selected only by maximum conformational stability. The corresponding T_m evaluation (Figure 66 – right) re-iterates the strong pH dependency of the conformational stability that was already discussed for the pH pre-screening and stabilizes the antibody with increasing pH values from pH 4.2 (F1) over pH 5.0 (F2) to pH 6.0 (F3). Comparing the buffer salts phosphate (F3), histidine (F4) and succinate (F5), a destabilizing effect of histidine is apparent. However, this fact has to be interpreted with care, as especially histidine shows a by approximately one decade more pronounced temperature effect on its pK_a value compared to the other buffer systems used[3,15,16]. This distinct property leads to a negative pH shift of ~0.9 pH units at 63 °C and ~1.1 pH units at 71 °C that lowers the actual pH value of the solution at T_m1 to pH 5.1, and at T_m2 to pH 4.9. Consistent with this argument is the observation that the apparent T_m1 value for Formulation 4 is between F3 (pH 6.0) and F2 (pH 5.0), while the T_m2 approaches the value for F2 even more. Excipients had a substantially less pronounced effect on the conformational stability compared to changes in the pH value. However, sorbitol (F7) and sucrose (F8) slightly stabilized the antibody while high salt concentrations (F10) destabilized. In order to put these results in context, the conformational stabilization by polyols and sugars is well described in literature and attributed to preferential hydration[17]. Additionally, a reduction of electrostatic repulsion in the native state is observed at increased salt contents for many mAbs and consequently leads to colloidal destabilization.[1]

VIII.2.1.2. Fluorescence Emission Spectroscopy (FES)

VIII.2.1.2.1. Nano Differential Scanning Fluorimetry (nanoDSF)

In the pH pre-screening, thermal unfolding detected by nanoDSF showed a strong pH dependence of unfolding and aggregation events. With increasing pH values, the thermal unfolding curves, detected by the ratio in intrinsic fluorescence emission at 350 nm/330 nm, were shifted to higher temperatures and hence overall conformational stability increased (Figure 67). In the melting temperature evaluation, this stability improvement holds true for the first as well as for the second unfolding transition. However, the increasing effect is considerably stronger for T_m1 and persists up to pH 6.2, whereas the T_m2 values reach a plateau at ~ 76 °C above pH 5.0.

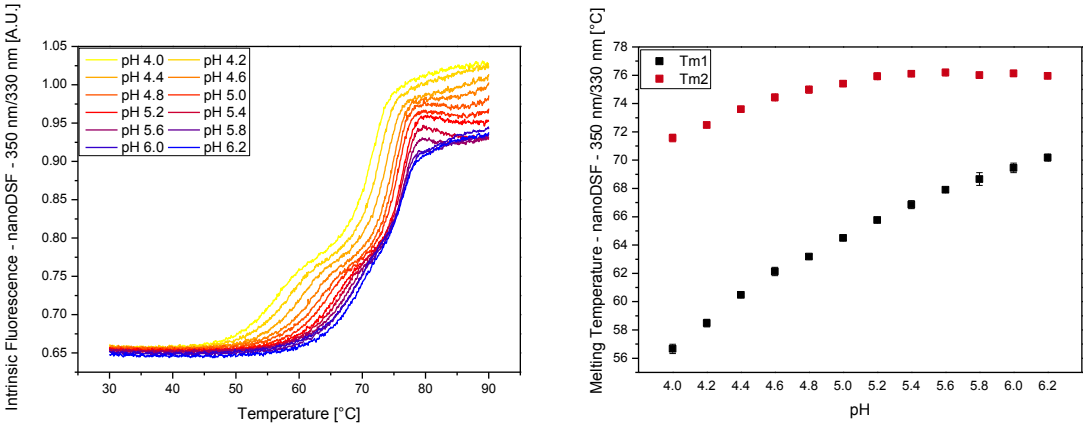

Figure 67: Benchmarking of the pH pre-screening results by using nanoDSF (1st up-scan). Left: Thermal unfolding monitored by the intrinsic fluorescence ratio of 350 nm/330 nm over temperature. Right: Conformational stability was calculated by determining the inflection points of the unfolding curves. All samples were measured in quadruplicates (n=4).

Furthermore, the propensity of non-native aggregation was tracked by measuring the reversibility of unfolding when performing a second consecutive temperature up-scan und re-evaluating the melting transitions, if present (Figure 68). Thereby, the inversely proportional trend of conformational and aggregation stability was reconfirmed, as the reversibility of unfolding and, therefore, the aggregation resistance decreased with increasing pH values. For the formulations from pH 4.0 to 5.4, protein unfolding was partially reversible, while with increasing pH values, the amplitude of the unfolding transition steadily decreased. This suggests the rise of an altered conformation on reheating, which is substantially influenced by pH. Nevertheless, consistent T_m2 values were obtained for all formulations in this range, while the first unfolding transition was only recurrent at pH 4.0. With the formulations at pH values higher than 5.4 showing no reversibility at all, these findings are in very good agreement with the MST results

where those pH values displayed an additional aggregation peak approaching lower temperatures with increasing pH values. Additionally, a µDSC study by Youssef[2] yielded highly comparable stability and reversibility data on the same mAb.

In summary, identical conclusions as for MST can be drawn, rendering intermediate pH values around 5.0 as lead conditions for further development, providing a suitable compromise between conformational stability and aggregation resistance.

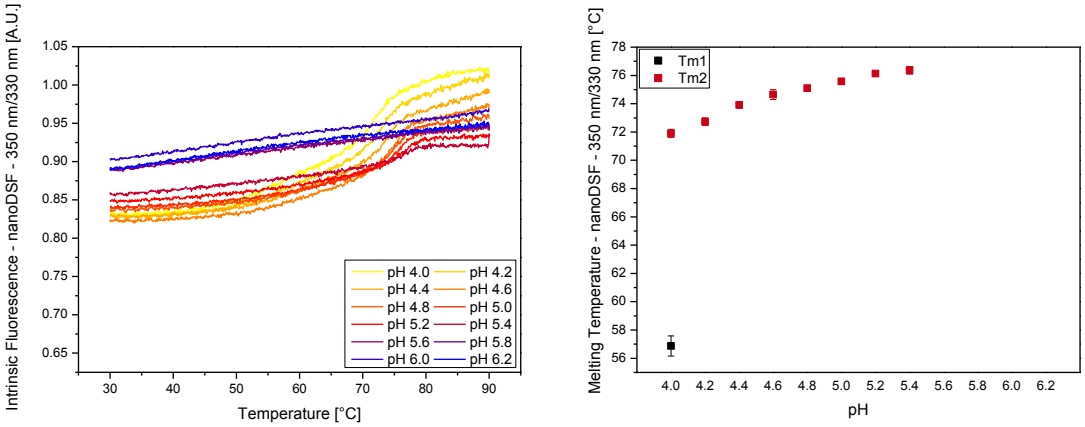

Figure 68: Benchmarking of the pH pre-screening results by using nanoDSF (2nd up-scan). Left: Colloidal stability was investigated by performing a second up-scan and checking for reversibility of unfolding. Right: Conformational stability was calculated by determining the inflection points of the unfolding curves. Evaluable T_m2 values were obtained for pH values in the range of 4.0 to 5.4, while a T_m1 value was observed for pH 4.0 only. All samples were measure in quadruplicates (n=4).

For the formulation excipient screening, the same assay was executed by performing two consecutive temperature up-scans from 30 °C to 90 °C and evaluating the conformational stability profile by melting temperature determination from the 1st and the aggregation propensity by unfolding reversibility from the 2nd ramp.

The first unfolding scan (Figure 69) very well validates the stability principles derived from the MST study. Once more, the strong pH influence on the unfolding stability of the mAb is highlighted, leading to the highest T_m value among the three phosphate buffers investigated (F1-F3, pH 4.2-pH 6.0) for pH 6.0 (F3). Furthermore, the buffer comparison of phosphate (F3), histidine (F4) and succinate (F3) shows identical trends for T_m1, revealing the reduced conformational stability for histidine which bears the risk of a negative pH shift upon heating, as described in the MST section (VIII.2.1). Surprisingly, the corresponding T_m2 does not show a destabilization for histidine and thus all buffer systems rank with comparable values. However, in general it is to mention that the stability trends for T_m2 in the nanoDSF results are considerably less pronounced compared to T_m1.The addition of polysorbate 80 (F6), glycerol (F9) or hydroxypropyl-beta-cyclodextrin (F11) had no effect on the melting temperatures of the 10 mM phosphate, pH 6.0 lead formulation, albeit we again revealed a slight

destabilization by sodium chloride (F10) and higher T_m values for sorbitol (F7) and sucrose (F8).

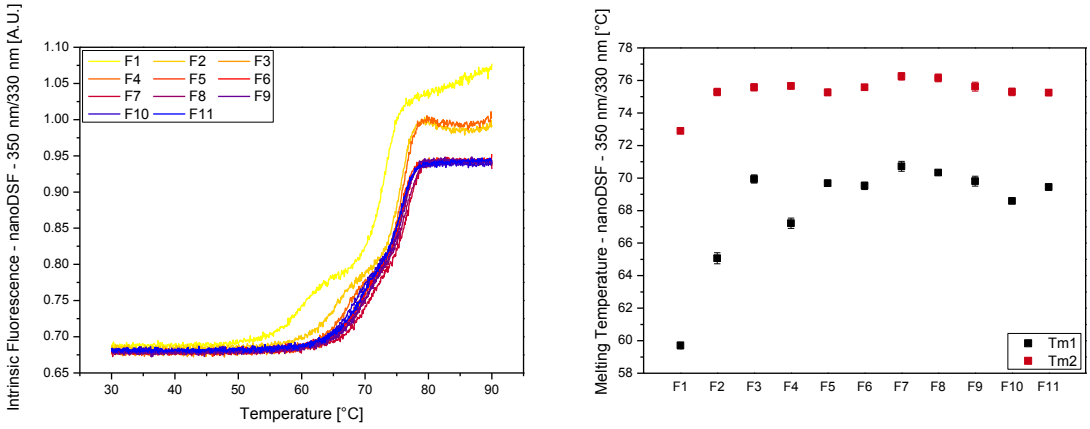

Figure 69: Benchmarking of the formulation screening results by using nanoDSF (1st up-scan). Left: Thermal unfolding monitored by the intrinsic fluorescence ratio of 350 nm/330 nm over temperature. Right: Conformational stability was calculated by determining the inflection points of the unfolding curves. All samples were measured in quadruplicates (n=4).

The second, consecutive unfolding scan of the formulation screening was performed by analogy to the first thermal ramp and elucidates the potential of intermediate protein refolding and formation of repetitive unfolding transitions with comparable melting temperatures (Figure 70). As already shown for the pH pre-screening, the mAb shows partial reversibility of unfolding when formulated in 10 mM phosphate buffer in the pH range between 4.0 and 5.4, which vanishes at higher pH values. Consequently, Formulation 1 (pH 4.2) and Formulation 2 (pH 5.0) were reversible to a certain degree, while Formulation 3 (pH 6.0) was not. Moreover, reversibility was confirmed to be mostly pH driven, as the addition of formulation excipients (F6-F11) had no effect on the second melting curve and were therefore not able to retrieve measurable changes in secondary or tertiary structure. In contrast to phosphate (F3) and succinate (F5), reversibility and repeatability was interestingly established for histidine buffer (F4) at pH 6.0. Taken the general thoughts about histidine as a buffer system (VIII.2.1) and the apparent T_m value into consideration, this finding may also be related to the expected negative pH shift occurring at elevated temperatures. Thus, Formulation 4 (histidine, pH 6.0) is expected to lower its pH value by up to one pH unit in the relevant temperature range and indeed reveals melting temperatures of the second unfolding transition (T_m2) comparable to Formulation 2 (phosphate, pH 5.0). Moreover, the fluorescence ratios (350 nm/330 nm) at 30 °C overlay almost perfect for Formulation 2 and 4 after performing the first temperature cycle. That implies the absence of irreversible aggregation and the formation of similar structures in a coherent refolding

mechanism that does not develop at elevated pH values. It is therefore assumed that aggregation and precipitation are closely associated with the pH and the resulting net charge of the antibody that is the main driving factor for colloidal interactions. This hypothesis is consistent with the pH dependence of unfolding and aggregation for different IgG1 type antibodies as reported by Sahin et al.[18] and Brummitt et al.[19].

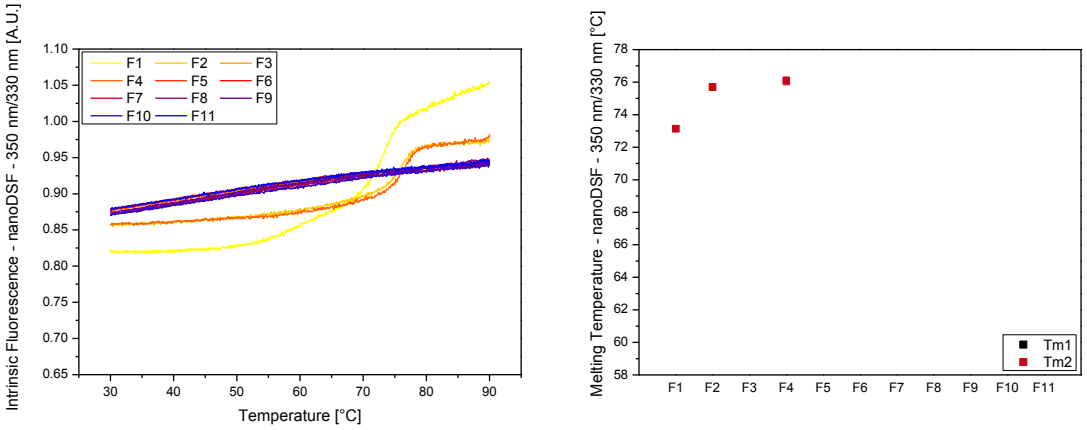

Figure 70: Benchmarking of the formulation screening results by using nanoDSF (2nd up-scan). Left: Colloidal stability was investigated by performing a second up-scan and checking for reversibility of unfolding. Right: Conformational stability was calculated by determining the inflection points of the unfolding curves. Evaluable T_m2 values were obtained for F1, F2 and F4 only. T_m1 values were not observed upon rescan. All samples were measure in quadruplicates (n=4).

VIII.2.1.2.2. Intrinsic Fluorescence Emission Spectroscopy (Intrinsic FES)

An alternative approach for benchmarking the MST results while measuring intrinsic fluorescence by the ratio of 350 nm/330 nm was investigated for the mAb formulation screening by using an Optim 1000 instrument. Comparably to the nanoDSF results, the melting curves (Figure 71 – left) resulted in a double sigmoidal curve showing two inflection points. However, the raw data quality is substantially lower for the Optim instrument when compared to the Prometheus, as the full spectrum fluorescence acquisition at every temperature step only allows for recording ~ 0.75 data points per °C and sample well when measuring 16 capillaries in a ramp of 1°C/min. For our measurement, this corresponds to ~ 45 data points per melting curve, which rather compares to the 60 data points measured in the MST setup. In comparison, the Prometheus instrument, operating with a dual wavelength detection emission filter setup, collected exactly 1009 data points per capillary, measuring the full formulation screening set in quadruplicates within one single run (44 capillaries in total). Given a temperature range of 30 °C to 90 °C in a slope of 1 °C/min, this leads to a resolution of ~ 16.6 measurements per capillary within one minute and a corresponding measurement interval of less than 4 seconds. These long measurement intervals for

the Optim setup led to an increased noise level for the raw data in the Optim and hence to a more imprecise T_m determination, especially for T_m1 due to the smaller unfolding transition (Figure 71 – right). These variations in the calculation of T_m1 introduce difficulties in the detailed evaluation of stabilizing and destabilizing trends, which are in general found to be larger for the first unfolding event. Nevertheless, the stability ranking determined for MST and nanoDSF was generally confirmed, although the influence of some excipients is covered by the standard deviations and therefore remains unresolved. In comparison, the medium resolution MST setup has the advantage of more pronounced thermophoresis unfolding peaks, which simplify the T_m determination and lead to a higher reproducibility of the results.

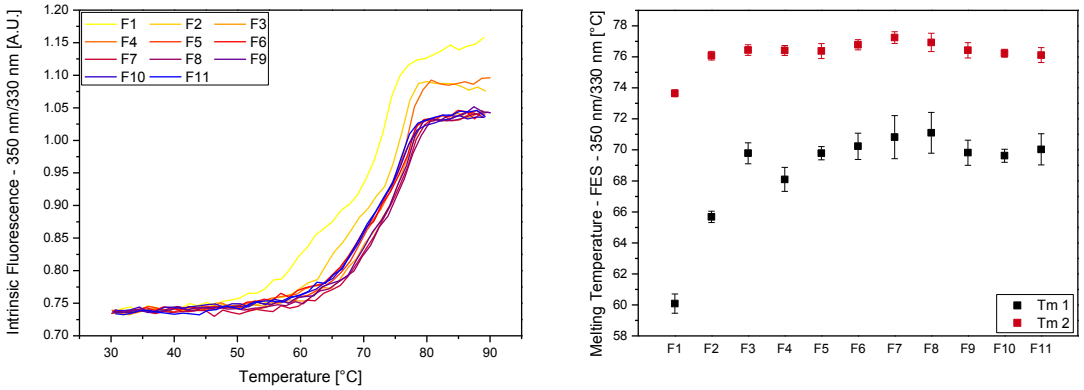

Figure 71: Benchmarking of the formulation screening results by using intrinsic FES. Left: Thermal unfolding monitored by the intrinsic fluorescence ratio of 350 nm/330 nm over temperature. Right: Conformational stability was calculated by determining the inflection points of the unfolding curves. All samples were measured at least in quadruplicates (n≥4).

VIII.2.1.2.3. Differential Scanning Fluorimetry (DSF)

Comparative measurements of thermal unfolding have been performed for the formulation screening by evaluating extrinsic fluorescence emission of the reporter dye SYPRO Orange (SO). Unfolding of the mAb resulted in very noisy but still evaluable raw data that showed low absolute fluorescence levels and only small melting transitions, especially for T_m2 (Figure 72). This low signal to noise ratio is reflected in larger standard deviations compared to the thermophoresis evaluation and the other benchmark methods. Only the T_m1 values determined by intrinsic FES measurements with the Optim instrument showed similar uncertainties as the T_m2 values found in the DSF approach. Whereas the large effects of different pH values (F1-F3) are still evaluable for both melting transitions, smaller influences, for example from different buffer salts or excipients, are covered by the large standard deviations of T_m2 and can only be interpreted using the more distinctive and less noisy T_m1 values. However, in

this way, the general ranking of conformational stabilities is very comparable and not impacted by the addition of a fluorescent dye. Both, the reduced melting point of histidine buffer (F4) and the stabilizing effect of sorbitol (F7) and sucrose (F8) can be derived and match the benchmark results nicely. Nevertheless, no unfolding transitions, and therefore no T_m values were received for the formulations containing 0.05% Tween 80 (F6) or 1% HP-β-CD (F11) as excipients. This was already observed for the rh-GCSF screening (VII.2.1.2) and therefore also expected for the mAb formulation screening. In contrast to all other formulations, F11 and especially F6 expose very high extrinsic fluorescence values from the beginning, which constantly decrease with increasing temperatures (data not shown). This fluorescence progression, caused by interactions of the excipients (Tween & HP-β-CD) with the dye, superimposes all melting transitions and makes the phrasing of a stability statement for these particular formulations impossible.

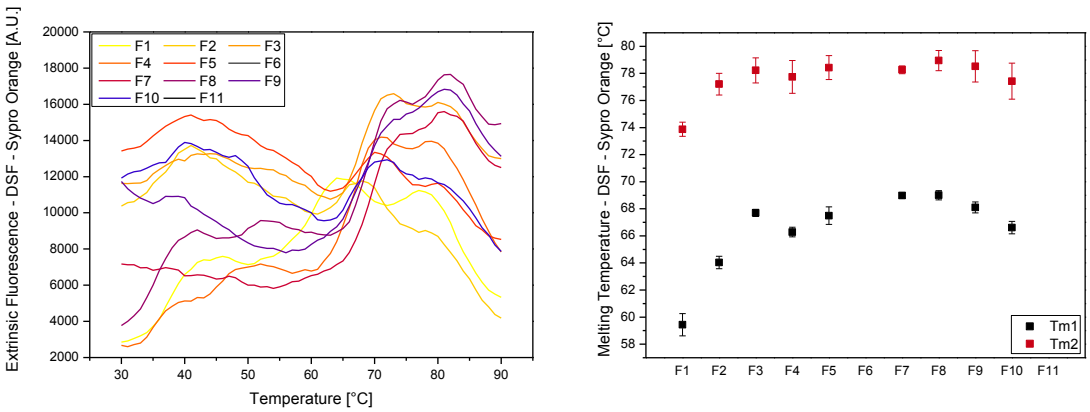

Figure 72: Benchmarking of the formulation screening results by using DSF with Sypro orange as unfolding sensitive dye. Left: Exemplary background corrected melting curves. Right: Evaluated meting temperatures. n≥4.

Furthermore, 9-(2,2-dicyanovinyl)julolidine (DCVJ) was investigated as a dye in DSF studies. This reporter molecule is described to eliminate the disadvantage of binding to certain formulation excipients and consequently enables the analysis of unfolding parameters in the presence of surfactants and potentially also other excipients which impede the detection of unfolding transitions by SO (e.g. cyclodextrins).[20-22] A concentration screening was performed using the mAb in order to evaluate the feasibility of using DCVJ as a fluorescent probe for stability screenings at low protein concentrations. Moreover, the upper measurable concentration limit and the effects of different concentrations on the derived melting temperatures were tested. Figure 73 displays exemplary normalized and staggered melting curves of all concentrations (left) and all evaluable melting temperatures (right). In the fluorescence readout, a

clear influence of concentration is apparent. For the low mAb concentrations of 0.1 and 0.5 mg/ml, the fluorescence traces do not considerably distinguish from the buffer reference and consequently develop no observable melting transitions. At 1.0 mg/ml, small peaks form and melting points were obtained for two out of four replicates. The unfolding events get more pronounced at higher concentrations and a reproducible and accurate T_m determination is enabled. Above a concentration of 5.0 mg/ml, a clear trending of the T_m1 values towards higher, and of the T_m2 values towards lower temperatures is received. The effect on the first melting transition could be explained by a more distinct peak formation and an appertaining right-shift of the inflection point on the ascending curve side. The decrease of T_m2 is observed as a true trend at higher concentrations and is attributed to instating protein aggregation and an associated discontinuation of fluorescence increase upon unfolding, which is well illustrated in the 15 mg/ml melting curve. Recapitulating, this leads to the conclusion that concentrations between 2.5 mg/ml and 10 mg/ml are required for a reasonable T_m determination. Thereby, an intermediate content of 5 mg/ml was determined to be the best compromise between weak signal intensities at lower and potential protein aggregation at higher concentrations. With these results, our pH pre-screening and the formulation screening are not measureable by using DCVJ as a dye for DSF.

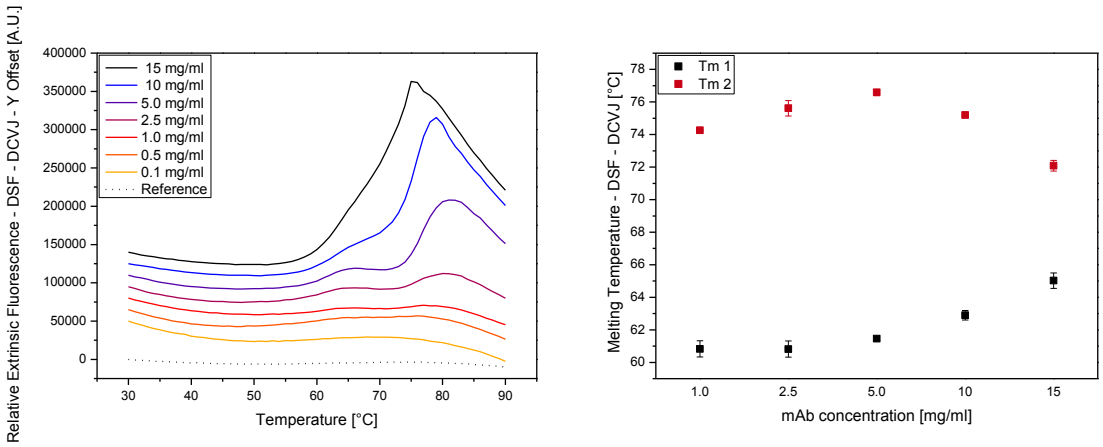

Figure 73: Influence of mAb concentration on DCVJ extrinsic fluorescence over temperature. Left: DCVJ fluorescence melting curve comparison. Values were set to 0 A.U. at 30 °C and then plotted with individual y-offset. Right: Comparison of the derived T_m values. n≥2.

VIII.2.1.3. Differential Scanning Micro-Calorimetry (µDSC)

µDSC, as the established gold-standard method for studying thermal protein unfolding events in high resolution including the possibility of evaluating thermodynamic parameters[23-26], was used for benchmark measurements in the mAb formulation screening. The changes in heat capacity (ΔC_p) clearly resolved both unfolding transitions of all examined formulations as endothermic peaks, which were shifting towards lower temperatures in destabilized formulations and towards higher temperatures under stabilizing conditions (Figure 74 – left). The respective peak maxima were assigned as transition midpoints (melting temperature, T_m) and evaluated in order to rank the formulations according to their conformational stability (Figure 74 – right).

The µDSC results fully confirmed the T_m comparison for the mAb formulation screening by MST. In detail, the stronger differentiation by T_m1 in comparison to T_m2, the strong stabilizing effect of higher pH values including the pH shift of histidine buffer (F4), the destabilization by high salt concentrations (F10), as well as the stabilization by sorbitol (F7) and sucrose (F8) were retrieved. Furthermore, high signal quality and reproducibility, showing only slight differences for F2, were obtained.

Additionally to conformational stability, µDSC indicated aggregation of the mAb by a sharp exothermal decline of the calorimetric signal at temperatures right above the second unfolding endotherm (Figure 74 – left). This aggregation event prevented the re-formation of a stable baseline after complete unfolding and present in the thermograms of all formulations except F1, F2 and F4. At the same time, these formulations showed reduced T_m values for both melting transitions. In comparison to all other formulations in the screening, which were adjusted to a pH value of 6.0, F1 (10 mM phosphate, pH 4.2) and F2 (10 mM phosphate, pH 5.0) were prepared at lower pH values, while F4 (10 mM histidine, pH 6.0) bears the property of lowering its pK_a value at elevated temperatures and therefore acidifying upon heating.

In conclusion, the only drawbacks of the calorimetric approach for the assessment of conformational stabilities and the indication of aggregation are the increased sample volume of ~ 600 µl per measurement and the low throughput of maximum three samples per day. Both the sample consumption, and the time-consuming handling and cleaning procedures are reduced when using the available sample handling robot. Nevertheless, the low volume and high-throughput assays like MST, nanoDSF, Optim, and extrinsic DSF are playing in an entirely different league.

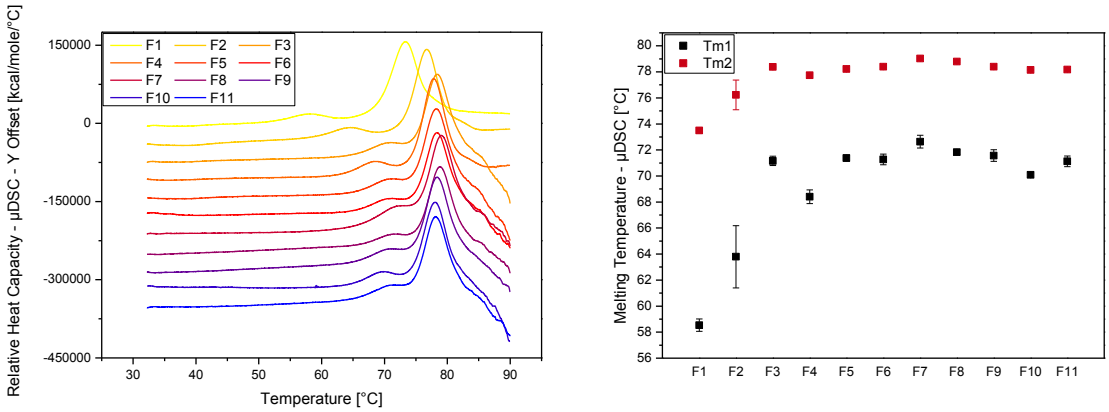

Figure 74: Benchmarking of the formulation screening results by using µDSC. µDSC thermograms are displayed with a customized Y offset for each formulation in order to emphasize and visualize differences in the curve shapes and peak positions (left). T_m values calculated by determining the peak maxima of the thermograms are shown (right, n≥3).

VIII.2.1.4. Static Light Scattering (SLS)

The linear aggregation study, simultaneously conducted with the Optim 1000 instrument, confirmed the impression on the principles of protein aggregation for this mAb which were thus far gathered by the MST, nanoDSF and µDSC analyses.

As Figure 75 illustrates, the changes in the SLS signal detected over increasing temperatures clearly emphasize the “low pH” formulations F1, F2 and F4 (after temperature induced pH shift) as the most aggregation resistant. Formulation 1 (10 mM phosphate, pH 4.2) showed neither at the scattering wavelength of 266 nm, nor at 473 nm any changes up to 90 °C, therefore no onset temperature of aggregation ($T_{agg\ onset}$) was determined. For Formulation 2 (10 mM phosphate, pH 5.0) and Formulation 4 (10 mM histidine, pH 6.0), the SLS at 266 nm increased only very minimally with $T_{agg\ onset}$ values above 74 °C. However, at 473 nm no aggregation was observed, which indicates the formation of very small particles, not detectable at the higher wavelength. All remaining formulations exhibited strong aggregation with very steep scattering slopes for both evaluations. The corresponding $T_{agg\ onset}$ values all range between 65 °C and 75 °C with slight tendencies of higher aggregation propensity for the preparations lacking a stabilizing excipient (F3 and F5) or containing low concentrations of Tween 80 (F6) or HP-β-CD (F11). With this said, the $T_{agg\ onset}$ values at 266 nm for F2 and F4 are indeed comparable with those for F7 (incl. 5% sorbitol) and F8 (incl. 5% sucrose), as the onset values are evaluated as the temperature, where the 10% of the maximum static light scattering increase is reached. However, the drastically increased final scattering level at ~ 80 °C for the

samples at pH 6.0 (F7 & F8) should also be considered in the overall reflection of aggregation propensities.

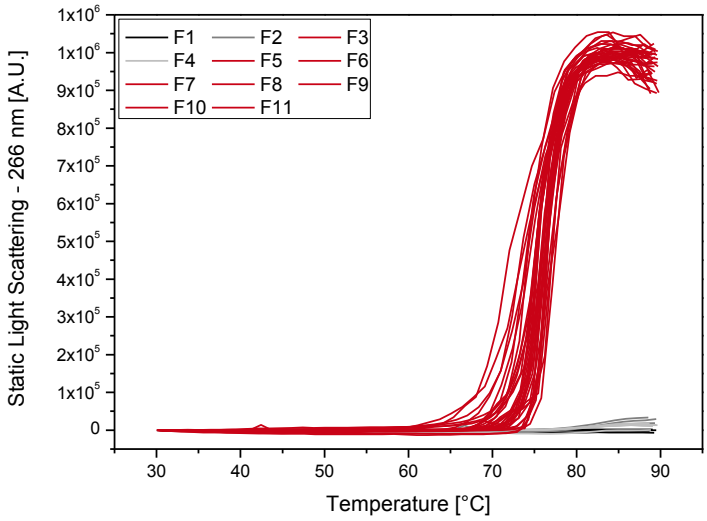

Figure 75: Benchmarking by using static light scattering. All individual measurements of all formulations are displayed. In order to easily distinguish between aggregating and non-aggregating formulations, F1, F2 and F4 are colored in grayscales, while all other formulations are shown in red.

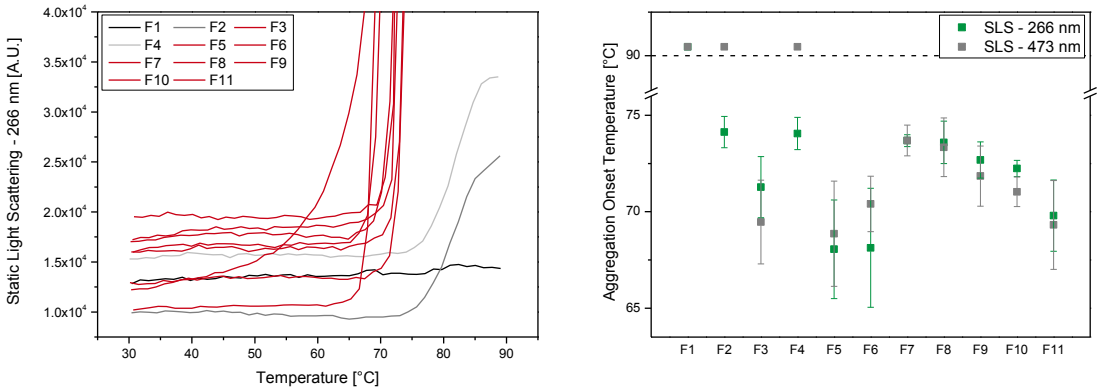

Figure 76: Benchmarking by using static light scattering. Left: Zoom-in of Figure 75, with only one set of formulations selected. Right: Evaluated aggregation onset temperatures for 266 nm and 473 nm. Formulations that showed no increase in light scattering over the complete temperature up-scan are assigned with a theoretical value above 90 °C (dashed line).

Moreover, the increase in static light scattering was found to be congruent with the second unfolding transition of the mAb, both ranging from ~ 70 °C to ~ 80 °C. This observation indicates a coherence of both events and a potential dependency of each other. For many antibodies, including commercial molecules, the presence of

aggregation prone regions (APRs) is described for the Fab part, especially the CDR loops.[26-28] Thermal unfolding of the Fab fragment potentially leads to the exposure of these hydrophobic or aromatic amino-acid rich regions, which in turn enable colloidal self-interactions and consequently lead to aggregation and precipitation. Evaluated for calorimetry[1,7,8,10] and anticipated for the fluorescence based techniques, the most prominent and in our case second unfolding transition reflects the above mentioned Fab unfolding. In combination with the pH value influencing the net charge of the mAbs in solution and therefore altering attractive and repulsive forces[29], a Fab unfolding induced aggregation by interaction of the APRs may serve as the overall hypothesis explaining the observed inversely proportional connection of conformational and colloidal stability.

VIII.2.1.5. Isothermal Chemical Denaturation (ICD) Assay

Isothermal chemical denaturation (ICD) was used as an alternative approach to thermal denaturation for studying the conformational stability of different mAb formulations.

Figure 77 displays the GuHCl induced unfolding curves, which were tracked by intrinsic fluorescence, as well as the derived unfolding denaturant concentrations C_m at the midpoints of unfolding. On the first impression, the unfolding traces were found to be very similar in comparison to the thermal melting curves and changing the pH value of the formulation (F1, F2, and F3) expose a high impact on the observed conformational stability. Moreover, the stabilizing effect of the added formulation excipients is again rather weak, whereas for sucrose (F8) and sorbitol (F7) stabilization was indicated. The conformational destabilization for F10, containing 150 mM sodium chloride, which was reported for the thermal assays, was not noticeable in the ICD approach. However, the main difference between chemical and thermal denaturation was observed for Formulation 4 (10 mM histidine, pH 6.0). In the thermal approach, lower T_m values were detected for the histidine based formulation in comparison to phosphate (F3) and succinate (F5). This observance was linked to the negative shift of the buffer pK_a value, when exposed to elevated temperatures. This hypothesis was recently substantiated by investigations of Svilenov et al.[3]. As the ICD approach is performed at a fixed temperature, this artifact does not occur and comparable conformational stabilities were expected for all buffer salts investigated. In fact, the C_m values (Figure 77 – right) exceeded all expectations and F4 was found to be suddenly the most stable formulation in the whole screening. Without studying an alternative to thermal unfolding and aggregation assays the histidine based formulation could have

been excluded from further investigations and the potential would have been overlooked. These results emphasize the necessity of considering orthogonal approaches and the reflecting the potential of chemical denaturation for the development of stable protein formulations.

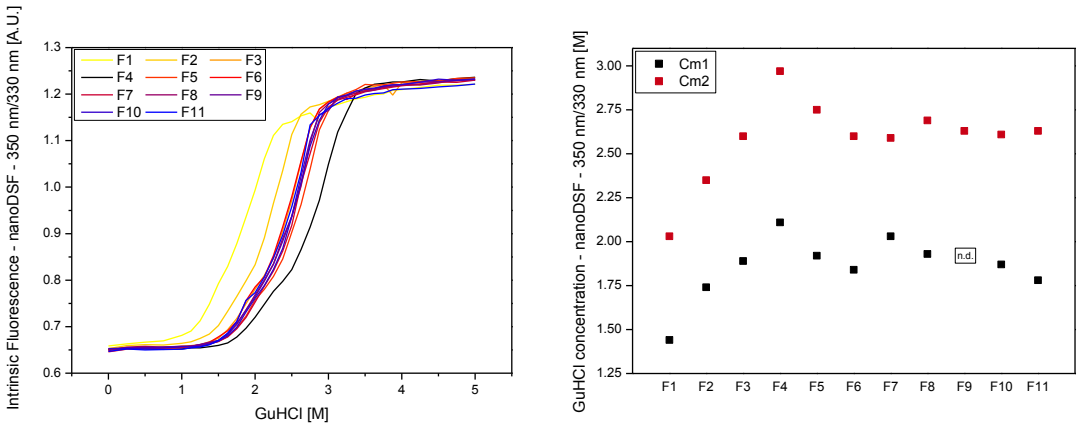

Figure 77: Benchmarking by using chemical denaturation. Guanidine hydrochloride was used as chaotropic excipient to unfold the protein without applying a thermal ramp. The unfolding event and the unfolding denaturant concentration was detected by using the intrinsic fluorescence ratio at 350 nm/330 nm (n=1). For Formulation 9, no Cm1 was detected.

VIII.2.1.6. Comparison and Evaluation of MST as a Tool for Unfolding and Aggregation Studies

In the pH pre-screening, MST and nanoDSF provided highly comparable and conclusive stability predictions over conformational stability and aggregation propensity. The evaluation of a single denaturation cycle by MST already contained information on both, protein unfolding and aggregation. In order to obtain a comparable information content by nanoDSF, two consecutive up-scans were performed and the reversibility of unfolding was analyzed. However, both up-scans by nanoDSF were executed within one third of the time, the single MST experiment took. Furthermore, instating protein aggregation had a strong influence on the unfolding signal in the MST setup, which impeded the calculation of melting temperatures for the formulation showing colloidal instabilities already at comparably low temperatures. On the contrary, the manifestation of unfolding transitions for the nanoDSF melting curves was not perturbed by aggregation and potentially precipitation. However, the T_m1 and T_m2 values that were not impacted by aggregation and therefore evaluable for both methods expose very high correlations with R^2 values above 0.99 (Figure 78). The acquired stability characteristics show a strong and inversely proportional dependence on pH, with decreasing melting temperatures but also reduced aggregate formation in acidified solutions. In conclusion, it was possible to determine pH 5.0 as a potential lead formulation, combining a minimum aggregation propensity with a maximum of conformational stability.

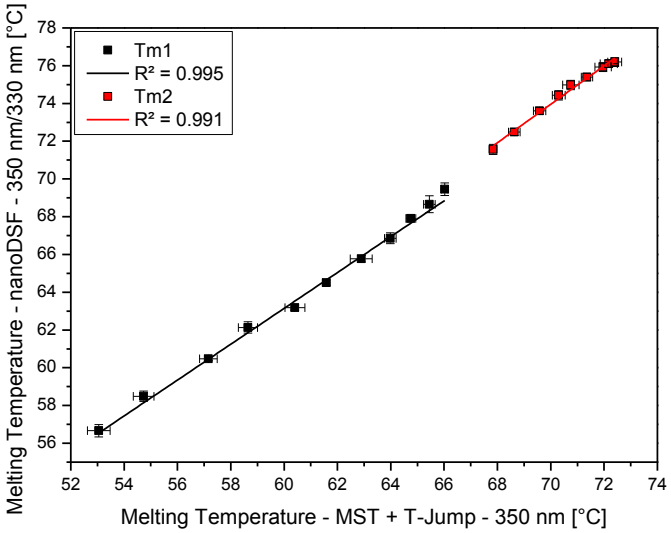

Figure 78: Correlation of the results for MST and nanoDSF within the mAb pH pre-screening.

Additionally, an extensive formulation screening benchmarking study was performed for the same monoclonal antibody. For the case study presented, the lead formulation was chosen only by maximum conformational stability in order to additionally investigate moderate stabilizing and destabilizing effects of different buffer salts and formulation excipients on the unfolding and aggregation characteristics. The MST results were compared to gold-standard methods for thermal denaturation and aggregation determination as well as chemical unfolding as a new approach in protein formulation development. Figure 79 displays the correlation of melting temperatures determined for thermophoresis and t-jump at 350 nm with benchmark results obtained by calorimetry, as well as extrinsic and intrinsic fluorescence emission. Thereby, very consistent data were obtained for the first unfolding transition (T_m1, $R^2 > 0.970$), while the correlation for the second unfolding event (T_m2) was found to be substantially weaker. The calculated T_m2 values for thermophoresis and t-jump clearly distinguish between stabilizing and destabilizing conditions, whereas the melting temperatures for the benchmark methods reach a plateau and only discriminate very minimally between the different formulations. Considering the lessons learned from the pH pre-screening, these deviations could be attributed to the measurement of protein aggregates in the MST setup, having a strong effect on the apparent T_m values and the resulting stability statement.

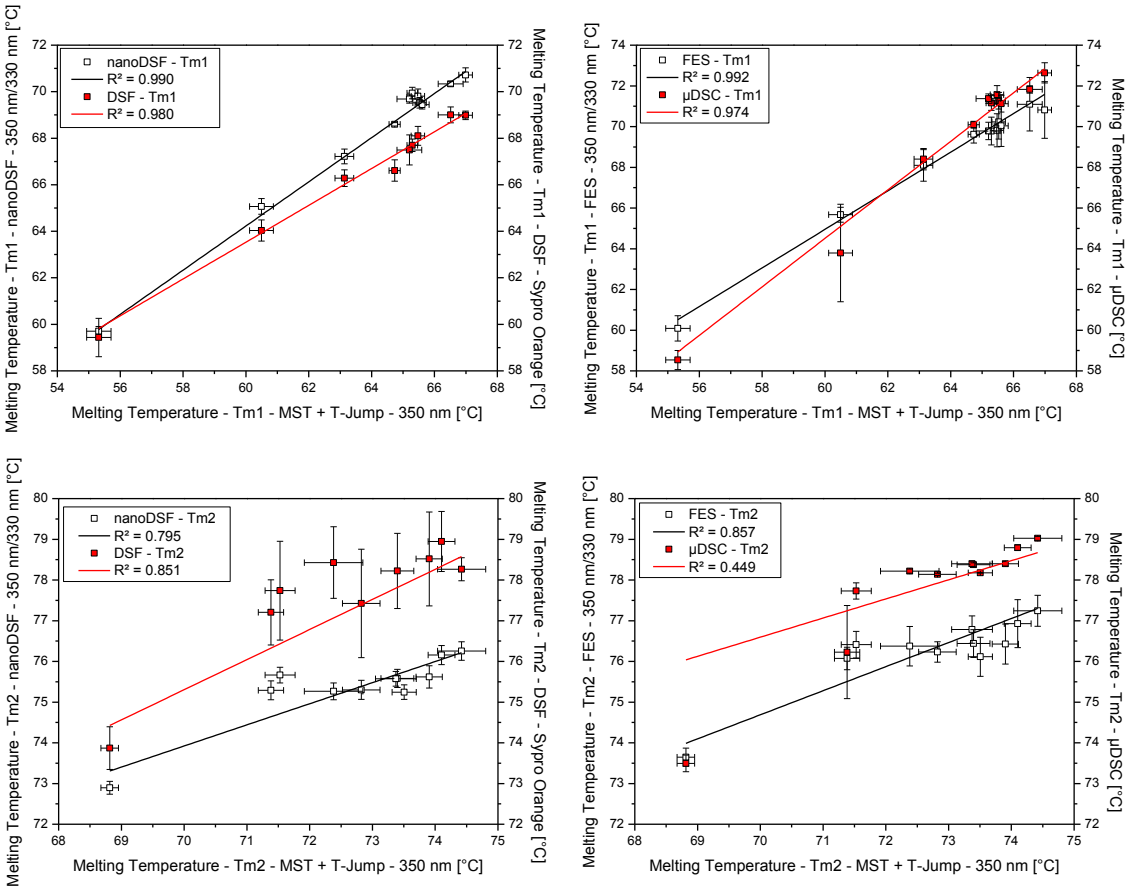

Figure 79: Correlation of the melting temperatures determined for the mAb formulation screening by thermophoresis with t-jump with the benchmark methods microcalorimetry (µDSC), intrinsic fluorescence (nanoDSF and FES), and extrinsic fluorescence (DSF). Tm1 (top) and Tm2 (bottom) values were correlated individually.

Chemical denaturation was tested as an alternative approach to the predominant thermal unfolding assays. Guanidine hydrochloride (GuHCl) was used as chaotropic agent that unfolds the mAb without the necessity of increasing the ambient temperature. Thereby, the temperature induced negative pH shift of approximately one pH unit, which was observed for the histidine based formulation (F4) during thermal denaturation, did not occur and the previously “destabilized” formulation showed by far the highest conformational stability among the formulations tested (Figure 80 – left). Interestingly, for all other formulations, very good correlations were received in the comparison of T_m2 and C_m2 values (Figure 80 – right, R^2=0.952). The first unfolding transitions showed a slightly reduced overlay for the two methods, which could be related to the difficulties in the precise determination of this transition by the limited number of data points for isothermal chemical denaturation. Overall, ICD was perceived as a valuable orthogonal tool for the assessment of conformational stabilities, especially for histidine buffered formulations.

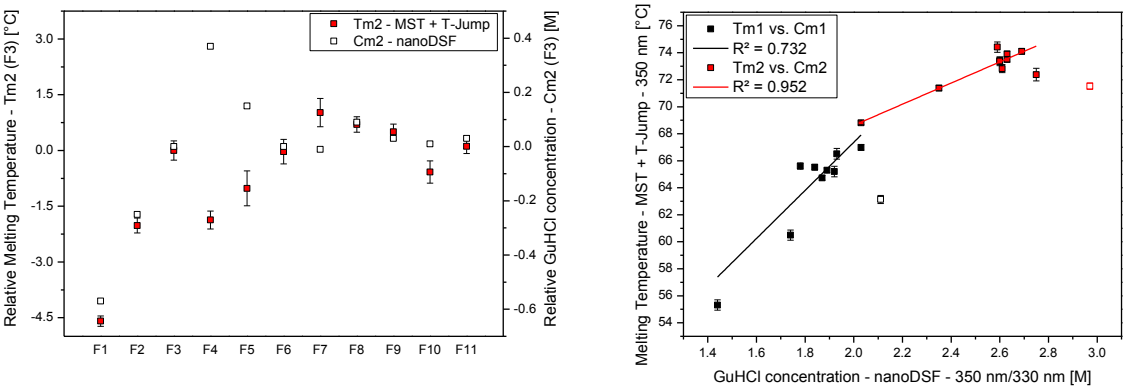

Figure 80: Comparison of chemical denaturation (nanoDSF) and thermal denaturation (thermophoresis with t-jump) within the mAb formulation screening. Left: Unfolding temperature/concentration comparison given relative to the second transition of F3. Right: Correlation of the T_m1/C_m1 and T_m2/C_m2 results in two individual fits. For linear fitting, the data points for F4 (open symbols) have been removed.

Thermal protein aggregation was directly measured by the increase in static light scattering, which most clearly differentiated between aggregation prone and aggregation resistant formulation conditions. Moreover, aggregation propensities were indirectly indicated by the emergence of additional peaks for thermophoresis, studying the reversibility of unfolding by intrinsic fluorescence and the baseline drop after the unfolding event for µDSC. All methods provided a comparable ranking on aggregation propensities, elucidating that increased pH values favor protein aggregation.

As expected, colloidal molecular interaction and the resulting aggregation were found to be mainly pH driven and hardly influenced by formulation excipients. Thus, approaching the isoelectric point (pI) of the mAb by changing the overall net charge could lead to strong molecular attraction and aggregation/precipitation.

In the following step, either a third round stability screening or storage stability studies could be performed. For both options, the lead candidate formulation would be optimized based on the present findings by choosing a reduced pH value (e.g. pH 5.0) and adding stabilizing excipients (e.g. sucrose or sorbitol). With this starting point, a compromise between high unfolding stability and a reduced aggregation propensity could be achieved.

VIII.2.2. Forced Degradation Studies

VIII.2.2.1. Thermo-Optical Protein Characterization (TOPC)

In Figure 81, the measurement of fluorescence changes over time during forced degradation in the course of the pH pre-screening is displayed. During the input of the IR-laser, the timetraces expose a distinct aggregation pattern by developing different fluorescence and scattering levels. The formulations with a pH up to 5.0 exhibited neither an increase in fluorescence nor in timetrace scattering and thus showed a high resistance to aggregation after unfolding. At higher pH values, the formation and accumulation of smaller soluble aggregates lead to a fluorescence enhancement over time. After approximately 90 seconds measurement time, the fluorescence scattering rapidly increased in the pH range from 5.6-6.2, which is attributed to the generation and growth of larger particles and precipitates, periodically flowing through the focal volume and blurring the visual appearance of the sample after the measurement. Moreover, a trend of earlier scattering onset times with higher pH values was apparent.

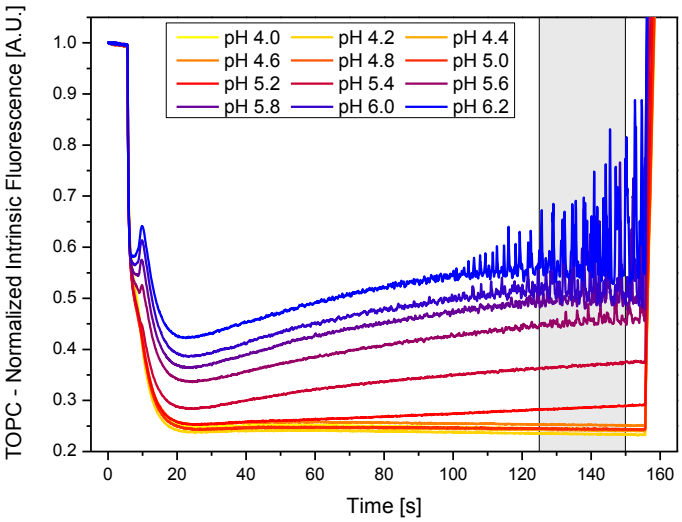

Figure 81: Normalized fluorescence timetraces over time of thermo-optical protein characterization within the pH pre-screening. IR-laser induced unfolding, aggregation and precipitation of monoclonal antibody formulations. The area between the horizontal bars (grey background) indicates the timeframe of the measurement that was used for further evaluation.

The chosen timeframe from 125 to 150 seconds as well as the data evaluation of three consecutive runs in terms of mean fluorescence values and standard deviations is displayed in Figure 82. While increasing mean fluorescence values display the formation of small aggregates, increasing standard deviations suggest the generation

of larger particles and precipitates. As both aggregation parameters increase at higher pH values, the first impressions from the raw data could be confirmed. Therefore, the unfolded monoclonal antibody shows a decreased colloidal stability with increasing pH values starting from pH 5.2. These observations corroborate the conclusions inferred from the thermal unfolding and aggregation investigations.

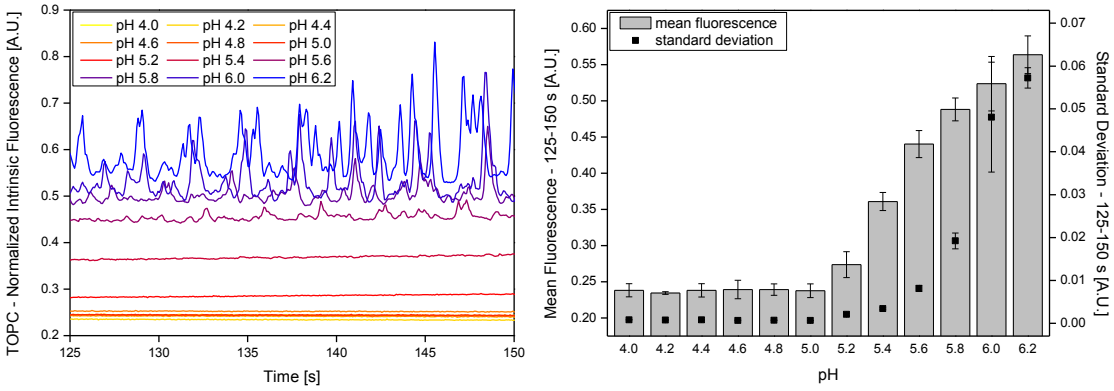

Figure 82: TOPC data evaluation. Left: Zoom-in of the chosen timeframe of 125-150 seconds to be used for further analysis. Right: Mean fluorescence value and standard deviation analysis of the thermo-optical protein characterization results. Increasing values precisely indicate protein aggregation and particle formation. Error bars were calculated by standard error (n=3).

In order to further investigate the effect of pH and beyond that target the impact of formulation excipients on the stability of the mAb, the formulation screening candidates (see page 135) have been included in the TOPC analysis (Figure 83).

As a first result, the TOPC assay was again able to distinguish rapidly between aggregating and non-aggregating samples. In accordance with the pH pre-screening results, changing the formulation pH exhibited a tremendous effect on the colloidal stability after unfolding, which consequently resulted in a much increased aggregation and precipitation propensity for the candidates formulated at a pH value of 6.0 (F3, F5-11) when compared to the formulations at low pH values of 4.2 (F1) and 5.0 (F2). While succinate (F4) and phosphate buffer (F3) expose equal aggregation and precipitation characteristics, the histidine formulation at pH 6.0 (F4) is of exceptional nature and must – due to its characteristic temperature dependent pH shift (see section VIII.2.1.1) – be evaluated with great care. In our selection of eleven formulations, F4 shows the highest aggregation resistance with very low fluorescence and scattering levels what points towards a strong temperature induced pH shift even below pH 4.2.

For the majority of excipients (F7-F11), a scattering, and therefore precipitation reducing effect was observed, when compared to the solely buffered formulation

composition (F3). However, this does not hold true for the addition of PS 80 (F6) and is surprisingly most pronounced for F10, where 150 mM NaCl were added. While a low stabilizing capability of polysorbate was already observed in the thermal unfolding and aggregation studies, a stabilizing effect of salt was never detected and the result for this formulation might be biased by the high salt concentrations potentially hindering the precipitation in this setup.

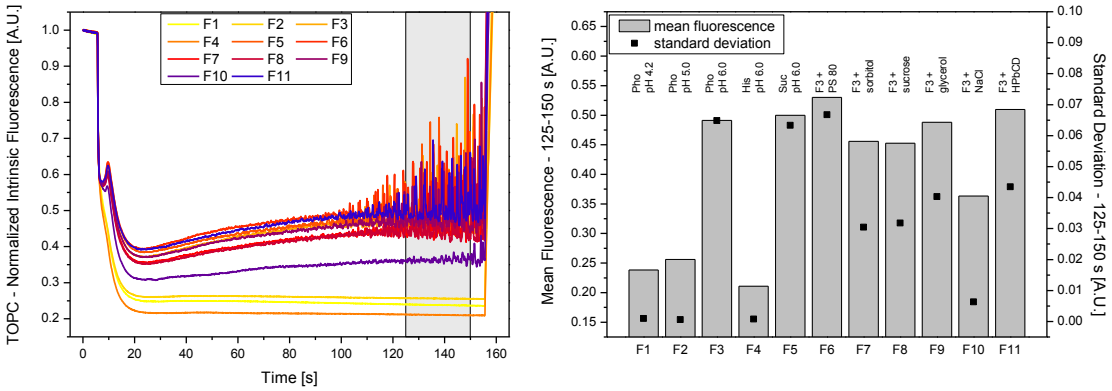

Figure 83: Normalized fluorescence timetraces over time (left) and data analysis (right) of thermo-optical protein characterization within the formulation screening.

VIII.2.2.2. Conventional Stress Testing

In order to benchmark the findings of the thermo-optical protein characterization measurements, we initiated a conventional forced degradation study. Therefore, in a first step, the protein formulations of the pH pre-screening were thermally stressed by intensive heat exposure and subsequently analyzed for aggregation and particle formation by dynamic light scattering (Figure 84 - left), turbidity (Figure 84 - right), and visual inspection (Figure 85) against a reference formulation. The study revealed corresponding results among each other and in comparison to the high power IR-laser heating experiments with pH 4.0 to 5.0 showing no to minimal increases in particle size and turbidity. DLS detected soluble aggregate growth in the nm to low µm range from pH 5.2 to 5.6 before larger precipitates exceeded the measurement range at higher pH values. In contrast, turbidity and visual inspection did not observe protein aggregation until pH 5.4 but enabled to detect even large aggregates and precipitates up to pH 6.2. Moreover, the latter exposed sedimentation of larger insoluble precipitates for the pH 5.8, 6.0 and 6.2 buffered formulations.

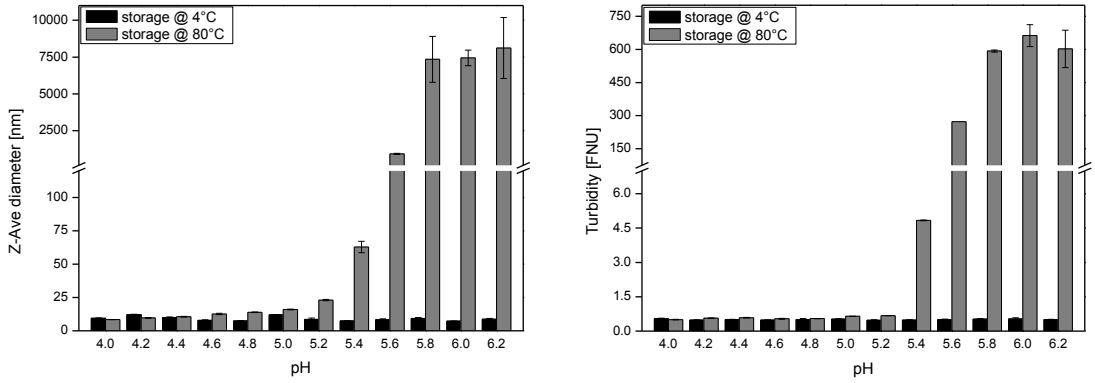

Figure 84: Benchmarking by forced degradation for the pH pre-screening. After incubation of the protein formulations at elevated temperatures, dynamic light scattering (left) and turbidity (right) was measured against a reference buffer. Error bars were calculated by standard error (n ≥ 3).

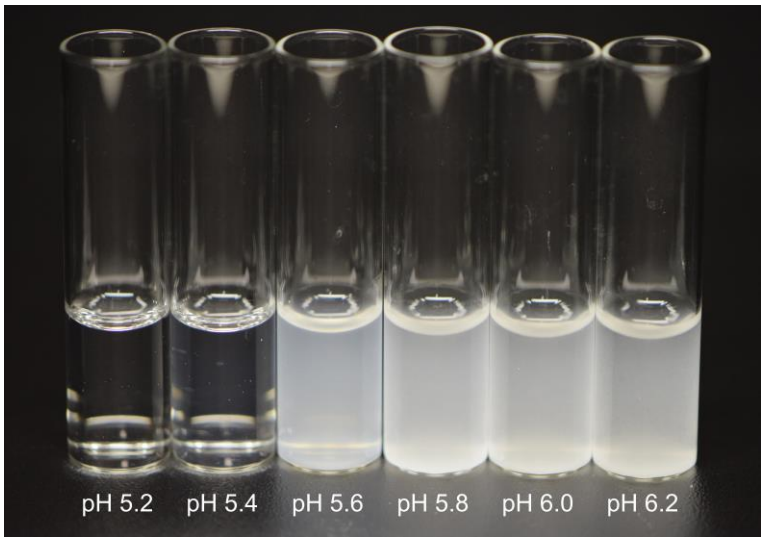

Figure 85: Visual Inspection after forced thermal degradation. While the formulation at pH 5.2 shows neither an increase in turbidity nor visible particles, visible aggregation and precipitation is apparent for higher pH values.

In a second step, stress testing was performed accordingly for the formulation screening samples. The analysis of the heat stressed formulations by DLS (Figure 86 – left) and turbidity (Figure 86 – right) measurements revealed consistent trends when compared to the TOPC results. For the formulations F3 and F5-F11 which showed elevated fluorescence levels and high scattering during TOPC, much increased Z-average diameters and turbidity values were received. On the contrary, F1, F2, and F4, which were found to be most aggregation resistant in TOPC, exposed only minor size and turbidity increases.

The only deviations between the heat incubated samples were found for the formulations F10 and F4. In the comparative forced degradation study, F10 shows a

similar stability profile as found for the other excipients, while the aggregation and precipitation propensity was reduced for the TOPC measurements. These results are congruent with the findings for the thermal unfolding and stability measurements and render the significance of TOPC results under widely varying tonicities questionable. Furthermore, F4 was ranked the most stable formulation in the TOPC assay, whereas this formulation shows a more pronounced size and turbidity increase in comparison to F1 and F2 when analyzed after the classical external forced degradation approach which is presented here. This variation could be attributed to different assay setups and incubation temperatures during heat exposure. In the forced degradation approach, the incubation temperature is fixed to 80 °C and the samples are analyzed after heat stressing and cooling down to room temperature. However, for the TOPC setup, the samples are IR-laser heated to temperatures exceeding the melting temperature and aggregation as well as precipitation characteristics are analyzed in-situ. Given the fact that the pH value of F4 is lowered during incubation at elevated temperatures and aggregation was less favored at lower pH values, the aggregation propensity is reduced in the TOPC assay when compared to the DLS and turbidity analysis at room temperature, where the pH returns to the initial value and the equilibrium between native and aggregated species is altered. This cooling step, which is necessary for the classical stress testing approach, is one major drawback of the procedure, as the molecular properties are prone to change and aggregation, as well as precipitation mechanisms could be induced or hindered.

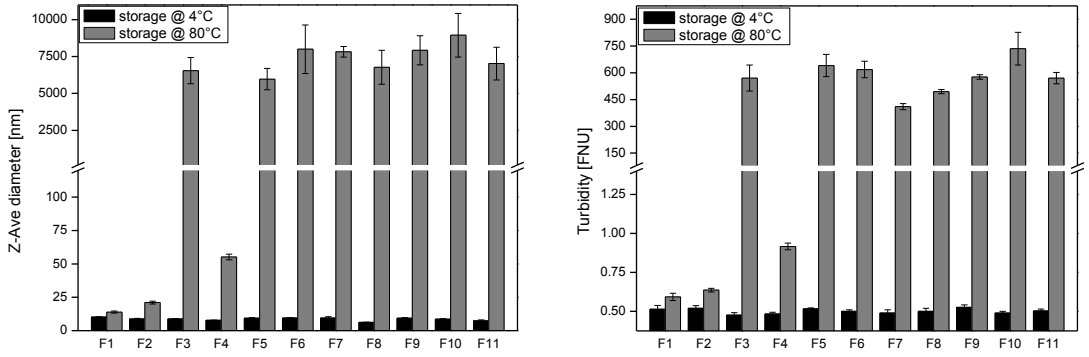

Figure 86: Benchmarking by forced degradation. After incubation of the protein formulations at elevated temperatures, dynamic light scattering (left) and turbidity (right) was measured against a reference buffer. Error bars were calculated by standard error (n=3).

Taken all aspects together thermo-optical protein particle characterization revealed a comparable aggregation and precipitation profiling in comparison to the forced-degradation benchmarking, but was able to differentiate more clearly between the

aggregating formulations in real-time by using much less time and experimental effort. However, it is to mention that the chosen heat stress conditions (storage at 80 °C) deviate from standard forced degradation approaches, where incubation usually is executed below the melting temperature of the protein. In our case, we wanted to mimic the condition during TOPC, where full denaturation of the protein is reached before aggregation is induced.

VIII.2.2.3. Comparison and Evaluation of TOPC as a Tool for Predictive Forced Degradation Studies

The present work introduced an innovative approach for fast and reliable differentiation between stabilizing and destabilizing formulation conditions for exemplary pH and formulation screenings of a monoclonal antibody (mAb). In the TOPC setup, changes in the intrinsic tryptophan fluorescence of the protein were measured during IR-laser-induced heating of the samples. This temperature increase led to characteristic fluorescence changes over time, which were attributed to separable effects of protein unfolding, aggregation, and precipitation, depending on the stability of the respective formulation. The obtained signals were compared with data from forced degradation and thermal stability measurements and correlated well both with the aggregation propensity and with the reversibility of unfolding in different formulations. Moreover, the most promising formulation in terms of maximal aggregation resistance and thermal stability was identified in combination with thermal unfolding measurements as shown in section VIII.2.1. These results, gathered with only 4 µL sample volume and 150 s measurement time per formulation, demonstrate that our straightforward approach facilitates preformulation studies by combining thermal stress testing with simultaneous protein aggregation and precipitation detection and therefore makes sophisticated instrumentation for temperature control, light scattering and turbidity detection redundant. In future investigations, Thermo-Optical Protein Characterization should be considered as a competitive orthogonal method for material and time saving early formulation and drugability screenings in academic and industrial settings, as it has the potential for general applicability in rapid candidate and formulation selections.

VIII.2.3. Protein-Excipient Interaction Analysis

VIII.2.3.1. Binding Studies with Cyclodextrins

VIII.2.3.1.1. MicroScale Thermophoresis (MST)

Binding of the mAb with three different cyclodextrins (α-CD, β-CD, and γ-CD) as well as two β-CD derivatives (HP-β-CD and SBE-β-CD) was investigated by using MST in two different assay buffers by only changing the solution pH. In Figure 87, the titration curves in 10 mM phosphate buffer pH 4.2 are shown, while Figure 88 displays the results in 10 mM phosphate buffer pH 6.0. For both experiments, data have been evaluated for thermophoresis (left) and intrinsic fluorescence (right).

At pH 4.2, thermophoresis remains constant over the whole concentration range and therefore no protein-excipient interaction is observed. However, in the intrinsic fluorescence evaluation, a binding event of SBE-β-CD to the mAb seems to occur. Binding is indicated by a drop in fluorescence by almost 30% between the titration points at 23.3 µM and 468 µM. Though, just after reaching lower thermophoresis plateau, the fluorescence intensity increases again and almost returns to the initial baseline values at 7500 µM SBE-β-CD. This curve progression could be the effect of an association of SBE-β-CD to the antibody at medium excipient concentrations, which is followed by a dissociation process taking place at increased concentrations of SBE-β-CD.

Increasing the assay pH to 6.0, neither thermophoresis, nor intrinsic fluorescence shows any signal change over the whole concentration range of the cyclodextrins, including SBE- β-CD. This observation might be caused by a decreased positive net charge of the antibody, when approaching the isoelectric point. Including the lessons learned from the rh-GCSF-excipient interactions, an ionic binding mechanism was only possible with a positively charged protein being able to bind to the strongly negative charged SBE-β-CD.

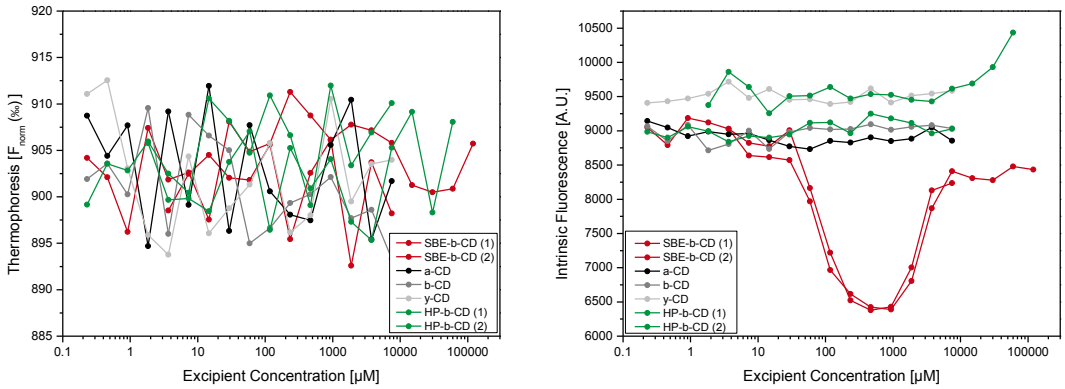

Figure 87: Binding studies of the mAb to various cyclodextrins in 10 mM phosphate buffer pH 4.2 evaluated by thermophoresis (left) and intrinsic fluorescence (right).

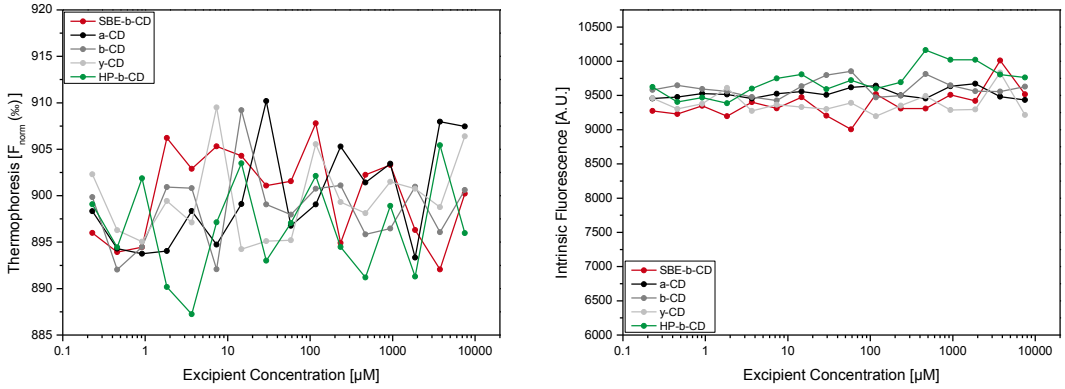

Figure 88: Binding studies of the mAb to various cyclodextrins in 10 mM phosphate buffer pH 6.0 evaluated by thermophoresis (left) and intrinsic fluorescence (right).

VIII.2.3.1.2. Nano Differential Scanning Fluorimetry (nanoDSF)

nanoDSF was used to verify the supposed binding mechanism between SBE-β-CD and the mAb by comparative thermal unfolding investigations with HP-β-CD in 10 mM phosphate buffer pH 4.2. Thus, for every titration step an unfolding scan was performed and changes in the unfolding curves, as well as the respective melting temperatures were evaluated from the intrinsic fluorescence emission ratio of 350 nm/330 nm.

Comparing the derived melting curves as shown in Figure 89, huge differences between HP-β-CD (right) and SBE-β-CD (left) are observed, which were also reflected in the melting temperature evaluation (Figure 90) Titrating HP-β-CD, both unfolding events remain unchanged at values of ~ 63.2 °C (T_m1) and ~ 74.6 °C (T_m2). For SBE-β-CD, a shift towards lower temperatures was apparent with increasing cyclodextrin

concentrations for the complete melting curve, reducing both respective T_m values to 52.9 °C (T_m1) and 66.7 °C (T_m2).

With these results an interaction between SBE-β-CD and the mAb in 10 mM phosphate buffer pH 4.2 is confirmed. Unfortunately, the binding seems to favor the stabilization of the unfolded state and therefore decreases the apparent melting temperatures. These findings are in good alignment with the study by Serno et al.[30,31], where no binding event between and IgG antibody and HP-β-CD could be resolved when using intrinsic fluorescence spectroscopy for binding detection. Furthermore, a considerable aggregation by SBE-β-CD addition was found for agitation and incubation at elevated temperature that was comparable or even deteriorated to a formulation without cyclodextrin. However, the adverse effects of agitation were effectively prevented by the use of HP-β-CD, while the resistance towards heat stress was slightly enhanced. Contrary to the original assumption, more recent studies by Serno[32] and Härtl [33,34] attribute the stabilizing effect of HP- β-CD against interfacial stress to weak direct interaction rather than competitive surface displacement.

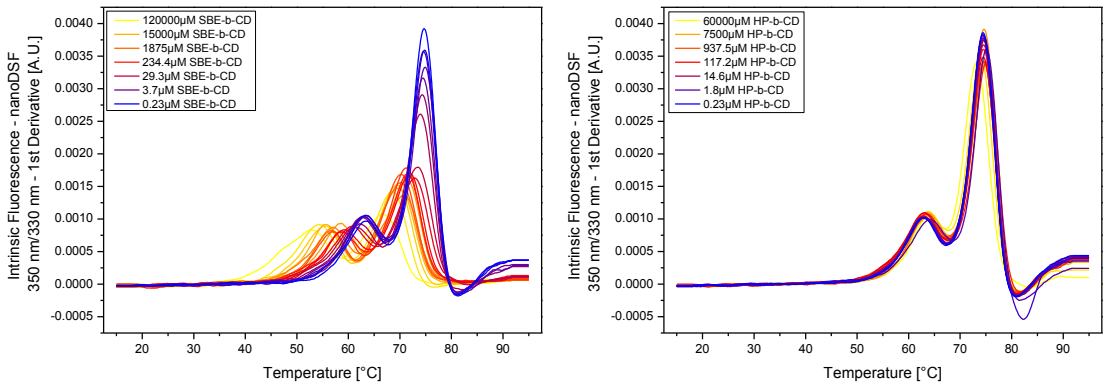

Figure 89: Thermal unfolding studies of the dilution series of SBE-β-CD (left) and HP-β-CD (right) to the mAb in 10 mM phosphate buffer pH 4.2. The unfolding events were tracked by nanoDSF and are displayed as the first derivative of the wavelength ratio 350 nm/330 nm. The color code corresponds to different cyclodextrin concentrations and changes from yellow over red to blue with progressing dilution.

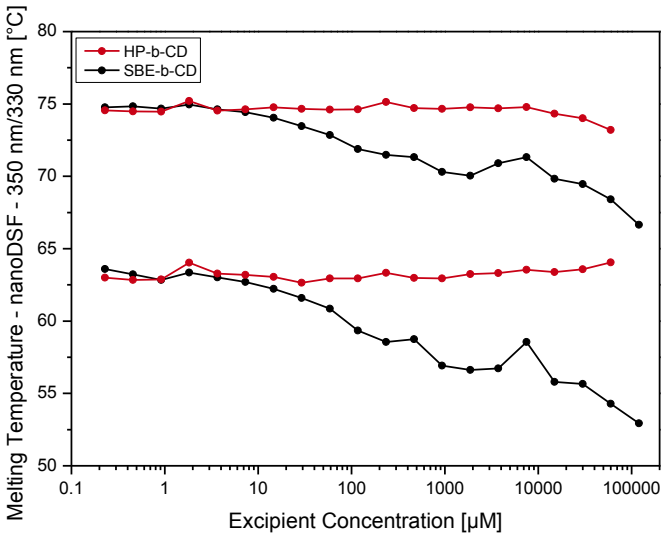

Figure 90: Melting temperature evaluation of the mAb thermal unfolding studies in 10 mM sodium phosphate buffer pH 4.2 at different concentrations of HP-β-CD and SBE-β-CD. For all excipient concentrations, two melting points were detected for the mAb, independent of the cyclodextrin titrated.

VIII.3. Summary and Conclusions

In the mAb case study presented, the strength and weaknesses of thermophoresis based approaches for protein formulation development were assessed within an extended formulation screening comprising a pH pre-screening step and a formulation excipient screening. Both, unfolding and aggregation studies by using MST, as well as forced degradation testing by using TOPC yielded in conclusive and highly comparable stability rankings of the formulations investigated.

With negligible sample volumes of only 10 µl, rapid assay set-ups, exceptionally short hands-on times, and a very broad application range, MST outperformed benchmark methods like µDSC, extrinsic DSF and ICD. Generally, the high sensitivity and accuracy of intrinsic fluorescence approaches was favorable over the addition of extrinsic dyes that led to artifacts and thus impacted the universal applicability. However, the gathered results by using MST match the benchmark results precisely but do not offer any further insights into conformation and aggregation propensities when compared to standard readouts like fluorescence or calorimetry. One drawback revealed for all thermal unfolding and aggregation assays was the fallacious assessment of stabilities for formulation candidates containing temperature sensitive buffer systems like histidine or tris. There, isothermal chemical denaturation (ICD) assays, performed at room temperature are beneficial.[3] In such assays, automated liquid handling and high-throughput fluorescence detection is of great advantage, while also MST can be used for evaluation.[35-37]

TOPC, as an innovative approach to forced degradation investigation and online aggregation monitoring, was compared to conventional stress testing by incubation at elevated temperature and subsequent analysis of turbidity and size distribution. Widely matching results were achieved in a fraction of the time and by using marginally sample volumes by using TOPC. However, the harsh stress condition used for sample incubation guaranteed for best comparability with the TOPC approach but deviates from standard forced-degradation temperatures, which are typically chosen below the unfolding temperature.

One further limitation of thermal unfolding and aggregation, as well as forced degradation is the missing correlation to long-term stability data at quiescent storage conditions, which would enable further insights into the predictive power of both short-term stability testing approaches.

Furthermore, the feasibility of rational excipient selection by using MST was investigated by targeting the binding of several cyclodextrin variants to the mAb and evaluating the stabilizing or destabilizing effect of the addition via thermal unfolding. In this study pH dependent binding was detected between the mAb and SBE-β-CD that led to adverse stability effects but nevertheless suggest a broader utilization of binding assays for excipient screenings.

VIII.4. References

1. Uchiyama S. 2014. Liquid formulation for antibody drugs. Biochimica et Biophysica Acta (BBA) - Proteins and Proteomics 1844(11):2041-2052.

2. Youssef AMK. 2010. Systematic studies to correlate microcalorimetry with stability studies on liquid formulations of various protein drugs. Dissertation. Ludwig-Maximilians-Universität München. Available at: https://edoc.ub.uni-muenchen.de/11623/1/Ahmed_Moustafa_Kamal_Youssef_Mohamed.pdf. Accessed: October 14, 2018.

3. Svilenov H, Markoja U, Winter G. 2018. Isothermal chemical denaturation as a complementary tool to overcome limitations of thermal differential scanning fluorimetry in predicting physical stability of protein formulations. European Journal of Pharmaceutics and Biopharmaceutics 125:106-113.

4. Freire E, Schön A, Hutchins BM, Brown RK. 2013. Chemical denaturation as a tool in the formulation optimization of biologics. Drug Discovery Today 18(19–20):1007-1013.

5. Fesinmeyer RM, Hogan S, Saluja A, Brych SR, Kras E, Narhi LO, Brems DN, Gokarn YR. 2009. Effect of ions on agitation-and temperature-induced aggregation reactions of antibodies. Pharmaceutical Research 26(4):903-913.

6. Brummitt RK, Nesta DP, Roberts CJ. 2011. Predicting accelerated aggregation rates for monoclonal antibody formulations, and challenges for low-temperature predictions. Journal of Pharmaceutical Sciences 100(10):4234-4243.

7. Garber E, Demarest SJ. 2007. A broad range of Fab stabilities within a host of therapeutic IgGs. Biochemical and Biophysical Research Communications 355(3):751-757.

8. Ionescu RM, Vlasak J, Price C, Kirchmeier M. 2008. Contribution of variable domains to the stability of humanized IgG1 monoclonal antibodies. Journal of Pharmaceutical Sciences 97(4):1414-1426.

9. Bork P, Holm L, Sander C. 1994. The immunoglobulin fold: Structural classification, sequence patterns and common core. Journal of Molecular Biology 242(4):309-320.

10. Wu H, Kroe-Barrett R, Singh S, Robinson AS, Roberts CJ. 2014. Competing aggregation pathways for monoclonal antibodies. FEBS Letters 588(6):936-941.

11. Sancho J. 2013. The stability of 2-state, 3-state and more-state proteins from simple spectroscopic techniques... plus the structure of the equilibrium intermediates at the same time. Archives of Biochemistry and Biophysics 531(1–2):4-13.

12. Garidel P, Hegyi M, Bassarab S, Weichel M. 2008. A rapid, sensitive and economical assessment of monoclonal antibody conformational stability by intrinsic tryptophan fluorescence spectroscopy. Biotechnology Journal 3(9-10):1201-1211.

13. Brader ML, Estey T, Bai S, Alston RW, Lucas KK, Lantz S, Landsman P, Maloney KM. 2015. Examination of thermal unfolding and aggregation profiles of a series of developable therapeutic monoclonal antibodies. Molecular Pharmaceutics 12(4):1005-1017.

14. Temel DB, Landsman P, Brader ML. 2016. Orthogonal methods for characterizing the unfolding of therapeutic monoclonal antibodies: Differential scanning calorimetry, isothermal chemical denaturation, and intrinsic fluorescence with concomitant static light scattering. Methods in Enzymology 567:359-389.

15. Reijenga JC, Gagliardi LG, Kenndler E. 2007. Temperature dependence of acidity constants, a tool to affect separation selectivity in capillary electrophoresis. Journal of Chromatography A 1155(2):142-145.

16. Zbacnik TJ, Holcomb RE, Katayama DS, Murphy BM, Payne RW, Coccaro RC, Evans GJ, Matsuura JE, Henry CS, Manning MC. 2017. Role of buffers in protein formulations. Journal of Pharmaceutical Sciences 106(3):713-733.

17. Arakawa T, Timasheff SN. 1982. Stabilization of protein structure by sugars. Biochemistry 21(25):6536-6544.

18. Sahin E, Grillo AO, Perkins MD, Roberts CJ. 2010. Comparative effects of pH and ionic strength on protein–protein interactions, unfolding, and aggregation for IgG1 antibodies. Journal of Pharmaceutical Sciences 99(12):4830-4848.

19. Brummitt RK, Nesta DP, Chang L, Chase SF, Laue TM, Roberts CJ. 2011. Nonnative aggregation of an IgG1 antibody in acidic conditions: Part 1. Unfolding, colloidal interactions, and formation of high-molecular-weight aggregates. Journal of Pharmaceutical Sciences 100(6):2087-2103.

20. Menzen T, Friess W. 2013. High-throughput melting-temperature analysis of a monoclonal antibody by differential scanning fluorimetry in the presence of surfactants. Journal of Pharmaceutical Sciences 102(2):415-428.

21. Hawe A, Filipe V, Jiskoot W. 2010. Fluorescent molecular rotors as dyes to characterize polysorbate-containing IgG formulations. Pharmaceutical Research 27(2):314-326.

22. Hawe A, Sutter M, Jiskoot W. 2008. Extrinsic fluorescent dyes as tools for protein characterization. Pharmaceutical Research 25(7):1487-1499.

23. Ahrer K, Buchacher A, Iberer G, Jungbauer A. 2006. Thermodynamic stability and formation of aggregates of human immunoglobulin G characterised by differential scanning calorimetry and dynamic light scattering. Journal of Biochemical and Biophysical Methods 66(1–3):73-86.

24. Bruylants G, Wouters J, Michaux C. 2005. Differential scanning calorimetry in life science: Thermodynamics, stability, molecular recognition and application in drug design. Current Medicinal Chemistry 12(17):2011-2020.

25. Cueto M, Dorta MJ, Munguía O, Llabrés M. 2003. New approach to stability assessment of protein solution formulations by differential scanning calorimetry. International Journal of Pharmaceutics 252(1–2):159-166.

26. Johnson CM. 2013. Differential scanning calorimetry as a tool for protein folding and stability. Archives of Biochemistry and Biophysics 531(1–2):100-109.

27. Wang X, Das TK, Singh SK, Kumar S. 2009. Potential aggregation prone regions in biotherapeutics: A survey of commercial monoclonal antibodies. mAbs 1(3):254-267.

28. van der Kant R, Karow-Zwick AR, Van Durme J, Blech M, Gallardo R, Seeliger D, Aßfalg K, Baatsen P, Compernolle G, Gils A, Studts JM, Schulz P, Garidel P, Schymkowitz J, Rousseau F. 2017. Prediction and reduction of the aggregation of monoclonal antibodies. Journal of Molecular Biology 429(8):1244-1261.

29. Lehermayr C, Mahler H-C, Mäder K, Fischer S. 2011. Assessment of net charge and protein-protein interactions of different monoclonal antibodies. Journal of Pharmaceutical Sciences 100(7):2551-2562.

30. Serno T, Carpenter JF, Randolph TW, Winter G. 2010. Inhibition of agitation-induced aggregation of an IgG-antibody by hydroxypropyl-β-cyclodextrin. Journal of Pharmaceutical Sciences 99(3):1193-1206.

31. Serno T. 2010. Inhibition of therapeutic protein aggregation by cyclodextrins. Dissertation. Ludwig-Maximilians-Universität München. Available at: https://edoc.ub.uni-muenchen.de/13125/1/Serno_Tim.pdf. Accessed: October 14, 2018.

32. Serno T, Härtl E, Besheer A, Miller R, Winter G. 2013. The role of polysorbate 80 and HPβCD at the air-water interface of IgG solutions. Pharmaceutical Research 30(1):117-130.

33. Härtl E, Dixit N, Besheer A, Kalonia D, Winter G. 2013. Weak antibody–cyclodextrin interactions determined by quartz crystal microbalance and dynamic/static light scattering. European Journal of Pharmaceutics and Biopharmaceutics 85(3):781-789.

34. Härtl E, Winter G, Besheer A. 2013. Influence of hydroxypropyl-beta-cyclodextrin on the stability of dilute and highly concentrated immunoglobulin G formulations. Journal of Pharmaceutical Sciences 102(11):4121-4131.

35. Alexander CG, Jürgens MC, Shepherd DA, Freund SMV, Ashcroft AE, Ferguson N. 2013. Thermodynamic origins of protein folding, allostery, and capsid formation in the human hepatitis B virus core protein. Proceedings of the National Academy of Sciences 110(30):E2782-2791.

36. Alexander CG, Wanner R, Johnson CM, Breitsprecher D, Winter G, Duhr S, Baaske P, Ferguson N. 2014. Novel microscale approaches for easy, rapid determination of protein stability in academic and commercial settings. Biochimica et Biophysica Acta (BBA) - Proteins and Proteomics 1844(12):2241-2250.

37. Jerabek-Willemsen M, André T, Wanner R, Roth HM, Duhr S, Baaske P, Breitsprecher D. 2014. Microscale thermophoresis: Interaction analysis and beyond. Journal of Molecular Structure 1077:101-113.

Chapter IX
Overall Summary and Conclusion

In this thesis, MicroScale Thermophoresis (MST) was developed and qualified as a versatile and reliable orthogonal tool for the high-throughput analysis and stability prediction of protein pharmaceuticals. This supports the quest for new straightforward analytical approaches in the early stages of biopharmaceutical development and thus enables a faster and more efficient lead formulation candidate selection. The application range demonstrated comprises investigations of (i) the conformational stability, (ii) the aggregation propensity, and (iii) protein-excipient interactions, as three major challenges and objectives in the field.

The main focus of our work was on the assessment of physical protein stabilities by using MicroScale Thermophoresis (MST) as a novel label-free high-throughput readout technique for thermal unfolding and aggregation investigations. Furthermore, a method termed Thermo-Optical Protein Characterization (TOPC) was developed as a screening tool investigating non-native aggregation propensities within minutes by IR-laser induced forced thermal degradation and in-situ intrinsic fluorescence readout. Besides innovative physical stability investigations, the commercialized and well-established MST interaction analysis assay was tested for the rational screening of formulation excipients and the examination of interaction mechanisms.

For both physical stability assessments, namely unfolding and aggregation investigations by using MST and forced degradation studies by using TOPC, extensive method and assay development was performed (Chapter IV). Prototype setups were constructed and steadily optimized in the course of the study, while measurement assays and data evaluation routines were developed and validated by the use of proof-of-principle investigations.

In the following, all thermophoresis based approaches were investigated as new tools for essentially label-free high-throughput stability and interaction analysis during formulation development. Four protein stability and formulation screening case studies were presented examining (i) engineered antibody derivatives (Chapter V), (ii) the model protein human serum albumin (HSA, Chapter VI), (iii) the cytokine recombinant human granulocyte colony stimulating factor (rh-GCSF, Chapter VII), and (iv) a model monoclonal antibody (mAb, Chapter VIII). All results were comprehensively benchmarked with established analytical methods, alternative assays and existing literature data.

Unfolding and aggregation investigations by using MST in a stepped thermal ramp assay (sections V.2.1, VI.2.1, VII.2.1, and VIII.2.1) showed two types of events that could be either correlated to protein unfolding transitions or to non-native protein aggregation. Protein melting transitions were reflected in distinct broad positive or negative peaks in the recorded melting curves for thermophoresis and/or t-jump, which were evaluated as apparent melting temperatures (T_m). In the same denaturation assay, occurring aggregation (and precipitation) was reflected in very sharp spike-like peaks, which were either used to simply indicate the formation of protein aggregates or to calculate aggregation onset temperatures ($T_{agg\ onset}$) and rank the formulations in terms of their aggregation stability. Thus, MST was capable of reliably detecting physical stability changes in the conformational state and aggregation behavior of multiple proteins and can be used for the rapid differentiation between stable and instable proteins and formulation conditions.

The derived stability predictions were found to be highly comparable and conclusive over conformational stability and aggregation propensity and correlate well with gold-standard reference techniques as intrinsic and extrinsic fluorescence, static and dynamic light scattering as well as calorimetry. Evaluating MST in the context of the benchmark methods (Table 25), our technique was classified with a low sample volume, short hands-on time and a very broad application range. Furthermore the measurement precision, resolution and repeatability were remarkable. However, the exceptional data density and resolution of µDSC is even beyond and allows for the analysis of even minute and overlapping unfolding transitions with reproducible data fitting and evaluation, when operated at an optimal protein concentration. The measurable concentration range is, in contrast, many times larger for MST, SLS and the intrinsic fluorescence approaches, which resulted in a comparably low noise level in the raw data and a smaller replicate deviation for the low concentrations investigated. Extrinsic fluorescence approaches (DSF) exclusively showed disadvantages compared to label-free assays, only covering a narrow dynamic range and additionally bearing the risks of altering the formulation stability and creating measurement artifacts by the addition of fluorescent reporter dyes.

Summarizing our findings for thermal unfolding and aggregation investigations, outstanding performance was received from in parallel developed intrinsic fluorescence approaches (i.e. Prometheus NT.48) that in the meantime clearly lead the field of straightforward, high-throughput and low material consuming stability assessments. In the end, no significant added value or benefit could be obtained from MST analysis on top of intrinsic fluorescence.

Forced degradation studies by using TOPC were utilized for rapid IR-laser heating and in-situ intrinsic fluorescence evaluation of emerging aggregation and precipitation over time (sections VI.2.2, VII.2.2, and VIII.2.2). Thereby, the accumulation of soluble protein aggregates in the focal area was tracked via increasing fluorescence baselines, while precipitation resulted in emerging and intensifying signal scattering, which is attributed to the periodical flow of particles through the measurement area. Our results were found to match the stability rankings from unfolding and aggregation investigations and furthermore coincide with conventional stress testing approaches by heat incubation and subsequent aggregate analysis. In comparison, TOPC enables online detection of protein aggregation and precipitation in real-time. Thus, a robust and reproducible stability profiling can be obtained in 150 s measurement time per formulation, which clearly outcompetes conventional stress testing approaches.

The assessment of protein-excipient interactions by using MST was used to further investigate molecular stabilization and destabilization mechanisms of excipients in protein formulations (sections VII.2.3 and VIII.2.3). The results of protein-cyclodextrin interaction studies were confirmed by determining the stability consequences of excipient addition by using nanoDSF. Consequently, the titration of binding excipients led to alterations in the conformational stability, while for the non-binding excipients no effect was observed. Furthermore, protein-surfactant interactions were investigate in MST binding studies and suggested a temperature and surfactant concentration dependent incorporation into pluronic F-127 micelles.

In summary, it can be stated that repetitive MST analysis in a stepped thermal ramp assay and IR-laser heating induced forced degradation via TOPC were successfully established as reliable orthogonal methods for the assessment of unfolding and aggregation parameters. Both methods provide multiple advantages over established approaches in terms of sample throughput, material consumption, precision, reproducibility, and application range. Furthermore, standard label-free MST was successfully applied for the fast and easy determination and quantification of protein-excipient interactions.

In conclusion, our results gained understanding for protein specific degradation pathways and interaction mechanisms, which both helped to derive a protein-specific stabilization strategy. For future investigations, this information can be used for a more rational excipient selection and to reduce the number of possible formulation candidates already in early development phases. A combination of conformation and aggregation sensitive analytics is proposed as gold-standard for the predictive stability

determination of protein formulations. Our results suggest performing these investigations either by using MST as a standalone technique covering both readouts, or by a combination of intrinsic fluorescence with an aggregation detecting technique.

Most useful combinations, as derived from our studies, consist of nanoDSF for unfolding analysis and TOPC or SLS for the investigation of protein aggregation and precipitation. The lately developed back-reflection aggregation detection optics, which was implemented as an add-on technique to nanoDSF within the Prometheus systems represents another highly interesting alternative. Furthermore, chemical denaturation should be considered as an alternative orthogonal approach to the predominant thermal unfolding assays, in order to not run in the risk of eliminating potentially stable formulations or selecting potentially instable systems due to pH changes occurring under elevated temperatures.

Table 25: Comparison of methods used for the determination of unfolding and aggregation stability parameters in thermal ramp setups.

Technique	Static light scattering (SLS)	Differential scanning micro-calorimetry (µDSC)	Fluorescence emission spectroscopy			Microscale thermophoresis (MST)
			DSF	Intrinsic FES	nanoDSF	
Device	Optim 1000	MicroCal VP-DSC	qTower	Optim 1000	Prometheus NT.48	Prototypes
Conformational stability	-	+	+	+	+	+
Aggregation stability	+	+/-	+/-	+/-	+/-	+/-
Sample throughput	+/-	-	+	+/-	+	+/-
Sample consumption	+	-	+/-	+	+	+
Resolution and precision	+/-	+	+/-	+/-	+	+/-
Application range	+	+/-	-	+	+	+